

TRACES OF NEW PHYSICS IN COLLIDER DATA

By
SIDDHARTH DWIVEDI
PHYS08201204008

Harish-Chandra Research Institute, Allahabad

A thesis submitted to the
Board of Studies in Physical Sciences
In partial fulfillment of requirements
for the Degree of
DOCTOR OF PHILOSOPHY
of
HOMI BHABHA NATIONAL INSTITUTE




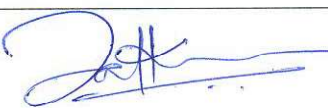

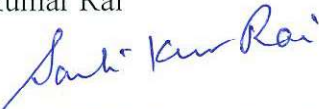


May, 2018

Homi Bhabha National Institute¹

Recommendations of the Viva Voce Committee

As members of the Viva Voce Committee, we certify that we have read the dissertation prepared by Mr. Siddharth Dwivedi entitled "Traces of New Physics in Collider Data" and recommend that it may be accepted as fulfilling the thesis requirement for the award of Degree of Doctor of Philosophy.

Chairman – Prof. Raj Gandhi		Date: 27/7/18
Guide / Convener – Prof. Biswarup Mukhopadhyaya		Date: 27.7.18
Examiner – Prof. Anindya Datta		Date: 27.7.18
Member 1- Prof. Dileep Jatkar		Date: 27/7/18
Member 2- Prof. Anirban Basu		Date: 27/7/18
Member 3- Prof. Santosh Kumar Rai		Date: 27/7/18

Final approval and acceptance of this thesis is contingent upon the candidate's submission of the final copies of the thesis to HBNI.

I/We hereby certify that I/we have read this thesis prepared under my/our direction and recommend that it may be accepted as fulfilling the thesis requirement.

Date: 27/07/2018

Place: Allahabad


Prof. Biswarup Mukhopadhyaya
Guide

¹ This page is to be included only for final submission after successful completion of viva voce.

STATEMENT BY AUTHOR

This dissertation has been submitted in partial fulfillment of requirements for an advanced degree at Homi Bhabha National Institute (HBNI) and is deposited in the Library to be made available to borrowers under rules of the HBNI.

Brief quotations from this dissertation are allowable without special permission, provided that accurate acknowledgement of source is made. Requests for permission for extended quotation from or reproduction of this manuscript in whole or in part may be granted by the Competent Authority of HBNI when in his or her judgment the proposed use of the material is in the interests of scholarship. In all other instances, however, permission must be obtained from the author.



Siddharth Dwivedi

DECLARATION

I, hereby declare that the investigation presented in the thesis has been carried out by me. The work is original and has not been submitted earlier as a whole or in part for a degree / diploma at this or any other Institution / University.



Siddharth Dwivedi

List of Publications arising from the thesis

Journal

1. "Reconstructing a light pseudoscalar in the Type-X Two Higgs Doublet Model", Eung Jin Chun, Siddharth Dwivedi, Tanmoy Mondal and Biswarup Mukhopadhyaya, *Physics Letters B*, **2017**, 774C, pp. 20- 25.
2. "Exploring anomalous $hb\bar{b}$ and $hb\bar{b}\gamma$ couplings in the context of the LHC and an e^+e^- collider", Siddharth Dwivedi, Subhadeep Mondal and Biswarup Mukhopadhyaya, *Phys. Rev. D*, **2017**, 96, 015035.
3. "Distinguishing CP-odd couplings of the Higgs boson to weak boson pairs", Siddharth Dwivedi, Dilip Kumar Ghosh, Biswarup Mukhopadhyaya and Ambresh Shivaji, *Phys. Rev. D*, **2016**, 93, 115039.
4. "Constraints on CP-violating gauge-Higgs operators", Siddharth Dwivedi, Dilip Kumar Ghosh, Biswarup Mukhopadhyaya and Ambresh Shivaji, *Phys. Rev. D*, **2015**, 92, 095015.

Presentation / Conferences

1. Attended SUSY17 conference at Tata Institute of Fundamental Research, Mumbai, India, 11-15 December, 2017 and presented a talk on " $h \rightarrow b\bar{b}\gamma$ at the LHC and an e^+e^- collider".
2. Attended XXII DAE-BRNS High Energy Physics Symposium at University of Delhi, 12-16 December, 2016 and presented a talk on "CP-violating gauge-Higgs Couplings at LHC : Role of CP-odd observables".

Others

1. Teaching Assistant for Quantum Mechanics II, Jan-May, 2018.
2. Teaching Assistant for Quantum Field Theory-I, Fall Semester, 2014.



Siddharth Dwivedi

Dedicated to

*My childhood days in Obra,
memory of which still
keeps me going.*

ACKNOWLEDGEMENTS

It is one of the rarest privileges for anyone to find a friend in his teacher or a teacher in his friend. Looking back at my academic life since my college days, I must admit that I have been really fortunate in this regard as I had both. Nearing the completion of my academic life at HRI, looking back, I have many names and faces that I owe my gratitude to in these past six years of stay in this campus. In case my memory fails me, I apologize to those whose names inadvertently do not find a mention here, but were an irreplaceable part of this wonderful episode in my life.

First and foremost, I convey my gratitude towards my supervisor Prof. Biswarup Mukhopadhyaya for his encouraging support and guidance during the past years. It has been a privilege to learn the deeper nuances of the subject from him and his insights have on many occasions taught me to think from a very different angle towards the solution of a problem.

I am deeply thankful to my teachers Prof. Rajesh Gopakumar, Prof. Ashoke Sen, Prof. Raj Gandhi, Prof. Santosh Kumar Rai, Prof. Asesh K. Datta, Prof. G.V. Pai, Prof. Anirban Basu, Prof. S. Naik, Prof. Sandhya Choubey, Prof. Prasenjit Sen, Prof. Anshuman Maharana, Prof. Dileep Jatkar and Prof. Sumathi Rao for their excellent teaching that provided a solid foundation before the plunge into the research years began. Even outside the classroom, discussions with them were always a constant source of fresh insights into the intricacies of theoretical physics. I take this opportunity to earnestly thank my collaborators Prof. Dilip Kumar Ghosh, Prof. Eung Jin Chun, Dr. Subhadeep Mondal, Dr. Tanmoy Mondal and Dr. Ambresh Shivaji, working with whom I have learned a lot about the subject.

I express my gratefulness to the Regional Centre for Accelerator- based Particle Physics (RECAPP) for providing computational resources and much needed travel support on several occasions.

No measure of admission of gratitude can do justice to my friends and colleagues who made this journey a lot more fun than I could have ever imagined. They were there through the thick and thin of things and for that I cannot thank them enough. It has been a privilege to have won friends for life in Rishu, Bhuvanesh, Kashi, Pramod, Abhishek, Krishna Mohan, Manish, Debajyoti, Tushar, Mrityunjay, Sitender, Satadal, Jyotiranjana, Samrat, Rajarshi, Ramlal, Vikas, Trilochan, Shubhroneel, Titas, Arif, Juhi, Sudipto, Debasis, Swapnamay, Avinanda, Masud, Tanumoy, Shankha, Nabarun, Saurabh, Manoj, Juhi, Anushree,

Ushoshi, Arunabha, Arijit, Indrani, Avirup, Arpan, Animesh, Niyogi, Ujjal and Dibya. All of these names have been a part of my day to-day life on campus and have made this journey worthwhile. Be it in the carefree banter in the guest house with the gang of Vikas, Abhishek, Ramlal, Trilochan and Rajarshi or in physics discussions with Kashi, Nabarun and Shubroneel or the life lessons from Bhuvanesh and Rishu, I have found myself always gaining from these experiences my little share of happiness, that would be a treasure to cherish for years to come.

I am deeply obliged to Nishita Desai and Pratishruti Saha who have helped me on numerous occasions whenever I got stuck with the technicalities of the discipline. I am also thankful to Prof. Bruce Mellado, Prof. Fawzi Boudjema, Prof. Rikard Enberg, Prof. Gunnar Ingelman, Prof. Dieter Zeppenfeld and Prof. Ritesh K Singh from whom I have gathered a lot of wisdom regarding my own work on occasions I got a chance to discuss it with them.

I also acknowledge the support received from the administrative and technical sections of HRI, in particular from Seema-ji, Archana-ji, Raachna-ji, Chandan and Rajiv.

At this stage I find it befitting to acknowledge the names whose motivation and support led me to this wonderful place. The names that come to mind are of Late Prof. D. Basu, Prof. Sayan Kar, Prof. Pratik Khastgir, Prof. Somnath Bharadwaj and Prof. Krishna Kumar who have been a perennial source of anchor during my college years and always motivated me with their guidance and wisdom. I find it rather unjust to extend “gratitude” to the friends who have been a part of my life for the past 14 years. I cannot escape mentioning Vivek, Amit, Himanshu Vikram, Nishant and Zohaib who were always there to push me to the next step after every set-back and assured me to keep the fight going.

Last but not the least, I am forever grateful to my family, my parents, my sister, and my wife, Priyanka who I have always looked up to for the much needed emotional and moral support to endure through all that has been, and for all that is to be.

Contents

SYNOPSIS	1
LIST OF FIGURES	3
LIST OF TABLES	8
1 Introduction	12
1.1 The Standard Model	12
1.2 SM: The Particle Directory	13
1.3 SM Lagrangian	14
1.3.1 The Gauge sector	14
1.3.2 The Fermionic sector	15
1.3.3 The Scalar Sector	16
1.4 The Higgs Mechanism: Giving them masses	17
1.4.1 Gauge boson masses	18
1.4.2 Fermion Masses	19
1.5 SM: The interactions	21
1.5.1 Electroweak currents	21
1.5.2 Higgs couplings in SM	23
1.6 Experimental validation of the SM	25
1.6.1 Deep Inelastic Scattering and the parton model	26
1.6.2 Discovery of gluon jets	26
1.6.3 Asymptotic freedom of QCD	26
1.6.4 Neutral currents and the Photon - Z interference	27
1.6.5 Discovery of W and Z bosons and the top quark	28
1.6.6 Precision tests of the standard model	28

1.6.7	Higgs discovery	30
2	The Quest for New Physics	32
2.1	Why Beyond the Standard Model ?	32
2.1.1	Theoretical motivations for BSM	32
2.1.2	Experimental hints towards BSM	34
2.2	Hunting new physics at LHC	36
2.2.1	Higgs production at the LHC :	36
2.2.2	Higgs Decay Channels:	38
2.2.3	Signal strength measurements at LHC	41
2.2.4	New physics in scaled Higgs couplings	43
2.2.5	New physics in modified Lorentz structure of Higgs couplings	45
3	Higher Dimensional Operators: The Gauge-Higgs Story	48
3.1	Introduction	48
3.2	Morphology of Gauge-Higgs Operators	50
3.3	Constraints from Electroweak Precision (EWP) Data	53
3.4	Constraints from LHC data	56
3.4.1	Higgs decay channels	56
3.4.2	Higgs production channels	58
3.4.3	Global analysis	59
3.5	Constraints from EDMs	65
3.6	Discussion	69
3.7	Summary	73
4	Distinguishing CP-odd couplings of the Higgs boson to weak boson pairs	75
4.1	Introduction	75
4.2	CP-odd anomalous couplings and their constraints	77
4.3	Isolating the effect of CP-odd couplings	80
4.3.1	Signal and backgrounds	80
4.3.2	Observables	82
4.3.3	Asymmetries vs couplings	83
4.4	Summary	91

5	Exploring anomalous $hb\bar{b}$ and $hb\bar{b}\gamma$ couplings at the LHC and an e^+e^- collider	92
5.1	Introduction	92
5.2	Higgs-bottom anomalous coupling	94
5.2.1	Parameterization of the interactions	94
5.2.2	Constraints from Higgs data and other sources	95
5.3	Collider Analysis	98
5.3.1	Effective $hb\bar{b}\gamma$ scenario	100
5.3.2	Effective $hb\bar{b}$ scenario	110
5.4	Summary	115
6	Two-Higgs doublet models	118
6.1	Two-Higgs doublet models (2HDM) : Motivation	118
6.2	The scalar potential in 2HDM models	121
6.3	Couplings to gauge bosons and fermions	123
6.4	Constraints on 2HDM parameters	124
6.4.1	Constraints from perturbativity and vacuum stability	125
6.4.2	EWP constraints	127
6.4.3	Flavor constraints on M_{H^\pm} and $\tan \beta$	127
6.4.4	Collider constraints	128
6.4.5	Constraints from muon g-2	129
6.5	Summary	130
7	Reconstructing a light pseudoscalar in the type X Two-Higgs doublet model	132
7.1	Introduction	132
7.2	The type X 2HDM Model and Constraints	134
7.3	Signal of a light A : An analysis for the LHC	136
7.3.1	Backgrounds	137
7.3.2	Simulation and event selection	138
7.4	Results and Discussion	140
7.5	Summary and Conclusion	143
8	Summary and conclusions	144

A Higher Dimensional Operators: The Gauge-Higgs Story	147
A.1 Gauge boson two-point functions in presence of CP-odd couplings	147
Bibliography	150

SYNOPSIS

The discovery of the 125 GeV Higgs boson at the Large Hadron Collider (LHC) [1,2] ushered in a new chapter in the study of fundamental structure of particle interactions. On one hand it gave a sound footing to the Standard Model (SM) of particle physics by completing the puzzle of "What gives masses to fermions and gauge bosons?", at the same time raising new questions, for example, about the stability of mass scales (naturalness problem). SM in its own right is a consistent theory, but still there are many questions which are left unanswered within its framework—no dark matter candidate, neutrino masses, naturalness, baryon asymmetry etc. to name a few. With the data collected from Run-I of the LHC and the ongoing Run-II, efforts have been directed towards shaping a better understanding of the couplings of the 125 GeV scalar to the other SM gauge bosons and fermions, to allow one to constrain the possible regions of the parameter space of the various viable scenarios, where in the signatures of new physics may be lurking. Such studies have been targeted both in a model-dependent framework (eg. SUSY, 2HDM, Higgs-portal, extra dimensions etc.) as well as in model-independent studies using higher-dimension gauge-invariant operators [3–13].

In the first study taken up during my PhD work, we consider the most general set of $SU(2) \times U(1)$ invariant CP-violating operators of dimension-six, which contribute to VVh interactions ($V = W, Z, \gamma$ and h is the 125 GeV Higgs boson). The effects of new physics are encoded within the Wilson coefficients of the higher-dimension operators (HDOs), suppressed by the powers of the cut-off scale, where the new physics is assumed to set in. The inclusion of these HDOs within the Lagrangian description results in a modification of the tensor structure of the gauge-Higgs couplings. These modified couplings can bring about deviations not just in the total signal rates, but also in the features of the kinematic distributions of the various observables constructed out of the spin and momenta of the final state particles, which can serve to hint at the kind of beyond Standard Model (BSM) scenario one is confronted with. Our aim is to constrain any CP-violating new physics above the electroweak scale via the effective couplings that arise when such physics is integrated out. For this purpose, we use, in turn, electroweak precision data, global fits of Higgs data at the Large Hadron Collider and the electric dipole moments of the neutron and the electron. We thus impose constraints mainly on two-parameter and three-parameter spaces. We find that the constraints from the

electroweak precision data are the weakest. Among the existing Higgs search channels, considerable constraints come from the diphoton signal strength. We note that potential contribution to $h \rightarrow \gamma Z$ may in principle be a useful constraining factor, but it can be utilized only in the high energy run. The contributions to electric dipole moments mostly lead to the strongest constraints, though somewhat fine-tuned combinations of more than one parameter with large magnitudes are allowed. We also discuss constraints on gauge boson trilinear couplings which depend on the parameters of the CP-violating operators .

In a follow-up study we consider the observable effects of CP-violating anomalous ZZh interaction arising from the above mentioned gauge-invariant dimension-six operators at the Large Hadron Collider (LHC), with the purpose of distinguishing them from not only the standard model effects but also those of CP-even anomalous interactions of similar nature. The postulation of a gauge-invariant origin makes various couplings of this kind interrelated. The updated constraints from the LHC as well as limits from neutron and electron dipole moments are used in selecting the benchmark interaction strengths. We use some asymmetry parameters defined over the kinematic distributions of CP-odd observables that have no contribution from standard or CP-even anomalous interactions. This is important since the differences in signal rates only cannot distinguish between the CP-even and CP-odd operators. Parton showering and detector level simulation is included to make our analysis as realistic as possible. On the whole, we conclude that gauge invariant interaction of strength $\geq 40/\text{TeV}^2$ can be successfully isolated using integrated luminosities in the 1.5–3.0 ab^{-1} range.

Subsequently, within the model-independent framework, we study the rare decay of the Higgs in the channel $h \rightarrow b\bar{b}\gamma$ using the anomalous $hb\bar{b}\gamma$ coupling and attempt to isolate the regions of phase space to maximize the discovery potential at the LHC as well as a future e^+e^- collider. A three body decay, as against a two body $h \rightarrow b\bar{b}$ decay is targeted with a view to capture more interesting features in the decay kinematics. The decay kinematics for $h \rightarrow b\bar{b}$ is difficult to use to one's benefit. This is because the two-body decay is isotropic in the rest frame of Higgs, a spinless particle, and moreover the b -hadrons mostly do not retain information such as that of the polarization of the b -quark formed. Such information could have potentially revealed useful clues on the Lorentz structure of the $hb\bar{b}$ coupling, where a small deviation from the SM nature could be a matter of great interest. The study also addresses the question of distinguishing the effects of anomalous $hb\bar{b}\gamma$ coupling from the anomalous $hb\bar{b}$ vertex which might contribute to similar final states. We construct observables which contrast the effects of the two scenarios. The study shows that within

the allowed range of the parameter space, satisfying the constraints on the invisible Higgs decay width [14], one can still see the signatures of anomalous $hb\bar{b}\gamma$ interaction within the luminosity reach of the 14 TeV LHC. We conclude that the anomalous $hb\bar{b}\gamma$ coupling can be probed at the LHC at 14 TeV at the 3σ level with an integrated luminosity of $\sim 2000 \text{ fb}^{-1}$, which an e^+e^- collider can probe at the 3σ level with $\sim 12(7) \text{ fb}^{-1}$ at $\sqrt{s} = 250(500) \text{ GeV}$.

Finally, within the context of a model-dependent BSM search we have investigated the detectability as well as reconstructibility of a light pseudoscalar particle A , of mass in the 50–60 GeV range, which is still allowed in type X (lepton-specific) two-Higgs doublet scenario [15–17]. Such a pseudoscalar can be pair-produced in the decay $h \rightarrow AA$ of the 125 GeV scalar h . The light pseudoscalar in the aforementioned range, helpful in explaining the muon anomalous magnetic moment, has not only substantial branching ratio in the $\tau^+\tau^-$ channel but also one of about 0.35% in the $\mu^+\mu^-$ final state. We show how to faithfully reconstruct the A mass using the $\mu^+\mu^-$ mode, and establish the existence of a pseudoscalar around 50–60 GeV, using the process $p p \rightarrow h \rightarrow AA \rightarrow \mu^+\mu^- \tau^+\tau^-$. The point emphasized in this work is that even though the decay of a light pseudoscalar prevents one from using the collinear approximation [18] to reconstruct the invariant mass of the tau-lepton pair directly, one can still bypass this requirement using suitable cuts on the phase space of the decay products, to reveal information about the mass of the pseudoscalar. The analysis reveals the discovery potential of this channel to be well within the high luminosity reach of the Run-II at LHC (*i.e.* 5σ discovery at $\sim \mathcal{O}(100 \text{ fb}^{-1})$).

List of Figures

1.1	The proton structure function F_2 vs Q^2 at fixed x showing scale invariance. The data are from the H1 and ZEUS experiments at the HERA ep collider [19], the muon-scattering experiments BCDMS [20] and NMC [21] at CERN, E665 at FNAL [22] and SLAC [23]. Figure taken from [24].	25
1.2	Summary of measurements of α_S as a function of the energy scale Q . Figure taken from [24].	27
1.3	Comparison of the measurements with the expectation of the SM for the various EW precision observables. Figure taken from [25].	29
1.4	Observation of Higgs as a bump in the invariant mass distribution of the diphoton system in the $h \rightarrow \gamma\gamma$ channel at ATLAS detector at CERN. Figure taken from [1] where the 125 GeV scalar has been denoted as “H”	31
2.1	Higgs production channels: (a) Gluon fusion, (b) Associated Higgs production, (c) Vector Boson Fusion (VBF) and (d) Associated top quark production.	37
2.2	Higgs production cross section vs. \sqrt{s} for $M_h = 125$ GeV. Figure taken from [24] where the 125 GeV scalar has been denoted as “H”.	38
2.3	Unpolarized parton distribution functions obtained in NNLO NNPDF3.0 global analysis [26] at scales $\mu^2 = 10$ GeV ² (left) and $\mu^2 = 104$ GeV ² (right), with $\alpha_S(M_Z^2) = 0.118$. The corresponding polarized parton distributions are shown (c,d), obtained in NLO with NNPDFpol1.1 [27]. Figure taken from [24].	39
2.4	Higgs BR as a function of Higgs mass. Figure is taken from [24].	40
2.5	Signal strengths corresponding to the channels in Table 2.3. The error bars indicate the 1σ intervals. The green bands indicate the theoretical uncertainties in the SM predictions. Figure is taken from [28] where 125 GeV scalar is denoted as “H”.	42

2.6	Best fit results for the production signal strengths for the combined ATLAS and CMS data. Results from both experiments are also shown separately. The error bars correspond to 1σ (thick lines) and 2σ (thin lines) intervals. Figure is taken from [28].	43
2.7	Best fit results for the signal strengths in Higgs decay channels for the combined ATLAS and CMS data. Results from both experiments are also shown separately. The error bars correspond to 1σ (thick lines) and 2σ (thin lines) intervals. Figure is taken from [28].	44
2.8	Fits for the coupling modifiers for the two cases: (a) Where we consider $\text{BR}_{\text{BSM}} \geq 0$ and $ \kappa_V \leq 1$ ($V = W, Z$), and (b) With $\text{BR}_{\text{BSM}} = 0$. Combined as well as individual results of ATLAS and CMS are shown along with with their uncertainties. The hatched areas show the non-allowed regions for the κ_t parameter, assumed to be positive without loss of generality. The error bars indicate the 1σ (thick lines) and 2σ (thin lines) intervals. For parameters with no sensitivity to the sign, only the absolute values are shown. Figure is taken from [28].	46
3.1	One-loop self energy corrections to electroweak vector bosons (oblique corrections) in presence of CP-odd operators. The blobs show the effective CP-odd vertices. These corrections are of $\mathcal{O}(1/\Lambda^4)$	54
3.2	Constraints from electroweak precision data keeping two parameters nonzero at a time and for $\Lambda = 1$ TeV.	55
3.3	Global fits of the CP-odd parameters keeping two parameters nonzero at a time. The point (0,0) corresponds to the SM point and the (*) represents the best fit point. The green region corresponds to the 68 percent confidence interval and the red region to the 95 percent confidence interval, respectively. The best fit point is doubly degenerate up to a sign flip of the best fit point coordinates.	62
3.4	Marginalized global fits of the CP-odd parameters \tilde{f}_B , \tilde{f}_W and \tilde{f}_{WW}	63
3.5	One-loop diagrams contributing to fermion EDMs. The blobs show the effective vertices arising out of the CP-odd operators.	65
3.6	EDM constraints keeping two parameters nonzero at a time for three representative values of $\Lambda = 1$ (blue), 5(green) & 10(red) TeV.	68
3.7	EDM constraints for non-zero \tilde{f}_B , \tilde{f}_W and \tilde{f}_{WW} with $\Lambda = 1$ TeV. Parameters are varied in the range between -200 to 200.	69

4.1	Differential cross-section distributions for \mathcal{O}_1 at $\sqrt{s} = 14$ TeV. (a) SM vs SM + CP-even case with $C_{ZZh} = 4.62$ and $C_{\gamma Zh} = 2.53$. (b) SM vs SM + CP-odd case with $\tilde{C}_{ZZh} = 40.0$ and $\tilde{C}_{\gamma Zh} = 0.0$. (c) We reverse the sign of the CP-odd coupling with $\tilde{C}_{ZZh} = -40.0$ and $\tilde{C}_{\gamma Zh} = 0.0$	84
4.2	Differential cross-section distributions for \mathcal{O}_2 at $\sqrt{s} = 14$ TeV. (a) SM vs SM + CP-even case with $C_{ZZh} = 4.62$ and $C_{\gamma Zh} = 2.53$. (b) SM vs SM + CP-odd case with $\tilde{C}_{ZZh} = 40.0$ and $\tilde{C}_{\gamma Zh} = 0.0$. (c) We reverse the sign of the CP-odd coupling with $\tilde{C}_{ZZh} = -40.0$ and $\tilde{C}_{\gamma Zh} = 0.0$	85
4.3	The asymmetry vs. coupling plot for the variable \mathcal{O}_1 at Luminosities 1 ab^{-1} , 1.5 ab^{-1} and 3 ab^{-1} , plotted for varying \tilde{C}_{ZZh} . The benchmark points are chosen such that $\tilde{C}_{\gamma Zh} = 0.0$. Statistical uncertainties are shown as error bars for different benchmark points. The zero line is shown to illustrate the offset of the non-vanishing asymmetry against the SM and CP-even case, for which a CP-odd observable has no asymmetry.	87
4.4	The asymmetry vs. coupling plot for the variable \mathcal{O}_2 at Luminosities 1 ab^{-1} , 1.5 ab^{-1} and 3 ab^{-1} , plotted for varying \tilde{C}_{ZZh} . The benchmark points are chosen such that $\tilde{C}_{\gamma Zh} = 0.0$	88
4.5	The asymmetry vs. coupling plot for the variable \mathcal{O}_1 at Luminosities 1 ab^{-1} , 1.5 ab^{-1} and 3 ab^{-1} , plotted for varying \tilde{C}_{ZZh} . The benchmark points are chosen such that $\tilde{C}_{\gamma Zh} = 1.5$	89
4.6	The asymmetry vs. coupling plot for the variable \mathcal{O}_2 at Luminosities 1 ab^{-1} , 1.5 ab^{-1} and 3 ab^{-1} , plotted for varying \tilde{C}_{ZZh} . The benchmark points are chosen such that $\tilde{C}_{\gamma Zh} = 1.5$	90
5.1	$h \rightarrow b\bar{b}\gamma$ via anomalous couplings $hb\bar{b}$ and $hb\bar{b}\gamma$	95
5.2	Contribution to the up-quark EDM arising from the anomalous $hb\bar{b}\gamma$ vertex at one loop.	97
5.3	The light blue, red, blue, cyan and black points indicate the regions of the parameter space excluded from the signal strength (μ) measurements of $\tau\bar{\tau}$, $b\bar{b}$, $\gamma\gamma$, WW^* and ZZ^* decay modes of the Higgs at 2σ level. The blank space is the allowed region.	98
5.4	Normalized distribution for $M_{b\bar{b}(j)\gamma}$ for the signal process ($d_1 = 5.0$, $d_2 = 5.0$) and various background channels : “bkgd1” refers to $pp \rightarrow Zh\gamma$, “bkgd2” to $pp \rightarrow t\bar{t}\gamma$, “bkgd3” to $pp \rightarrow \ell^+\ell^-b\bar{b}\gamma$ and “bkgd4” to $pp \rightarrow \ell^+\ell^-jj\gamma$ respectively.	102

5.5	Normalized distribution for $\Delta\phi(\gamma, \ell^+\ell^-)$ for the signal process ($d_1 = 5.0, d_2 = 5.0$) and various background channels : “bkgd1” refers to $pp \rightarrow Zh\gamma$, “bkgd2” to $pp \rightarrow t\bar{t}\gamma$, “bkgd3” to $pp \rightarrow \ell^+\ell^-b\bar{b}\gamma$ and “bkgd4” to $pp \rightarrow \ell^+\ell^-jj\gamma$ respectively.	103
5.6	Normalized distribution for m_{rec} for the signal process ($d_1 = 5.0, d_2 = 5.0$) and the backgrounds at $\sqrt{s} = 250$ GeV. “bkgd1” refers to $e^+e^- \rightarrow Zh\gamma, Z \rightarrow \ell^+\ell^-, h \rightarrow b\bar{b}$, “bkgd2” to $e^+e^- \rightarrow \ell^+\ell^-b\bar{b}\gamma$ and “bkgd3” to $e^+e^- \rightarrow \ell^+\ell^-jj\gamma$ respectively.	106
5.7	Normalized distribution for \cancel{E} for the signal process and the backgrounds at $\sqrt{s} = 500$ GeV. “bkgd1” refers to $e^+e^- \rightarrow \nu\bar{\nu}h\gamma, h \rightarrow b\bar{b}$, “bkgd2” to $e^+e^- \rightarrow \nu\bar{\nu}b\bar{b}\gamma$ and “bkgd3” to $e^+e^- \rightarrow \nu\bar{\nu}jj\gamma$ respectively.	108
5.8	Normalized distribution for $M_{b\bar{b}(j)\gamma}$ for the signal process and the backgrounds at $\sqrt{s} = 500$ GeV.	109
5.9	Normalized distribution for $M_{b\bar{b}(j)}$ for the signal process and the backgrounds at $\sqrt{s} = 500$ GeV.	110
5.10	Normalized distribution for $M_{b\bar{b}(j)}$ for the signal process $e^+e^- \rightarrow \nu\bar{\nu}h, h \rightarrow b\bar{b}\gamma$ corresponding to the $hb\bar{b}\gamma$ and $hb\bar{b}$ effective vertex scenarios at $\sqrt{s} = 500$ GeV.	113
5.11	Normalized distribution for $\Delta\phi(\gamma, \vec{\cancel{E}})$ for the signal processes ($c_1 = -2.0, c_2 = 0.5$). “signal1” and “signal2” correspond to $e^+e^- \rightarrow \nu\bar{\nu}h, h \rightarrow b\bar{b}\gamma$ and $e^+e^- \rightarrow \nu\bar{\nu}h\gamma, h \rightarrow b\bar{b}$ respectively. The plot has been done with events generated at $\sqrt{s} = 500$ GeV.	116
6.1	M_A - $M_{H\pm}$ plane in 2HDMs with $\beta - \alpha = \pi/2$ and $M_h = 126$ GeV. The darker to lighter gray regions in the left panel correspond to $\Delta M \equiv M_H - M_{H\pm} = \{20, 0, -30\}$ GeV and $\lambda_1 = \sqrt{4\pi}$. The allowed regions in the right panel correspond to $\lambda_1 = \{\sqrt{4\pi}, 2\pi, 4\pi\}$ and vanishing ΔM . Both plots are obtained for $\tan\beta = 50$, but the change with respect to values of $\tan\beta \in [5, 100]$ is negligible. Figure taken from [16].	126
6.2	Allowed region in the M_A vs. $\Delta M_H = M_H - M_{H\pm}$ plane from EWP constraints for different values of $M_{H\pm} = 200, 400$ and 600 GeV. Plots are benchmarked for $\beta - \alpha = \pi/2$ and $M_h = 126$ GeV. The green, yellow, gray regions correspond to 68.3, 95.4, and 99.7% confidence intervals respectively, of a chi-square fit to the EWP data. Figure taken from [16].	127
6.3	Two-loop contribution to muon $g - 2$ from a Barr-Zee diagram with a light A and a fermion loop.	129

6.4	The 1σ , 2σ and 3σ regions allowed by Δa_μ in the M_A - $\tan\beta$ plane taking the limit of $\beta - \alpha = \pi/2$ and $M_{h(H)} = 126$ (200) GeV in type X 2HDM. The regions below the dashed (dotted) lines are allowed at 3σ (1.4σ) by Δa_e . The vertical dashed line corresponds to $M_A = M_h/2$. Figure taken from [16].	131
7.1	The invariant mass of the 2 tau-tagged jets for $M_A = 50$ and $M_A = 60$. The figures illustrate how the higher $p_T(j_\tau)$ threshold leads to more precise reconstruction of the peak at M_A .	138
7.2	The invariant mass of the 2μ and 2 tau-tagged jets for $M_A = 50$ and $M_A = 60$. The figures illustrate how the higher $p_T(j_\tau)$ threshold leads to more precise reconstruction of the peak at $M_h = 125$ GeV.	139
7.3	Discovery potential of the light pseudoscalar decaying to di-muon and di-tau channel using invariant mass variables for BP1(left panel) and BP2(right panel) at 14 TeV LHC.	142

List of Tables

1.1	<i>Charges of the SM chiral fields . 1,2, 3 denote if the field belongs to the singlet, doublet or triplet representation of the corresponding group respectively. T_3 is the third component of weak isospin, Y is the hypercharge quantum number and Q is the electric charge.</i>	14
2.1	Higgs production cross section at LHC at various collision energies (\sqrt{s}). The numbers are from [24].	37
2.2	The branching ratios and the relative uncertainty for a 125 GeV SM Higgs boson. Numbers are taken from [24].	40
2.3	Best fit values of μ_{if} for each specific channel $i \rightarrow h \rightarrow f$, using the combined ATLAS and CMS data for $\sqrt{s} = 7$ and 8 TeV. The results are shown together with their total uncertainties (statistical and systematic combined). The entries labelled with a “–” are either not measured with a meaningful precision and therefore not quoted (for $h \rightarrow ZZ^*$ decay channel for the Wh , Zh , and $t\bar{t}h$ production modes), or not measured at all and therefore fixed to their corresponding SM predictions($h \rightarrow bb$ decay mode for the ggF and VBF production processes).	41
3.1	CP-odd VVh and WWV coupling factors and their effective strengths. . . .	53
3.2	Higgs production cross section in the SM [29]	60
3.3	LHC data used in the global analysis.	61
3.4	Limits on CP-odd coupling strengths from LHC data and EDM measurements for $\Lambda=1$ TeV. 2P and 3P stand for two parameter nonzero and three parameter nonzero cases respectively.	71
4.1	CP-odd VVh coupling factors and their effective strengths.	78

4.2	Limits on CP-odd coupling strengths from LHC data and EDM measurements for $\Lambda=1$ TeV. 2P and 3P stand for two parameter nonzero and three parameter nonzero cases respectively.	79
5.1	ATLAS and CMS $\sqrt{s}=7$ and 8 TeV combined μ values along with their total uncertainties for different Higgs boson decay channels as quoted in Table 11 of Ref. [30].	96
5.2	Cross sections at LHC for our signal processes at $\sqrt{s}=8$ TeV and 14 TeV.	104
5.3	Cross-sections for the signal (corresponding to $d_1 = d_2 = 5.0$) and various background channels are shown in pb alongside the number of expected events for the individual channels at 1000 fb^{-1} luminosity after each of the cuts C0-C4 as listed in the text. NEV \equiv number of events.	104
5.4	Cross-section for the signal process ($d_1 = 5.0, d_2 = 5.0$) presented at $\sqrt{s} = 250$ GeV, before applying the cuts C0, D1 and D2	107
5.5	Cross-section and expected number of events at 250 fb^{-1} luminosity for the signal and various processes contributing to background at $\sqrt{s} = 250$ GeV. We have used $d_1 = d_2 = 5.0$, with $\Lambda = 1$ TeV.	107
5.6	Individual cross-sections of the contributing production channels for the signal process $e^+e^- \rightarrow \nu\bar{\nu}h, h \rightarrow b\bar{b}\gamma$ presented at $\sqrt{s} = 250$ and $\sqrt{s} = 500$ GeV, before applying the cuts I0 - I3 . We have used $d_1 = d_2 = 5.0$, with $\Lambda = 1$ TeV.	111
5.7	Cross-section and expected number of events at 100 fb^{-1} luminosity for the signal and various processes contributing to background at $\sqrt{s} = 250$ and $\sqrt{s} = 500$ GeV . We have used $d_1 = d_2 = 5.0$, with $\Lambda = 1$ TeV.	112
5.8	cross sections for various processes contributing to signal at $\sqrt{s} = 500$ GeV and 1 TeV. Here $c_1 = -2.0$ and $c_2 = 0.5$	114
5.9	Cross-section and expected number of events at 500 fb^{-1} luminosity for the signal and various processes contributing to background at $\sqrt{s} = 500$ GeV and 1 TeV. The Higgs-driven events include both the SM contributions and those due to non-vanishing $\{c_1, c_2\}$	115
5.10	Required integrated luminosities to attain 3σ statistical significance corresponding to the final state $b\bar{b}\gamma + \cancel{E}$ at the centre-of-mass energy, $\sqrt{s} = 500$ GeV for different values of $hb\bar{b}\gamma$ anomalous couplings, $\{d_1, d_2\}$	117
6.1	Models which lead to natural flavour conservation. The superscript i is a generation index.	121

6.2	The multiplicative factors in each type of Yukawa interactions in Eq. (6.3.4)	124
7.1	The multiplicative factors of Yukawa interactions in type X 2HDM	135
7.2	Benchmark points for studying the discovery prospects of light pseudoscalar in Type X 2HDM model at 14 TeV run of LHC. λ_{hAA} is in units of $v = 246$ GeV.	137
7.3	Cut flow table for signal BP1(BP2) and different background processes with two different set of $p_T(j_\tau)$ cuts as described in Section 7.3.2. The number of events are computed with integrated luminosity of 3000 fb^{-1} . The number of background events also depends on benchmark points as M_A changes.	141

Chapter 1

Introduction

1.1 The Standard Model

The Standard Model (SM) is a theoretical framework that successfully describes the three fundamental interactions in nature i.e. the strong, weak and electromagnetic interactions among elementary particles [31–35]. The first step in this direction was to provide an intertwined quantum description of weak and electromagnetic forces, based on the principle of gauge invariance. Once the gauge group for strong interactions too is incorporated as a direct product, the symmetry group that defines the theory is $SU(3)_C \times SU(2)_L \times U(1)_Y$. Here C stands for colour, L for left-handed chiral fields and Y for the hypercharge quantum number respectively. Within the direct product group mentioned above, the $SU(3)_C$ part is responsible for generating strong interactions, whereas the group $SU(2)_L \times U(1)_Y$ is accountable towards all the electromagnetic phenomena and the processes involving weak interactions, for example, beta-decay [31] of nuclei.

Over the years, the SM has stood tall, moving through the discovery of the W and Z gauge-bosons at CERN in 1983 [36–39], the top quark discovery at Fermilab in 1995 [40, 41] and finally celebrating the discovery of the Higgs boson at the Large Hadron Collider (LHC) in 2012 [1, 2].

In the following sections we review the particle content of the SM and the Lagrangian construct of the theory.

1.2 SM: The Particle Directory

SM is a chiral theory of the matter fields (fermions), the gauge bosons (W^\pm , Z bosons and the photon) and the Higgs boson (h). The fermions include the leptons (electron (e), muon (μ) and tau (τ)) along with their corresponding neutrinos (ν_e, ν_μ, ν_τ) and three families of quarks:

$$\begin{pmatrix} u \\ d \end{pmatrix}, \begin{pmatrix} c \\ s \end{pmatrix}, \begin{pmatrix} t \\ b \end{pmatrix}$$

where $u = \text{up}$, $d = \text{down}$, $c = \text{charm}$, $s = \text{strange}$, $t = \text{top}$ and $b = \text{bottom}$ respectively. The fermionic fields are arranged into the doublet and singlet representations of the $SU(2)_L$, given as:

$$\text{Leptons : } \begin{pmatrix} \nu_L \\ e_L \end{pmatrix} \quad e_R, \quad (\nu = \nu_e, \nu_\mu, \nu_\tau ; e = e, \mu, \tau)$$

$$\text{Quarks : } \begin{pmatrix} u_L \\ d_L \end{pmatrix} \quad u_R \quad d_R \quad (u = u, c, t ; d = d, s, b)$$

Here, the subscripts L and R refer to the left-handed and right-handed chiral fields respectively. This splitting of the chiral fields into doublets and singlets is because only the left-chiral fields transform non-trivially under $SU(2)_L$ (hence the name) and carry the weak isospin charge (T). Note that there is no right handed neutrino within the SM. The electric charge Q carried by a particle is related to the third component of the weak isospin T_3 and hypercharge Y by the following relation:

$$Q = T_3 + \frac{Y}{2} \tag{1.2.1}$$

The charge assignments for the various fields are given in Table 1.1.

After having assigned the various quantum numbers to the fermions we proceed to describe the SM Lagrangian constructed out of all possible renormalizable terms respecting the $SU(3)_C \times SU(2)_L \times U(1)_Y$ gauge invariance.

Chiral fields	$SU(3)_C$	$SU(2)_L$	T_3	Y	$Q = T_3 + \frac{Y}{2}$
ν_L	1	2	$\frac{1}{2}$	-1	0
e_L	1	2	$-\frac{1}{2}$	-1	-1
e_R	1	1	0	-2	-1
u_L	3	2	$\frac{1}{2}$	$\frac{1}{3}$	$\frac{2}{3}$
d_L	3	2	$-\frac{1}{2}$	$\frac{1}{3}$	$-\frac{1}{3}$
u_R	3	1	0	$\frac{4}{3}$	$\frac{2}{3}$
d_R	3	1	0	$-\frac{2}{3}$	$-\frac{2}{3}$

Table 1.1: *Charges of the SM chiral fields* . **1,2, 3** denote if the field belongs to the singlet, doublet or triplet representation of the corresponding group respectively. T_3 is the third component of weak isospin, Y is the hypercharge quantum number and Q is the electric charge.

1.3 SM Lagrangian

The SM Lagrangian can be broken into three parts :

$$\mathcal{L}_{SM} = \mathcal{L}_G + \mathcal{L}_F + \mathcal{L}_H \quad (1.3.1)$$

where \mathcal{L}_G is the pure gauge sector, \mathcal{L}_F denotes the fermionic (+ gauge) part and \mathcal{L}_H is the scalar sector (including Yukawa interactions) of the of the Lagrangian.

1.3.1 The Gauge sector

The gauge sector of the Lagrangian is comprised of four electroweak gauge bosons, W_μ^i , ($i = 1..3$), which couple to the weak isospin and B_μ which couples to the hypercharge. In addition, the strong force is mediated by eight gluons G_μ^a , ($a = 1..8$), carrying the colour charge. The gauge-sector of the SM can be expressed as,

$$\mathcal{L}_G = -\frac{1}{4}F^{i\mu\nu}F_{\mu\nu}^i - \frac{1}{4}B^{\mu\nu}B_{\mu\nu} - \frac{1}{4}G^{a\mu\nu}G_{\mu\nu}^a \quad (1.3.2)$$

where $F_{\mu\nu}^i$ is the $SU(2)_L$ field strength,

$$F_{\mu\nu}^i = \partial_\mu W_\nu^i - \partial_\nu W_\mu^i + g\epsilon^{ijk}W_\mu^j W_\nu^k \quad (1.3.3)$$

and $B_{\mu\nu}$ is the $U(1)_Y$ field strength,

$$B_{\mu\nu} = \partial_\mu B_\nu - \partial_\nu B_\mu \quad (1.3.4)$$

The gluonic field strength tensor $G_{\mu\nu}^a$ is

$$G_{\mu\nu}^a = \partial_\mu G_\nu^a - \partial_\nu G_\mu^a + g_s f^{abc} G_\mu^b G_\nu^c \quad (1.3.5)$$

Here the non-abelian field strengths $F_{\mu\nu}^i$ and $G_{\mu\nu}^a$ are characterized by their respective couplings, g , g_s and the completely antisymmetric structure constants ϵ^{ijk} and f^{abc} respectively. These structure constants enter into the defining equations of the Lie algebras of the corresponding groups :

$$[\tau^i, \tau^j] = i\epsilon^{ijk} \tau^k \quad (1.3.6)$$

$$[T^a, T^b] = if^{abc} T^c \quad (1.3.7)$$

where τ^i , T^a are the generators of the $SU(2)$ and $SU(3)$ algebras respectively. $\tau^i = \frac{1}{2}\sigma^i$, σ^i ($i = 1, 2, 3$) being the Pauli matrices and $T^a = \frac{1}{2}\lambda^a$, λ^a ($a = 1, \dots, 8$) being the eight Gell-Mann matrices.

1.3.2 The Fermionic sector

The fermionic sector is broken down into left chiral fields and right chiral fields and can be expressed as

$$\mathcal{L}_F = \sum_{\psi_L} \bar{\psi}_L i \not{D} \psi_L + \sum_{\psi_R} \bar{\psi}_R i \not{D} \psi_R \quad (1.3.8)$$

Here, $\not{D} = \gamma^\mu D_\mu$. Since the left chiral fields couple to weak isospin but the right chiral ones do not, the action of the covariant derivative is different on them, *i.e.*

$$D_\mu \psi_R = \left(\partial_\mu - i \frac{g'}{2} Y B_\mu - i \frac{g_s}{2} \lambda^a G_\mu^a \right) \psi_R, \quad (1.3.9)$$

g' being the $U(1)_Y$ coupling constant and,

$$D_\mu \psi_L = \left(\mathbf{I} \left(\partial_\mu - i \frac{g'}{2} Y B_\mu \right) - i g \frac{\vec{\sigma}}{2} \cdot \vec{W}_\mu - i \frac{g_s}{2} \lambda^a G_\mu^a \right) \psi_L \quad (1.3.10)$$

where $\mathbf{I}, \vec{\sigma}$ are the identity and the Pauli matrices respectively. The terms proportional to g_s , of course, arise for quarks only.

1.3.3 The Scalar Sector

The short-ranged nature of the weak forces requires one to break the $SU(2)_L \times U(1)_Y$ gauge group to an unbroken $U(1)_{\text{EM}}$ corresponding to the electromagnetic interaction. This can be done consistently with renormalizability via the mechanism called spontaneous symmetry breaking (SSB), where some fundamental scalars with non-zero vev are required. The scalar sector in SM is constructed out of a complex $SU(2)$ doublet Φ of spin-zero Higgs fields with the electric charge assignments as shown below

$$\Phi = \begin{pmatrix} \phi^+ \\ \phi^0 \end{pmatrix} = \frac{1}{\sqrt{2}} \begin{pmatrix} \phi_1 + i\phi_2 \\ \phi_3 + i\phi_4 \end{pmatrix} \quad (1.3.11)$$

Eq. 1.2.1 dictates the hypercharge of the scalar doublet to be equal to 1.

The scalar Lagrangian can be separated into a gauge-Higgs part \mathcal{L}_{gh} constructed out of only the scalar doublet and its covariant derivatives and a Yukawa sector \mathcal{L}_{Yukawa} , involving the interactions of the Higgs doublet with the fermions. These are given as,

$$\mathcal{L}_{gh} = (D_\mu \Phi)^\dagger (D^\mu \Phi) - V(\Phi) \quad (1.3.12)$$

where

$$D_\mu \Phi = \left(\mathbf{I} \left(\partial_\mu - i \frac{g'}{2} Y B_\mu \right) - ig \frac{\vec{\sigma}}{2} \cdot \vec{W}_\mu \right) \Phi, \quad (1.3.13)$$

and $V(\Phi)$ is the Higgs potential,

$$V(\Phi) = \mu^2 \Phi^\dagger \Phi + \lambda (\Phi^\dagger \Phi)^2 \quad (1.3.14)$$

with $\mu^2 < 0$ and $\lambda > 0$.

The Yukawa sector Lagrangian is,

$$\mathcal{L}_{Yukawa} = -y_u^{ij} \bar{q}_L^i \tilde{\Phi} u_R^j - y_d^{ij} \bar{q}_L^i \Phi d_R^j - y_e^{ij} \bar{l}_L^i \Phi e_R^j + \text{h.c.} \quad (1.3.15)$$

In Eq. 1.3.15, $y_{u,d,e}^{ij}$ denote the Yukawa couplings (complex in general) for the up-type, down-type quarks and leptons respectively. q_L and l_L stand for the $SU(2)$ quark and lepton doublets within a given generation. The indices i, j run over the three generations of quarks and leptons. Here, $\tilde{\Phi} = i\sigma_2 \Phi^*$ is again an $SU(2)_L$ doublet with $Y = -1$. The up-type quarks couple differently than the down type quark. The quadratic and quartic terms in the scalar potential determine the mass and self-interaction strength of the Higgs boson. they get related by the electroweak symmetry breaking scale.

1.4 The Higgs Mechanism: Giving them masses

Looking at equations 1.3.12, 1.3.13, 1.3.14 and 1.3.15 one can infer that there is no explicit mass term for the gauge-bosons or the fermions within the SM. This is because such a mass would violate gauge-invariance. However the masses for the electroweak gauge bosons (W^\pm, Z) and fermions are generated by what is known as the Higgs mechanism [42–44], which involves spontaneous breaking of the $SU(2) \times U(1)$ symmetry of the SM Lagrangian owing to the fact that the Higgs field acquires a non-zero vacuum expectation value. This can be understood as follows: For $\mu^2 < 0$ in 1.3.14 minimization of $V(\Phi)$ gives us the ground-state Higgs configuration as,

$$V'(\Phi) = 0 \implies |\Phi|(\mu^2 + 2\lambda|\Phi|^2) = 0 \quad (1.4.1)$$

where $|\Phi| = \sqrt{\langle \Phi^\dagger \Phi \rangle_0}$, $\sqrt{\langle \Phi^\dagger \Phi \rangle_0}$ being the vacuum expectation value of the Higgs field. This admits of two solutions, *i.e.*

$|\Phi| = 0$, which is the trivial solution and the non-trivial solution,

$$|\Phi| = \sqrt{-\frac{\mu^2}{2\lambda}} = \frac{v}{\sqrt{2}} \quad (1.4.2)$$

where v is the Higgs vacuum expectation value (vev). A nontrivial vacuum Higgs configuration which spontaneously breaks the $SU(2)_L \times U(1)_Y$ symmetry and respects the conservation of electrical charge Q ($U(1)_Q$ is unbroken) is,

$$\langle \Phi \rangle_0 = \begin{pmatrix} 0 \\ v \\ \frac{v}{\sqrt{2}} \end{pmatrix} \quad (1.4.3)$$

Thus one can reparameterize the complex Higgs doublet as,

$$\Phi = \exp\left(i\frac{\vec{\theta}(\mathbf{x}) \cdot \vec{\tau}}{2v}\right) \begin{pmatrix} 0 \\ v+h \\ \frac{v}{\sqrt{2}} \end{pmatrix} \quad (1.4.4)$$

with the 4 ϕ_i s in 1.3.11 being replaced by 3 real fields $\vec{\theta}(\mathbf{x})$ and the physical Higgs field h . One can get rid of the exponential factor in 1.4.4 by a finite $SU(2)_L$ transformation, *i.e.*

$$\Phi \rightarrow \exp\left(-i\frac{\vec{\theta}(\mathbf{x}) \cdot \vec{\tau}}{2v}\right) \Phi$$

This is the unitary gauge, where the Higgs doublet becomes,

$$\Phi = \frac{1}{\sqrt{2}} \begin{pmatrix} 0 \\ v+h \end{pmatrix} \quad (1.4.5)$$

1.4.1 Gauge boson masses

Using the above definition of the Higgs in the unitary gauge (1.4.4), we can rewrite the the gauge covariant derivative for the Higgs field as,

$$\begin{aligned}
D_\mu \Phi &= \left[\mathbf{I} \partial_\mu - i \frac{g}{2} \begin{pmatrix} W_\mu^3 & W_\mu^1 - iW_\mu^2 \\ W_\mu^1 + iW_\mu^2 & W_\mu^3 \end{pmatrix} - i \frac{g'}{2} \begin{pmatrix} B_\mu & 0 \\ 0 & B_\mu \end{pmatrix} \right] \frac{1}{\sqrt{2}} \begin{pmatrix} 0 \\ v+h \end{pmatrix} \\
\Rightarrow D_\mu \Phi &= \frac{1}{\sqrt{2}} \begin{bmatrix} \partial_\mu - \frac{i}{2}(gW_\mu^3 + g'B_\mu) & -i \frac{g}{2}(W_\mu^1 - iW_\mu^2) \\ -i \frac{g}{2}(W_\mu^1 - iW_\mu^2) & \partial_\mu + \frac{i}{2}(gW_\mu^3 - g'B_\mu) \end{bmatrix} \begin{pmatrix} 0 \\ v+h \end{pmatrix} \quad (1.4.6)
\end{aligned}$$

Redefining the fields as,

$$\begin{aligned}
W_\mu^\pm &= \frac{1}{\sqrt{2}}(W_\mu^1 \mp iW_\mu^2) \text{ and,} \\
Z_\mu &= W_\mu^3 \cos \theta_W - B_\mu \sin \theta_W, \\
A_\mu &= W_\mu^3 \sin \theta_W + B_\mu \cos \theta_W \quad (1.4.7)
\end{aligned}$$

where the weak mixing angle (or Weinberg angle) θ_W is given as,

$$\tan \theta_W = \frac{g'}{g} \quad (1.4.8)$$

and W^\pm, Z are the physical electroweak gauge bosons and A is the photon. Using these redefinitions the gauge covariant derivative becomes,

$$\begin{aligned}
\Rightarrow D_\mu \Phi &= \frac{1}{\sqrt{2}} \begin{bmatrix} \partial_\mu - i \frac{g}{2 c_W} (Z_\mu c_{2W} + A_\mu s_{2W}) & -i \frac{g}{\sqrt{2}} W_\mu^+ \\ -i \frac{g}{\sqrt{2}} W_\mu^- & \partial_\mu + i \frac{g}{2 c_W} Z_\mu \end{bmatrix} \begin{pmatrix} 0 \\ v+h \end{pmatrix} \\
\Rightarrow D_\mu \Phi &= \frac{1}{\sqrt{2}} \begin{bmatrix} -i \frac{g}{\sqrt{2}} (v+h) W_\mu^+ \\ \partial_\mu h + i \frac{g}{2 c_W} (v+h) Z_\mu \end{bmatrix} \quad (1.4.9)
\end{aligned}$$

Here $c_W = \cos \theta_W$, $s_W = \sin \theta_W$, $c_{2W} = \cos 2\theta_W$, $s_{2W} = \sin 2\theta_W$.

Gauge boson masses can be seen to arise from the term $(D_\mu\Phi)^\dagger(D^\mu\Phi)$ (ignoring the terms with h),

$$(D_\mu\Phi)^\dagger(D^\mu\Phi) \rightarrow \frac{g^2v^2}{4}W_\mu^+W^{-\mu} + \frac{1}{2}\frac{g^2v^2}{4c_W^2}Z_\mu Z^\mu + \dots$$

From which one can read off,

$$M_W = \frac{v}{2}g \text{ and } M_Z = \frac{v}{2}\frac{g}{c_W} = \frac{v}{2}\sqrt{g^2 + g'^2} \quad (1.4.10)$$

It is in the unitary gauge that the degrees of freedom corresponding to the Goldstone bosons get absorbed as the longitudinal components of the W and Z fields. Notice that the photon (A_μ) remains massless. Also within the standard model the ratio,

$$\rho = \frac{M_W^2}{M_Z^2 c_W^2} = 1 \quad (1.4.11)$$

This ρ parameter being unity is a consequence of a global custodial symmetry which protects the mass relation of the W and Z gauge bosons [45–48].

1.4.2 Fermion Masses

The mass terms for quarks and leptons can be seen to arise from the Yukawa terms in 1.3.15 after plugging in Eq. 1.4.5 for the Higgs doublet,

$$\mathcal{L}_{quarks} = -\frac{y_u^{ij}}{\sqrt{2}} \begin{pmatrix} \bar{u}_L^i & \bar{d}_L^i \end{pmatrix} \begin{pmatrix} v+h \\ 0 \end{pmatrix} u_R^j - \frac{y_d^{ij}}{\sqrt{2}} \begin{pmatrix} \bar{u}_L^i & \bar{d}_L^i \end{pmatrix} \begin{pmatrix} 0 \\ v+h \end{pmatrix} d_R^j + \text{h.c.} \quad (1.4.12)$$

$$\mathcal{L}_{leptons} = -\frac{y_e^{ij}}{\sqrt{2}} \begin{pmatrix} \bar{\nu}_L^i & \bar{e}_L^i \end{pmatrix} \begin{pmatrix} 0 \\ v+h \end{pmatrix} e_R^j + \text{h.c.} \quad (1.4.13)$$

where we have substituted $\begin{pmatrix} \bar{u}_L^i & \bar{d}_L^i \end{pmatrix}$ for \bar{q}_L^i and $\begin{pmatrix} \bar{\nu}_L^i & \bar{e}_L^i \end{pmatrix}$ for \bar{l}_L^i

Looking at the quarks first we have for the mass terms

$$\mathcal{L}_{quarks}^{mass} = -\frac{v}{\sqrt{2}} y_u^{ij} \bar{u}_L^i u_R^j - \frac{v}{\sqrt{2}} y_d^{ij} \bar{d}_L^i d_R^j + \text{h.c.} \quad (1.4.14)$$

Rewriting this in matrix notation,

$$\mathcal{L}_{quarks}^{mass} = -\frac{v}{\sqrt{2}} \bar{u}_L Y_u u_R - \frac{v}{\sqrt{2}} \bar{d}_L Y_d d_R + \text{h.c.} \quad (1.4.15)$$

where $\bar{u}_L = \begin{pmatrix} \bar{u}_L & \bar{c}_L & \bar{t}_L \end{pmatrix}$, $\bar{d}_L = \begin{pmatrix} \bar{d}_L & \bar{s}_L & \bar{b}_L \end{pmatrix}$ and

$$u_R = \begin{pmatrix} u_R \\ c_R \\ t_R \end{pmatrix}, d_R = \begin{pmatrix} d_R \\ s_R \\ b_R \end{pmatrix} \text{ with } Y_u \text{ and } Y_d \text{ being the } 3 \times 3 \text{ matrices (complex in general)}$$

corresponding to y_u^{ij} and y_d^{ij} respectively. Since we need to diagonalize the matrices Y_u and Y_d to get the mass terms for the quarks, we proceed as follows: Consider two unitary matrices U_u and W_u which diagonalize the hermitian matrix Y_u via

$$Y_u = U_u M_u W_u^\dagger, \quad (1.4.16)$$

with M_u being a diagonal matrix with real positive entries. Similarly for the down-type quarks we have,

$$Y_d = U_d M_d W_d^\dagger, \quad (1.4.17)$$

Substituting for Y_u and Y_d in Eq. 1.4.15 we get

$$\mathcal{L}_{quarks}^{mass} = -\frac{v}{\sqrt{2}} \bar{u}_L U_u M_u W_u^\dagger u_R - \frac{v}{\sqrt{2}} \bar{d}_L U_d M_d W_d^\dagger d_R + \text{h.c.} \quad (1.4.18)$$

Now transforming the fields as,

$$\begin{aligned} u'_L &= U_u^\dagger u_L, & u'_R &= W_u^\dagger u_R \\ d'_L &= U_d^\dagger d_L, & d'_R &= W_d^\dagger d_R \end{aligned} \quad (1.4.19)$$

Eq. 1.4.18 becomes

$$\mathcal{L}_{quarks}^{mass} = -\frac{v}{\sqrt{2}} \bar{u}'_L M_u u'_R - \frac{v}{\sqrt{2}} \bar{d}'_L M_d d'_R + \text{h.c.} \quad (1.4.20)$$

where the diagonal entries of the matrices M_u and M_d are related to quark masses as

$$m_u^i = \frac{v}{\sqrt{2}} M_u^{ii}, \quad m_d^i = \frac{v}{\sqrt{2}} M_d^{ii} \quad (1.4.21)$$

Thus in the mass diagonal basis we can rewrite the quark terms in the Yukawa sector as

$$\mathcal{L}_{quarks} = -m_u^i \bar{u}'_L u'_R \left(1 + \frac{h}{v}\right) - m_d^i \bar{d}'_L d'_R \left(1 + \frac{h}{v}\right) + \text{h.c.} \quad (1.4.22)$$

Similarly for the leptonic part, we have for the mass term,

$$\mathcal{L}_{leptons}^{mass} = -\frac{v}{\sqrt{2}} y_e^{ij} \bar{e}'_L e'_R + \text{h.c.} = -\frac{v}{\sqrt{2}} \bar{e}_L Y_e e_R + \text{h.c.} \quad (1.4.23)$$

can define the diagonalizing unitary matrices U_e and W_e such that $Y_e = U_e M_e W_e^\dagger$, where M_e is a 3×3 diagonal matrix. Again redefining the fields in the mass basis,

$$e'_L = U_e^\dagger e_L, \quad \nu'_L = U_e^\dagger \nu_L, \quad e'_R = W_e^\dagger e_R \quad (1.4.24)$$

we can rewrite the leptonic Yukawa terms as

$$\mathcal{L}_{leptons} = -m_e^i \bar{e}'_L{}^i e'_R{}^i \left(1 + \frac{h}{v}\right) + \text{h.c.} \quad (1.4.25)$$

where $m_e^i = \frac{v}{\sqrt{2}} M_e^{ii}$ are the charged lepton masses.

Notice that here we are making the same unitary rotation on both the components of the $SU(2)$ doublet $l_L = (\nu_L \ e_L)$. This results in the leptonic sector having CP conserving interactions and also lepton number in each generation is conserved separately. This is different from the quark sector as we shall see in the following section.

1.5 SM: The interactions

After having written the SM Lagrangian in terms of the physical scalar h , and having diagonalized the various mass matrices corresponding to the gauge bosons and fermions we can see the resulting interactions among the physical fields i.e. between fermions and gauge bosons (electroweak currents), fermions and Higgs (Yukawa interactions) and between gauge bosons and Higgs and also the self interactions between gauge bosons themselves and the Higgs.

1.5.1 Electroweak currents

The interaction terms between the fermions and gauge bosons arise from the gauge covariant derivative terms in Eq. 1.3.8. If we rewrite the covariant derivative for the left chiral fermions in terms of the physical gauge bosons,

$$D_\mu \psi_L = \left(\partial_\mu - i \frac{g}{\sqrt{2}} (W_\mu^+ T^+ + W_\mu^- T^-) - i \frac{g}{c_W} (T_3 - Q s_W^2) Z_\mu - ie Q A_\mu \right) \psi_L \quad (1.5.1)$$

where $T^\pm = \frac{1}{2}(\sigma^1 \pm \sigma^2)$, $Q = T_3 + \frac{Y}{2}$. From here we can also identify,

$$e = g s_W = g' c_W, \quad (1.5.2)$$

e being the electromagnetic coupling constant.

Similarly for the ψ_R fields we get,

$$D_\mu \psi_R = \left[\partial_\mu + i \frac{g}{c_W} \left(\frac{Y}{2} s_W^2 \right) Z_\mu - i e \frac{Y}{2} A_\mu \right] \psi_L \quad (1.5.3)$$

Using these two equations 1.5.1 and 1.5.3, the gauge-fermion interactions can be expanded in flavor basis as,

$$\mathcal{L}_{int} = g(W_\mu^+ J_W^{\mu+} + W_\mu^- J_W^{\mu-} + Z_\mu J_Z^\mu) + e A_\mu J_{EM}^\mu \quad (1.5.4)$$

with the charged W boson currents given by,

$$\begin{aligned} J_W^{\mu+} &= \frac{1}{\sqrt{2}} (\bar{\nu}_L \gamma^\mu e_L + \bar{u}_L \gamma^\mu d_L) \\ J_W^{\mu-} &= \frac{1}{\sqrt{2}} (\bar{e}_L \gamma^\mu \nu_L + \bar{d}_L \gamma^\mu u_L) \end{aligned} \quad (1.5.5)$$

From the above form of the charged currents one can relate the Fermi constant G_F of the 4-Fermi theory to M_W and v by,

$$\frac{G_F}{\sqrt{2}} = \frac{g^2}{8M_W^2} = \frac{1}{2v^2} \quad (1.5.6)$$

Also, the neutral currents corresponding to the Z boson and photon are

$$\begin{aligned} J_Z^\mu &= \frac{1}{c_W} \left[\bar{\nu}_L \gamma^\mu \left(\frac{1}{2} \right) \nu_L + \bar{e}_L \gamma^\mu \left(-\frac{1}{2} + s_W^2 \right) e_L + \bar{e}_R \gamma^\mu (s_W^2) e_R \right. \\ &\quad + \bar{u}_L \gamma^\mu \left(\frac{1}{2} + \frac{2}{3} s_W^2 \right) u_L + \bar{u}_R \gamma^\mu \left(-\frac{2}{3} s_W^2 \right) u_R \\ &\quad \left. + \bar{d}_L \gamma^\mu \left(-\frac{1}{2} + \frac{1}{3} s_W^2 \right) d_L + \bar{d}_R \gamma^\mu \left(\frac{1}{3} s_W^2 \right) d_R \right] \end{aligned} \quad (1.5.7)$$

$$J_{EM}^\mu = \bar{e} \gamma^\mu (-1) e + \bar{u} \gamma^\mu \left(+\frac{2}{3} \right) u + \bar{d} \gamma^\mu \left(-\frac{1}{3} \right) d \quad (1.5.8)$$

One can see from Eqs. 1.4.19 and 1.4.24 in section 1.4.2 that the unitary rotations of the quarks and leptons from the flavor to the mass basis would still keep the neutral currents J_Z^μ and J_{EM}^μ diagonal. But such is not the case for the charge currents. For the leptonic charged currents one would still get

$$J_W^{\mu+}(\text{leptons}) \rightarrow \frac{1}{\sqrt{2}} \bar{\nu}'_L U_e^\dagger \gamma^\mu U_e e'_L \rightarrow \frac{1}{\sqrt{2}} \bar{\nu}'_L \gamma^\mu e'_L \quad \text{and,}$$

$$J_W^{\mu-}(\text{leptons}) \rightarrow \frac{1}{\sqrt{2}} \bar{e}'_L U_e^\dagger \gamma^\mu U_e \nu'_L \rightarrow \frac{1}{\sqrt{2}} \bar{e}'_L \gamma^\mu \nu'_L \quad (1.5.9)$$

where the Unitary matrices U_e and U_e^\dagger can move through γ^μ since they act on flavor basis while γ^μ are in spinor space. But when one considers the charged current corresponding to quarks, for example,

$$J_W^{\mu+}(\text{quarks}) \rightarrow \frac{1}{\sqrt{2}} \bar{u}'_L \gamma_\mu U_u^\dagger U_d d'_L \rightarrow \frac{1}{\sqrt{2}} \bar{u}'_L \gamma_\mu \mathbf{V}_{\text{CKM}} d'_L \quad (1.5.10)$$

where the quark mixing matrix $\mathbf{V}_{\text{CKM}} = U_u^\dagger U_d$ being product of two unitary matrices is also a unitary matrix. The matrix elements of \mathbf{V}_{CKM} cannot be theoretically calculated within SM, but are phenomenologically extracted from experiments. For the two generation case, \mathbf{V}_{CKM} reduces to the *Cabibbo* matrix [49] and for the three generations it is called the *Cabibbo-Kobayashi-Maskawa* matrix [50] given as,

$$\mathbf{V}_{\text{CKM}} = \begin{pmatrix} V_{ud} & V_{us} & V_{ub} \\ V_{cd} & V_{cs} & V_{cb} \\ V_{td} & V_{ts} & V_{tb} \end{pmatrix} \quad (1.5.11)$$

This 3×3 unitary matrix can be expressed in terms of four parameters, *i.e.* three angles and a complex phase. The presence of this complex phase brings in CP violation within the SM. Associated with this CKM matrix there is a phase convention independent measure of CP violation, the Jarlskog invariant. J is defined as $J = \text{Im}(V_{ij} V_{kl} V_{il}^* V_{kj}^*)$ where Im stands for the imaginary part. From the experiments, the magnitudes of the various CKM elements and the Jarlskog invariant J are constrained to be [24],

$$\mathbf{V}_{\text{CKM}} = \begin{pmatrix} 0.97434_{-0.00012}^{+0.00011} & 0.22506 \pm 0.00050 & 0.00357 \pm 0.00015 \\ 0.22492 \pm 0.00050 & 0.97351 \pm 0.00013 & 0.0411 \pm 0.0013 \\ 0.00875_{-0.00033}^{+0.00032} & 0.0403 \pm 0.0013 & 0.999915 \pm 0.00005 \end{pmatrix} \quad (1.5.12)$$

and the Jarlskog invariant $J = 3.04_{-0.20}^{+0.21} \times 10^{-5}$.

1.5.2 Higgs couplings in SM

Using the Eq. 1.4.5 in the Higgs potential $V(\Phi)$ (Eq. 1.3.14) we can write the scalar self interaction terms as

$$\mathcal{L}_{\text{scalar}}^{\text{int}} = -V(\Phi) = -\lambda v^2 h^2 - \lambda v h^3 - \frac{\lambda}{4} h^4 \quad (1.5.13)$$

from where we can read the Higgs mass,

$$M_h = 2\lambda v^2 \quad (1.5.14)$$

Rewriting $\mathcal{L}_{scalar}^{int}$ in terms of M_h ,

$$\mathcal{L}_{scalar}^{int} = -V(\Phi) = -\frac{1}{2}M_h^2 h^2 - \frac{M_h^2}{2v}h^3 - \frac{M_h^2}{8v^2}h^4 \quad (1.5.15)$$

from where we can read off the interaction vertices for the cubic and quartic terms,

$$\begin{aligned} h^3 \text{ vertex} &: -i \frac{3M_h^2}{v} \\ h^4 \text{ vertex} &: -i \frac{3M_h^2}{v^2} \end{aligned} \quad (1.5.16)$$

The gauge-Higgs interactions come from the term $(D_\mu\Phi)^\dagger(D^\mu\Phi)$ and using the form in Eq. 1.4.9 we get the three and four point gauge-Higgs vertices to be

$$(D_\mu\Phi)^\dagger(D^\mu\Phi) \rightarrow \frac{M_Z^2}{v}Z^\mu Z_\mu h + \frac{M_Z^2}{2v^2}Z^\mu Z_\mu h^2 + \frac{2M_W^2}{v}W^{+\mu}W_\mu^- h + \frac{M_W^2}{v^2}W^{+\mu}W_\mu^- h^2. \quad (1.5.17)$$

Thus for the generic $V_1^\mu V_2^\nu h$ and $V_1^\mu V_2^\nu h^2$ vertices the Vertex factors are,

$$\begin{aligned} V_1^\mu V_2^\nu h &: i \frac{2M_V^2}{v} g_{\mu\nu} \\ V_1^\mu V_2^\nu h^2 &: i \frac{2M_V^2}{v^2} g_{\mu\nu} \end{aligned} \quad (1.5.18)$$

with $g_{\mu\nu}$ being the Minkowski metric, $g_{\mu\nu} = \text{diag}(1, -1, -1, -1)$.

Lastly, the interactions of the fermions with Higgs can be read off from Eqs. 1.4.22 and 1.4.25 to have the form

$$\mathcal{L}_{Yukawa}^{int} = -\frac{m_f}{v} \bar{f} f h \quad (1.5.19)$$

where m_f is the mass of the Dirac fermion f .

Having reviewed the theoretical construct of the SM, in terms of the interactions between the electroweak gauge bosons, fermions and the Higgs, we now take a look at how over the years, various experiments have corroborated the same. This has led to stronger foundations for the SM to be realised as a consistent theory not just at the tree level but also incorporating the quantum effects that come into play as corrections to the tree level predictions.

1.6 Experimental validation of the SM

Theoretical framework of the SM has been tested and verified in a series of experiments spanning over almost five decades involving various international collaborations. These experiments have tested the robustness of the predictions of the SM, not only at the tree level but also incorporating the quantum corrections to the various observables and parameters within the theory. Here we look at some of the high points of this experimental journey.

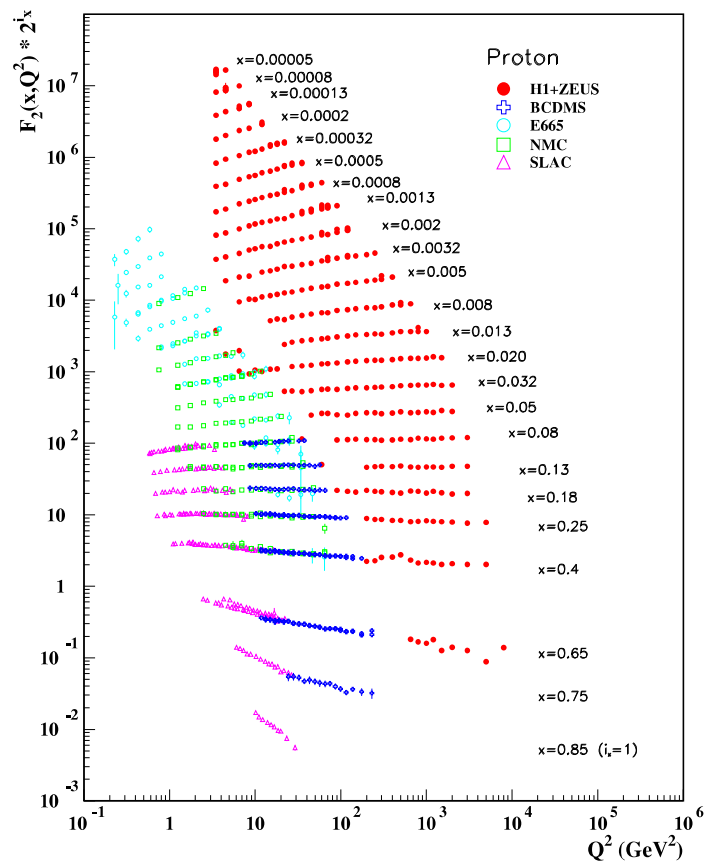


Figure 1.1: The proton structure function F_2 vs Q^2 at fixed x showing scale invariance. The data are from the H1 and ZEUS experiments at the HERA ep collider [19], the muon-scattering experiments BCDMS [20] and NMC [21] at CERN, E665 at FNAL [22] and SLAC [23]. Figure taken from [24].

1.6.1 Deep Inelastic Scattering and the parton model

A series of inelastic scattering experiments were carried out at SLAC around late 1960s, which had high energy electrons bombarding on proton targets [51, 52]. The aim of these experiments was to probe the structure of the target nucleons. The scattering is mediated by a photon or Z boson with a momentum transfer Q^2 accompanied by a energy loss ν carried by the scattered electron. The experiments confirmed that the structure functions associated with the amplitude of such scattering are essentially independent of Q^2 for a fixed value of $x = \frac{Q^2}{2M\nu}$, M being the proton mass. This approximate independence of the form factors associated with deep inelastic scattering (DIS)(Fig. 1.1), known as Bjorken scaling [53] signals towards proton being a composite object made of essentially free constituents (partons) [54, 55]. These and subsequent experiments [56–58] validated the spin-half nature of the constituent partons and also that they carry fractional electrical charges. Moreover, it was also confirmed that the charged partons carried only about 50% of the proton momentum, giving way for the gluons to enter the scene.

1.6.2 Discovery of gluon jets

Gluon was theoretically a strong contender to account for the missing fraction of the momenta other than carried by the electrically charged partons but its direct evidence came from the e^+e^- collisions in the PETRA collider at DESY in 1979 [59–62]. The physics of these collision events involves an e^+e^- pair annihilating into a quark-antiquark pair, with a gluon emitted from the final state quarks even before they hadronise and form collimated jets. These gluons can result into a separately identifiable third jet if there is a large angular separation of the same from the quark-jets. Such three-jet final states served as a strong evidence for the gluon as the missing parton.

1.6.3 Asymptotic freedom of QCD

Quantum Chromodynamics QCD has the essential feature of being asymptotically free [63, 64], which implies that the strong coupling constant becomes smaller (or more perturbative) at large momentum transfers ($\sim \mathcal{O}(100 \text{ GeV} - 1 \text{ TeV})$). A series of experimental measurements of the strong coupling constant at various energy scales have led to a confirmation of the above stated behaviour (Fig. 1.2). These include measurements of $\alpha_S(m_Z)$ from e^+e^- colliders (in particular LEP), from deep inelastic scattering and from the hadron Colliders (Tevatron and LHC) [24, 65].

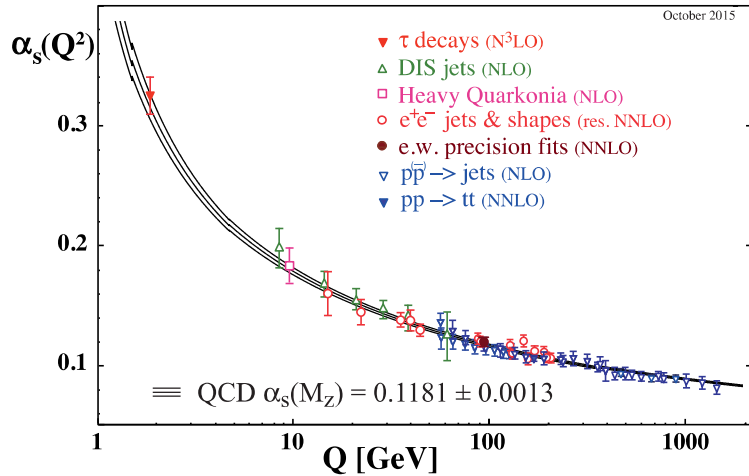


Figure 1.2: Summary of measurements of α_s as a function of the energy scale Q . Figure taken from [24].

The data on the α_s firmly establishes QCD as a perturbative formulation at higher energy scales of the order of a few hundred GeV to 1 TeV.

1.6.4 Neutral currents and the Photon - Z interference

Neutral current (NC) interactions were first experimentally observed at CERN in 1973 in the elastic scattering of ν_μ and $\bar{\nu}_\mu$ from nuclear targets [66, 67]. The reactions involved were of the kind,

$\nu_\mu(\bar{\nu}_\mu) + N \rightarrow \nu_\mu(\bar{\nu}_\mu) + \text{hadrons}$, in addition to the leptonic interactions $\nu_\mu(\bar{\nu}_\mu) + e^- \rightarrow \nu_\mu(\bar{\nu}_\mu) + e^-$ (via scattering off atomic electrons). Thus one could calculate the ratio of the hadronic neutral current interactions to the charged current (CC) ones of the kind,

$$\nu_\mu(\bar{\nu}_\mu) + N \rightarrow \mu^-(\mu^+) + \text{hadrons}$$

and the ratio turned out to be

$$\left(\frac{\text{NC}}{\text{CC}}\right)_\nu = 0.21 \pm 0.03, \quad \left(\frac{\text{NC}}{\text{CC}}\right)_{\bar{\nu}} = 0.45 \pm 0.09$$

In addition to the above data, the observation of a single event in the channel $\bar{\nu}_\mu + e^- \rightarrow \bar{\nu}_\mu + e^-$ confirmed the presence of the weak neutral current. Also, from the hadronic interaction $\sin^2 \theta_W$ was constrained between 0.3 – 0.4 whereas in the leptonic mode due to poor

statistics the constraint was looser, *i.e.* $0.1 < \sin^2 \theta_W < 0.6$ at 90% confidence level.

The effects of such neutral current interactions, noticed first in the deep inelastic scattering of neutrinos, can also be investigated through the interference effects they have on the process like $e^+e^- \rightarrow f\bar{f}$, where f can be a charged lepton or quark. The interference between the vector and the axial vector interactions in such processes can be noticed in the observables constructed via integration of the differential cross section over selected regions of the phase space. Thus one can construct a forward backward asymmetry, non-vanishing value of which is a smoking gun signal of the neutral current interactions of the above kind, where the presence of the Z is essential. One of the earliest measurements of the interference effects between the weak and electromagnetic amplitudes was made in the inelastic scattering of polarized electron beams from unpolarized deuterium target around 1978 at SLAC [68, 69]. Further experiments which made observations to this effect were done at DESY around 1983 involving annihilations of e^+e^- to a pair of muons or τ leptons [70, 71]. These led to an experimental determination of $\sin^2 \theta_W$ in the range $\sin^2 \theta_W = 0.27 \pm 0.08$.

1.6.5 Discovery of W and Z bosons and the top quark

The discovery of the W and Z at the UA-1 and UA-2 experiments at CERN [36–39] was an important step in validating the gauge structure of the GSW model. The masses obtained in these experiments were close to the predictions from the neutrino deep inelastic experiments [72]. For example the W and Z masses from the UA-2 experiment were reported to be, $M_W = 80_{-6}^{+10}$ GeV and $M_Z = 91.9 \pm 1.3 \pm 1.4$ GeV.

In addition to the discovery of the massive gauge bosons, the top quark discovery by the DO and CDF experiments in 1995 [40, 41] completed the validation of the three generation picture of the quark sector of the SM.

1.6.6 Precision tests of the standard model

The work of Veltman and 't Hooft [73, 74] had established SM as a renormalizable QFT. This implied that one could calculate the loop induced corrections to the various tree level observables and all such finite corrections could be matched against the experimental results to test the theory at the quantum level. The precision measurements at Z resonance in the channel $e^+e^- \rightarrow f\bar{f}$ at LEP and SLC [25] led to the determination of the properties of the Z boson, *i.e.* its mass, width, the couplings to fermions etc. with unprecedented accuracy

that allowed for testing of the SM predictions at loop level. For example the mass and width were measured to be,

$M_Z = 91.1875 \pm 0.0021$ GeV, $\Gamma_Z = 2.4952 \pm 0.0023$ GeV. From the contribution of the invisible decay of the Z to its total width, one could restrict the number of neutrino flavors to be,

$N_\nu = 2.9840 \pm 0.0082$, in agreement with the SM.

Thus in addition to the above, a number of other EW observables were measured, eg. forward backward asymmetries, predictions for M_W and M_t etc. These measured values when pitted against the loop corrected calculations within the SM, tested the robustness of the predictability of SM. Fig. 1.3 shows a comparison of the values of the various EW observables compared to their SM best fit values. Note that for the observables involving hadronic final states, QCD corrections play a significant role in such estimates.

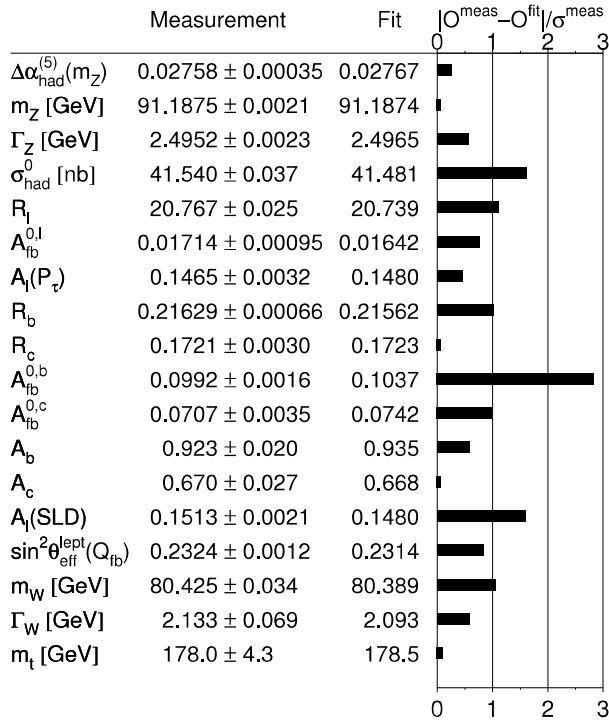


Figure 1.3: Comparison of the measurements with the expectation of the SM for the various EW precision observables. Figure taken from [25].

Departures from the standard model behaviour can be probed quite effectively in the so-called oblique electroweak observables or the Peskin-Takeuchi parameters [75]. They are functions of the corrections to the gauge boson two point functions and are given as [76],

$$\begin{aligned}
T &= \frac{1}{\alpha_e} \left(\frac{\Pi_{WW}^{\text{new}}(0)}{M_W^2} - \frac{\Pi_{ZZ}^{\text{new}}(0)}{M_Z^2} \right) = \frac{\rho - 1}{\alpha_e}, \\
S &= \frac{4c_W^2 s_W^2}{\alpha_e} \left[\frac{\Pi_{ZZ}^{\text{new}}(M_Z^2) - \Pi_{ZZ}^{\text{new}}(0)}{M_Z^2} - \frac{c_W^2 - s_W^2}{c_W s_W} \frac{\Pi_{\gamma Z}^{\text{new}}(M_Z^2)}{M_Z^2} - \frac{\Pi_{\gamma\gamma}^{\text{new}}(M_Z^2)}{M_Z^2} \right], \\
U &= \frac{4s_W^2}{\alpha_e} \left[\frac{\Pi_{WW}^{\text{new}}(M_Z^2) - \Pi_{WW}^{\text{new}}(0)}{M_W^2} - \frac{c_W}{s_W} \frac{\Pi_{\gamma Z}^{\text{new}}(M_Z^2)}{M_Z^2} - \frac{\Pi_{\gamma\gamma}^{\text{new}}(M_Z^2)}{M_Z^2} \right] - S \quad (1.6.1)
\end{aligned}$$

with $\alpha_e = \alpha_e(M_Z)$. The superscript “new“ stands for the fact that S , T and U are defined after subtracting out the SM contribution. Thus in all such cases where new physics can potentially give contributions to the gauge boson two point functions, experimental bounds on the oblique parameters would be pivotal in constraining the corresponding parameter spaces. Current experimental values of these are [24]: $S = 0.03 \pm 0.10$, $T = 0.01 \pm 0.12$, $U = 0.05 \pm 0.10$. The parameters S and T are able to provide constraints on the new physics beyond the SM. S gets contributions from a new generation of fermions and T being equivalent to ρ signifies the extent of isospin violation *i.e.* the mass splitting between the members of the new doublet. As an example, the Technicolor theories became strongly disfavoured as the contributions to the S parameter were in conflict with the experimental data [76]. Similarly, the existence of additional sequential fermion families have been constrained by the precision observables.

1.6.7 Higgs discovery

The discovery of the Higgs boson at CERN in 2012 [1, 2] with a mass in the range 125-126 GeV was a much awaited moment as it cleared a lot of dust on the mass generation mechanism in the SM. With this discovery, the spontaneous symmetry breaking mechanism got singled out as the one responsible for generating masses of the weak gauge bosons and the fermions.

The discovery of the Higgs has been followed up by a series of investigations into the CP properties of the scalar and its couplings to the fermions and gauge bosons. The purpose of such studies has been to get a better and detailed understanding of the electroweak symmetry

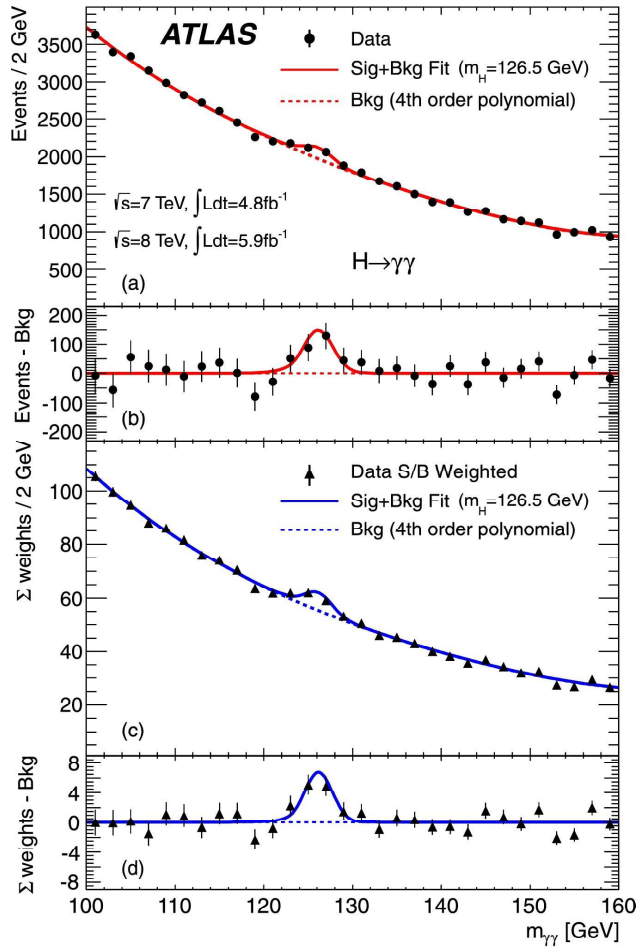


Figure 1.4: Observation of Higgs as a bump in the invariant mass distribution of the diphoton system in the $h \rightarrow \gamma\gamma$ channel at ATLAS detector at CERN. Figure taken from [1] where the 125 GeV scalar has been denoted as “H” .

breaking mechanism and also seek any lurking hints on the physics beyond the SM. We will have more to say on this in the following chapter.

Chapter 2

The Quest for New Physics

2.1 Why Beyond the Standard Model ?

The standard model (SM) over decades has successfully stood against experimental scrutiny and its predictions have been verified by the data collected from various experiments. This has resulted in increased faith in the predictive power of the theory even at the quantum level. With the discovery of the Higgs in 2012 [1,2] the missing link was discovered explaining particle masses in terms of spontaneous symmetry breaking mechanism. With all these experimental successes in sight, SM seems to be a consistent framework, working well within the ambit of present-day experimental precision.

However, there still are a lot of questions from a theoretical and experimental point of view which SM fails to answer. These issues motivate one to search for scenarios beyond the standard model (BSM) which have SM as their low energy limit in the electroweak scale.

2.1.1 Theoretical motivations for BSM

- **Lack of unification:** Although SM incorporates the strong, weak and electromagnetic forces in a gauge invariant framework, the theory has three different coupling constants g_s , g and g' which seem to have no common origin. SM has no way to embed these three different couplings into the gauge-invariant description of a bigger symmetry group with a single coupling constant i.e. a Grand Unified Theory (GUT) [77–80]. In other words, assuming only SM dynamics, the renormalization group running of these couplings does not lead them to converge at a higher scale (GUT scale), where one could have hoped for a unification [81–85]. In addition, SM still is incapable of incorporating

gravity in a renormalizable framework with the other fundamental forces. This is an obvious statement of its shortcoming as a unified theory if one seeks a description all the way up to the Planck scale *i.e.* $M_{pl} \sim 10^{19}$ GeV, where quantum effects of gravity become relevant.

- **The naturalness or fine tuning problem :** When one computes loop corrections to mass squared of the Higgs, one is confronted with the problem of quadratic sensitivity to the masses of the heavier scales [86, 87]. This drives the corrections away from the observed scale of ~ 125 GeV towards the heavier scales in the problem. Thus if one assumes SM to have a cut-off at scale Λ , the corrections to M_h^2 scale as,

$$\delta M_h^2 \propto \Lambda^2$$

To tame the corrections to the order of the electroweak scale then one requires a delicate cancellation or fine tuning among the parameters involved. This is known as the fine tuning problem. It is evident that higher the mass scales entering in the loop correction, more acute is the fine tuning required. Moreover, one has to fine-tune parameters at every perturbative order. The desirability of avoiding such fine tuned cancellations is one of the reasons towards motivating new physics to arrive at TeV scale. One has to further ensure that the new physics introduced does not lead to further divergent contributions. Supersymmetry, or boson-fermion symmetry, is an elegant solution to the fine tuning problem. It helps in controlling the scalar mass corrections via exact cancellations between the quadratically divergent bosonic and fermionic contributions to the loops [88].

- **Strong CP problem :** The gauge sector of the SM lagrangian allows for the inclusion of a CP and P violating term of the form,

$$\mathcal{L}_\theta = \bar{\theta} \varepsilon^{\mu\nu\alpha\beta} F_{\mu\nu}^a F_{\alpha\beta}^a \quad (2.1.1)$$

where $\bar{\theta}$ is known as the strong CP phase. One of the most problematic consequences of this is an unacceptably large contribution to the neutron electric dipole moment (EDM).

The current experiments [89] put an upper limit on the magnitude of the neutron EDM at,

$$|d_n| < 2.9 \times 10^{-26} e \text{ cm (90\% C.L.)}.$$

From this, $\bar{\theta}$ is constrained to be, $\bar{\theta} < 10^{-10}$ [90,91]. However there is no symmetry in the SM which forces $\bar{\theta}$ to be so tightly constrained. This smallness of $\bar{\theta}$ is known as the strong CP problem.

Apart from these theoretical considerations, there are experimental observations which hint towards fundamental physics beyond the SM.

2.1.2 Experimental hints towards BSM

- **Neutrino masses and mixing:** The experimental evidence of neutrino oscillations points towards neutrinos being massive [24,92,93]. Various experiments have measured the parameters that determine the mixing between the flavor states and the mass splittings amongst the physical states in the mass diagonal basis. Mixing requires non-degenerate masses for three sequential neutrinos. However, within SM the absence of a right handed partner does not allow the existence of a dirac mass term for the neutrinos. On the other hand, $\Delta L = 2$ Majorana masses, too, are not forbidden by any fundamental consideration, but will take one beyond the SM. There are scenarios like $SO(10)$ GUTs [94,95] and left-right symmetric models [96] incorporating heavy sterile neutrinos, where one can give mass to the light neutrinos using the seesaw mechanism.
- **Hierarchy of fermion masses and mixings :** The masses of fermions in SM range from $\mathcal{O}(10^{-3})$ GeV for electrons to $\mathcal{O}(100)$ GeV for the top quark. Also for the quarks and leptons we see a successive gradation in the masses of the three generations. Apart from the masses, within the quark sector, the CKM matrix reveals a nearly diagonal structure, with the magnitudes of the in-family CKM elements being close to 1, and the off-diagonal ones being only significant for the first two quark families. There is no inherent explanation in SM for this hierarchy of masses and the CKM mixings.
- **No dark matter candidate :** From the data on the rotation curves of the galaxies, first set of evidence was collected towards the presence of a non-interacting “dark” matter in and around the visible matter in the galaxies [97–99]. The data collected from Planck [100] and WMAP [101] suggest that cold dark matter constitutes about 23% of the matter content in the universe. SM has no such dark matter candidate within its particle spectrum.
- **Matter-antimatter asymmetry :** The present universe seems to be comprised es-

entially of matter. The net baryon asymmetry is given by the ratio [101],

$$\eta_B = \frac{n_B - n_{\bar{B}}}{n_\gamma} \sim 6 \times 10^{-10} \quad (2.1.2)$$

where n_B and $n_{\bar{B}}$ are the baryon and anti-baryon number densities and n_γ is the photon number density. There are three necessary conditions for successful baryogenesis, given by Sakharov [102]: I) baryon number violation, II) C and CP -violation and III) a deviation from thermal equilibrium. SM and cosmology in principle fulfill all three Sakharov conditions [103, 104], but the magnitude of CP -violation in SM, contributed by the complex phase of the CKM matrix [50] is not sufficient to generate the observed baryon asymmetry. Thus one needs to go beyond the SM to answer for the observed matter-antimatter asymmetry.

- **Muon $g-2$ discrepancy** : The experimental determination of the anomalous magnetic moment of the muon reveals a $\sim 3\sigma$ level of discrepancy from the SM estimate of the same [24, 105, 106], *i.e.*,

$$\Delta a_\mu = a_\mu^{exp} - a_\mu^{SM} = 268(63)(43) \times 10^{11} \quad (2.1.3)$$

where the errors from experiment and theory are combined in quadrature. This has invited attention towards possible new physics scenarios which may give additive loop contributions to the muon $g - 2$ and answer for the discrepancy. For example SUSY particles in the loops [107] or a light pseudoscalar in leptophilic two-Higgs doublet models (L2HDM) [16] are some of the plausible candidates.

The above observations provide a compelling argument in favor of new physics beyond the SM framework. In the rest of this thesis we will indicate how the discovery of the Higgs boson at the LHC has triggered investigations on possible traces of new physics in the newly available data. Such investigations have led to better insights into the possible new physics scenarios and regions in the corresponding parameter spaces that qualify as potential solutions to the problems of the SM.

2.2 Hunting new physics at LHC

As everybody knows, the Large Hadron Collider (LHC) is yet to unravel any signal for new physics. However, what looks very similar to the SM Higgs boson has been discovered. This has given impetus to new physics searches using the discovered scalar as a probe, through attempts to answer the question: “Is it the Higgs or a Higgs?” Since the discovery of the Higgs boson at the LHC, the ATLAS and CMS experiments have embarked upon a dedicated program to further investigate the CP properties of the Higgs and its couplings to the other SM particles. These efforts can improve our understanding of spontaneous symmetry breaking and also narrow down new physics scenarios. In what follows we discuss the various production and decay modes of the Higgs and how the data on the same has led to insights on the possible signatures of new physics.

2.2.1 Higgs production at the LHC :

The main Higgs production channels at the LHC are the following [24, 108] (Fig. 2.1):

- Gluon fusion (ggF) : $gg \rightarrow h + X$
- Vector Boson Fusion (VBF) : $q\bar{q} \rightarrow q\bar{q}h$, yielding a pair of forward jets.
- Associated production with a gauge boson (Z, W) : $q\bar{q} \rightarrow Vh$
- Associated production with a top-antitop pair ($t\bar{t}h$): $gg \rightarrow t\bar{t}h$

The scattering cross section for the scattering of two hadrons (protons) A and B to a given final state Y can be written as a sum over the sub-process cross sections from the constituent partons:

$$\sigma(AB \rightarrow YX) = \sum_{a,b} \int dx_a dx_b f_{a/A}(x_a, Q^2) f_{b/B}(x_b, Q^2) \hat{\sigma}(ab \rightarrow Y) \quad (2.2.1)$$

where x_a and x_b are the momentum fraction of the constituent partons a and b in the protons A and B. The functions $f_{a/A}(x_a, Q^2)$ and $f_{b/B}(x_b, Q^2)$ are the parton distribution functions corresponding to a and b partons. The scale Q^2 is the factorization scale of the parton-level hard scattering process. The cross section for this can be calculated perturbatively in QCD, while the parton distribution functions parameterize the non-perturbative part.

The dominant production mode is ggF, followed by VBF, associated Vh production and then the $t\bar{t}h$ mode. Table 2.1 lists the SM cross sections for the various production channels

at various collision energies of the proton-proton scattering. Fig. 2.2 shows the same for a 125 GeV Higgs. Gluon fusion is the dominant mode of production despite being a loop induced process as Fig. 2.1 (a) shows. This is because of the large gluon flux at low momentum fraction of the proton momentum (Fig. 2.3).

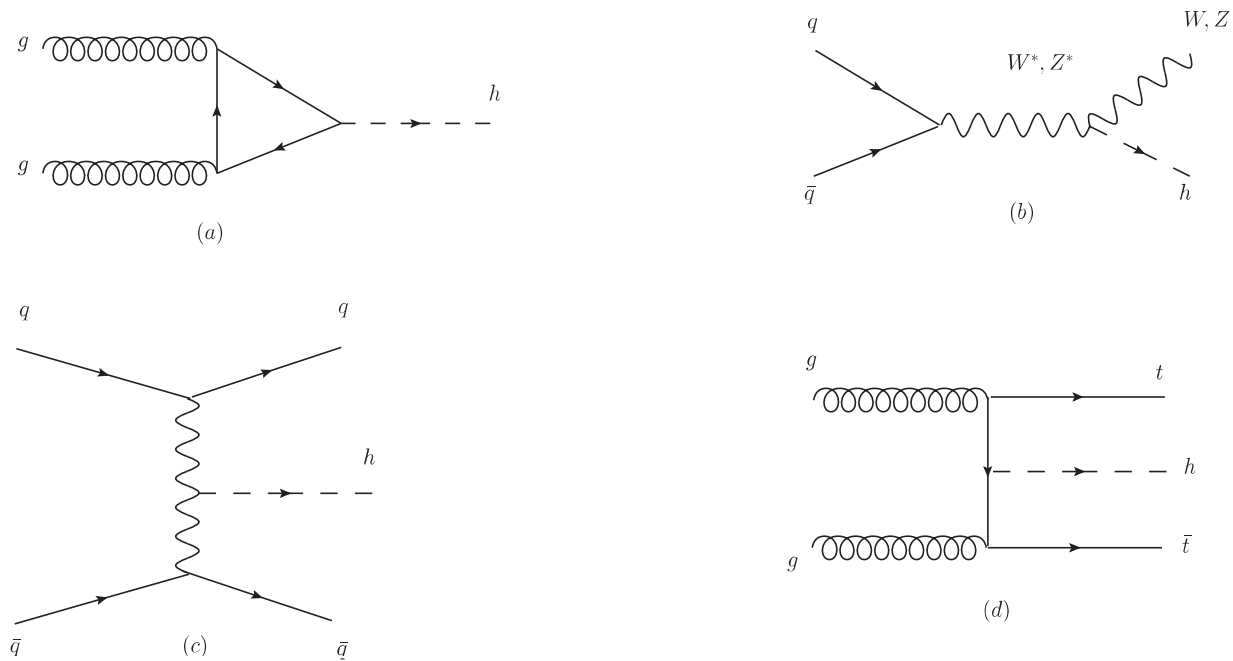


Figure 2.1: Higgs production channels: (a) Gluon fusion, (b) Associated Higgs production, (c) Vector Boson Fusion (VBF) and (d) Associated top quark production.

\sqrt{s} (TeV)	Higgs Production cross section (pb) $M_h = 125$ GeV				
	ggF	VBF	Wh	Zh	$t\bar{t}h$
7	$15.3^{+10\%}_{-10\%}$	$1.24^{+2\%}_{-2\%}$	$0.58^{+3\%}_{-3\%}$	$0.34^{+4\%}_{-4\%}$	$0.09^{+8\%}_{-14\%}$
8	$19.5^{+10\%}_{-11\%}$	$1.60^{+2\%}_{-2\%}$	$0.70^{+3\%}_{-3\%}$	$0.42^{+5\%}_{-5\%}$	$0.13^{+8\%}_{-13\%}$
13	$44.1^{+11\%}_{-11\%}$	$3.78^{+2\%}_{-2\%}$	$1.37^{+2\%}_{-2\%}$	$0.88^{+5\%}_{-5\%}$	$0.51^{+9\%}_{-13\%}$
14	$49.7^{+11\%}_{-11\%}$	$4.28^{+2\%}_{-2\%}$	$1.51^{+2\%}_{-2\%}$	$0.99^{+5\%}_{-5\%}$	$0.61^{+9\%}_{-13\%}$

Table 2.1: Higgs production cross section at LHC at various collision energies (\sqrt{s}). The numbers are from [24].

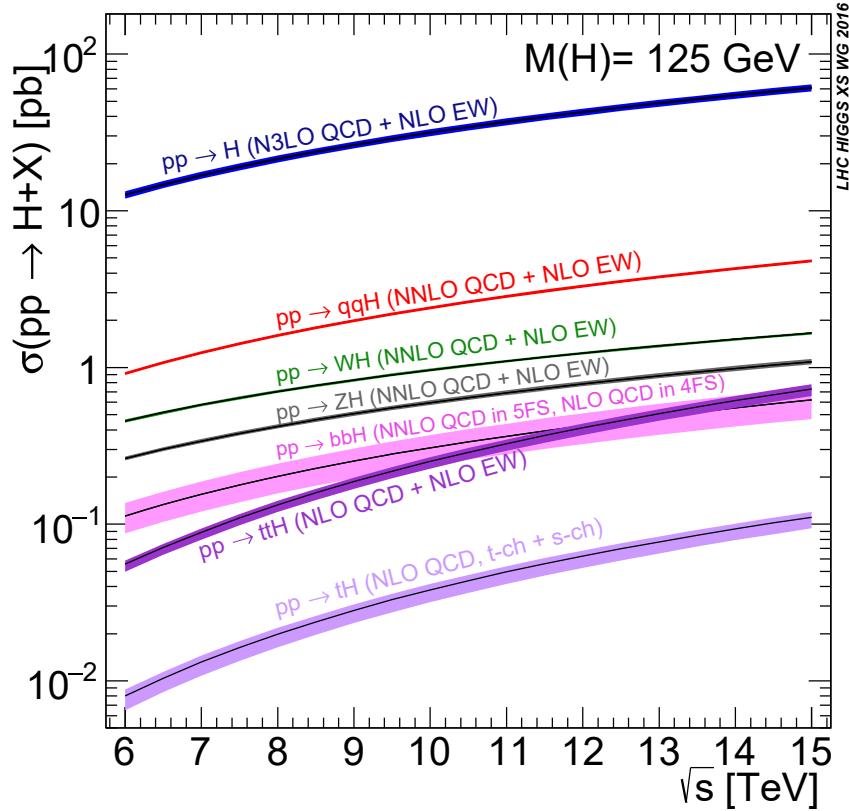


Figure 2.2: Higgs production cross section vs. \sqrt{s} for $M_h = 125$ GeV. Figure taken from [24] where the 125 GeV scalar has been denoted as “H”.

2.2.2 Higgs Decay Channels:

The dominant decay modes are $h \rightarrow b\bar{b}$ and $h \rightarrow WW$, followed by $h \rightarrow gg$, $h \rightarrow \tau^+\tau^-$, $h \rightarrow c\bar{c}$ and $h \rightarrow ZZ^*$. Because of loop suppression, Higgs decays into $h \rightarrow \gamma\gamma$, $h \rightarrow \gamma Z$ with much smaller rates. This is followed by $h \rightarrow \mu^+\mu^-$ owing to the small Yukawa coupling because of the small μ mass. Since the decays into gluons, diphotons and γZ modes are loop induced, they can provide information on the Higgs couplings to WW , ZZ and $t\bar{t}$ which enter into the loops for the above decays. Table 2.2 lists the branching ratios (BRs) for the SM 125 GeV Higgs into various final states. The variation of the Higgs BR with Higgs mass is shown in Fig 2.4. The total width of a 125 GeV SM Higgs boson is $\Gamma_h = 4.07 \times 10^3$ GeV, with a relative uncertainty of $^{+4.0\%}_{-3.9\%}$. The $h \rightarrow \gamma\gamma$ and $h \rightarrow ZZ^* \rightarrow 4\ell$ channels, even with their modest BRs have the advantage that the final state particles can be precisely reconstructed with an excellent mass resolution of 1 – 2%. It is because of this reason that these two final states were very crucial to the Higgs discovery [24]. For the $h \rightarrow W^+W^- \rightarrow \ell^+\nu_\ell\ell'^-\bar{\nu}_{\ell'}$

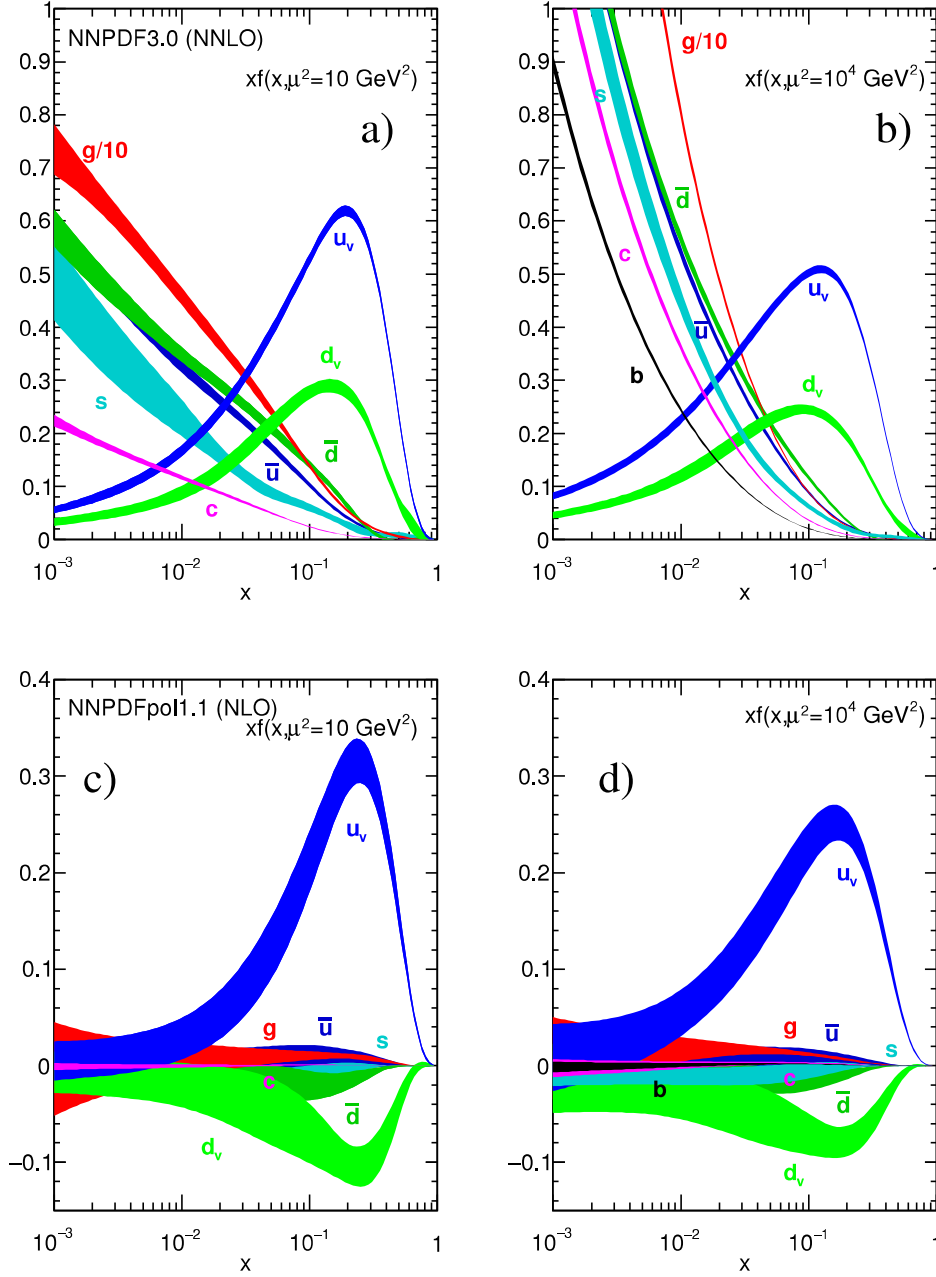


Figure 2.3: Unpolarized parton distribution functions obtained in NNLO NNPDF3.0 global analysis [26] at scales $\mu^2 = 10 \text{ GeV}^2$ (left) and $\mu^2 = 10^4 \text{ GeV}^2$ (right), with $\alpha_S(M_Z^2) = 0.118$. The corresponding polarized parton distributions are shown (c,d), obtained in NLO with NNPDFpol1.1 [27]. Figure taken from [24].

the mass resolution is poor owing to the presence of neutrinos in the final state. The $h \rightarrow b\bar{b}$ and the $h \rightarrow \tau^+\tau^-$ channels have to compete against large backgrounds and a rather poor

mass resolution of 10 – 15%.

Table 2.2: The branching ratios and the relative uncertainty for a 125 GeV SM Higgs boson.

Numbers are taken from [24].

Decay mode	Branching Ratio	Relative Uncertainty
$h \rightarrow \gamma\gamma$	2.27×10^{-3}	+5.0% -4.9%
$h \rightarrow ZZ^*$	2.62×10^{-2}	+4.3% -4.1%
$h \rightarrow WW^*$	2.14×10^{-1}	+4.3% -4.2%
$h \rightarrow \tau^+\tau^-$	6.27×10^{-2}	+5.7% -5.7%
$h \rightarrow b\bar{b}$	5.84×10^{-1}	+3.2% -3.3%
$h \rightarrow \gamma Z$	1.53×10^{-3}	+9.0% -8.9%
$h \rightarrow \mu^+\mu^-$	2.18×10^{-4}	+6.0% -5.9%

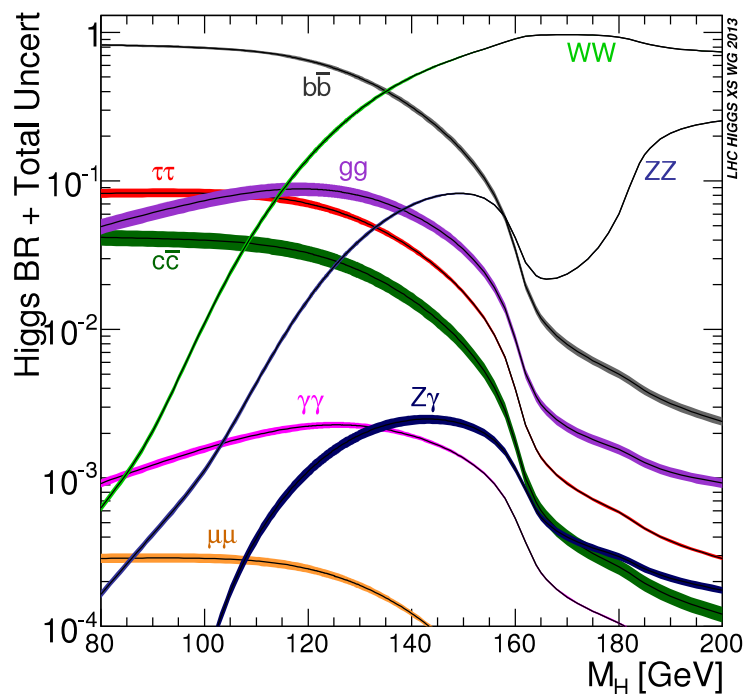


Figure 2.4: Higgs BR as a function of Higgs mass. Figure is taken from [24].

	$\gamma\gamma$	ZZ^*	WW^*	$\tau^+\tau^-$	$b\bar{b}$
ggF	$1.10^{+0.23}_{-0.22}$	$1.13^{+0.34}_{-0.31}$	$0.84^{+0.17}_{-0.17}$	$1.0^{+0.6}_{-0.6}$	—
VBF	$1.3^{+0.5}_{-0.5}$	$0.1^{+1.1}_{-0.6}$	$1.2^{+0.4}_{-0.4}$	$1.3^{+0.4}_{-0.4}$	—
Wh	$0.5^{+1.3}_{-1.2}$	—	$1.6^{+1.2}_{-1.0}$	$-1.4^{+1.4}_{-1.4}$	$1.0^{+0.5}_{-0.5}$
Zh	$0.5^{+3.0}_{-2.5}$	—	$5.9^{+2.6}_{-2.2}$	$2.2^{+2.2}_{-1.8}$	$0.4^{+0.4}_{-0.4}$
$t\bar{t}h$	$2.2^{+1.6}_{-1.3}$	—	$5.0^{+1.8}_{-1.7}$	$1.9^{+3.7}_{-3.3}$	$1.1^{+1.0}_{-1.0}$

Table 2.3: Best fit values of μ_{if} for each specific channel $i \rightarrow h \rightarrow f$, using the combined ATLAS and CMS data for $\sqrt{s} = 7$ and 8 TeV. The results are shown together with their total uncertainties (statistical and systematic combined). The entries labelled with a “—” are either not measured with a meaningful precision and therefore not quoted (for $h \rightarrow ZZ^*$ decay channel for the Wh , Zh , and $t\bar{t}h$ production modes), or not measured at all and therefore fixed to their corresponding SM predictions ($h \rightarrow b\bar{b}$ decay mode for the ggF and VBF production processes).

2.2.3 Signal strength measurements at LHC

Given the values of the production cross section and branching ratios of the Higgs within the SM, the data collected by the ATLAS and CMS experiments in various production and decay channels can be used to quantify the deviations from the SM expectations. One such measure is the signal strength ratio defined for a channel $i \rightarrow h \rightarrow f$ by

$$\mu_{if} = \frac{\sigma(i \rightarrow h) \times \text{BR}(h \rightarrow f)}{\sigma_{\text{SM}}(i \rightarrow h) \times \text{BR}_{\text{SM}}(h \rightarrow f)} \quad (2.2.2)$$

where $\sigma(i \rightarrow h)$ is the production cross section for Higgs in the i^{th} channel ($i = \text{ggF}, \text{VBF}, Wh, Zh, t\bar{t}h$) and $\text{BR}(h \rightarrow f)$ is the branching ratio for Higgs to final state f ($f = ZZ^*, WW^*, \tau^+\tau^-, \gamma\gamma, b\bar{b}$). The denominator is the product of the corresponding quantities in SM. Table 2.3 lists the signal strengths (also shown in Fig.2.5) for the various production and decay channels corresponding to the combined ATLAS and CMS data for $\sqrt{s} = 7$ and 8 TeV [28].

One can also fit the signal strength data by assuming that there is no new physics in the Higgs decay, *i.e.* $\frac{\text{BR}(h \rightarrow f)}{\text{BR}_{\text{SM}}(h \rightarrow f)} = 1$. This can then be interpreted as the limits on the ratio

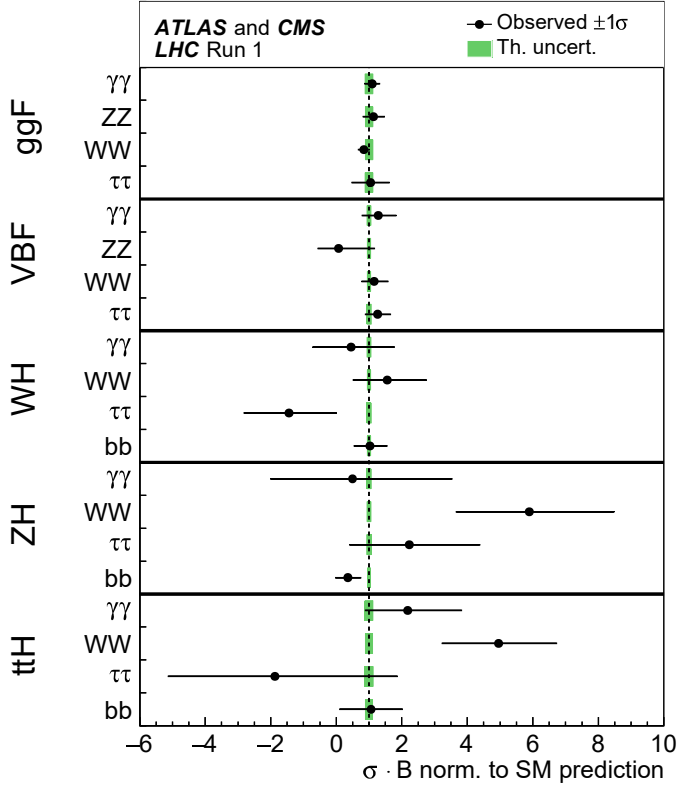


Figure 2.5: Signal strengths corresponding to the channels in Table 2.3. The error bars indicate the 1σ intervals. The green bands indicate the theoretical uncertainties in the SM predictions. Figure is taken from [28] where 125 GeV scalar is denoted as “H”.

$\mu_i = \frac{\sigma(i \rightarrow h)}{\sigma_{\text{SM}}(i \rightarrow h)}$ from the signal strength measurements. Fig. 2.6 lists the signal strengths for the five main Higgs production channels *i.e.*, μ_{ggF} , μ_{VBF} , μ_{Wh} , μ_{Zh} and μ_{tth} .

A similar approach towards the Higgs decay allows one to establish limits on the ratio

$\mu_f = \frac{\text{BR}(h \rightarrow f)}{\text{BR}_{\text{SM}}(h \rightarrow f)}$ assuming there is no new physics in the Higgs production channels. Fig. 2.7 lists the signal strengths corresponding to the five Higgs decay modes, $\mu_{\gamma\gamma}$, μ_{ZZ^*} , μ_{WW^*} , $\mu_{\tau^+\tau^-}$ and μ_{bb} .

The above data on the signal strength measurements can be translated into limits on the deviations of the Higgs couplings to SM particles from their SM values. To this end, one can at first go assume that the new physics is such that the couplings are modified only by a constant scaling and no modification is introduced to their Lorentz structure. In the following subsection we discuss how these constraints look like for the case when

- One assumes that there is no new decay mode coming from the new physics, *i.e.*

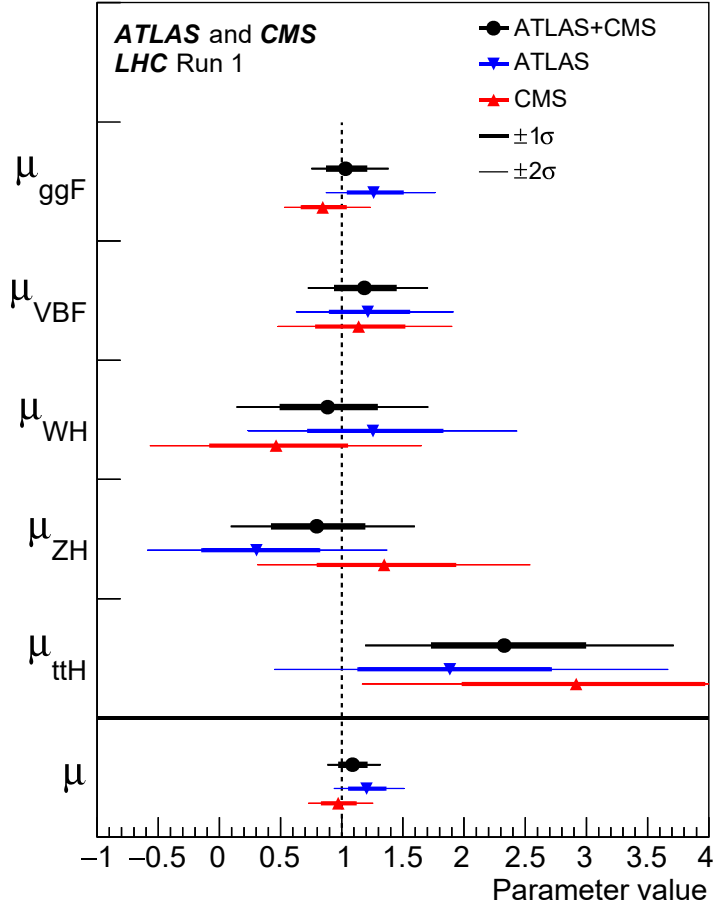


Figure 2.6: Best fit results for the production signal strengths for the combined ATLAS and CMS data. Results from both experiments are also shown separately. The error bars correspond to 1σ (thick lines) and 2σ (thin lines) intervals. Figure is taken from [28].

$$\text{BR}_{\text{BSM}} = 0.$$

- One allows for $\text{BR}_{\text{BSM}} \geq 0$.

2.2.4 New physics in scaled Higgs couplings

For a given Higgs production or decay channel denoted by “ i ”, a scaling factor or coupling modifier corresponding to that channel is given by [28]

$$\kappa_i^2 = \frac{\sigma_i}{\sigma_i^{\text{SM}}} \text{ (production) or } \kappa_i^2 = \frac{\Gamma_i}{\Gamma_i^{\text{SM}}} \text{ (decay)}. \quad (2.2.3)$$

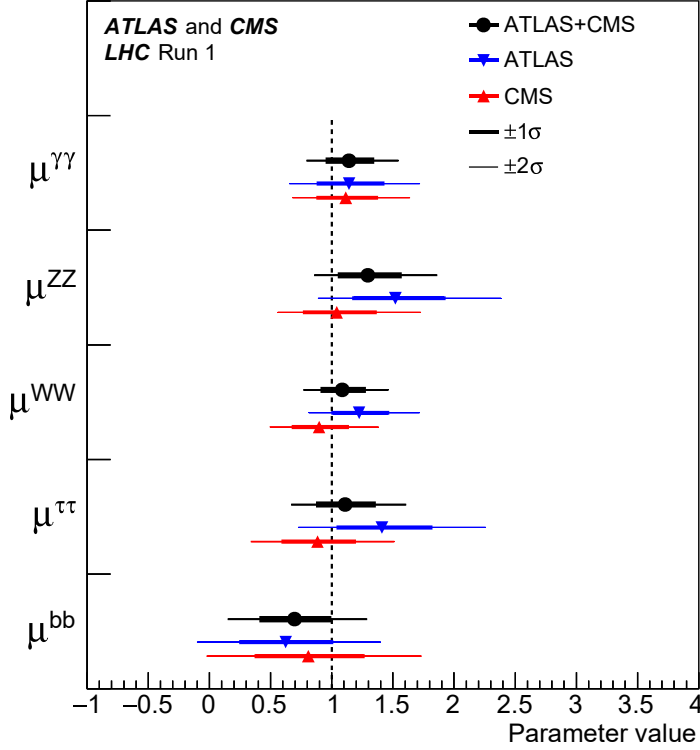


Figure 2.7: Best fit results for the signal strengths in Higgs decay channels for the combined ATLAS and CMS data. Results from both experiments are also shown separately. The error bars correspond to 1σ (thick lines) and 2σ (thin lines) intervals. Figure is taken from [28].

These coupling modifiers are basically associated with the scaling of the SM Higgs couplings to the SM gauge bosons or fermions. Thus we have κ_W , κ_Z , κ_t , κ_b , and κ_τ at tree level corresponding to the WWh , ZZh , $t\bar{t}h$, $b\bar{b}h$ and $h\tau\tau$ couplings. Since the Run-I LHC data are insensitive to the coupling modifiers κ_c and κ_s , and have limited sensitivity to κ_μ , it is assumed that κ_c varies as κ_t , κ_s as κ_b , and κ_μ as κ_τ . Other coupling modifiers (κ_u , κ_d , and κ_e) are irrelevant provided they are of order unity. Apart from the tree level scalings of the Higgs interactions we also have two effective coupling modifiers, κ_g and κ_γ , corresponding to the loop induced hgg and $h\gamma\gamma$ couplings. This is under the assumption that BSM particles that might contribute to these effective couplings are not expected to significantly modify the kinematics of the corresponding processes involving these vertices. Thus the $gg \rightarrow h$ production and $h \rightarrow \gamma\gamma$ decay can be studied, either through these effective coupling modifiers, or through the coupling modifiers corresponding to the SM particles that enter into these loops.

The above scaling of the Higgs couplings will result in a variation of the Higgs boson

width. Thus we define the scaling of the overall Higgs width as

$$\kappa_h^2 = \sum_i \text{BR}_i^{\text{SM}} \kappa_i^2 \quad (2.2.4)$$

When only the SM decay modes of the Higgs boson are allowed ($\text{BR}_{\text{BSM}} = 0$), we have $\kappa_h^2 = \frac{\Gamma_h^{\text{SM}}}{\Gamma_h}$. If instead deviations from the SM are introduced in the decays ($\text{BR}_{\text{BSM}} \geq 0$), the modified Higgs width Γ_h becomes

$$\Gamma_h = \frac{\kappa_h^2 \Gamma_h^{\text{SM}}}{1 - \text{BR}_{\text{BSM}}} \quad (2.2.5)$$

where BR_{BSM} is the total branching fraction into BSM decays. Such BSM decays can be of three types:

- Decays into BSM particles that go undetected because of their feeble interactions with ordinary matter.
- Decays into BSM particles that go undetected because they are associated with the final states that are not searched for.
- Decays involving modification of the branching fractions into SM particles in decay channels that are not directly measured, such as $h \rightarrow c\bar{c}$.

Fig. 2.8 shows the fits to the scaling factors κ_W , κ_Z , κ_t , κ_b , κ_τ , κ_g and κ_γ assuming either $|\kappa_V| \leq 1$ ($V = W, Z$) and $\text{BR}_{\text{BSM}} \geq 0$ or $\text{BR}_{\text{BSM}} = 0$. In the former case, an upper limit of $\text{BR}_{\text{BSM}} = 0.34$ at 95% CL is obtained, compared to an expected upper limit of 0.39. For details see [28].

2.2.5 New physics in modified Lorentz structure of Higgs couplings

Other than the possibility of Higgs couplings being modified by just constant scaling of the couplings, one can also consider the case where new physics can invite modification to the Lorentz structure of the Higgs couplings. In the previous case the total rates of production and decay channels can differ from their SM counterparts, but the kinematic properties of the Higgs boson in each channel are unchanged. But when new Lorentz structures are allowed, this can lead to modified kinematics which can be probed in the differential distributions

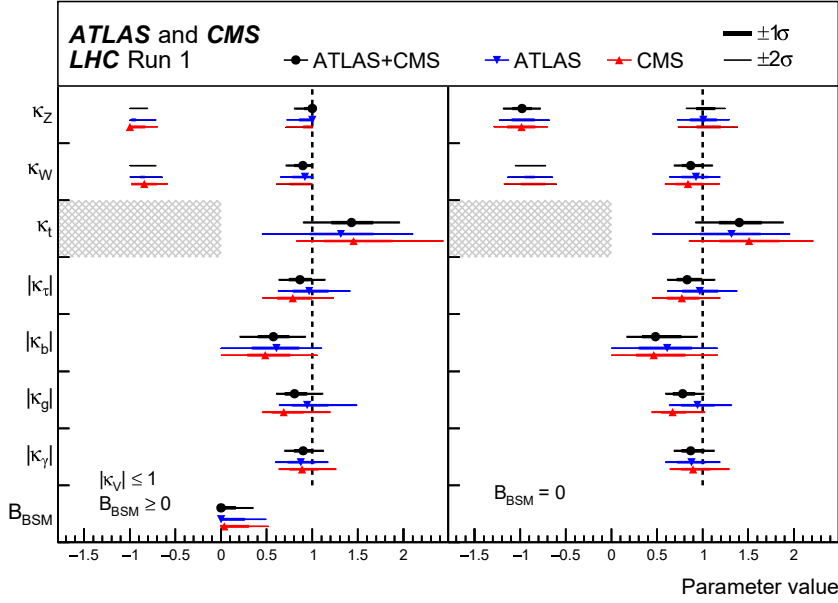


Figure 2.8: Fits for the coupling modifiers for the two cases: (a) Where we consider $\text{BR}_{\text{BSM}} \geq 0$ and $|\kappa_V| \leq 1$ ($V = W, Z$), and (b) With $\text{BR}_{\text{BSM}} = 0$. Combined as well as individual results of ATLAS and CMS are shown along with their uncertainties. The hatched areas show the non-allowed regions for the κ_t parameter, assumed to be positive without loss of generality. The error bars indicate the 1σ (thick lines) and 2σ (thin lines) intervals. For parameters with no sensitivity to the sign, only the absolute values are shown. Figure is taken from [28].

of the various kinematic observables constructed out of the spin-momenta of the particles involved in a given production and decay channel.

The second possibility has been investigated by the ATLAS collaboration [109] in a model-independent framework using effective field theory (EFT) approach [3, 12, 108, 110–112], whereby the SM Lagrangian is modified by addition of CP-even and CP-odd gauge-invariant operators of dimension six. The $SU(2) \times U(1)$ gauge-invariance is postulated because these operators are obtained by integrating out physics above the scale of electroweak symmetry breaking. These result in new tensor structures for the interactions between the Higgs boson and the SM particles, which lead to modified Higgs boson kinematic distributions as well as those of the associated jets. The presence of higher dimension operators [3, 12, 108, 110–112]

leads to gauge-Higgs couplings with a generic tensor structure of the form

$$\mathcal{L}_{VVh} = \frac{2}{v} [aM_V^2 g_{\mu\nu} + b(k_1^\nu k_2^\mu - g^{\mu\nu} k_1 \cdot k_2) + \tilde{b} \epsilon_{\mu\nu\alpha\beta} k_1^\alpha k_2^\beta] V^\mu(k_1) V^\nu(k_2) h(k) \quad (2.2.6)$$

where the ‘ a ’ term is just the scaling of the Higgs coupling, ‘ b ’ term is contributed by the higher dimension CP-even operators and the ‘ \tilde{b} ’ term arises out of CP-odd operators. Similarly for the Yukawa couplings, we have an admixture of the CP-even and odd terms in the form

$$\mathcal{L}_{f\bar{f}h} = \bar{f}(c + id\gamma_5)fh \quad (2.2.7)$$

Here ‘ c ’ is the scaling of the SM Yukawa coupling and ‘ d ’ term is the CP-odd contribution. From the data on the Higgs decays to diboson final states the pure CP-odd resonance has been ruled out at 99.98% CL [113] but an admixture of CP-even and odd states still is allowed with a dominant CP-even component. We will explore the above mentioned higher dimension operators and their effects on the kinematics of the various production and decay channels in further detail in the following chapters.

Chapter 3

Higher Dimensional Operators: The Gauge-Higgs Story

3.1 Introduction

As we have already mentioned, although the discovery of “a Higgs-like boson” at the Large Hadron Collider (LHC) has been a refreshing development [1, 2], there is no clear signal yet for physics beyond the standard model (SM). It is therefore natural that physicists are trying to wring the last drop out of the Higgs sector itself, in attempts to read fingerprints of new physics.

One approach to that end is to examine all available data in terms of specific new models, such as supersymmetry or just additional Higgs doublets. In the other approach, one can take a model-independent stance, parametrize possible modifications of the interaction terms of the Higgs with pairs of SM particles, and examine them in the light of the available data. Such modifications can again be of two types. In the first category, they are just multiplicative modifications of the coupling strengths, the Lorentz structures remaining the same as in the SM. Constraints on such modifications have already been derived from the available Higgs data [28, 114–118]. In the second class, one considers additional operators with new Lorentz structures satisfying all symmetries of the SM [3, 12, 112, 119–122]. Gauge-invariance of such operators in their original forms may be expected, since they are obtained by integrating out new physics that arises at scales higher than the electroweak scale. Sets of such higher-dimensional operators contributing to the effective coupling of the Higgs to, say a pair of electroweak vector bosons have been studied extensively. Here it makes sense to include

only $SU(2) \times U(1)$ invariant operators in one's list to start with, because the yet unknown new physics lies at least a little above the electroweak symmetry breaking scale. With the inclusion of such higher-dimensional operators the effective Lagrangian at the electroweak scale can be given as

$$\mathcal{L}_{eff} = \mathcal{L}_{SM} + \sum_{d,n} \frac{f_n^{(d)}}{\Lambda^{d-4}} \mathcal{O}_n^{(d)} \quad (3.1.1)$$

where d is the dimensionality of the operator $\mathcal{O}_n^{(d)}$ and $f_n^{(d)}$ is the Wilson coefficient corresponding to that operator. The scale Λ is the heavy scale at which new physics has been integrated out. An exhaustive list of dimension-six terms can be found in [3, 12].

A host of such gauge-invariant higher-dimensional operators have been, and are being, analyzed with considerable rigor, and now there exist limits on them, using data ranging from electroweak precision measurements to global fits of LHC results [4–11, 13, 113, 123–143]. Most of such analyses include higher-dimensional operators that conserve charge conjugation (C), parity (P) and time-reversal (T). However, there is evidence of C, P and CP-violation in weak interactions [24], and there are speculations about other sources of CP-violation as well, especially with a view to explaining the baryon asymmetry in our universe [102, 144]. The possibility of CP-nonconservation cannot therefore be ruled out in the new physics currently sought after. Thus one may in principle also obtain higher-dimensional interaction terms involving the Higgs and a pair of gauge bosons. The constraints on such terms, and identification of regions in the parameter space where they can be phenomenologically significant, form the subject-matter of this chapter.

The CP-violating effective couplings, interestingly, are not constrained by the oblique electroweak parameters at one-loop level up to $\mathcal{O}(\frac{1}{\Lambda^2})$, where Λ is the cutoff scale of the effective theory. The leading contributions to self-energy corrections to electroweak gauge bosons at one-loop level occur at $\mathcal{O}(\frac{1}{\Lambda^4})$. Therefore, electroweak precision (EWP) data are not expected to provide severe constraints on CP-odd parameters. In addition to this, Higgs-mediated event rates in various channels receive contributions from these couplings at $\mathcal{O}(\frac{1}{\Lambda^4})$. Thus they can also be constrained from global fits of the LHC data. The strongest limits on them, however, arise from the contributions to the electric dipole moments (EDMs) of the neutron and the electron, both of which are severely restricted from experiments. As we shall see in the following sections, a single CP-violating operator taken at a time may in certain cases be limited to a very small strength from the above constraints, while two or three such operators considered together can have relatively larger, but highly correlated coefficients. Some of these operators can have interesting phenomenological implications, especially in

the context of the LHC. A study in similar lines can be found in Refs. [123, 128, 134, 140].

In the following section we analyse the set of dimension-six gauge-Higgs operators that contribute to the modification of the VVh ($V = W, Z, \gamma$) couplings and the relationship between the Wilson coefficients and the various CP-odd vertices.

3.2 Morphology of Gauge-Higgs Operators

In the effective Lagrangian approach that has been followed here, the effects of new physics at the low energy can be described by the Lagrangian \mathcal{L}_{eff} in Eq.(3.1.1) comprising only of the SM fields. The information about the high scale theory is encoded in the Wilson coefficients of the operators, suppressed by the powers of the cut-off scale Λ . The operators constructed out of the Higgs doublet and the $SU(2) \times U(1)$ gauge fields are of even dimensions, and at the leading order they have mass dimension $d = 6$. The dimension-six CP-even gauge invariant operators constructed out of the Higgs doublet (Φ) and the electroweak gauge fields (B_μ, W_μ^a), that modify the gauge-Higgs couplings are given as follows:

$$\begin{aligned}
O_W &= \frac{f_W}{\Lambda^2} (D_\mu \Phi)^\dagger \hat{W}^{\mu\nu} (D_\nu \Phi); & O_B &= \frac{f_B}{\Lambda^2} (D_\mu \Phi)^\dagger \hat{B}^{\mu\nu} (D_\nu \Phi); \\
O_{BB} &= \frac{f_{BB}}{\Lambda^2} \Phi^\dagger \hat{B}^{\mu\nu} \hat{B}_{\mu\nu} \Phi; & O_{WW} &= \frac{f_{WW}}{\Lambda^2} \Phi^\dagger \hat{W}^{\mu\nu} \hat{W}_{\mu\nu} \Phi; \\
O_{BW} &= \frac{f_{BW}}{\Lambda^2} \Phi^\dagger \hat{B}^{\mu\nu} \hat{W}_{\mu\nu} \Phi.
\end{aligned} \tag{3.2.1}$$

In the above, we have defined $\hat{B}_{\mu\nu} = i\frac{g'}{2} B_{\mu\nu}$ and $\hat{W}_{\mu\nu} = i\frac{g}{2} \tau^a W_{\mu\nu}^a$. g and g' are the electroweak coupling parameters corresponding to $SU(2)$ and $U(1)$ gauge groups respectively, and τ^a ($a = 1, 2, 3$) are the three Pauli matrices. We define the gauge covariant derivative as $D_\mu \equiv \partial_\mu - i\frac{g}{2} \tau^a W_\mu^a - i\frac{g'}{2} Y B_\mu$, where Y is the hypercharge quantum number. With this choice of the definition of gauge covariant derivative, field strength tensor $W_{\mu\nu}^a$ is given by, $W_{\mu\nu}^a = \partial_\mu W_\nu^a - \partial_\nu W_\mu^a + g\epsilon^{abc} W_\mu^b W_\nu^c$. The constraints on CP-even parameters and their collider implications have been studied extensively in the literature [4, 9, 126, 129, 131, 136, 143]. Here we are interested in the corresponding CP-violating dimension six gauge-Higgs operators. These are

$$\begin{aligned}
\tilde{O}_W &= \frac{\tilde{f}_W}{\Lambda^2} (D_\mu \Phi)^\dagger \hat{\tilde{W}}^{\mu\nu} (D_\nu \Phi); & \tilde{O}_B &= \frac{\tilde{f}_B}{\Lambda^2} (D_\mu \Phi)^\dagger \hat{\tilde{B}}^{\mu\nu} (D_\nu \Phi); \\
\tilde{O}_{BB} &= \frac{\tilde{f}_{BB}}{\Lambda^2} \Phi^\dagger \hat{\tilde{B}}^{\mu\nu} \hat{\tilde{B}}_{\mu\nu} \Phi; & \tilde{O}_{WW} &= \frac{\tilde{f}_{WW}}{\Lambda^2} \Phi^\dagger \hat{\tilde{W}}^{\mu\nu} \hat{\tilde{W}}_{\mu\nu} \Phi; \\
\tilde{O}_{BW} &= \frac{\tilde{f}_{BW}}{\Lambda^2} \Phi^\dagger \hat{\tilde{B}}^{\mu\nu} \hat{\tilde{W}}_{\mu\nu} \Phi,
\end{aligned} \tag{3.2.2}$$

where, $\hat{W}^{\mu\nu} = \frac{1}{2}\epsilon^{\mu\nu\alpha\beta}\hat{W}_{\alpha\beta}$ and $\hat{B}^{\mu\nu} = \frac{1}{2}\epsilon^{\mu\nu\alpha\beta}\hat{B}_{\alpha\beta}$, $\epsilon^{\mu\nu\alpha\beta}$ being the four-dimensional fully antisymmetric tensor with $\epsilon^{0123} = 1$.

However, all five of these CP-violating operators are not independent, and are related by the following constraint equations, which arise from using the SM equations of motion: ¹

$$\begin{aligned} 2\tilde{O}_B &= \frac{\tilde{f}_B}{\tilde{f}_{BB}}\tilde{O}_{BB} + \frac{\tilde{f}_B}{\tilde{f}_{BW}}\tilde{O}_{BW}, \\ 2\tilde{O}_W &= \frac{\tilde{f}_W}{\tilde{f}_{WW}}\tilde{O}_{WW} + \frac{\tilde{f}_W}{\tilde{f}_{BW}}\tilde{O}_{BW} \end{aligned} \quad (3.2.3)$$

The above set of constraints in Eq.(3.2.3) entails only three of the five operators in Eq.(3.2.2) to be independent of each other. For the purpose of our study we take \tilde{O}_B , \tilde{O}_W and \tilde{O}_{WW} to be comprising an independent set of CP-violating gauge-Higgs operators. In principle, the CP-even operators [Eq.(3.2.1)] could have been assumed to exist simultaneously with the CP-odd ones considered here. However, such an approach generates far too large a set of free parameters, where the signature of the CP-violating effective couplings would be drowned. Moreover, the CP-even operators are independent of the CP-odd ones (and vice versa); therefore, setting them to zero is a viable phenomenological approach. We therefore postulate that the new physics above scale Λ is such that *only CP-violating dimension six effective operators are appreciable*, and the corresponding CP-conserving ones are much smaller. Such a ‘‘simplified approach,’’ we reiterate, is unavoidable for unveiling CP-violating high scale physics, as has been recognized in the literature [128, 145–147]. Studies focusing exclusively on the generation of CP-violating terms in specific new physics frameworks can also be found, an example being those in the context of extra space-time dimensions [148, 149].

After electroweak symmetry breaking, these CP-odd operators contribute to following three-point vertices of our interest²

$$\mathcal{L}_{WW}h = -\frac{gm_W}{\Lambda^2}(\tilde{f}_W + 2\tilde{f}_{WW})\epsilon^{\mu\nu\alpha\beta}k_{1\alpha}k_{2\beta}W_\mu^+(k_1)W_\nu^-(k_2)h(k), \quad (3.2.4)$$

$$\begin{aligned} \mathcal{L}_{ZZ}h &= -\frac{gm_W}{\Lambda^2}\left[\frac{c_W^2\tilde{f}_W + s_W^2\tilde{f}_B}{c_W^2} + 2c_W^2\tilde{f}_{WW}\right] \\ &\quad \epsilon^{\mu\nu\alpha\beta}k_{1\alpha}k_{2\beta}Z_\mu(k_1)Z_\nu(k_2)h(k), \end{aligned} \quad (3.2.5)$$

¹We thank Wouter Dekens and Jordy de Vries for helpful comments on this matter.

² The CP-odd operators considered here also contribute to four-point and five-point vertices like $VVhh$, $VVVh$ and $VVVhh$. However, as we will see in following sections, all the observables used in our analysis are sensitive to only three-point vertices at the leading order.

$$\begin{aligned}\mathcal{L}_{\gamma\gamma h} &= -2\left(\frac{gm_W}{\Lambda^2}\right)s_W^2 \tilde{f}_{WW} \\ &\quad \epsilon^{\mu\nu\alpha\beta}k_{1\alpha}k_{2\beta}A_\mu(k_1)A_\nu(k_2)h(k),\end{aligned}\tag{3.2.6}$$

$$\begin{aligned}\mathcal{L}_{\gamma Zh} &= \left(\frac{gm_W}{2\Lambda^2}\right)t_W \left[(-\tilde{f}_W + \tilde{f}_B) - 4c_W^2\tilde{f}_{WW}\right] \\ &\quad \epsilon^{\mu\nu\alpha\beta}k_{1\alpha}k_{2\beta}A_\mu(k_1)Z_\nu(k_2)h(k),\end{aligned}\tag{3.2.7}$$

$$\begin{aligned}\mathcal{L}_{WW\gamma} &= \left(\frac{gm_W^2}{2\Lambda^2}\right)s_W(\tilde{f}_W + \tilde{f}_B) \\ &\quad \epsilon^{\mu\nu\alpha\beta}k_\beta W_\mu^+(k_1)W_\nu^-(k_2)A_\alpha(k),\end{aligned}\tag{3.2.8}$$

$$\begin{aligned}\mathcal{L}_{WWZ} &= -\left(\frac{gm_W^2}{2\Lambda^2}\right)s_W t_W(\tilde{f}_W + \tilde{f}_B) \\ &\quad \epsilon^{\mu\nu\alpha\beta}k_\beta W_\mu^+(k_1)W_\nu^-(k_2)Z_\alpha(k).\end{aligned}\tag{3.2.9}$$

In the above equations $s_W = \sin \theta_W$, $c_W = \cos \theta_W$, $t_W = \tan \theta_W$, and $c_{2W} = \cos 2\theta_W$, where θ_W is the Weinberg angle. Here ks are the four-momenta of the fields that enter the vertex. We have taken all momenta to be inflowing toward the three-point vertex in establishing the Feynman rules. From the list of CP-odd interaction vertices shown above, one can observe a general tensor structure of the form $\epsilon^{\mu\nu\alpha\beta}k_{1\alpha}k_{2\beta}$ in VVh vertices and a general tensor structure of the form $\epsilon^{\mu\nu\alpha\beta}k_\beta$ in trilinear gauge boson couplings (WWV). Because of this the CP-odd couplings are linear combinations of the parameters \tilde{f}_i . Note that we have not included the CP-odd operator involving gluon-Higgs coupling,

$$\tilde{O}_{GG} = \frac{\tilde{f}_{GG}}{\Lambda^2}\Phi^\dagger \hat{G}^{\mu\nu} \hat{G}_{\mu\nu} \Phi.\tag{3.2.10}$$

This operator introduces a θ_{QCD} term [150, 151], and it is severely constrained by the experimental measurement of neutron EDM [24]. In Table 3.1, we list various couplings and their effective strengths ignoring the overall dimension full factor of $\frac{gm_W}{\Lambda^2}$ in \tilde{C}_{VVh} and the dimensionless factor of $\frac{gm_W^2}{\Lambda^2}$ in \tilde{C}_{WWV} couplings. Note that only ZZh and γZh couplings receive contribution from all three CP-odd operators. The operators which contribute to $WW\gamma$ also contribute to WWZ and these couplings are related by, $\tilde{C}_{WWZ} = -t_W \tilde{C}_{WW\gamma}$.

Having discussed the Lorentz structure of the anomalous three-point VVh and WWV vertices, we now move on to discuss the constraints on these CP-odd couplings arising from the precision electroweak data, the LHC data on the Higgs production and decay and finally from the experimental bounds on the fermionic electric dipole moments.

Coupling	Effective coupling strength
\tilde{C}_{WWh}	$(-\tilde{f}_W - 2\tilde{f}_{WW})$
\tilde{C}_{ZZh}	$-\frac{1}{c_W^2} [c_W^2 \tilde{f}_W + s_W^2 \tilde{f}_B + 2c_W^4 \tilde{f}_{WW}]$
$\tilde{C}_{\gamma\gamma h}$	$-2s_W^2 (\tilde{f}_{WW})$
$\tilde{C}_{\gamma Zh}$	$\frac{t_W}{2} [(-\tilde{f}_W + \tilde{f}_B) - 4c_W^2 \tilde{f}_{WW}]$
$\tilde{C}_{WW\gamma}$	$\frac{s_W}{2} (\tilde{f}_W + \tilde{f}_B)$
\tilde{C}_{WWZ}	$-\frac{s_W t_W}{2} (\tilde{f}_W + \tilde{f}_B)$

Table 3.1: CP-odd VVh and WWV coupling factors and their effective strengths.

3.3 Constraints from Electroweak Precision (EWP) Data

We note that unlike some of the CP-even ($d = 6$) operators, the CP-odd operators do not contribute to the gauge boson propagator corrections at tree level, hence are not expected to receive severe bounds from the electroweak precision data. This is due to the antisymmetry of the epsilon tensor which is present in all CP-odd operators. In fact, because of the same reason, all quantum corrections to gauge boson two-point functions up to $\mathcal{O}(\frac{1}{\Lambda^2})$ vanish ³

³These corrections are proportional to $\epsilon^{\mu\nu\alpha\beta} p_\alpha p_\beta$ (p being the four-momentum of gauge boson) which is zero.

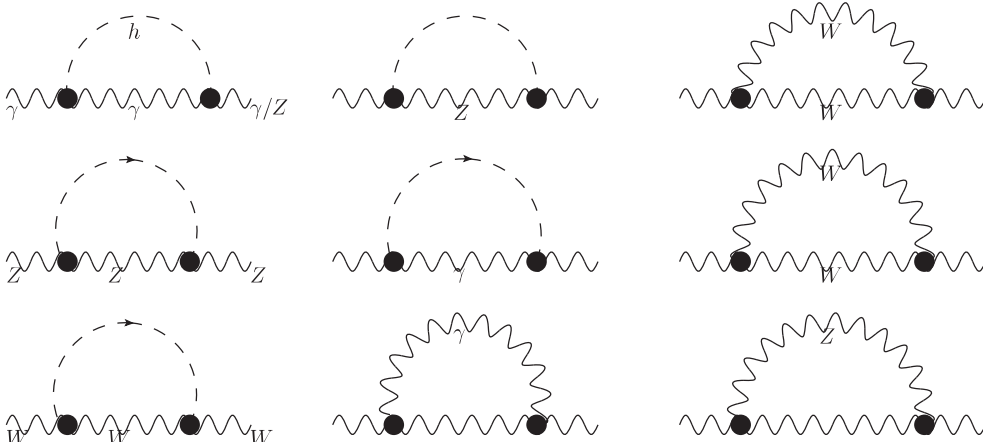


Figure 3.1: One-loop self energy corrections to electroweak vector bosons (oblique corrections) in presence of CP-odd operators. The blobs show the effective CP-odd vertices. These corrections are of $\mathcal{O}(1/\Lambda^4)$.

and first nonzero contributions due to CP-odd operators appear at $\mathcal{O}(\frac{1}{\Lambda^4})$. As we will see in section 4, the CP-odd couplings contribute to observables related to LHC Higgs data at this order. It would be interesting to discuss the implications of the electroweak precision measurement constraints on the parameters of CP-odd operators.

It is well known that the dominant effects of new physics can be conveniently parametrized in terms of Peskin-Takeuchi parameters [75]. These are related to the gauge boson two-point functions as

$$\alpha S = 4c_W^2 s_W^2 \left(\Pi'_{ZZ}(0) - \Pi'_{\gamma\gamma}(0) - \frac{c_W^2 - s_W^2}{s_W c_W} \Pi'_{\gamma Z}(0) \right) \quad (3.3.1)$$

$$\alpha T = \frac{\Pi_{WW}(0)}{m_W^2} - \frac{\Pi_{ZZ}(0)}{m_Z^2} \quad (3.3.2)$$

$$\alpha U = 4s_W^2 \left(\Pi'_{WW}(0) - c_W \Pi'_{ZZ}(0) - s_W^2 \Pi'_{\gamma\gamma}(0) - 2c_W s_W \Pi'_{\gamma Z}(0) \right) \quad (3.3.3)$$

where, $\Pi_{V_1 V_2}(p^2)$ and $\Pi'_{V_1 V_2}(p^2)$ are the coefficients of $g^{\mu\nu}$ in the two-point function and its derivative with respect to p^2 , respectively. The relevant one-loop Feynman diagrams are shown in Fig. 3.1. We have regularized ultraviolet (UV) singularities of these diagrams in dimensional regularization (DR). The expressions for $\Pi_{V_1 V_2}(p^2)$ in terms of standard one-loop scalar functions are given in Appendix A.1. We find that $\Pi_{\gamma\gamma}(0) = \Pi_{\gamma Z}(0) = 0$ which is expected due to the transverse nature of the photon. The renormalization of UV singularity is carried out in $\overline{\text{MS}}$ scheme which introduces scale dependence in these expressions. We have identified the renormalization scale with the cutoff scale Λ . Thus the gauge boson two-point

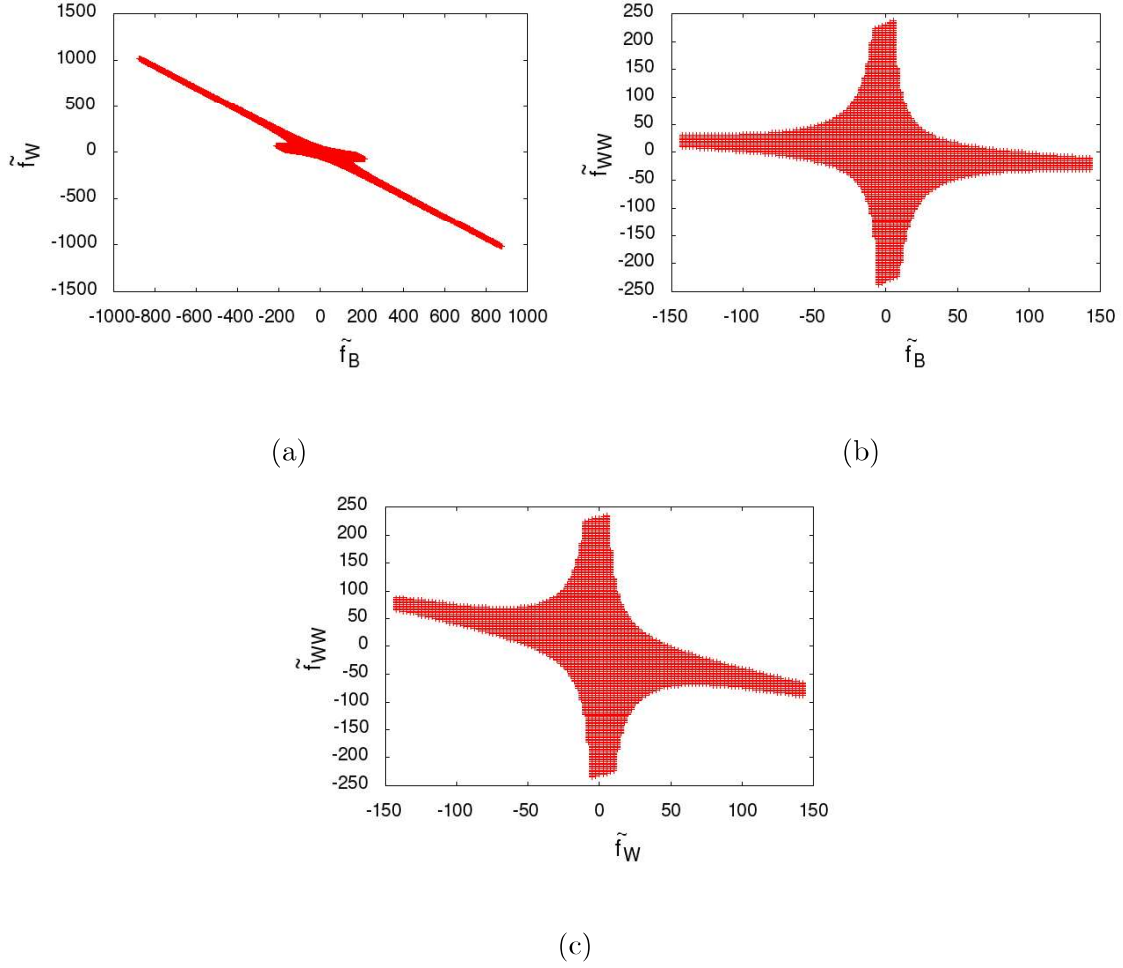


Figure 3.2: Constraints from electroweak precision data keeping two parameters nonzero at a time and for $\Lambda = 1$ TeV.

functions also have $\ln(\Lambda)$ dependence apart from the overall $1/\Lambda^4$ dependence coming from CP-odd couplings. Because of this an explicit choice of Λ is necessary in deriving the EWP constraints on \tilde{f}_i s.

For $\Lambda = 1$ TeV, the Peskin-Takeuchi parameters due to CP-odd couplings are given by,

$$S = (-3.36 \tilde{C}_{\gamma\gamma h}^2 - 1.28 \tilde{C}_{\gamma Zh}^2 + 4.64 \tilde{C}_{ZZh}^2 - 4.49 \tilde{C}_{\gamma\gamma h} \tilde{C}_{\gamma Zh} - 6.21 \tilde{C}_{\gamma Zh} \tilde{C}_{ZZh}) \times 10^{-5} \quad (3.3.4)$$

$$T = -9.74 \times 10^{-5} \tilde{C}_{WW\gamma}^2 \quad (3.3.5)$$

$$U = (-0.960 \tilde{C}_{\gamma\gamma h}^2 - 4.69 \tilde{C}_{\gamma Zh}^2 - 4.64 \tilde{C}_{ZZh}^2 + 5.67 \tilde{C}_{WWh}^2 + 2.76 \tilde{C}_{WW\gamma}^2 - 3.59 \tilde{C}_{\gamma\gamma h} \tilde{C}_{\gamma Zh} - 4.96 \tilde{C}_{\gamma Zh} \tilde{C}_{ZZh}) \times 10^{-5}. \quad (3.3.6)$$

We can also express them in terms of \tilde{f}_i s using their relation with C_i s given in Table 3.1. The

experimental limits on S, T and U parameters are obtained by fitting the data on various electroweak observables with these parameters. The limits are [24]⁴

$$S = -0.03 \pm 0.10, T = 0.01 \pm 0.12, U = 0.05 \pm 0.10. \quad (3.3.7)$$

In Eqs. (3.3.4), (3.3.5) and (3.3.6) the coefficients of various couplings are $\sim 10^{-5}$ suggesting that the EWP constraints cannot be very strong. Therefore, we only consider the case where any two out of three parameters are nonzero. In Fig. 3.2, we display the allowed range for CP-odd parameters which satisfy the above limits on S, T and U parameters for all combinations of two parameters taken together. Here we have varied parameters freely to ensure that we obtain a bounded region. As we turn on other parameters, these constraints become weaker. Also, for a larger cutoff scale the allowed parameter space grows as one would expect.

3.4 Constraints from LHC data

The presence of CP-odd operators introduces modifications in the strength of the gauge-Higgs couplings, and hence changes the Higgs production and decay rates in channels involving these couplings. Since we are interested in CP-even observables, the SM VVh couplings which are CP-even, do not interfere with the CP-odd VVh couplings. Hence the lowest order (tree level) modifications to the decay widths (Γ) and production cross sections (σ) are of the order $\frac{1}{\Lambda^4}$. To quantify these changes we define the following ratios for various decay and production channels,

$$\alpha_Y = \frac{\Gamma^{\text{BSM}}(h \rightarrow Y)}{\Gamma^{\text{SM}}(h \rightarrow Y)} \quad (3.4.1)$$

$$\gamma_X = \frac{\sigma^{\text{BSM}}(X \rightarrow h)}{\sigma^{\text{SM}}(X \rightarrow h)} \quad (3.4.2)$$

where Y and X are used to label the final state and initial state particles in the Higgs decay and production channels respectively.

3.4.1 Higgs decay channels

In the SM, the 126 GeV Higgs boson predominantly decays into $b\bar{b}$ and WW^* followed by gg , $\tau^+\tau^-$, $c\bar{c}$ and ZZ^* . It also decays to $\gamma\gamma$, γZ and $\mu^+\mu^-$ with much suppressed rates. Out of these, $h \rightarrow gg$, $h \rightarrow \gamma\gamma$ and $h \rightarrow \gamma Z$ are loop-induced decay modes and hence are

⁴These limits have been updated in the latest version. The numbers presented here are from PDG 2014.

sensitive to new physics. The decay channels which are affected by the CP-odd operators are $h \rightarrow \gamma\gamma$, $h \rightarrow \gamma Z$, $h \rightarrow WW^*$ and $h \rightarrow ZZ^*$. The expressions for the ratio of the decay widths, α_{ij} in various two body Higgs decay channels are as follows ⁵:

$$\alpha_{\gamma\gamma} = 1 + 2.84 \left(\frac{\tilde{C}_{\gamma\gamma h}^2}{\Lambda^4} \right) \quad (3.4.4)$$

$$\alpha_{\gamma Z} = 1 + 0.856 \left(\frac{\tilde{C}_{\gamma Zh}^2}{\Lambda^4} \right) \quad (3.4.5)$$

$$\alpha_{WW^*} = 1 + 3.35 \times 10^{-6} \left(\frac{\tilde{C}_{WWh}^2}{\Lambda^4} \right) \quad (3.4.6)$$

$$\alpha_{2\ell 2\nu} = 1 + 3.56 \times 10^{-6} \left(\frac{\tilde{C}_{WWh}^2}{\Lambda^4} \right) \quad (3.4.7)$$

$$\alpha_{ZZ^*} = 1 + 1.40 \times 10^{-6} \left(\frac{\tilde{C}_{ZZh}^2}{\Lambda^4} \right) \quad (3.4.8)$$

$$\alpha_{4\ell} = 1 + 1.54 \times 10^{-6} \left(\frac{\tilde{C}_{ZZh}^2}{\Lambda^4} \right) \quad (3.4.9)$$

Since the set of gauge-Higgs operators considered in our analysis do not alter the Higgs coupling with gluons (g) and fermions (f), we have $\alpha_{ff} = \alpha_{gg} = 1$. The ratios $\alpha_{2\ell 2\nu}$ [Eq.(3.4.7)] and $\alpha_{4\ell}$ [Eq.(3.4.9)] correspond to the $h \rightarrow WW^* \rightarrow 2\ell 2\nu$ and $h \rightarrow ZZ^* \rightarrow 4\ell$ respectively. Here ℓ stands for electron and muon, and ν for corresponding neutrinos. The ratios α_{WW^*} and α_{ZZ^*} which include both leptonic and hadronic decays of W and Z bosons are used in calculating modified total Higgs decay width. As mentioned earlier, the modifications to Higgs partial decay widths at leading order are $\mathcal{O}(1/\Lambda^4)$. It is in contrast to the case of CP-even dimension six gauge-Higgs operators where such modifications occur at $\mathcal{O}(1/\Lambda^2)$. Unlike WWh and ZZh couplings, the $\gamma\gamma h$ and γZh couplings are loop-induced in the SM. In the presence of CP-odd operators these vertices receive contributions at tree level. This explains the relatively large coefficients in the expressions for $\alpha_{\gamma\gamma}$ [Eq.(3.4.4)] and $\alpha_{\gamma Z}$ [Eq.(3.4.5)] as compared to the other decay width ratios. This would imply most stringent constraints on the parameters contributing to these decay channels.

⁵ We disagree with the CP-odd part of the analytic expression for $\alpha_{\gamma Z}$ in Eq. (3.17) of Ref. [134]. The correct expression for CP-odd term in the notations of Ref. [134] turns out to be,

$$\alpha_{\gamma Z} = 1 + \left| \frac{4\sqrt{2}\pi^2 \tilde{a}_2}{G_F \Lambda^2 s_W^2 (A_F + A_W)} \right|^2, \quad (3.4.3)$$

where \tilde{a}_2 can be identified with the factor $\frac{1}{2}\tilde{C}_{\gamma Zh}$ in our notation.

3.4.2 Higgs production channels

As discussed before, at the LHC, the dominant mode to produce Higgs boson is gluon-gluon fusion (ggF) mediated by a top quark loop. The other major production channels include: vector boson fusion (VBF), associated production with a weak boson (Vh) and associated production with a pair of top quark ($t\bar{t}h$). Except ggF and $t\bar{t}h$ production channels, all other channels are affected in presence of anomalous gauge-Higgs CP-odd vertices. Like the decay width ratios, the production cross section ratios also receive leading order modifications at $\mathcal{O}(1/\Lambda^4)$. The ratios of the Higgs production cross sections, γ_X in various channels at $\sqrt{s} = 8(7)$ TeV LHC are given below.

$$\gamma_{pp \rightarrow Wh} = 1 + 5.61(5.37) \times 10^{-4} \left(\frac{\tilde{C}_{WW}^2}{\Lambda^4} \right) \quad (3.4.10)$$

$$\gamma_{pp \rightarrow Wh \rightarrow h\nu} = 1 + 5.67(5.16) \times 10^{-4} \left(\frac{\tilde{C}_{WW}^2}{\Lambda^4} \right) \quad (3.4.11)$$

$$\begin{aligned} \gamma_{pp \rightarrow Zh} = & 1 + 4.09(3.92) \times 10^{-4} \left(\frac{\tilde{C}_{ZZh}^2}{\Lambda^4} \right) + 2.45(2.32) \times 10^{-4} \left(\frac{\tilde{C}_{\gamma Zh}^2}{\Lambda^4} \right) \\ & + 2.55(2.44) \times 10^{-4} \left(\frac{\tilde{C}_{ZZh}}{\Lambda^2} \right) \left(\frac{\tilde{C}_{\gamma Zh}}{\Lambda^2} \right) \end{aligned} \quad (3.4.12)$$

$$\begin{aligned} \gamma_{\text{VBF}} = & 1 + 7.02(5.62) \times 10^{-6} \left(\frac{\tilde{f}_B^2}{\Lambda^4} \right) + 1.50(1.44) \times 10^{-4} \left(\frac{\tilde{f}_W^2}{\Lambda^4} \right) \\ & + 6.98(6.75) \times 10^{-4} \left(\frac{\tilde{f}_{WW}^2}{\Lambda^4} \right) - 1.32(1.14) \times 10^{-5} \left(\frac{\tilde{f}_B \tilde{f}_W}{\Lambda^4} \right) \\ & - 5.06(5.03) \times 10^{-5} \left(\frac{\tilde{f}_B \tilde{f}_{WW}}{\Lambda^4} \right) + 6.22(5.98) \times 10^{-4} \left(\frac{\tilde{f}_W \tilde{f}_{WW}}{\Lambda^4} \right) \end{aligned} \quad (3.4.13)$$

$$\gamma_{pp \rightarrow t\bar{t}h} = \gamma_{\text{GGF}} = 1. \quad (3.4.14)$$

These expressions have been obtained by computing the SM and BSM cross sections at tree level using `Madgraph` [152] under the assumption that the K-factors (due to higher order corrections) are same in the SM and BSM cases. For that we have implemented our effective Lagrangian in `FeynRules` [153] and used the generated UFO model file in `Madgraph`. The cross sections have been calculated using `cteq611` parton distribution functions [154] and with default settings for renormalization and factorization scales.

We would like to point out that there is an additional diagram other than the one involving the ZZh coupling, which contributes to $pp \rightarrow Zh$ production. This is due to the tree level CP-odd γZh coupling. Similarly, in VBF channel additional diagrams appear besides the one involving WWh and ZZh vertices due to the contributions from the anomalous $\gamma\gamma h$ and γZh couplings. Because of a different parametrization, this information is not explicit in the expression for VBF. We find this parametrization more convenient in terms of evaluating the coefficients in Eq.(3.4.13). Also, the VBF coefficients reported above do not have any Vh contamination and this can be ensured in `Madgraph` at the process generation level. One can notice that the modifications induced by the CP-odd operators are relatively weak because the SM cross sections are already tree level effects in the modified production channels.

One important fact in relation to these production cross section ratios (γs) is that the numerical coefficients present in these expressions are very much cut dependent. This is associated with the fact that the anomalous couplings induced by the gauge-Higgs operators have a different Lorentz structure (therefore, different kinematic dependence) than their SM counterparts. Hence in general the SM and BSM cut efficiencies are not the same for a given process. The differences between the two become more pronounced for higher values of the CP-odd couplings. But for reasonably low values of the same one can still work under the approximation that the two cut efficiencies are the same. In this work we have taken this approximation into consideration, and taken only default cuts in `Madgraph` to simulate any production or decay channel. Since we have taken data only from individual production channels and not from combined channel data (e.g. Vh combined channel) in our chi-square analysis, this approximation finds a stronger footing.

3.4.3 Global analysis

The quantitative measure of the difference between the Higgs data from the LHC, and its corresponding SM predictions is given by what we call the signal strength, defined as,

$$\mu^{X,Y} = \frac{\sigma^{\text{BSM}}(X \rightarrow h)\text{BR}^{\text{BSM}}(h \rightarrow Y)}{\sigma^{\text{SM}}(X \rightarrow h)\text{BR}^{\text{SM}}(h \rightarrow Y)} \quad (3.4.15)$$

where, $\text{BR}(h \rightarrow Y) = \frac{\Gamma(h \rightarrow Y)}{\Gamma_{\text{total}}}$ is the branching ratio for Higgs decaying into Y final state, and Γ_{total} is the total Higgs decay width. For 126 GeV Higgs boson $\Gamma_{\text{total}}^{\text{SM}} = 4.2$ MeV. The total Higgs decay width in the BSM construct $\Gamma_{\text{total}}^{\text{BSM}}$ can be expressed in terms of the SM total Higgs decay width $\Gamma_{\text{total}}^{\text{SM}}$ by,

$$\Gamma_{\text{total}}^{\text{BSM}} = S_{\text{total}}\Gamma_{\text{total}}^{\text{SM}}. \quad (3.4.16)$$

S_{total} is given in terms of the various branching fractions of the Higgs in the SM as,

$$S_{total} \sim \text{BR}_{bb}^{\text{SM}} + \text{BR}_{cc}^{\text{SM}} + \text{BR}_{\tau\tau}^{\text{SM}} + \alpha_{\gamma\gamma} \text{BR}_{\gamma\gamma}^{\text{SM}} + \alpha_{\gamma Z} \text{BR}_{\gamma Z}^{\text{SM}} \\ + \alpha_{WW^*} \text{BR}_{WW^*}^{\text{SM}} + \alpha_{ZZ^*} \text{BR}_{ZZ^*}^{\text{SM}} + \alpha_{gg} \text{BR}_{gg}^{\text{SM}} \quad (3.4.17)$$

which becomes on solving,

$$S_{total} \sim 0.736 + 0.0023\alpha_{\gamma\gamma} + 0.0016\alpha_{\gamma Z} + 0.23\alpha_{WW^*} + 0.029\alpha_{ZZ^*}. \quad (3.4.18)$$

The SM branching fractions for 126 GeV Higgs are taken from [29]. The signal strength in Eq.(3.4.15) can be rewritten in a compact form using the decay and the productions cross section ratios defined above,

$$\mu^{X,Y} = \gamma_X \frac{\alpha_Y}{S_{total}}. \quad (3.4.19)$$

Production channel	8 TeV cross section (pb)	7 TeV cross section (pb)
ggF	18.97	14.89
VBF	1.568	1.211
Wh	0.686	0.563
Zh	0.405	0.327
$t\bar{t}h$	0.1262	0.0843
$b\bar{b}h$	0.198	0.152

Table 3.2: Higgs production cross section in the SM [29].

To perform the global fit of our CP-odd parameters, we use the standard definition of the chi-square function,

$$\chi^2 = \sum_{X,Y} \frac{(\mu_{th}^{X,Y} - \mu_{exp}^{X,Y})^2}{\Sigma_{X,Y}^2} \quad (3.4.20)$$

where $\mu_{th}^{X,Y}$ is the theoretical signal strength expected in presence of CP-odd operators, and $\mu_{exp}^{X,Y}$ is the experimental signal strength reported by the LHC experiments. $\Sigma_{X,Y}$ is the experimental uncertainty in $\mu_{exp}^{X,Y}$. The experimental data reported generally has unsymmetrical uncertainties $\Sigma_{X,Y}^+$ and $\Sigma_{X,Y}^-$. The $\Sigma_{X,Y}$ that we use symmetrizes these uncertainties in quadrature through the following definition [126, 131],

$$\Sigma_{X,Y} = \sqrt{\frac{(\Sigma_{X,Y}^+)^2 + (\Sigma_{X,Y}^-)^2}{2}}. \quad (3.4.21)$$

Since the LHC data that we use includes data from both 7 and 8 TeV LHC runs, the theoretical signal strength in Eq.(3.4.20) is obtained after combining the signal strengths calculated for 7 and 8 TeV LHC. For that we have used following formula [126],

$$\mu_{th}^{XY} = \frac{\mu_{th,8}^{XY} \sigma_8^{\text{SM}} \mathcal{L}_8 + \mu_{th,7}^{XY} \sigma_7^{\text{SM}} \mathcal{L}_7}{\sigma_8^{\text{SM}} \mathcal{L}_8 + \sigma_7^{\text{SM}} \mathcal{L}_7} \quad (3.4.22)$$

where \mathcal{L}_7 and \mathcal{L}_8 are the luminosities at 7 and 8 TeV, respectively, and σ_7^{SM} and σ_8^{SM} are the SM cross sections at those energies. These cross sections are listed in Table 3.2.

Production channel	Decay channel	Signal strength	Energy in TeV (Luminosity in fb^{-1})
ggF (ATLAS)	$h \rightarrow \gamma\gamma$	1.32 ± 0.38 [155]	7(4.5) + 8(20.3)
VBF (ATLAS)	$h \rightarrow \gamma\gamma$	0.8 ± 0.7 [155]	7(4.5) + 8(20.3)
Wh (ATLAS)	$h \rightarrow \gamma\gamma$	1.0 ± 1.6 [155]	7(4.5) + 8(20.3)
Zh (ATLAS)	$h \rightarrow \gamma\gamma$	$0.1^{+3.7}_{-0.1}$ [155]	7(4.5) + 8(20.3)
$t\bar{t}h$ (ATLAS)	$h \rightarrow \gamma\gamma$	$1.6^{+2.7}_{-1.8}$ [155]	7(4.5) + 8(20.3)
ggF (CMS)	$h \rightarrow \gamma\gamma$	$1.12^{+0.37}_{-0.32}$ [156]	7(5.1) + 8(19.7)
VBF (CMS)	$h \rightarrow \gamma\gamma$	$1.58^{+0.77}_{-0.68}$ [156]	7(5.1) + 8(19.7)
$t\bar{t}h$ (CMS)	$h \rightarrow \gamma\gamma$	$2.69^{+2.51}_{-1.81}$ [156]	7(5.1) + 8(19.7)
ggF + $t\bar{t}h$ + $b\bar{b}h$ (ATLAS)	$h \rightarrow ZZ^* \rightarrow 4\ell$	$1.7^{+0.5}_{-0.4}$ [157]	7(4.5) + 8(20.3)
ggF + $t\bar{t}h$ (CMS)	$h \rightarrow ZZ^* \rightarrow 4\ell$	$0.8^{+0.46}_{-0.36}$ [158]	7(5.1) + 8 (19.7)
ggF (ATLAS)	$h \rightarrow WW^* \rightarrow 2\ell 2\nu$	$1.01^{+0.27}_{-0.25}$ [159]	7(4.5) + 8(20.3)
VBF (ATLAS)	$h \rightarrow WW^* \rightarrow 2\ell 2\nu$	$1.28^{+0.53}_{-0.45}$ [159]	7(4.5) + 8(20.3)
ggF (CMS)	$h \rightarrow WW^* \rightarrow 2\ell 2\nu$	$0.74^{+0.22}_{-0.20}$ [160]	7(4.9) + 8 (19.4)
VBF (CMS)	$h \rightarrow WW^* \rightarrow 2\ell 2\nu$	$0.6^{+0.57}_{-0.46}$ [160]	7(4.9) + 8 (19.4)
$Wh \rightarrow h\ell\nu$ (CMS)	$h \rightarrow WW^* \rightarrow 2\ell 2\nu$	$0.56^{+1.27}_{-0.95}$ [160]	7(4.9) + 8 (19.4)

Table 3.3: LHC data used in the global analysis.

In our analysis we have taken altogether 15 data points as listed in Table 3.3. Note that due to large uncertainty, we do not include Higgs data in $h \rightarrow \gamma Z$ decay channel [161, 162] from CMS and ATLAS. Since the LHC observables have an overall cutoff scale dependence, the ratio \tilde{f}_i/Λ^2 can be taken as the effective parameter to be constrained. In other words, the constraints from global analysis can be easily predicted for any value of Λ of interest.

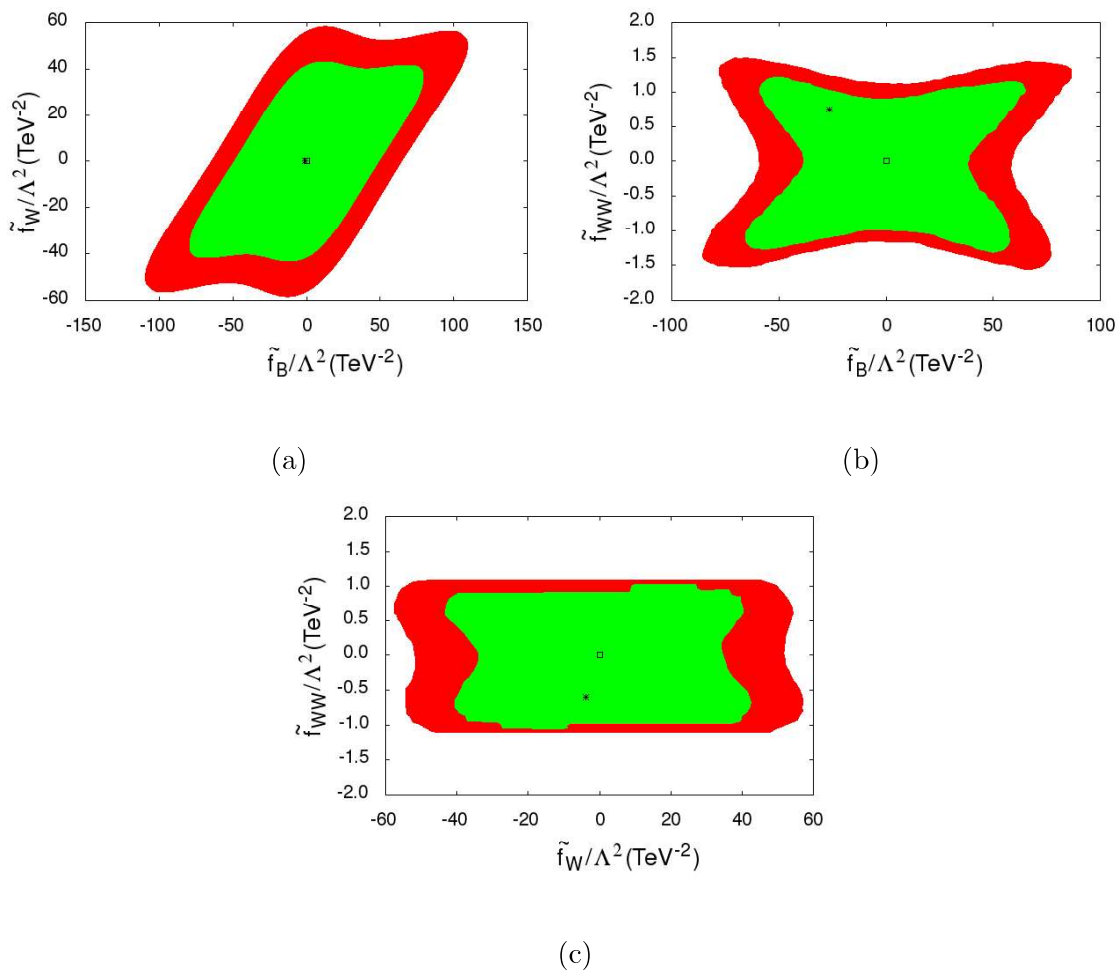


Figure 3.3: Global fits of the CP-odd parameters keeping two parameters nonzero at a time. The point (0,0) corresponds to the SM point and the (*) represents the best fit point. The green region corresponds to the 68 percent confidence interval and the red region to the 95 percent confidence interval, respectively. The best fit point is doubly degenerate up to a sign flip of the best fit point coordinates.

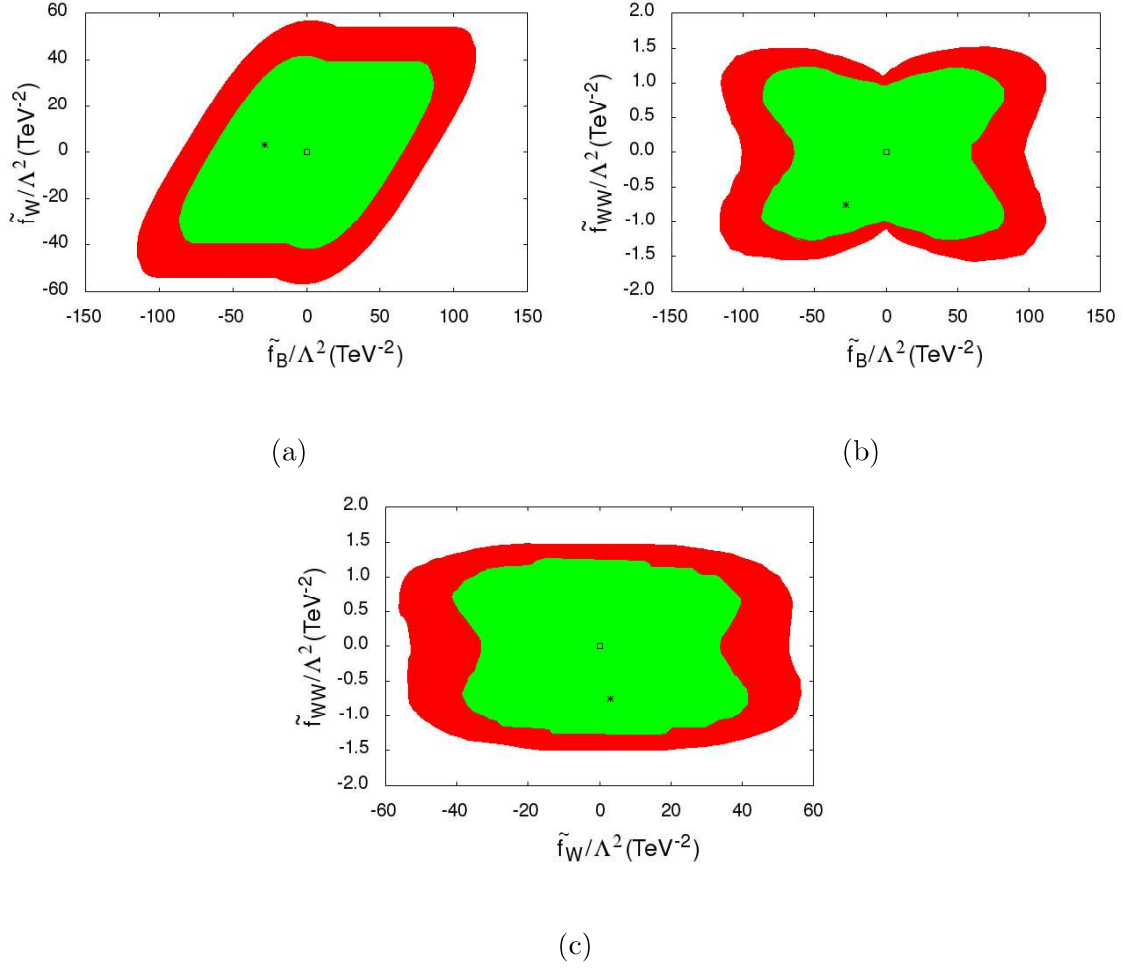


Figure 3.4: Marginalized global fits of the CP-odd parameters \tilde{f}_B , \tilde{f}_W and \tilde{f}_{WW} .

We organize the constraints on CP-odd parameters from global fit of LHC data in the following two parts.

- In the first case, we consider any two of the CP-odd parameters (\tilde{f}_B , \tilde{f}_W and \tilde{f}_{WW}) to be non-zero and put limits on them. The allowed parameter space with 68% and 95% confidence levels are shown in Fig.3.3. In generating these plots we have varied parameters freely. We can see that in all cases the allowed parameter space is bounded. The parameter which enters the $\gamma\gamma h$ vertex *i.e.*, \tilde{f}_{WW} is in general more constrained than those which do not enter the $\gamma\gamma h$ vertex *i.e.*, \tilde{f}_B and \tilde{f}_W . This is exemplified by Fig. 3.3b and 3.3c where we find that \tilde{f}_{WW} is much tightly constrained and allowed values are of $\mathcal{O}(1)$. The nature of slope in these figures is related to the relative sign among the parameters entering into the coupling definitions in Table 3.1. We also note

that out of \tilde{f}_B and \tilde{f}_W , \tilde{f}_W is always more constrained. For example, the maximum allowed value for \tilde{f}_B is ~ 100 while the allowed values of \tilde{f}_W are less than 60, see Fig. 3.3a. This observation can be attributed to the relative size of their coefficients in various observables.

- In the second case we consider three parameters at a time in the global analysis. The allowed parameter space for the three parameters are shown in Fig. 3.4. The two-parameter constraint planes here are obtained after marginalizing over the third parameter. As compared to two-parameter plots (see Fig. 3.3), the allowed region here is more diffused due to the presence of the third parameter. We find that \tilde{f}_{WW} being present in all VVh couplings gets stronger bounds. Here also, as in two parameter fit, \tilde{f}_{WW} being the only parameter contributing to the $\gamma\gamma h$ vertex, is very tightly constrained as shown by the plots in Figs. 3.4b and 3.4c.

It is also found that the constraints on CP-odd parameters from the direct and indirect measurements of the Higgs total width [158, 163] are weaker than those obtained from the global analysis. On the whole, since \tilde{f}_{WW} contributes to the $\gamma\gamma h$ vertex at tree level, thus is constrained rather tightly compared to \tilde{f}_B and \tilde{f}_W . The fact that one has SM contribution at the one-loop level only is responsible for this. \tilde{f}_B and \tilde{f}_W are relatively loosely constrained since they contribute to vertices which have a CP-even SM contribution at the tree level. Also there is lack of sufficient data on the channel $h \rightarrow \gamma Z$, to which they contribute.

The constraints on the parameter space of the CP-violating operators, as obtained from global fits of the (7 + 8) TeV data, are expected to be improved in the high energy runs. A tentative estimate of such improvements, as also that in a linear e^+e^- collider, can be found, for example, in [164]. Going by the estimates of [164], the uncertainty in the signal strength measurements in the next run can be reduced to 33% of the present uncertainties as obtained by both ATLAS and CMS for the $\gamma\gamma$ and WW^* final states in the gluon fusion channel. A precise answer on the improvement of these limits, however, depends also on any possible shift in the central values of the measured signal strengths in different channels. This in turn is also a function of the various systematic uncertainties in the new run, and therefore we have to wait for more data before some precise conclusions can be drawn. A similar consideration applies to a linear collider; precision in coupling measurements down to 1% is expected there in principle [164], but the available statistics as well as the systematics need to be known before concrete estimates emerge.

3.5 Constraints from EDMs

The fermionic electric dipole moment receive an additional contribution from these new CP-odd higher-dimensional operators involving Higgs and pair of gauge bosons. Nonobservation of any fermionic EDMs puts severe constraints on the parameters \tilde{f}_i s. The fermion EDM operator is defined as,

$$-\frac{1}{2} d_f \bar{\psi}(p_2) i\gamma^5 \sigma^{\mu\nu} \psi(p_1) F_{\mu\nu}, \quad (3.5.1)$$

where, $\sigma^{\mu\nu} = \frac{i}{2}[\gamma^\mu, \gamma^\nu]$ and d_f is known as the fermion EDM form factor. Nonvanishing EDMs provide clear hint of CP-violation [165, 166]. In the standard model, CP violation occurs due to quark mixing and it is quite weak (1 part in 1000) [24]. On top of that the first nonzero contribution to EDM operator in the SM appears at three loop level in quark sector, while, for leptons it arises at four loop level. The present upper limits on electron and neutron EDMs are much larger than the values predicted by the SM [167]. In presence of CP-odd gauge-Higgs operators $\gamma\gamma h$, γZh and $WW\gamma$ couplings are modified, because of which the leading contribution to fermion EDMs appears at one-loop level. Due to this the fermion EDM measurements can provide stringent bounds on the CP-odd parameters. Note that the contribution to the fermion EDMs from CP-odd WWh and ZZh vertices can result only at two-loop level. Since the two-loop effects are expected to be subdominant, we will derive constraints on the CP-odd parameters from one-loop fermion EDM calculations. The diagrams that contribute to the fermion EDM at one-loop level are shown in Fig.3.5.

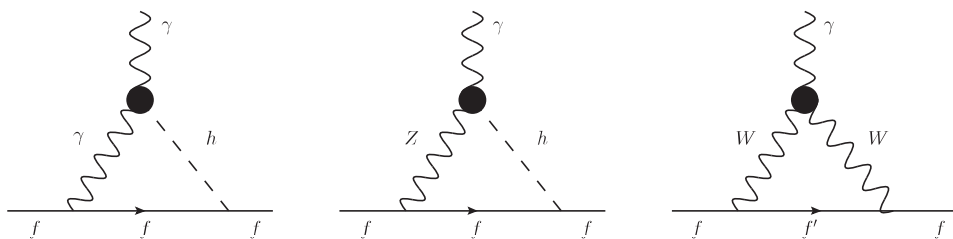


Figure 3.5: One-loop diagrams contributing to fermion EDMs. The blobs show the effective vertices arising out of the CP-odd operators.

The expression for the fermion EDM form factor d_f at one-loop due to the $\gamma\gamma h$, γZh and

$WW\gamma$ vertices is given by the following equation⁶:

$$d_f = \frac{m_f e \alpha}{\pi v^2} \left[\tilde{a}_1 K_1(\Lambda, m_h) + \tilde{a}_2 K_2(\Lambda, m_Z, m_h) + \tilde{a}_3 K_1(\Lambda, m_W) \right] \quad (3.5.2)$$

where,

$$\tilde{a}_1 = -\frac{Q_f}{4s_W^2} \tilde{C}_{\gamma\gamma h}; \quad \tilde{a}_2 = \frac{\left(\frac{1}{2}I_f - Q_f s_W^2\right)}{t_W s_W^2} \tilde{C}_{\gamma Zh}; \quad \tilde{a}_3 = -\frac{I_f}{4s_W^3} \tilde{C}_{WW\gamma}. \quad (3.5.3)$$

Here, v is the electroweak symmetry breaking scale, α is the fine structure constant, I_f is the third component of the fermion Isospin and Q_f is its electric charge quantum number. We have neglected the fermion masses (m_f) with respect to other mass scales in the loop. The one-loop factors K_1 and K_2 are calculated in dimensional regularization ($d = 4 - 2\epsilon$). Since these loops are UV divergent, we renormalize them in $\overline{\text{MS}}$ scheme and identify the renormalization scale with the cutoff Λ . The expressions for K_1 and K_2 are given by,

$$K_1(\Lambda, x) = \frac{v^2}{\Lambda^2} \left[\frac{1}{2} \ln \frac{\Lambda^2}{x^2} + \frac{3}{4} \right], \quad (3.5.4)$$

$$K_2(\Lambda, x, y) = \frac{v^2}{\Lambda^2} \left[\frac{1}{2} \frac{x^2 \ln \frac{\Lambda^2}{x^2} - y^2 \ln \frac{\Lambda^2}{y^2}}{x^2 - y^2} + \frac{3}{4} \right]. \quad (3.5.5)$$

The latest experimental bounds on the electron and neutron EDMs are [168, 169],

$$\begin{aligned} |d_e| &< 8.7 \times 10^{-29} \text{ e cm} \\ |d_n| &< 2.9 \times 10^{-26} \text{ e cm.} \end{aligned} \quad (3.5.6)$$

Note that the EDM contribution is $\mathcal{O}(\frac{1}{\Lambda^2})$ in the cutoff scale, therefore, it is expected to provide stronger bounds on CP-odd parameters than those obtained from EWP and LHC data. Like the electroweak precision observables calculated in section 3, the EDMs also have explicit dependence on Λ . Due to this, we provide EDM constraint equations for three different choices of cutoff scale $\Lambda = 1, 5$ and 10 TeV.

- $\Lambda = 1$ TeV

$$\begin{aligned} |d_e| &\equiv |233.86 \tilde{f}_B + 260.45 \tilde{f}_W - 337.72 \tilde{f}_{WW}| < 1 \\ |d_n| &\equiv |7.02 \tilde{f}_B + 13.81 \tilde{f}_W + 4.66 \tilde{f}_{WW}| < 1 \end{aligned} \quad (3.5.7)$$

⁶We have observed a relative sign change in the contribution of the $WW\gamma$ diagram to the EDM, for the u and d quarks, which is taken care of by the factor I_f in \tilde{a}_3 . It was unaccounted by Ref. [134] where a similar calculation is done.

- $\Lambda = 5$ TeV

$$\begin{aligned}
|d_e| &\equiv |13.87\tilde{f}_B + 15.63\tilde{f}_W - 21.08\tilde{f}_{WW}| < 1 \\
|d_n| &\equiv |0.40\tilde{f}_B + 0.85\tilde{f}_W + 0.33\tilde{f}_{WW}| < 1
\end{aligned}
\tag{3.5.8}$$

- $\Lambda = 10$ TeV

$$\begin{aligned}
|d_e| &\equiv |3.95\tilde{f}_B + 4.47\tilde{f}_W - 6.08\tilde{f}_{WW}| < 1 \\
|d_n| &\equiv |0.11\tilde{f}_B + 0.24\tilde{f}_W + 0.10\tilde{f}_{WW}| < 1
\end{aligned}
\tag{3.5.9}$$

The neutron EDM form factor (d_n) is calculated in terms of constituent quark EDMs using the relation $d_n = \frac{4}{3}d_d - \frac{1}{3}d_u$, from the chiral-quark model [170]. In calculating the above constraints on the EDMs we take $\alpha = 1/137$ and $M_H = 126$ GeV. Because of a stronger experimental limit on electron EDM, the coefficients of parameters in d_e are larger than those in d_n . The constraint equations for electron EDM form factor differ by an order of magnitude from those obtained in Ref. [134] mainly because the most updated experimental bound on electron EDM [169] has been considered.

We first consider the case when only two of the three parameters are kept nonzero. In this case, we freely vary the parameters. The constraints on the parameters are shown in Fig 3.6 for $\Lambda = 1, 5$ and 10 TeV respectively. In all combinations we get bounded regions. The inclinations of the constraint regions can be understood from the relative sign between the parameters in the expressions for the EDMs. As expected, the constraints for $\Lambda = 1$ TeV are tighter than those for $\Lambda = 5$ and 10 TeV and this is corroborated by the size of the coefficients entering in EDM expressions. In $\Lambda = 1$ TeV case, the allowed values for parameters can reach $\mathcal{O}(1)$ values at maximum. As we push the cutoff scale higher, the allowed range for parameters also increases. For example, for $\Lambda = 10$ TeV the allowed values can become $\mathcal{O}(10)$ or larger in some cases.

When three parameters are taken to be nonzero at a time, the parameters are scanned in the range -200 to 200. Fig 3.7, shows two dimensional projection plots of the three dimensional constraint region for $\Lambda = 1$ TeV. We can see that with three parameters present, the constraints are more relaxed than when only two of them are nonzero. However, the parameters are still quite correlated. In fact it is very difficult to obtain closed boundaries. As we increase the range for parameter scan the allowed values for CP-odd parameters become very large [$\gg \mathcal{O}(100)$]. However, it is important to note that for too large values of parameters, the two-loop EDM constraints may become relevant and, therefore, should also be taken into account.

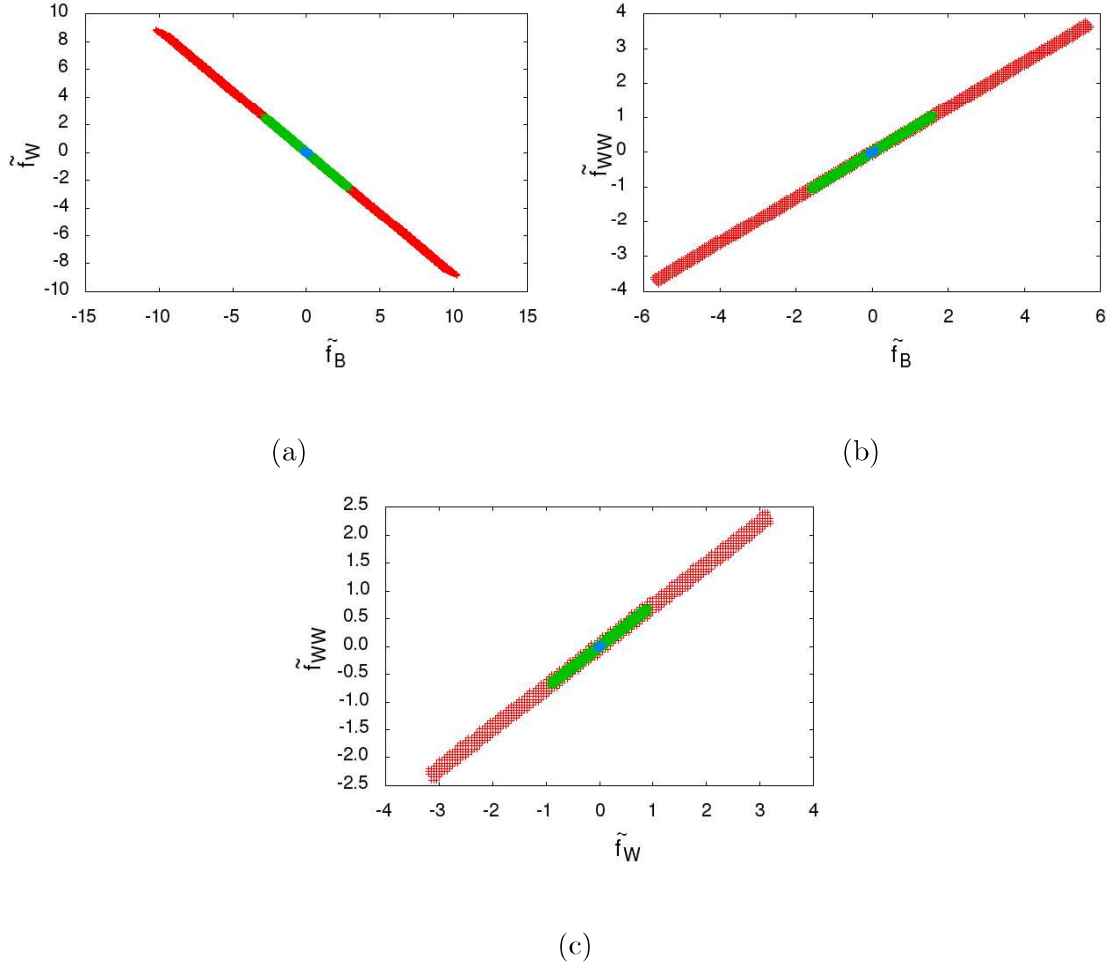


Figure 3.6: EDM constraints keeping two parameters nonzero at a time for three representative values of $\Lambda = 1$ (blue), 5 (green) & 10 (red) TeV.

From the experimental perspective, a number of new EDM experiments promise to improve the level of sensitivity by one to two orders of magnitude in the coming years. For example, The Institut Laue Langevin (ILL) cryogenic experiment and the Spallation Neutron Source (SNS) nEDM experiment [171–173] aim at improving the upper limit on neutron EDM by two orders of magnitude, i.e down to $\mathcal{O}(10^{-28})e.cm$. This would imply that the numerical coefficients in the constraint equations for d_n in Eqs. (3.5.7), (3.5.8) and (3.5.9) would become stronger by almost two orders of magnitude and thus the allowed parameter space for \tilde{f} s will be even more severely constrained, unless, of course, there is direct evidence of neutron EDM in the aforesaid experiments.

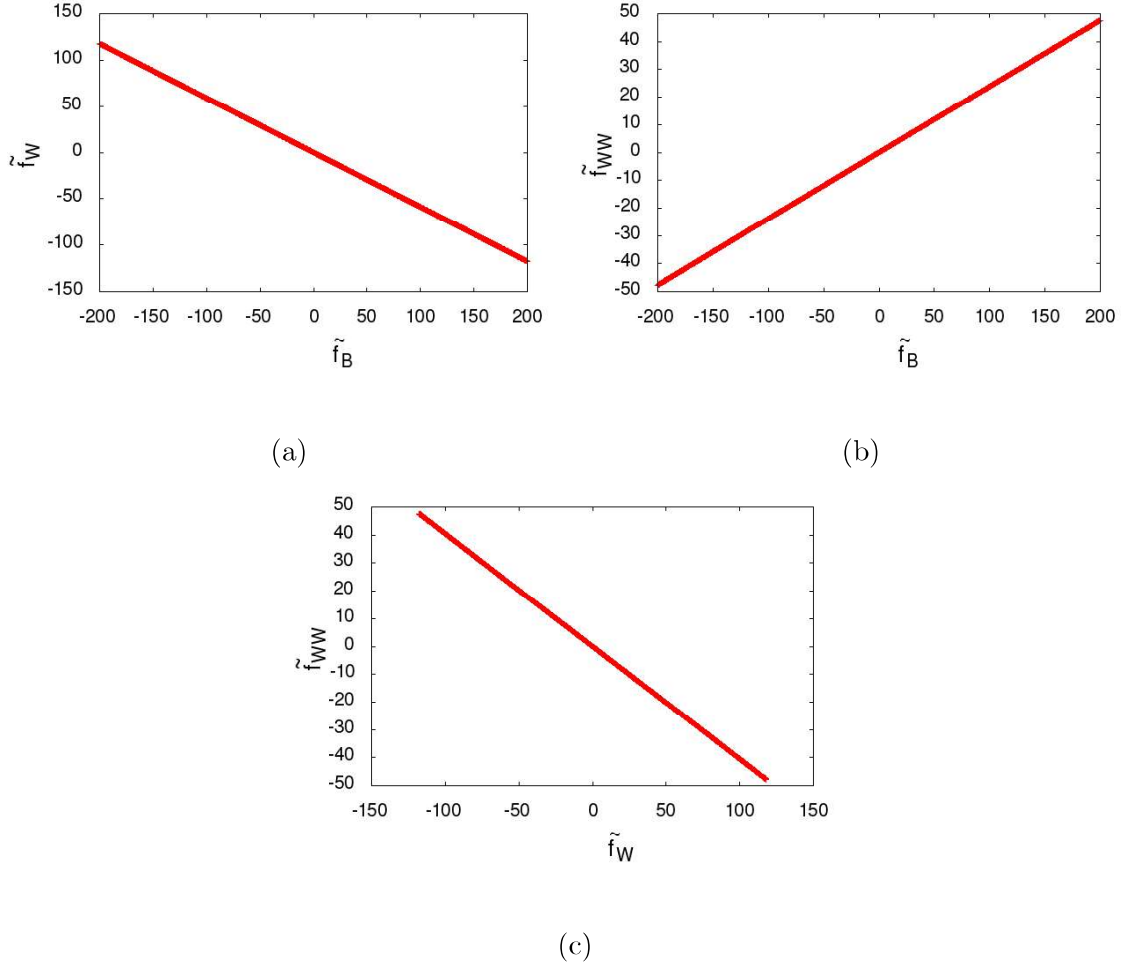


Figure 3.7: EDM constraints for non-zero \tilde{f}_B , \tilde{f}_W and \tilde{f}_{WW} with $\Lambda = 1$ TeV. Parameters are varied in the range between -200 to 200.

3.6 Discussion

We now highlight the important features of the analysis presented in sections 3.3, 3.4 and 3.5. We try to draw a comparative picture and address some of the issues relevant to the analysis.

- In the two parameter case, among all the constraints, the EWP constraints on CP-odd parameters are always the weakest while EDM constraints are the strongest. In general, the correlation among parameters is stronger in EWP and EDM cases as compared to the LHC case.
- In case of global fit of LHC data whatever contributes to $h \rightarrow \gamma\gamma$ receives stronger

constraints, since here the “tree level” contributions from the dimension six operators are essentially at the same level as the “one-loop” SM contributions.

- The same should apply to parameters contributing to $h \rightarrow \gamma Z$ channel which also includes \tilde{f}_B and \tilde{f}_W . However the limits based on current data are rather weak there and are not considered in this analysis. The global fit puts some limits on \tilde{f}_B and \tilde{f}_W as the γZh coupling modifies the Zh and VBF production channels and the total Higgs decay width.
- The channels dependent on the $WW h$ and $ZZ h$ couplings yield relatively weak constraints from the global fits as a whole, since the higher dimensional interactions are inadequate to override the tree level SM contributions.
- In three parameter case, the bounds from LHC data are stronger than those obtained from EDMs. However, the parameters constrained from EDMs still display a tight correlation.
- If we allow dimension-6 CP-even operators to coexist with the CP-odd ones, the EWP and LHC observables would receive contributions at $\mathcal{O}(1/\Lambda^2)$ (as a result of interference with the SM) as well as at $\mathcal{O}(1/\Lambda^4)$. Since there is no interference between CP-odd and CP-even operators in total rates, the CP-odd interactions analyzed here should contribute to signal strengths at $\mathcal{O}(1/\Lambda^4)$. For the sake of consistency, at $\mathcal{O}(1/\Lambda^4)$ the contribution from dimension-8 CP-even operators via its interference with the SM should also be considered. Thus, in the presence of CP-even operators, the constraints from LHC and precision data can be relaxed. However, under the assumption that the effect of CP-conserving new physics is not significantly large, the constraints obtained on CP-odd operators here are in a way the most conservative estimates of the allowed parameter space. Of course, the limits from EDM analyses remain the same in all the cases.
- A comparison between the relative strengths of the EDM and LHC constraints is most transparent only when the CP-violating operators alone are considered, since the CP-conserving ones have no role in EDMs. Their inclusion, albeit via marginalization in the LHC global fits, will serve to relax the corresponding limits beyond what have been obtained. But then, it ceases to be a one-to-one comparison between the two kinds of constraints, something that was intended from the beginning.

Couplings	LHC data		EDM	
	2P case	3P case	2P case	3P case
$ \tilde{C}_{WWh} $	0 – 60	0 – 60	0 – 0.17	0 – 55
$ \tilde{C}_{ZZh} $	25 – 80	25 – 80	0.11 – 0.20	0.15 – 33
$ \tilde{C}_{\gamma h} $	0 – 0.8	0 – 0.8	0 – 0.16	0.02 – 52
$ \tilde{C}_{\gamma Zh} $	15 – 25	15 – 25	0.03 – 0.25	0.05 – 110
$ \tilde{C}_{WW\gamma} $	0 – 40	15 – 40	0 – 0.15	0.02 – 47

Table 3.4: Limits on CP-odd coupling strengths from LHC data and EDM measurements for $\Lambda=1$ TeV. 2P and 3P stand for two parameter nonzero and three parameter nonzero cases respectively.

We have already seen that the Lorentz structure of anomalous CP-odd couplings is unique and these are just some linear combinations of the CP-odd parameters (see Table 3.1). Since in all the observables these couplings enter directly, it is instructive to know the kind of values these couplings can take as a result of the analysis presented above. In the calculation of S , T and U parameters all the CP-odd couplings directly enter. In the global analysis only \tilde{C}_{VVh} couplings participate, therefore, constraints on \tilde{C}_{WWV} from the LHC data are indirect. In EDM calculations only $\tilde{C}_{\gamma h}$, $\tilde{C}_{\gamma Zh}$ and $\tilde{C}_{WW\gamma}$ enter directly and therefore limits obtained on \tilde{C}_{WWh} and \tilde{C}_{ZZh} are also indirect. The limits on the strengths of the anomalous couplings are listed in Table 3.4. Since electroweak precision bounds on \tilde{f}_i are the weakest ⁷, in the table we

⁷Although the EWP constraints are weaker in general, we find that the limits on \tilde{C}_{WWV} from EWP and LHC data are comparable in 2P case.

compare bounds on couplings due to LHC data and EDMs. The comparison is presented for both the two parameter (2P) and three parameter (3P) cases. Since \tilde{C}_{WWZ} is proportional to $\tilde{C}_{WW\gamma}$, the limits on $\tilde{C}_{WW\gamma}$ can be easily translated to limits on \tilde{C}_{WWZ} . Looking at the LHC limits on the couplings we find that $\tilde{C}_{\gamma\gamma h}$ is the most constrained coupling. Also, the LHC limits in 2P and 3P cases are comparable. On the other hand the EDM limits on couplings in 2P case is always stronger than in 3P case.

The triple gauge boson couplings (TGCs) $WW\gamma$ and WWZ can also be constrained using the collider data on gauge boson pair production. Data from Tevatron and LHC are used mainly to constrain the CP-even anomalous couplings as the observables used are not sensitive to CP-odd couplings [174–179]. On the other hand, the experimental analyses at LEP which studied the angular distribution of final state particles are sensitive to CP-odd TGCs. A comparison between the CP-odd sector of TGC Lagrangian [146, 180, 181] and our effective couplings (3.1) implies

$$\frac{\tilde{C}_{WW\gamma}}{\Lambda^2} = \frac{s_W}{m_W^2} \tilde{\kappa}_\gamma \quad (3.6.1)$$

$$\frac{\tilde{C}_{WWZ}}{\Lambda^2} = \frac{c_W}{m_W^2} \tilde{\kappa}_Z. \quad (3.6.2)$$

Using the relation between $\tilde{C}_{WW\gamma}$ and \tilde{C}_{WWZ} we get, $\tilde{\kappa}_Z = -t_W^2 \tilde{\kappa}_\gamma$. At 68% CL, the combined LEP limits on $\tilde{\kappa}_Z$ are [182]

$$-0.14 \leq \tilde{\kappa}_Z \leq -0.06. \quad (3.6.3)$$

These limits when translated on \tilde{C}_{WWZ} and $\tilde{C}_{WW\gamma}$ become,

$$\begin{aligned} -0.19 &\leq \frac{\tilde{C}_{WWZ}}{\Lambda^2} [\text{TeV}^{-2}] \leq -0.08, \\ 0.15 &\leq \frac{\tilde{C}_{WW\gamma}}{\Lambda^2} [\text{TeV}^{-2}] \leq 0.36. \end{aligned} \quad (3.6.4)$$

Note that these limits are comparable to the limits obtained from EDMs in 2P case, however, information on the sign of the couplings is also available.

Other than the VVh vertices considered in our analysis, quartic $VVhh$ vertices also arise out of gauge invariant CP violating operators. One can thus expect some correlated phenomenology from the trilinear and quartic interactions, since the former arise essentially on replacing one Higgs by its vacuum expectation value in the quartic terms. In the analysis presented in this work, the production and decay channels considered are not affected at tree level by such quartic $VVhh$ vertices. Thus in the context of the present analysis, any constraints on

such quartic vertices from observed data are likely to be weaker than those obtained from the $VVh(V = W, Z, \gamma)$ effective interactions, since the quartic couplings would entail Higgs pair production. For example, the $VVhh$ vertex may contribute in addition to the hhh vertex toward a di-Higgs final state. However, one needs to wait for a large volume of data on Higgs pair production to see such correlated phenomena. In general, limits stronger than what we have obtained are not expected. Also, the contributions from such $VVhh$ CP-odd vertices to EDMs and EWP observables come at higher loop levels and thus are expected to be substantially weaker than what we have obtained for the trilinear terms.

It is a well-known fact that the observed baryon asymmetry in our universe cannot be explained by just the CP-violating phase of the Cabibbo-Kobayashi-Maskawa (CKM) matrix in the SM. The presence of additional sources of CP-violating operators arising from the anomalous VVh interactions may in principle explain the observed baryon asymmetry of the universe. However, a more careful scrutiny of this picture reveals that these CP-violating operators are not sufficient to trigger strongly the first order electroweak phase transition required for the baryogenesis. For this, one has to extend the Higgs sector of the SM by introducing new particles which couple to the Higgs boson and thus modify the Higgs potential such that it leads to a strongly first order electroweak phase transition [183]. The phenomenological implications of the operators under study, however, continue to be of considerable interest, especially in a bottom-up search for new physics starting at the electroweak symmetry breaking scale.

3.7 Summary

We have analyzed CP-odd $VVh(V = W, Z, \gamma)$ and $WWV(V = Z, \gamma)$ interactions in terms of gauge-invariant dimension-six operators, obtained as the artifacts of physics beyond the standard model. Constraints on the coefficients of such operators have been investigated using electroweak precision data, LHC data on Higgs and limits on the electric dipole moments of the neutron and the electron. With Λ as the scale suppressing the CP-violating operators, precision parameters as well as LHC observables receive contributions $\sim 1/\Lambda^4$ from the CP-odd couplings, while contributions $\sim 1/\Lambda^2$ to EDM observables are expected. The constraints obtained from the S, T and U parameters are the weakest, while the bounds from EDMs are the strongest with two non vanishing operators. The global analysis of Higgs data from the LHC puts stronger constraints on those CP-odd effective couplings which contribute to $h \rightarrow \gamma\gamma$, as compared to those which do not. We also indicate situations

where large values of certain couplings are allowed by all constraints, when they appear in combination. The constraints coming from LEP on CP-odd couplings $\tilde{C}_{WW\gamma}$ and \tilde{C}_{WWZ} are consistent with the limits obtained from EDMs in the case when any two out of three parameters are nonzero. It may be of interest to find out new physics scenarios where, by integrating out heavy degrees of freedom, one may arrive at large correlated values of such operators.

In the next chapter we try to answer the question of how to see the signatures of the anomalous vertices discussed here at the LHC, and the kind of correlations one has to look for in digging out the CP-violating physics from the CP-conserving effects.

Chapter 4

Distinguishing CP-odd couplings of the Higgs boson to weak boson pairs

4.1 Introduction

Chapter 3 presented a detailed analysis of the constraints on the set of three CP-odd dimension-six gauge-invariant operators, i.e. \tilde{O}_B , \tilde{O}_W and \tilde{O}_{WW} , coming from

- The electroweak precision data.
- The global fits of the signal strengths in Higgs production and decay channels.
- The upper limits on the neutron and electron EDMs.

Once we have the constraints on the CP-odd couplings, we can move on to ask how one can see the signatures of such CP-violating vertices at the LHC. To put it more precisely, one would like to disentangle the signatures of the high scale CP-violating physics from the CP-even physics contributed by the SM along with the corresponding higher-dimension CP-even operators. Such a quest is highly warranted in exploring any non-standard interactions of the 125 GeV resonance discovered at the LHC. The confirmation of such deviations from the SM expectations may bring into light some novel features of the underlying symmetries of the high scale theory and may help us better answer the question as to whether what we have found is “the Higgs” of the SM or “a Higgs” within a richer particle directory.

As pointed out in the previous chapter, since these CP-even operators can contribute to the Higgs production and decays at $\mathcal{O}(\frac{1}{\Lambda^2})$ via interference terms with the SM vertices,

they are relatively more constrained than their CP-odd counterparts. However, if they are present in conjunction with the CP-odd operators, they may have non-negligible contributions via interference effects to certain kinematic observables that might serve to highlight the CP-violating signatures against the background of CP-conserving effects. The role of such observables constructed out of the spin/momenta of the final state particles is the focus of this chapter. As a natural follow-up of the material reported in Chapter 3, this has been analyzed here in the context of the associated Higgs production channel, $pp \rightarrow Zh$, where the anomalous \tilde{C}_{ZZh} and $\tilde{C}_{\gamma Zh}$ couplings contribute. Many studies along similar lines have taken place over the years, probing higher-dimensional WWh and ZZh interactions, often taking them in isolation and predicting observable phenomena in terms of the new operators [5, 6, 8, 10, 11, 13, 113, 124, 125, 135–137, 139, 141, 142, 146, 181, 184–215].

In the sections that follow, we present a brief review of the Lagrangian terms and the CP-odd vertices that come about, along with a table of constraints on the CP-odd VVh vertices, previously discussed in Chapter 3. With a view to make the analysis generic and inclusive, the CP-odd terms are supplemented with a CP-even gauge-Higgs operator which, as mentioned before, can contribute via interference effects.

This is followed up by collider analysis of the $pp \rightarrow Zh$ channel, in connection to which we construct some asymmetry observables which are shown to give non-vanishing contributions if and only if there are CP-violating terms in the Lagrangian. The contributions of the CP-even operators to the suggested asymmetries at the LHC lie within the 1σ error-bars of the SM, while the CP-odd ones are shown to lead to values that steer clear of these error-bars over extended regions of the parameter space. Since the prediction of observable asymmetries is based on detailed event generation, including showering, jet formation and detector simulation, it leads to comparatively realistic estimates of what can be observed. The predictions of CP-violating asymmetries and suppression of the effects of CP-even operators are projected for various luminosities, giving an idea of the luminosity required to obtain useful conclusions.

4.2 CP-odd anomalous couplings and their constraints

The set of CP-violating gauge-Higgs operators of dimension-six that we have considered in our analysis [216] is listed below :

$$\tilde{O}_W = \frac{\tilde{f}_W}{\Lambda^2} (D_\mu \Phi)^\dagger \hat{W}^{\mu\nu} (D_\nu \Phi); \quad \tilde{O}_B = \frac{\tilde{f}_B}{\Lambda^2} (D_\mu \Phi)^\dagger \hat{B}^{\mu\nu} (D_\nu \Phi); \quad \tilde{O}_{WW} = \frac{\tilde{f}_{WW}}{\Lambda^2} \Phi^\dagger \hat{W}^{\mu\nu} \hat{W}_{\mu\nu} \Phi \quad (4.2.1)$$

Here Λ is the cut-off scale above which the high scale physics sets in. For the purpose of this study Λ is taken to be 1 TeV. Since for the LHC observables, \tilde{f}_i/Λ^2 ($i = B, W, WW$) is the effective parameter that gets constrained, the global fit constraints can be predicted for any value of Λ , with the constraints on the parameters \tilde{f}_i 's being appropriately scaled. However, for the constraints coming from EDM measurements, one finds that EDMs have an explicit cut-off dependence other than the one coming via the parameters \tilde{f}_i/Λ^2 . This dependence coming from loop contributions is logarithmic in nature [216].

These operators give rise to the CP-odd VVh interaction vertices of following form,

$$\tilde{\mathcal{L}}_{VVh} = \frac{gm_W}{\Lambda^2} \tilde{C}_{VVh} [\epsilon_{\mu\nu\alpha\beta} k_1^\alpha k_2^\beta] V^\mu(k_1) V^\nu(k_2) h(k), \quad (4.2.2)$$

where $V = W, Z, \gamma$. The coefficients \tilde{C}_{VVh} denote the effective coupling strengths of CP-odd VVh couplings and, are listed in Table 4.1. The VVh interaction vertices arising from corresponding CP-even operators are derived in Ref. [4].

Our aim in the present work is to include scenarios where both CP-odd and-even operators are present, and to discriminate between them via appropriately defined asymmetry parameters. We demonstrate this by turning on the CP-even operator,

$$O_{WW} = \frac{f_{WW}}{\Lambda^2} \Phi^\dagger \hat{W}^{\mu\nu} \hat{W}_{\mu\nu} \Phi, \quad (4.2.3)$$

which contributes to all the VVh vertices. The additional interaction terms thus playing a role in our analysis have the following form [4]:

$$\mathcal{L}_{VVh} = \frac{gm_W}{\Lambda^2} C_{VVh} [k_1^\nu k_2^\mu - g^{\mu\nu} (k_1 \cdot k_2)] V_\mu(k_1) V_\nu(k_2) h(k). \quad (4.2.4)$$

The coupling strengths of CP-even VVh couplings are given by

$$C_{WWh} = -2f_{WW}; \quad C_{ZZh} = -2c_W^2 f_{WW}; \quad C_{\gamma\gamma h} = -2s_W^2 f_{WW}; \quad C_{\gamma Zh} = -2c_W s_W f_{WW}, \quad (4.2.5)$$

which are similar to the corresponding CP-odd couplings receiving contributions from \tilde{O}_{WW} operator.

Coupling	Effective coupling strength
\tilde{C}_{WWh}	$(-\tilde{f}_W - 2\tilde{f}_{WW})$
\tilde{C}_{ZZh}	$-\frac{1}{c_W^2} [c_W^2 \tilde{f}_W + s_W^2 \tilde{f}_B + 2c_W^4 \tilde{f}_{WW}]$
$\tilde{C}_{\gamma\gamma h}$	$-2s_W^2 (\tilde{f}_{WW})$
$\tilde{C}_{\gamma Zh}$	$\frac{t_W}{2} [(-\tilde{f}_W + \tilde{f}_B) - 4c_W^2 \tilde{f}_{WW}]$

Table 4.1: CP-odd VVh coupling factors and their effective strengths.

In [216] we derived limits on the parameters of the CP-odd operators using the collider data (from LEP and LHC) and measurements of electron and neutron EDMs. These limits were obtained taking mainly two parameters (2P) and three parameters (3P) nonzero at a time. The limits on parameters were further used to constrain the effective CP-odd VVh couplings which are listed in Table 4.2.

As has been already stated, these constraints can get relaxed when we keep a linearly independent set of CP-violating gauge-Higgs operators to be non-zero at the same time along with the other fermion-Higgs dimension-six operators (which contribute to fermionic EDMs), and also include at least some of their CP-conserving counterparts. Such operators can be obtained directly by extending those listed in [12] (Table 2). While the CP-violating ones contribute to EDMs, they do not affect the phenomenology of VVh interactions. The consequent enlargement of the parameter space, however, relaxes the otherwise stringent constraints from EDMs.

The allowed values of the coefficients of the dimension-six operators apparently threaten perturbative unitarity in $V_L V_L \rightarrow V_L V_L (V = W, Z)$ at scales of the order of few TeV. The exact value of this scale depends on the specific choice of the operators involved and the

Couplings	LHC data		EDM	
	2P case	3P case	2P case	3P case
$ \tilde{C}_{WWh} $	0 – 60	0 – 60	0 – 0.17	0 – 55
$ \tilde{C}_{ZZh} $	25 – 80	25 – 80	0.11 – 0.20	0.15 – 33
$ \tilde{C}_{\gamma\gamma h} $	0 – 0.8	0 – 0.8	0 – 0.16	0.02 – 52
$ \tilde{C}_{\gamma Zh} $	15 – 25	15 – 25	0.03 – 0.25	0.05 – 110

Table 4.2: Limits on CP-odd coupling strengths from LHC data and EDM measurements for $\Lambda=1$ TeV. 2P and 3P stand for two parameter nonzero and three parameter nonzero cases respectively.

corresponding anomalous couplings they generate [217,218]. However, the effective operators are not reliable at such scales. There one has to include the actual heavy fields of mass $\mathcal{O}(\Lambda)$ (for weakly coupled ultraviolet completion), which are integrated out to obtain the effective coupling terms. These additional degrees of freedom are trusted to restore unitarity when the full theory is switched on. In the context of the study presented here, the range of \tilde{C}_{ZZh} is varied up to $\mathcal{O}(70)$. Even though \tilde{C}_{ZZh} is varied up to this range, the effective coupling parameter that will decide the perturbativity of the loop expansion is given by [11],

$$\tilde{b} = \frac{gm_W v}{2\Lambda^2} \tilde{C}_{ZZh} \quad (4.2.6)$$

Here, $v = 246$ GeV is the Higgs vacuum expectation value. Thus even for $\tilde{C}_{ZZh} \lesssim \mathcal{O}(70)$, $\tilde{b} \lesssim \mathcal{O}(1)$ and the loop expansion in terms of \tilde{b} remains perturbative.

4.3 Isolating the effect of CP-odd couplings

In any elementary particle scattering process, the size and shape of certain kinematic distributions involving leptons and jets can change non-trivially with respect to the purely standard model prediction in the presence of both CP-odd and even higher-dimensional operators. For generic observables like p_T and rapidity distributions which are affected by both CP-even as well as CP-odd couplings, it may not be possible to separate the effect of the two couplings with sufficient statistical significance. In other words, for values of anomalous couplings, consistent with the available experimental data, it would require analyzing a huge amount of data/events to confirm the effect of CP-odd couplings on top of the effect of CP-even couplings using generic observables. Therefore, it is more economical to work with observables which are unambiguously sensitive to the definite CP-property of the couplings.

In the present work, we are interested in CP-odd observables. The CP-odd observables can be categorized as \hat{T} -even or \hat{T} -odd type¹. CP-odd, \hat{T} -even observables may arise only in the presence of absorptive phases. The triple cross products constructed using the particle momenta/spin on the other hand, are \hat{T} -odd observables and they genuinely reflect CP violating interaction [219]. In this section, we quantitatively establish such characteristics of the chosen observables after a realistic simulation of a suitable process at the LHC.

4.3.1 Signal and backgrounds

With the above considerations in view, we take up the analysis of the process, $pp \rightarrow Zh \rightarrow \ell^+ \ell^- b \bar{b}$ with $\ell = e, \mu$. We consider the decay of Higgs to $b \bar{b}$ final state to ensure sufficient event rates. The final state is required to have two opposite sign leptons and exactly two b -tagged jets. The proton-proton collisions are simulated at the center-of-mass energy of 14 TeV. In presence of dimension-six operators, this process also receives contribution from a tree-level diagram involving γZh vertex, which is not present in the SM. Thus there is an interference of the two s -channel diagrams involving the ZZh and γZh vertices at the amplitude level. This is because the same gauge-Higgs operators that give rise to the anomalous \tilde{C}_{ZZh} coupling also give rise to the $\tilde{C}_{\gamma Zh}$ interaction [Table 4.1].

Throughout our analysis we consider $M_h = 126$ GeV. We implement the anomalous couplings in `Madgraph` [152] using the package `FeynRules` [153]. The cross sections are calculated using `nn23lo1` [220] parton distribution functions with default settings for renor-

¹ \hat{T} is the naive time reversal transformation that flips the sign of the particle spin and momenta, without interchanging the initial and final states.

malization and factorization scales. While the parton level events are generated in **Madgraph**, the Pythia [221] switch is turned on to incorporate showering, hadronization and initial and final state radiation (ISR/FSR) effects. The HEP file obtained from this interfacing is passed to **Delphes-3.1.1.2** [222] which gives a ROOT [223] file as output. Jets are formed using the anti-kt algorithm in **Delphes** with a cone size of 0.6. A p_T dependent tagging efficiency is employed for b -jets, namely, 0.7-0.5 for p_T in the range 20-500 GeV. We also use a mis-tagging efficiency of 0.001 for light jets and a p_T dependent mis-tagging efficiency for c -induced jets, which varies from 0.14-0.08 for $20 < p_T < 500$ GeV. The ROOT file thus obtained is fed to the analysis code to generate the distributions.

We start with following basic cuts on the transverse momentum, rapidity and separation of leptons (ℓ) and jets (J), where $J = j, b$; j being the light quark jets and b corresponds to the b -induced jets.

1. $p_{T,J,\ell} > 20$ GeV and $|\eta_{J,\ell}| < 2.5$: We demand that our final state leptons and jets should lie in the central rapidity region each with a minimum transverse momentum of 20 GeV.
2. $\Delta R_{JJ,J\ell} > 0.4$: We demand that both the jets should be well separated from each other as well as from leptons.
3. $\Delta R_{\ell\ell} > 0.2$: There will be sufficiently large opening angle between the two leptons.

The SM cross section for the signal after the generation level cuts is 12.4 fb.

The major background to the signal comes from the following SM processes:

1. $pp \rightarrow b\bar{b} \ell^+\ell^-$ (QCD)
2. $pp \rightarrow t\bar{t} \rightarrow b\bar{b} \ell^+\ell^- \nu\bar{\nu}$
3. $pp \rightarrow jj \ell^+\ell^-$ (QCD)
4. $pp \rightarrow Z \ell^+\ell^- \rightarrow b\bar{b} \ell^+\ell^-$ (EW)

To suppress the above sources of the background, we employ the following additional selection cuts :

1. $p_{T_j} > 50$ GeV
2. $105 < M_{JJ} < 130$ GeV

3. $|M_U - M_Z| < 15 \text{ GeV}$

4. The p_T of the reconstructed Z boson is taken to be $> 150 \text{ GeV}$

The asymmetrical cut on the invariant mass of the two b -tagged jets (M_{JJ}) in the final state around the peak (approximately 116 GeV) is helpful in suppressing backgrounds from $pp \rightarrow b\bar{b} \ell^+\ell^-$ and $pp \rightarrow Z \ell^+\ell^- \rightarrow b\bar{b} \ell^+\ell^-$ processes. We have taken such a window for the invariant mass of the two b -tagged jets because owing to the effects of hadronization and showering, the peak of the invariant mass distribution shifts from M_h to about 116 GeV. Thus we gain in terms of signal events by choosing such an invariant mass cut. Further, requiring exactly two b -tagged jets in the final state significantly reduces the background coming from $pp \rightarrow jj \ell^+\ell^-$.

In order to suppress the $t\bar{t}$ backgrounds, use has been made of the fact that our signal events are hermetic in the ideal situation. In contrast, similar final states from the $t\bar{t}$ background will be necessarily associated with missing- E_T . Thus we propose to distinguish the signal by also demanding $\cancel{E}_T < 20 \text{ GeV}$ [11].

4.3.2 Observables

Next, we discuss two CP-odd, \hat{T} -odd quantities used in the rest of the analysis to isolate the effect of CP-odd couplings from the CP-even ones. These observables are constructed using the 3-momentum information of the final state particles. The first one, also discussed in Refs. [11, 199] is given by,

$$\mathcal{O}_1 = \frac{(\vec{p}_+ \times \vec{p}_-) \cdot \hat{z}}{|\vec{p}_+ \times \vec{p}_-|} \text{sign}[(\vec{p}_+ - \vec{p}_-) \cdot \hat{z}] \quad (4.3.1)$$

Here \vec{p}_+ and \vec{p}_- are the 3-momenta of ℓ^+ and ℓ^- respectively, and \hat{z} is the unit vector along the incoming quark(or anti-quark) direction or the collision axis. The factor $\text{sign}[(\vec{p}_+ - \vec{p}_-) \cdot \hat{z}]$ is the sign of the difference of the momentum projections of the outgoing leptons along the \hat{z} axis. Since the dot product with the \hat{z} unit vector occurs twice in the definition of the observable, the observable is rendered independent of the choice of the direction of the incoming quark momentum. This is important in the context of LHC, as there is ambiguity associated with the momentum direction of the initial quark with respect to which proton it is from. The definition of \mathcal{O}_1 removes this ambiguity and makes it uniquely measurable.

The second observable that we consider uses \vec{p}_{j_1} and \vec{p}_{j_2} , the three-momenta of the two b -tagged jets in addition to the oppositely signed leptons in the final state and is given as:

$$\mathcal{O}_2 = \frac{((\vec{p}_{j_1} + \vec{p}_{j_2}) \times (\vec{p}_+ - \vec{p}_-)) \cdot \hat{z}}{|(\vec{p}_{j_1} + \vec{p}_{j_2}) \times (\vec{p}_+ - \vec{p}_-)|} \text{sign}[(\vec{p}_+ - \vec{p}_-) \cdot \hat{z}], \quad (4.3.2)$$

These observables are CP-odd and \hat{T} -odd, and thus generated from the dispersive part of the amplitude. It should also be noted that, since the in-state partons from the two colliding proton beams do not always carry equal momenta, the lab frame and the center of mass (cm) frame for the colliding partons are in general different. Thus, except for the cm frame *i.e.* when the two initial partons come with the same x -value, where $\vec{p}_{j_1} + \vec{p}_{j_2} + \vec{p}_+ + \vec{p}_- = 0$, the observables \mathcal{O}_1 and \mathcal{O}_2 are distinct. Also, due to the showering effects, an exact momentum balance between the final state b -jets and leptons does not hold true. The difference in the observables is evident from their distributions. By definition, each of them ranges from -1.0 to +1.0.

The distinguishability of the CP-odd operators is quantified more effectively in terms of the asymmetries A_i defined as:

$$A_i = \frac{\sigma(\mathcal{O}_i > 0) - \sigma(\mathcal{O}_i < 0)}{\sigma(\mathcal{O}_i > 0) + \sigma(\mathcal{O}_i < 0)} \quad (4.3.3)$$

We show in Figs. 4.1 and 4.2 histograms of the differential cross section distributions corresponding to observables \mathcal{O}_1 and \mathcal{O}_2 respectively. In both the figures, to tune in the CP-even Lagrangian, we have taken the benchmark value $f_{WW} = -3.0$ [224] which corresponds to $C_{ZZh} = 4.62$ and $C_{\gamma Zh} = 2.53$. As for the CP-odd terms, we take the benchmark point as $\tilde{f}_B = \tilde{f}_W = -30.77$ such that $\tilde{C}_{ZZh} = 40.0$ and $\tilde{C}_{\gamma Zh} = 0.0$ [Table 4.1]. Both of these benchmarks are consistent with existing constraints [216, 224]. The histograms in the two figures are indicative of the induced asymmetry in the distributions for both \mathcal{O}_1 and \mathcal{O}_2 when the CP-violating coupling is turned on. It is important to note that unlike total rates and other CP-even observables which depend on CP-odd couplings quadratically, a comparison of distributions in second and third panel confirms that these observables have linear dependence on \tilde{C}_{ZZh} coupling in the numerator of the expression for the asymmetry [Eq. 4.3.3]. The qualitative features of the histograms remain similar when the $\tilde{C}_{\gamma Zh}$ coupling is also taken to be non-zero and interference effects of both \tilde{C}_{ZZh} and $\tilde{C}_{\gamma Zh}$ couplings are considered.

4.3.3 Asymmetries vs couplings

To assess the possibility of seeing the signatures of CP-violating physics in isolation, we need to calculate the statistical significance at which one can establish the existence of

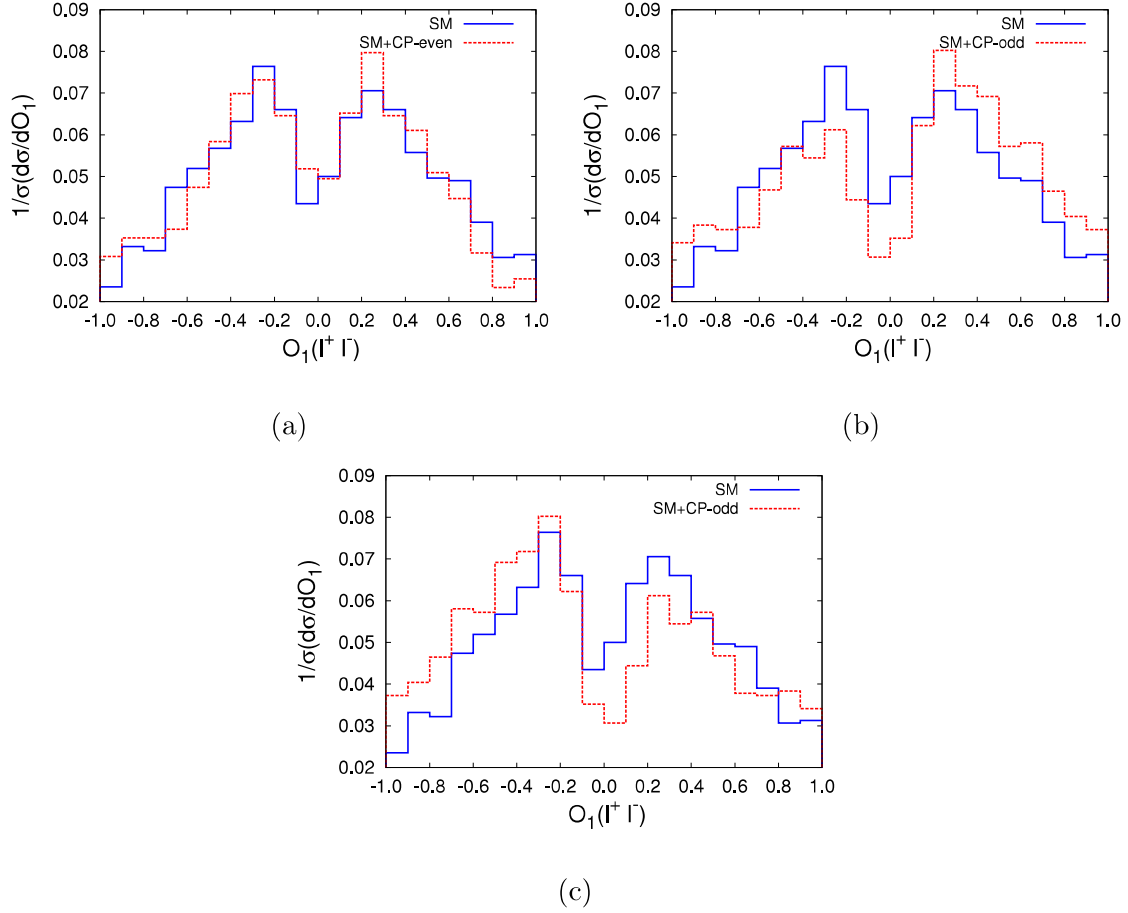


Figure 4.1: Differential cross-section distributions for \mathcal{O}_1 at $\sqrt{s} = 14$ TeV. (a) SM vs SM + CP-even case with $C_{ZZh} = 4.62$ and $C_{\gamma Zh} = 2.53$. (b) SM vs SM + CP-odd case with $\tilde{C}_{ZZh} = 40.0$ and $\tilde{C}_{\gamma Zh} = 0.0$. (c) We reverse the sign of the CP-odd coupling with $\tilde{C}_{ZZh} = -40.0$ and $\tilde{C}_{\gamma Zh} = 0.0$.

non-vanishing asymmetry over and above the CP-conserving effects coming from the SM background. If N_S is the number of signal events and N_B the number of background events, then the observed asymmetry A_i^{obs} , corresponding to observable \mathcal{O}_i at the detector is related to the theoretical asymmetry in the signal distribution *i.e.* A_i , given in Eq. (4.3.3) by the following relation:

$$A_i^{\text{obs}} = A_i \left(\frac{N_S}{N_S + N_B} \right) \quad (4.3.4)$$

The statistical error in the observed asymmetry is given by,

$$\Delta A_i^{\text{obs}} = \frac{1}{\sqrt{N_S + N_B}} = \frac{1}{\sqrt{N}}, \quad (4.3.5)$$

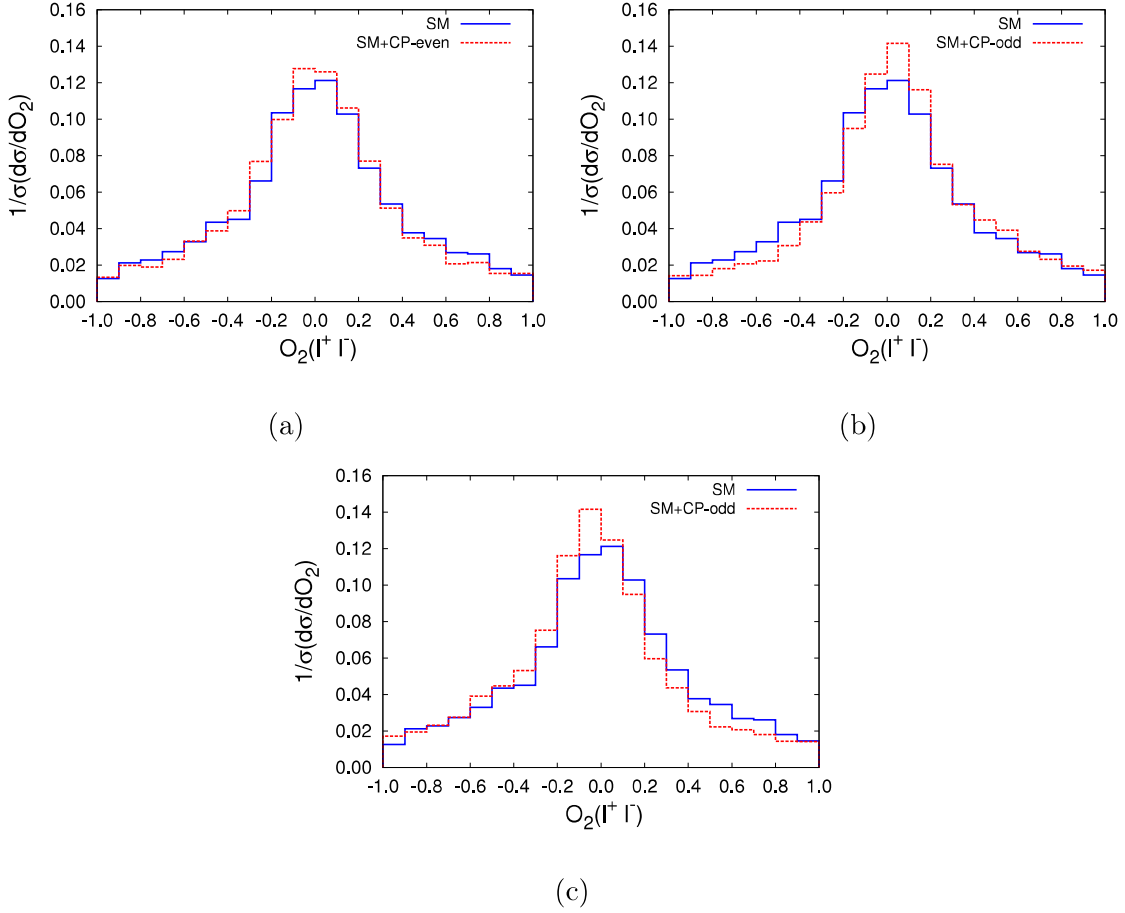


Figure 4.2: Differential cross-section distributions for \mathcal{O}_2 at $\sqrt{s} = 14$ TeV. (a) SM vs SM + CP-even case with $C_{ZZh} = 4.62$ and $C_{\gamma Zh} = 2.53$. (b) SM vs SM + CP-odd case with $\tilde{C}_{ZZh} = 40.0$ and $\tilde{C}_{\gamma Zh} = 0.0$. (c) We reverse the sign of the CP-odd coupling with $\tilde{C}_{ZZh} = -40.0$ and $\tilde{C}_{\gamma Zh} = 0.0$.

where $N = N_S + N_B$ is the total number of signal and background events. Using the above information, the significance S , associated with an observed asymmetry is given by [10],

$$S = A_i^{\text{obs}} \sqrt{N} = A_i \frac{N_S}{\sqrt{N}} \quad (4.3.6)$$

With this in mind, we plot the variation of the asymmetry against the value of the coupling parameter \tilde{C}_{ZZh} as shown in Figures 4.3 to 4.6. Figures 4.3 and 4.4 show the variation of asymmetry for observables \mathcal{O}_1 and \mathcal{O}_2 respectively. For both of them we vary \tilde{C}_{ZZh} keeping $\tilde{C}_{\gamma Zh} = 0.0$, whereas Figures 4.5 and 4.6 show the asymmetry plots for the same observables, although this time we fix the $\tilde{C}_{\gamma Zh}$ coupling at 1.5. For each of the Figures 4.3 to 4.6 we present the error bars on the asymmetries for the various benchmark points. We have

not included any specific values of systematic uncertainties which can in principle change the asymmetries by a few percent.

Our calculations yield near vanishing asymmetry for SM and CP-even cases, which are consistent with zero within 0.5σ for the chosen integrated luminosities. Looking at Figures 4.3 to 4.6 one can infer that the statistical significance improves as we go from a luminosity reach of 1 ab^{-1} to 3 ab^{-1} . For example, in Fig. 4.3, we see that for $\tilde{C}_{ZZh} = 40.0$, the sensitivity improves from 2σ to about 4σ in going from 1 ab^{-1} to 3 ab^{-1} . Another important feature to notice is that the asymmetry does not monotonically increase as we increase the magnitude of the coupling parameter. This is due to the fact that for higher values of couplings, the higher order term (quadratic in \tilde{C}_{ZZh}) in the total cross section starts competing with the SM contribution in the denominator of Eq. 4.3.3. This is corroborated by the marginal decrease in the asymmetry curve beyond $\tilde{C}_{ZZh} = 40.0$ in Figures 4.3 and 4.4. The analysis done here agrees at the parton level to the work presented in [11], but once we fold in the ISR/FSR and detector effects, the statistical significance gets lowered in comparison to what one gets for the parton level analysis.

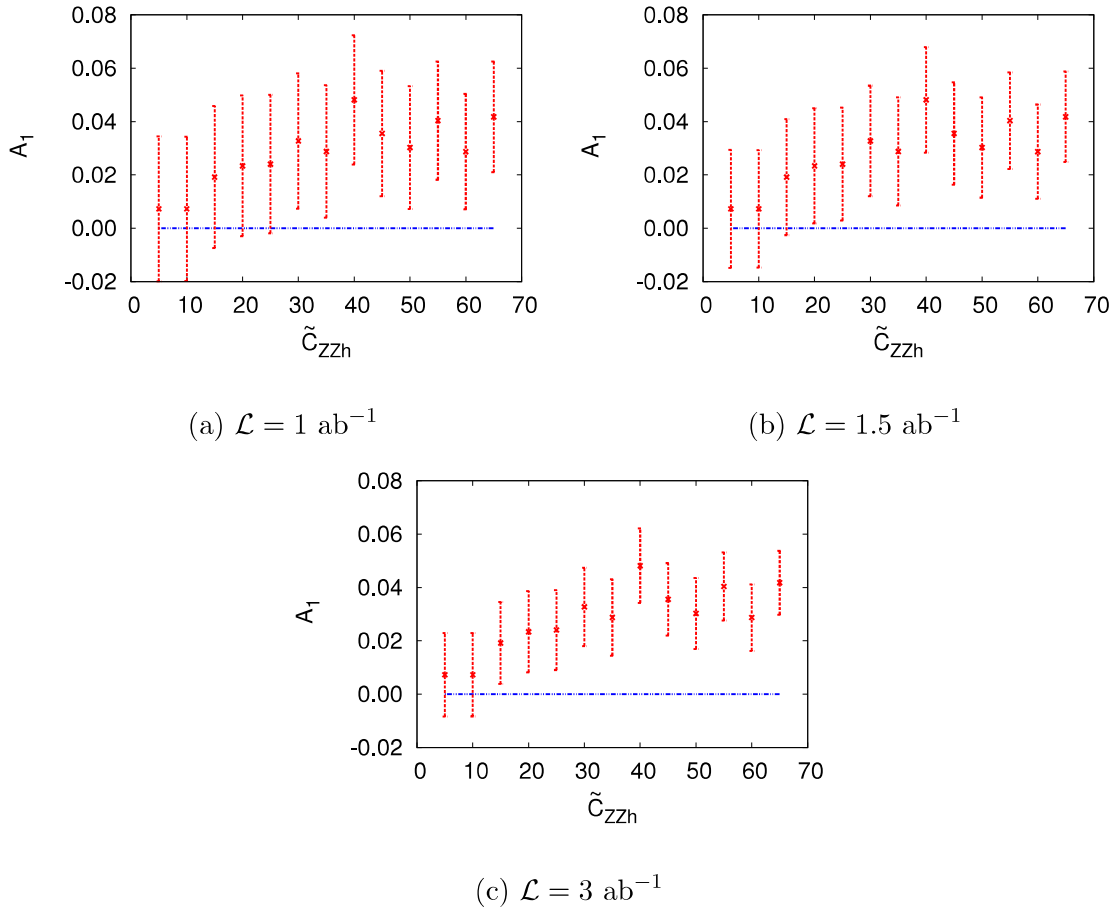
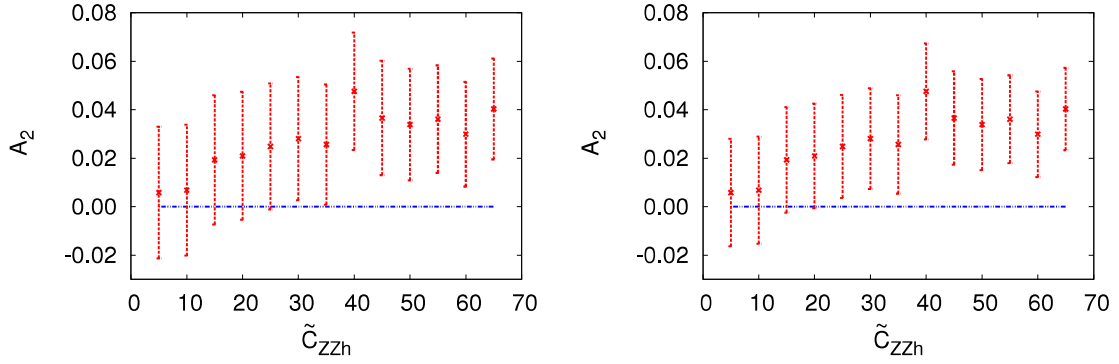
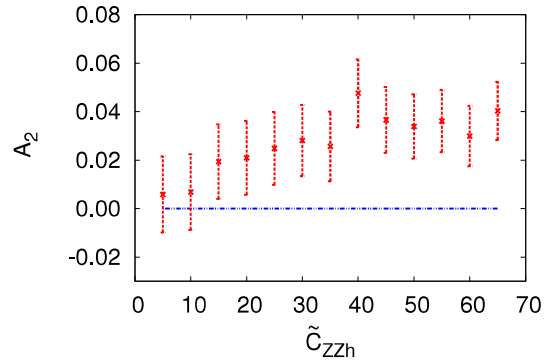


Figure 4.3: The asymmetry vs. coupling plot for the variable \mathcal{O}_1 at Luminosities 1 ab^{-1} , 1.5 ab^{-1} and 3 ab^{-1} , plotted for varying \tilde{C}_{ZZh} . The benchmark points are chosen such that $\tilde{C}_{\gamma Zh} = 0.0$. Statistical uncertainties are shown as error bars for different benchmark points. The zero line is shown to illustrate the offset of the non-vanishing asymmetry against the SM and CP-even case, for which a CP-odd observable has no asymmetry.



(a) $\mathcal{L} = 1 \text{ ab}^{-1}$

(b) $\mathcal{L} = 1.5 \text{ ab}^{-1}$



(c) $\mathcal{L} = 3 \text{ ab}^{-1}$

Figure 4.4: The asymmetry vs. coupling plot for the variable \mathcal{O}_2 at Luminosities 1 ab^{-1} , 1.5 ab^{-1} and 3 ab^{-1} , plotted for varying \tilde{C}_{ZZh} . The benchmark points are chosen such that $\tilde{C}_{\gamma Zh} = 0.0$.

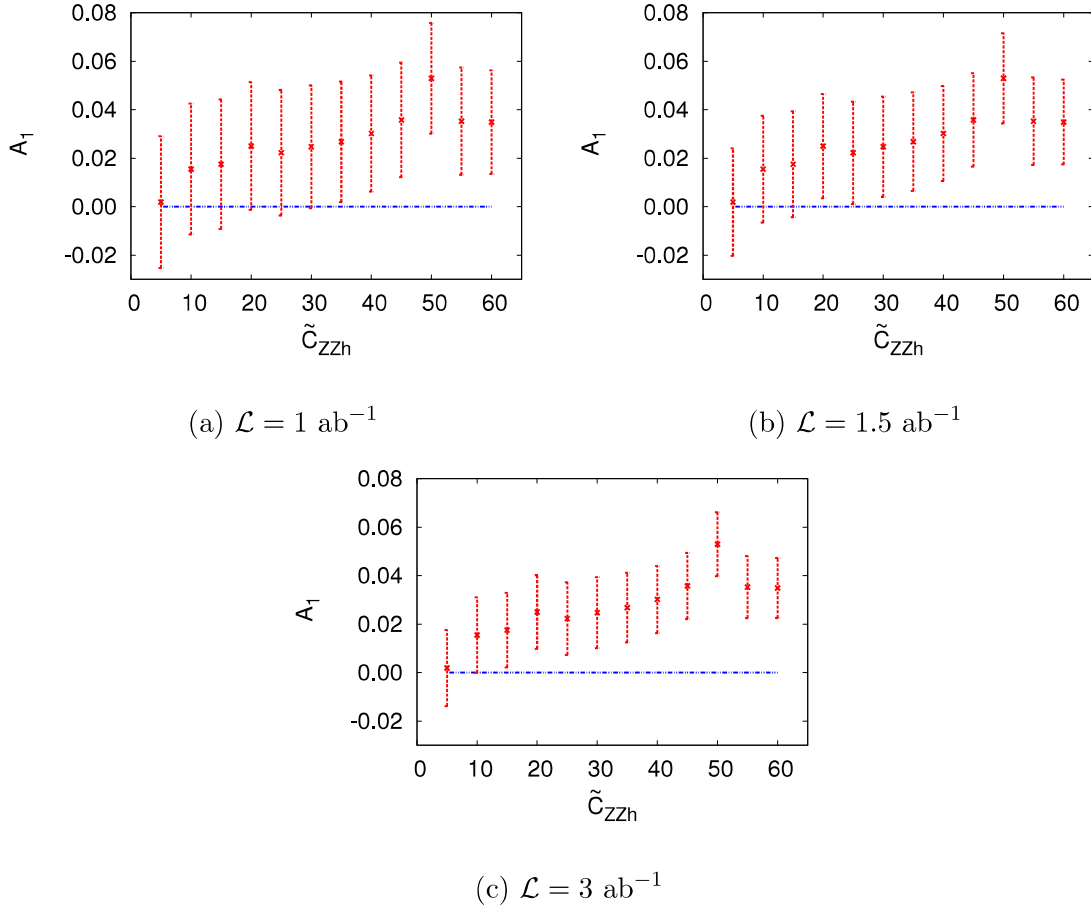


Figure 4.5: The asymmetry vs. coupling plot for the variable \mathcal{O}_1 at Luminosities 1 ab^{-1} , 1.5 ab^{-1} and 3 ab^{-1} , plotted for varying \tilde{C}_{ZZh} . The benchmark points are chosen such that $\tilde{C}_{\gamma Zh} = 1.5$.

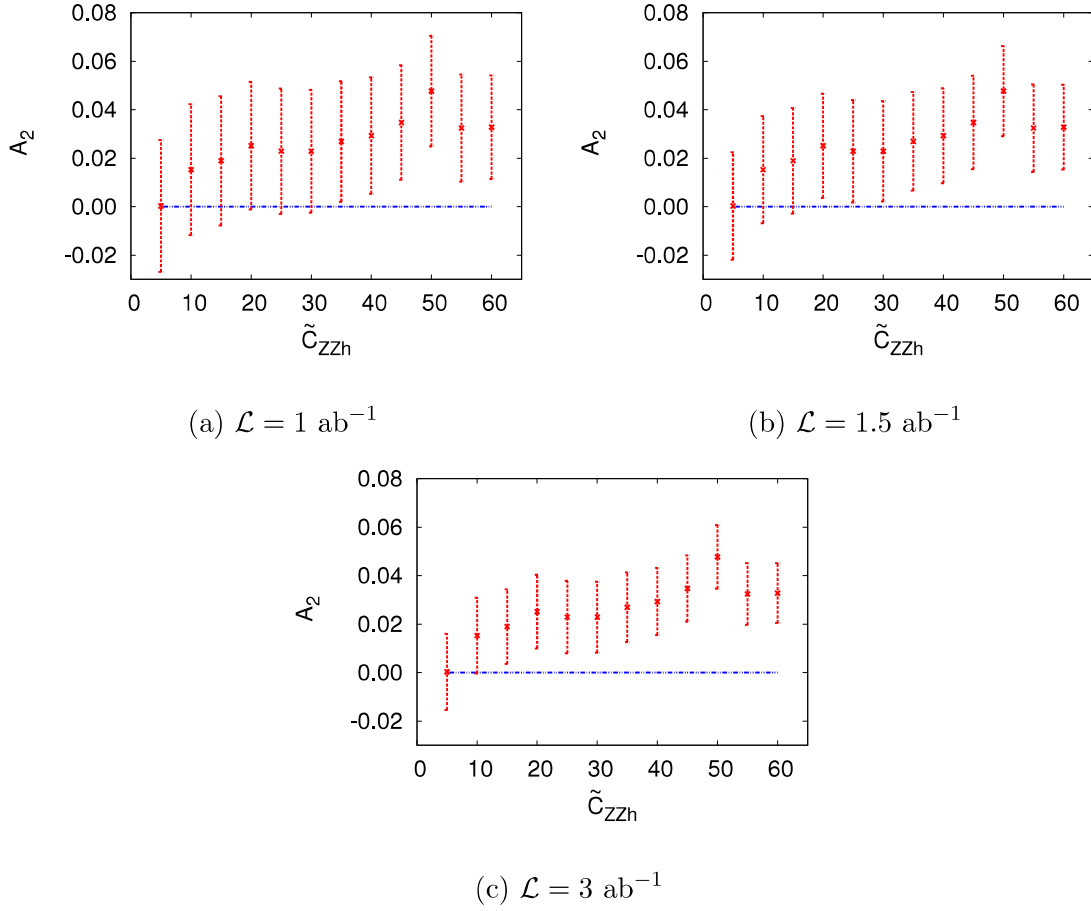


Figure 4.6: The asymmetry vs. coupling plot for the variable \mathcal{O}_2 at Luminosities 1 ab^{-1} , 1.5 ab^{-1} and 3 ab^{-1} , plotted for varying \tilde{C}_{ZZh} . The benchmark points are chosen such that $\tilde{C}_{\gamma Zh} = 1.5$.

4.4 Summary

We have looked for experimentally realizing the effects of dimension-six CP-violating gauge-Higgs operators that give rise to anomalous VVh couplings. Values of the couplings consistent with global fits of the LHC data are taken. We have studied *Higgstrahlung* process ($pp \rightarrow Zh$) in presence of both CP-even and CP-odd couplings. The effects of parton showers and detector simulation have been included to make our estimates as realistic as possible. The presence of non vanishing asymmetries over and above the statistical errors is seen as the litmus test for testing the presence of CP-violating new physics. This was demonstrated by the construction of CP-odd and \hat{T} -odd observables from the momenta of the final state particles. The presence of CP-violating gauge-Higgs operators is seen to give rise to non-vanishing asymmetries for such observables, thus clearly demarcating the presence of CP-violating high scale physics. It is observed that for a benchmark value of $\tilde{C}_{ZZh} = 40.0$, asymmetry can be established at about 4σ level with 3 ab^{-1} in the 14 TeV run of the LHC.

Chapter 5

Exploring anomalous $hb\bar{b}$ and $hb\bar{b}\gamma$ couplings at the LHC and an e^+e^- collider

5.1 Introduction

A fairly generic parameterization of non-standard couplings in the gauge-Higgs sector has been exemplified in Chapters 3 and 4 using the set of dimension-six CP-odd and even operators. A model-independent approach has been taken in exploring non-standard Lorentz structures of the couplings of the Higgs to the gauge bosons and the kind of kinematic observables that are sensitive to the new physics in this sector have also been discussed. Along similar lines, one may hope to seek new physics in Higgs decay channels which are “rare” within SM. Such rare or suppressed decays are expected to be sensitive to any new physics that may have distinct signatures in select regions of the phase space of the corresponding decay channels. One such rare decay of the higgs within SM, *i.e.* $h \rightarrow b\bar{b}\gamma$ is discussed here, the underlying purpose being the search for anomalous $hb\bar{b}\gamma$ interactions.

One can argue for such a three body decay to be a viable probe candidate because as much as the (effective) couplings of the ‘Higgs’ to gauge boson pairs are being probed with increasing precision (largely because of either the abundance or the distinctiveness of the resulting final states), the measurements of Higgs couplings to fermion pairs, especially those to $b\bar{b}$ and $\tau^+\tau^-$ pairs, still exhibit considerable uncertainty. For $hb\bar{b}$ interaction, in particular, the measurement of total rates of two-body decays (as reflected in the so-called

signal strength, namely, $\mu = \sigma/\sigma_{SM}$) remains the only handle, and is beset with a big error-bar. The decay kinematics for $h \rightarrow b\bar{b}$ is also difficult to use to one's benefit. This is because (a) the two-body decay is isotropic in the rest frame of h , a spinless particle, and (b) the b -hadrons mostly do not retain information such as that of the polarisation of the b -quark formed.

Such information could have potentially revealed useful clues on the Lorentz structure of the $hb\bar{b}$ coupling, where a small deviation from the SM nature could be a matter of great interest. This is what stonewalls investigations based on model-independent, gauge-invariant effective couplings, of which exhaustive lists exist in the literature [3, 12].

Under such circumstances, one line of thinking, where one may be greeted by new physics, is to look *not* for effective couplings involving the Higgs-like object and a $b\bar{b}$ -pair, but *those which lead to three-body decays of the h rather than a two-body one*. We investigate this possibility by considering the $hb\bar{b}\gamma$ effective interaction. This interaction should exhibit departure from the SM character as a result of new physics in the sector comprising the h and the bottom quark, contributing to the three-body radiative decay $h \rightarrow b\bar{b}\gamma$. Just like the $hb\bar{b}$ effective coupling, the anomalous ‘radiative coupling’, too, can be motivated from dimension-six gauge-invariant effective operators. However, the coefficients of such operators are much less constrained from existing data. This immediately implies possible excess/modification in the signal rate for $pp \rightarrow hX \rightarrow b\bar{b}\gamma X$. The signal, however, can be mimicked by not only SM channels but also radiative Higgs decays where anomalous $hb\bar{b}$ interactions play a part. We show that current constraints allow such values of the effective $hb\bar{b}\gamma$ coupling strength, for which the resulting three-body radiative Higgs decays can be distinguished from standard model backgrounds at the LHC as well as high-energy e^+e^- colliders. Furthermore, they lead to excess $b\bar{b}\gamma$ events at a rate which cannot be faked by anomalous $hb\bar{b}$ interaction, given the existing constraints on the latter.

In section 5.2 we discuss the effective Lagrangian terms sourcing the above mentioned couplings parameterising the BSM contribution to the Higgs interaction terms. In this section, we also discuss the higher-dimensional operators which can give rise to such terms, and show the constraints on the new parameters using Higgs measurement data at the LHC. In section 5.3, we present the collider analyses for the two BSM scenarios (those involving anomalous $hb\bar{b}\gamma$ as well as $hb\bar{b}$ couplings) we consider here in the context of both the LHC and e^+e^- colliders. A kinematic variable is also proposed which can help to distinguish between a two-body and a three-body Higgs decay giving rise to similar final states. We summarise and conclude in section 5.4.

5.2 Higgs-bottom anomalous coupling

5.2.1 Parameterization of the interactions

As has already been stated, we adopt a model-independent approach, parameterizing the anomalous $hb\bar{b}\gamma$ vertex in terms of Wilson coefficients that encapsulate the effects of the high scale theory entering into low-energy physics. Such interaction terms follow from $d > 4$, $SU(2) \times U(1)$ gauge-invariant operators. This is consistent with the assumption that their origin lies above the electroweak symmetry breaking scale.

The anomalous interactions relevant for our study are as follows:

- The $hb\bar{b}\gamma$ vertex of the form

$$\mathcal{L}_{hb\bar{b}\gamma} = \frac{1}{\Lambda^2} F^{\mu\nu} \bar{b} \sigma_{\mu\nu} (d_1 + id_2 \gamma_5) b h \quad (5.2.1)$$

Such an effective coupling can arise out of dimension-six operators of the form [12]

$$O_{dB} \sim \frac{1}{\Lambda^2} (\bar{q}_p \sigma^{\mu\nu} d_r) \Phi B_{\mu\nu} \quad (5.2.2)$$

and

$$O_{dW} \sim \frac{1}{\Lambda^2} (\bar{q}_p \sigma^{\mu\nu} d_r) \tau^i \Phi W_{\mu\nu}^i \quad (5.2.3)$$

where Φ , q and d are the scalar doublet, left-handed quark doublet and right-handed down type quarks respectively, and $B_{\mu\nu}$ and $W_{\mu\nu}$ are the $U(1)$ and $SU(2)_L$ field strength tensors respectively. Λ is the cut-off scale at which new physics sets in ¹.

- An $hb\bar{b}$ anomalous vertex modifying the SM coupling strength, can be a potential contributor to the process $h \rightarrow b\bar{b}\gamma$. The modification to the SM $hb\bar{b}$ coupling may be written as

$$\mathcal{L}_{hb\bar{b}} = \left(\frac{gm_b}{2m_W} \right) \bar{b} (c_1 + ic_2 \gamma_5) b h. \quad (5.2.4)$$

where m_b and m_W are the b -quark and W -boson mass respectively. Again, such interactions may be generated from dimension-six fermion-Higgs operators of the kind [12]

$$O_{d\phi} \sim \frac{C}{\Lambda^2} (\Phi^\dagger \Phi) (\bar{q}_p d_r \Phi) + \text{h.c.} \quad (5.2.5)$$

¹Throughout this work, we have assumed $\Lambda = 1$ TeV

for a complex C . It should be noted that both the sets $\{d_1, d_2\}$ and $\{c_1, c_2\}$ include the possibility of CP-violation, a possibility that cannot be ruled out in view of observations such as the baryon-antibaryon asymmetry in our universe. Thus both of the paired parameters in each case should affect event rates at colliders, irrespectively of whether CP-violating effects can be discerned.

Note that only the contribution from the third family in Eqs. 5.2.2, 5.2.3 and 5.2.5 have been included in the present study. While all possible higher-dimensional operators are in principle to be included in an effective field theory approach, the proliferation of terms (and free parameters) caused by such universal inclusion will make any phenomenological study difficult. Keeping in mind and remembering that our purpose here is to look for non-standard Higgs signals based on b -quark interactions, we have assumed that only the terms with $p=r=3$ are non-vanishing in Eqs. 5.2.2, 5.2.3 and 5.2.5.

Fig. 5.1 illustrates how the anomalous couplings affect the three-body decay of the Higgs boson into $b\bar{b}\gamma$ in the two scenarios described above. As has been mentioned in the introduction, our interest is primarily on the first set of anomalous operators, as they have not yet been investigated. However, any observable effect arising from them can in principle be always faked by interactions of the second kind, and therefore the latter need to be treated with due merit in the study of the final states of our interest.

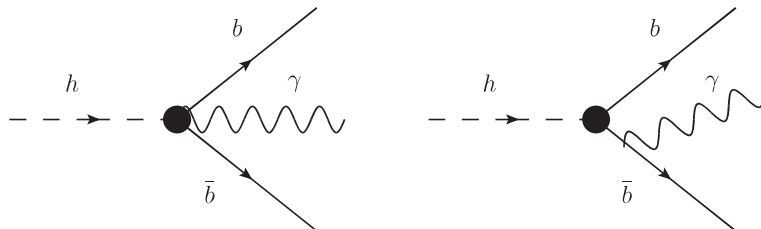


Figure 5.1: $h \rightarrow b\bar{b}\gamma$ via anomalous couplings $hb\bar{b}$ and $hb\bar{b}\gamma$.

5.2.2 Constraints from Higgs data and other sources

The addition of a non-standard Higgs vertex or having the standard interaction terms with modified coefficients will change the Higgs signal strengths ($\mu = \sigma/\sigma_{SM}$). The Higgs-related data at the LHC already put strong constraints on such deviations, the measured values of μ being always consistent with unity at the 2σ -level. The non-standard effects under consideration here will have to be consistent with such constraints to start with. In applying these constraints, we have taken the most updated measurements of various μ -values provided by

ATLAS and CMS so far [30, 155–158, 160, 225–230]. These values and their corresponding 1σ error bars, based on the (7+8) TeV data, are shown in Table 5.1. The non-standard effective

Decay channel	ATLAS+CMS
$\mu^{\gamma\gamma}$	$1.16_{-0.18}^{+0.20}$ [155, 156]
μ^{ZZ}	$1.31_{-0.24}^{+0.27}$ [157, 158]
μ^{WW}	$1.11_{-0.17}^{+0.18}$ [160, 226, 229]
$\mu^{\tau\tau}$	$1.12_{-0.23}^{+0.25}$ [228, 230]
μ^{bb}	$0.69_{-0.27}^{+0.29}$ [225, 227]

Table 5.1: ATLAS and CMS $\sqrt{s}=7$ and 8 TeV combined μ values along with their total uncertainties for different Higgs boson decay channels as quoted in Table 11 of Ref. [30].

interaction terms in Eq. 5.2.1 and 5.2.4 have been added to the existing SM Lagrangian using FeynRules [153, 231] modifying the CP-even coupling coefficient in the $hb\bar{b}$ vertex in the latter case to $(1 + c_1)\frac{gm_b}{2m_W}$.

First consider the effective $hb\bar{b}\gamma$ vertex scenario. This vertex does not contribute to any of the standard Higgs decay modes and gives rise to the three-body decay $h \rightarrow b\bar{b}\gamma$. This invites an additional perturbative suppression by α_{em} within the framework of the SM, and also in presence of the anomalous couplings $\{c_1, c_2\}$. However, the dimension-6 operators shown in Eq. 5.2.2 and 5.2.3 can in principle boost this decay channel, depending on the values of d_1 and d_2 . To the best of our understanding, no dedicated search for $h \rightarrow b\bar{b}\gamma$ has been reported so far. We therefore depend on global fits of the LHC data which yield an upper limit of about 23% [14] on any non-standard decay branching ratio (BR) of the 125 GeV scalar at 95% confidence level. This includes, for example, invisible decays as well as decays into light-quark or gluon jets. In our case, the same limit is assumed to apply on $\text{BR}(h \rightarrow b\bar{b}\gamma)$, which translates into a bound on the couplings $|d_1|, |d_2| \leq 10$ for $d_1 \approx d_2$. However, such a large BR for $h \rightarrow b\bar{b}\gamma$ might affect the event count for a $h \rightarrow b\bar{b}$ study if the photon goes untagged. Also, it might come into conflict with the predicted two-gluon BR for the Higgs, if the invisible decay width gets further constrained by even a small amount. In view of this, this analysis incorporates a relatively conservative choice, namely, $|d_1|, |d_2| \leq 5$. It is found that, even with such values, the contribution to $\text{BR}(h \rightarrow b\bar{b}\gamma)$ is about one order higher than what could come from purely SM interactions. Thus the effects of such additional couplings are unlikely to be faked by SM effects. The new physics parameters d_1 and d_2 are

not constrained from any other experimentally measured quantities. In principle, d_2 could be constrained from neutron electric dipole moment (nEDM) measurement [165, 167, 168, 232] since the presence of the $hb\bar{b}\gamma$ vertex can lead to contribution to the up quark EDM at one-loop level as shown in Fig. 5.2. The contribution to the up quark EDM (d_u) coming

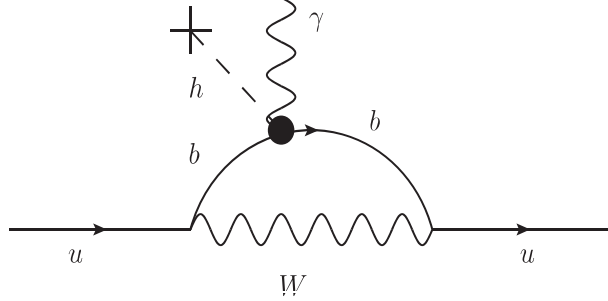


Figure 5.2: Contribution to the up-quark EDM arising from the anomalous $hb\bar{b}\gamma$ vertex at one loop.

from this anomalous vertex is given as

$$\frac{d_u}{e} \simeq \frac{d_2}{3} \frac{m_u m_b}{m_W^2 - m_b^2} \left(\frac{|V_{ub}|g}{2\sqrt{2}} \right)^2 \left(\frac{v}{\Lambda^2} \right) K(\Lambda, m_W, m_b) \quad (5.2.6)$$

where $K(\Lambda, m_W, m_b) = \frac{1}{4\pi^2} \left[\frac{5}{8} + \frac{3}{4} \ln\left(\frac{\Lambda^2}{m_W^2}\right) - \ln\left(\frac{\Lambda^2}{m_b^2}\right) \right]$.

Here m_u is the up quark mass, m_W is the mass of W boson, m_b is the b -quark mass and v is the Higgs vacuum expectation value respectively. As is evident from Eq. 5.2.6, the contribution to nEDM from such a diagram is proportional to the amplitude squared of the quark mixing element *i.e.*, $|V_{ub}|^2$. The smallness of $|V_{ub}|$ ($\sim 4 \times 10^{-3}$) results in a suppressed nEDM contribution and thus the constraint on d_2 becomes much more relaxed as compared to that derived from non-standard Higgs decay branching ratio constraint.

The situation is different for the anomalous effective $hb\bar{b}$ vertex scenario. Since this vertex directly affects the most dominant Higgs decay mode, *i.e.* $h \rightarrow b\bar{b}$, the existing Higgs data impose a much more severe constraint on the non-standard couplings in this case, since even a small change in the $\text{BR}(h \rightarrow b\bar{b})$ can alter the other SM Higgs signal strengths significantly. In order to ascertain the consequently allowed values of $\{c_1, c_2\}$, we compute the corresponding μ -values within our effective theory framework. Non-vanishing c_1, c_2 are assumed to keep the Higgs production rate unaffected, and all other Higgs couplings are assumed to be SM-like for simplicity of the analysis. The allowed regions thus obtained at the 95.6% C.L. are shown in Fig. 5.3.

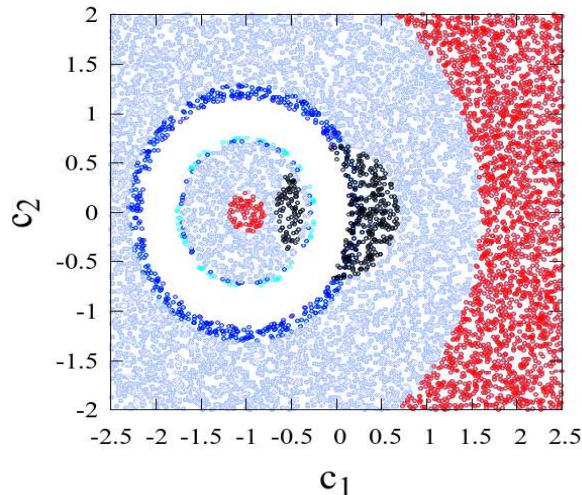


Figure 5.3: The light blue, red, blue, cyan and black points indicate the regions of the parameter space excluded from the signal strength (μ) measurements of $\tau\bar{\tau}$, $b\bar{b}$, $\gamma\gamma$, WW^* and ZZ^* decay modes of the Higgs at 2σ level. The blank space is the allowed region.

The white annular region in Fig. 5.3 represents the allowed 95.6% C.L. parameter space in the c_1 - c_2 plane. The light blue, red, blue, cyan and black regions are excluded by the measurement of $\mu^{\tau\tau}$, μ^{bb} , $\mu^{\gamma\gamma}$, μ^{WW} and μ^{ZZ} respectively. Note that large positive values of c_1 will be disfavored since it tends to enhance $\text{BR}(h \rightarrow b\bar{b})$ beyond acceptable limits.

5.3 Collider Analysis

Collider signatures of possible anomalous Higgs vertices have been studied both theoretically, see e.g. [4, 5, 13, 116, 135, 136, 141, 193, 200–203, 206, 233–239], and experimentally [109, 240]. However, as has been already stated, none of these studies include three-body decays such as $h \rightarrow b\bar{b}\gamma$ and their possible signals at colliders.

Keeping collinear divergences in mind, we have retained the b-quark mass. In addition, we make sure that the photon is well-separated from the b -partons at the generation level. The non-standard effective Lagrangian terms have been encoded using FeynRules in order to generate the model files for implementation in MadGraph [152, 241] which was used for computing the required cross-sections and generating events for collider analyses. The Higgs branching ratios are calculated at the tree-level.

We have put a minimum isolation, namely, $\Delta R > 0.4$, between any two visible particles

in the final state while generating the events at the parton level. Additionally, we have put minimum p_T thresholds on both the b -jets and the photon, namely, $p_T^b > 20$ GeV and $p_T^{\gamma,\ell} > 10$ GeV. These cuts ensure that a certain angular separation is maintained among the final state particles, thus avoiding the infrared and collinear divergences in the lowest order calculation. For the effective $hb\bar{b}\gamma$ scenario, MadGraph treats $h \rightarrow b\bar{b}\gamma$ as just another non-standard decay of the Higgs at the tree level. However, for the effective $hb\bar{b}$ scenario, the γ has to be radiated from one of the b -partons originating from h . The cancellation of the already mentioned infrared/collinear divergences in such a case calls for a full one-loop calculation. We have checked using MadGraph that the one-loop corrected Higgs decay width in the framework of the SM differs from that at the leading order by a factor of ~ 1.1 . Hence with such loop-corrected Higgs decay width the relevant branching ratio ($\approx 10^{-4}$) does not differ by more than 1-2%. We have thus retained the tree-level branching ratio for $h \rightarrow b\bar{b}\gamma$.

After generating events with MadGraph, we have used PYTHIA [221] for the subsequent decay, showering and hadronization of the parton level events. For the LHC analysis we have used the nn23lo1 [26] parton distribution function and the default dynamic renormalisation and factorisation scales [242] in MadGraph for our analysis. Finally, detector simulation was done using Delphes3 [222]. The b -tagging efficiency and mistagging efficiencies of the light jets as b -jets incorporated in Delphes3 can be found in [243, 244]². Jets were constructed using the anti- k_T algorithm [245]. The following cuts were applied on the jets, leptons and photons at the parton level in Madgraph while generating all the events throughout this work:

- All the charged leptons and jets including b -jets are selected with a minimum transverse momentum cut of 20 GeV, $p_T^{b,\ell} > 20$ GeV. They must also lie within the pseudo-rapidity window $|\eta|^{b,\ell} < 2.5$. For e^+e^- collider analysis, the lepton p_T requirement is changed to $p_T^\ell > 10$ GeV following [246].
- All the photons in the final state must satisfy $p_T^\gamma > 10$ GeV and $|\eta|^\gamma < 2.5$.
- In order to make sure that all the final state particles are well-separated, we demand

² b -tagging efficiency used in the context of the LHC: $0.8 \times \tanh(0.003 p_T^b) \times \frac{30.0}{1+0.086 p_T^b}$ and that in the context of e^+e^- collider: $0.85 \times \tanh(0.002 p_T^b) \times \frac{25.0}{1+0.063 p_T^b}$. Mistagging efficiency of a c -jet as a b -jet in the context of LHC: $0.2 \times \tanh(0.02 p_T^c) \times \frac{1.0}{1+0.0034 p_T^c}$ and that in the context of e^+e^- collider: $0.25 \times \tanh(0.018 p_T^c) \times \frac{1.0}{1+0.0013 p_T^c}$. The mistagging efficiency of the other light-jets as b -jets is $\sim 0.2\%$ and $\sim 1\%$ at the LHC and e^+e^- colliders respectively.

$\Delta R > 0.4$ between all possible pairs.

Note that the hardest photon in the final state has been tagged in order to reconstruct the 125 GeV Higgs mass. In the signal process we always obtain one such hard photon arising from Higgs decay. However, for the background processes, events can be found with an isolated bremsstrahlung photon or one coming from π^0 decay. In general, photons from showering as well as initial state radiation do constitute backgrounds to our signal, and the selection cuts need to be chosen so as to suppress them.

5.3.1 Effective $hb\bar{b}\gamma$ scenario

LHC Search

To start with, we are concerned with $b\bar{b}$ -pairs (along with a photon) being produced in Higgs decay. Existing studies indicate that, in such a case, Z -boson associated production, with Z decaying into an opposite-sign same-flavor lepton pair, is the most suitable one for studying such final states [227]. We thus concentrate on

$$pp \rightarrow Zh, h \rightarrow b\bar{b}\gamma, Z \rightarrow \ell^+\ell^- \quad (5.3.1)$$

leading to the final state $\ell^+\ell^-b\bar{b}\gamma$, with $\ell = e, \mu$. One can also look for associated Wh production where W decays leptonically to yield the $\ell + b\bar{b}\gamma$ final state ($\ell = e, \mu$). However, the signal acceptance efficiency is smaller compared to that for the Z -associated production channel [227], where the invariant mass of the lepton-pair from Z -decay can be used to one's advantage. Higgs production via vector boson fusion (VBF) can be another possibility which, however, is more effective in probing gauge-Higgs anomalous vertex [6, 195]. Higgs production associated with a top-pair has a much smaller cross-section [247] and hence is not effective for such studies. Finally, the most dominant Higgs production mode at the LHC, namely, gluon fusion, can give rise to a $b\bar{b}\gamma$ final state which is swamped by the huge SM background.

The main contribution to the SM background comes from the following channels:

1. $pp \rightarrow Zh\gamma, h \rightarrow b\bar{b}, Z \rightarrow \ell^+\ell^-$
2. $pp \rightarrow t\bar{t}\gamma, t \rightarrow bW^-, W^- \rightarrow \ell^-\nu$
3. $pp \rightarrow \ell^+\ell^-b\bar{b}\gamma$
4. $pp \rightarrow \ell^+\ell^-jj\gamma$

Let us re-iterate that the radiative process can in each case be faked by the corresponding process without the photon emission but with the photon arising through showering. Such showering photons, however, are mostly softer than what is expected of the signal photons, since the latter come from three-body decays of the 125 GeV scalar, and thus their p_T peaks at values close to 40 GeV.

We use the following criteria (**C0**) for the pre-selection of our final state:

- The number of jets in the final state: $N_j \geq 2$.
- At least one, and not more than two b -jets: $1 \leq N_b \leq 2$.
- One hard photon with $E_T \geq 20$ GeV.
- Two same-flavor, opposite-sign charged leptons (e, μ).

Such final states are further subjected to the following kinematical criteria:

- **C1:** $\cancel{E}_T < 30$ GeV.
- **C2:** An invariant mass window for the invariant mass $M_{b\bar{b}(j)\gamma}$ (see Fig. 5.4): $105 \text{ GeV} \leq M_{b\bar{b}(j)\gamma} \leq 135 \text{ GeV}$. When two b -jets are tagged, both are included. When only one b is identified, it is combined with the hardest of the remaining jets together with the hardest photon.
- **C3:** An invariant mass window for the associated lepton pair: $(m_Z - 15 \text{ GeV}) \leq M_{\ell^+\ell^-} \leq (m_Z + 15 \text{ GeV})$.
- **C4:** Finally, the Z and h are produced almost back-to-back in the transverse plane for our signal process. This, along with the fact that the Higgs decay products are considerably boosted in the direction of the Higgs, prompts us to impose an azimuthal angle cut between the photon and the dilepton system (Fig. 5.5): $\Delta\phi(\gamma, \ell^+\ell^-) > 1.5$.

Among the selection criteria listed above, we have checked that **C2** and **C4** are effective in reducing the contamination from showering photons.

We present the results of our analysis for $\sqrt{s} = 14$ TeV. Signal events were generated for $d_1 = d_2 = 5.0$ which results in $\text{BR}(h \rightarrow b\bar{b}\gamma) \simeq 5\%$.

Tables 5.2 and 5.3 show the signal rates and the response of signal and background events to the cuts mentioned above. Since the production cross-section is small to start with, one

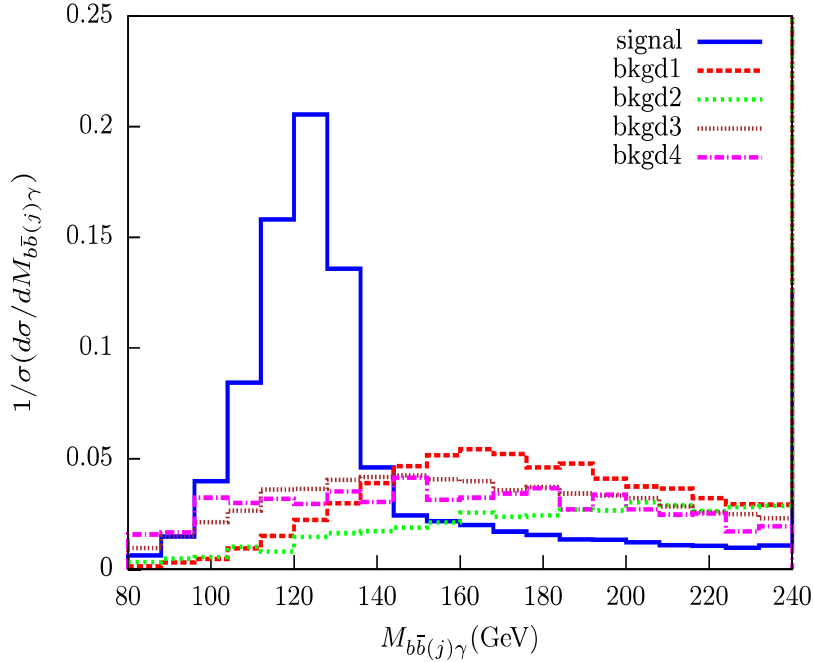


Figure 5.4: Normalized distribution for $M_{b\bar{b}(j)\gamma}$ for the signal process ($d_1 = 5.0$, $d_2 = 5.0$) and various background channels : “bkgd1” refers to $pp \rightarrow Zh\gamma$, “bkgd2” to $pp \rightarrow t\bar{t}\gamma$, “bkgd3” to $pp \rightarrow \ell^+\ell^-b\bar{b}\gamma$ and “bkgd4” to $pp \rightarrow \ell^+\ell^-jj\gamma$ respectively.

depends on the high luminosity run of the LHC. As seen from Table 5.2, the 8 TeV run has understandably been inadequate to reveal the signal under investigation. Hence any hope of seeing the signal events lies in the high-energy run (14 TeV). A detailed cut-flow table for both the signal and background events is shown in Table 5.3.

As we can see, contributions to the background from $pp \rightarrow Zh\gamma$ is reduced by the cuts rather significantly, whereas $pp \rightarrow \ell^+\ell^-jj\gamma$ contributes the most. Demanding two b -tagged jets in the final state would have significantly reduced this background, given the faking probability of a light jet as a b -jet (as emerging from DELPHES). However, that would have reduced our signal events further, since the second hardest b -jet peaks around 30 GeV, and thus the tagging efficiency drops. The next largest contributor to the background events is the process $pp \rightarrow \ell^+\ell^-b\bar{b}\gamma$. The invariant mass and $\Delta\phi$ cuts play rather important roles in reducing both this background and the one discussed in the previous paragraph. The $t\bar{t}\gamma$ production channel, too, could contribute menacingly to the background. However, the large missing transverse energy associated with this channel allows us to suppress its effects, by requiring $\cancel{E}_T < 30$ GeV. Further enhancement of the signal significance occurs via invariant mass cuts on the $b\bar{b}\gamma$ and $\ell^+\ell^-$ systems. In principle, one may also expect some significant

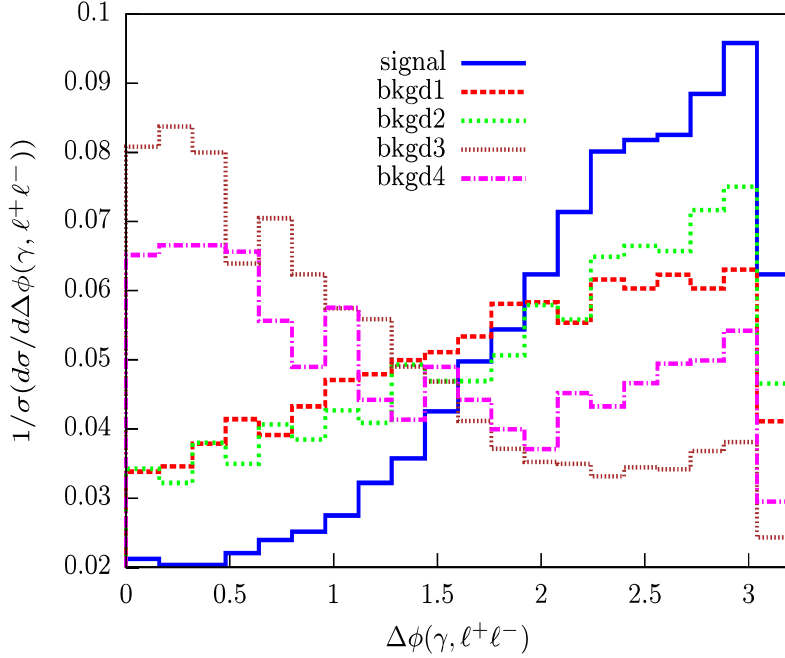


Figure 5.5: Normalized distribution for $\Delta\phi(\gamma, \ell^+\ell^-)$ for the signal process ($d_1 = 5.0, d_2 = 5.0$) and various background channels : “bkgd1” refers to $pp \rightarrow Zh\gamma$, “bkgd2” to $pp \rightarrow t\bar{t}\gamma$, “bkgd3” to $pp \rightarrow \ell^+\ell^-b\bar{b}\gamma$ and “bkgd4” to $pp \rightarrow \ell^+\ell^-jj\gamma$ respectively.

contribution to the background from the production channels $t\bar{t}W^\pm\gamma$ and $W^+W^-\gamma + \text{jets}$. However, these channels are associated with large \cancel{E}_T . We have checked that the our \cancel{E}_T and $M_{b\bar{b}(j)\gamma}$ requirements render these background contributions negligible. On the whole, the background contributions add up to a total of 165 events compared to 29 signal events at 1000 fb^{-1} for our choice of $d_1 = d_2 = 5.0$, which amounts to a statistical significance³ of 2.2σ for the $\ell^+\ell^-b\bar{b}\gamma$ final state. Hence a 3σ statistical significance can be achieved for such a signal at 14 TeV with a luminosity $\sim 1900 \text{ fb}^{-1}$. Such, and higher, luminosities should be able to probe the signature of the the $hb\bar{b}\gamma$ effective interaction with strength well within the present experimental limits.

Search at an e^+e^- collider

It is evident from the previous section that the scenario under consideration can be probed at least with moderate statistical significance at the LHC at high luminosity at the 14 TeV

³The statistical significance (\mathcal{S}) of the signal (s) events over the SM background (b) is calculated using $\mathcal{S} = \sqrt{2 \times [(s+b)\ln(1 + \frac{s}{b}) - s]}$.

Process	$\sqrt{s} = 8 \text{ TeV}$	$\sqrt{s} = 14 \text{ TeV}$
	$\sigma \text{ (pb)}$	$\sigma \text{ (pb)}$
$pp \rightarrow Zh, h \rightarrow b\bar{b}\gamma$	1.795×10^{-4}	3.332×10^{-4}

Table 5.2: Cross sections at LHC for our signal processes at $\sqrt{s} = 8 \text{ TeV}$ and 14 TeV .

Process	$\sqrt{s} = 14 \text{ TeV}$					
	$\sigma \text{ (pb)}$	NEV ($\mathcal{L} = 1000 \text{ fb}^{-1}$)				
		C0	C1	C2	C3	C4
$pp \rightarrow Zh, h \rightarrow b\bar{b}\gamma$	3.332×10^{-4}	83	70	41	39	29
$pp \rightarrow Zh\gamma$	4.765×10^{-5}	17	13	1	1	-
$pp \rightarrow t\bar{t}\gamma$	0.03144	5214	586	31	5	4
$pp \rightarrow \ell^+\ell^-b\bar{b}\gamma$	0.01373	3149	2507	345	98	54
$pp \rightarrow \ell^+\ell^-jj\gamma$	3.589	5355	4523	427	213	107

Table 5.3: Cross-sections for the signal (corresponding to $d_1 = d_2 = 5.0$) and various background channels are shown in pb alongside the number of expected events for the individual channels at 1000 fb^{-1} luminosity after each of the cuts **C0-C4** as listed in the text. NEV \equiv number of events.

run. We next address the question as to whether an electron-positron collider can improve the reach.

An e^+e^- machine is expected to provide a much cleaner environment compared to the LHC. Here the dominant Higgs production modes are the Z -boson mediated s-channel process and gauge boson fusion processes, resulting in the production of Zh and $h\nu\bar{\nu}$ respectively [248]. The Zh mode has the largest cross-section at relatively lower center-of-mass energies (\sqrt{s}), peaking around $\sqrt{s} = 250 \text{ GeV}$. However, as \sqrt{s} increases, this cross-section goes down, making this channel less significant while the W -boson fusion production mode dominates. Hence we include both these production modes in our analysis and explore our scenario at two different center-of-mass energies, namely, $\sqrt{s} = 250 \text{ GeV}$ and 500 GeV . For $\sqrt{s} = 250 \text{ GeV}$, we consider two possible final states depending on whether Z decays into a

pair of leptons or a pair of neutrinos. For the latter final state, there is also some contribution from the W -fusion diagram, which is small but not entirely negligible. For $\sqrt{s} = 500$ GeV, however, most of the contribution comes from the $h\nu\bar{\nu}$ production via W fusion along with a small contribution from Zh production. The production channels we consider are therefore

$$e^+e^- \rightarrow Zh, Z \rightarrow \ell^+\ell^-, h \rightarrow b\bar{b}\gamma \quad (5.3.2)$$

$$e^+e^- \rightarrow \nu\bar{\nu}h, h \rightarrow b\bar{b}\gamma \quad (5.3.3)$$

resulting in the final state $\ell^+\ell^-b\bar{b}\gamma$ or $b\bar{b}\gamma + \cancel{E}$. Let us first take up the $\ell^+\ell^-b\bar{b}\gamma$ final state, which is relevant for $\sqrt{s} = 250$ GeV. The major SM background contributions are:

1. $e^+e^- \rightarrow Zh\gamma, Z \rightarrow \ell^+\ell^-, h \rightarrow b\bar{b}$
2. $e^+e^- \rightarrow \ell^+\ell^-b\bar{b}\gamma$
3. $e^+e^- \rightarrow \ell^+\ell^-jj\gamma$. with at least one j faking a b -jet.

After passing through the pre-selection cuts **C0**, the signal as well as the background events are further subjected to the following kinematical requirements:

- **D1** : Since we have two same-flavor opposite-sign leptons in the event arising from Z -decay, their momentum information can be used to reconstruct the Higgs boson mass irrespective of its decay products via the recoil mass variable defined as

$$m_{rec} \equiv \sqrt{(\sqrt{s} - E_{\ell^+\ell^-})^2 - \vec{p}_{\ell^+\ell^-}^2} \quad (5.3.4)$$

where $E_{\ell^+\ell^-}$ and $\vec{p}_{\ell^+\ell^-}$ are the net energy and three-momentum of the $\ell^+\ell^-$ system or that of the reconstructed Z -boson. This variable is free from jet tagging and smearing effects and shows a much sharper peak at the Higgs mass (M_h) compared to $M_{b\bar{b}(j)\gamma}$ as shown in Fig. 5.6. This variable is thus more effective in reducing the SM background. We demand $122 \text{ GeV} \leq m_{rec} \leq 128 \text{ GeV}$.

- **D2** : As before, we select an invariant mass window for the associated lepton pair: $(m_Z - 15 \text{ GeV}) \leq M_{\ell^+\ell^-} \leq (m_Z + 15 \text{ GeV})$.

We summarise our results for our signal and background analysis in the subsequent Tables 5.4 and 5.5. As evident from Table 5.5, variable m_{rec} is highly effective in reducing the background events resulting in a statistical significance of 3σ and 5σ at $\sim 85 \text{ fb}^{-1}$ and $\sim 250 \text{ fb}^{-1}$ integrated luminosities respectively.

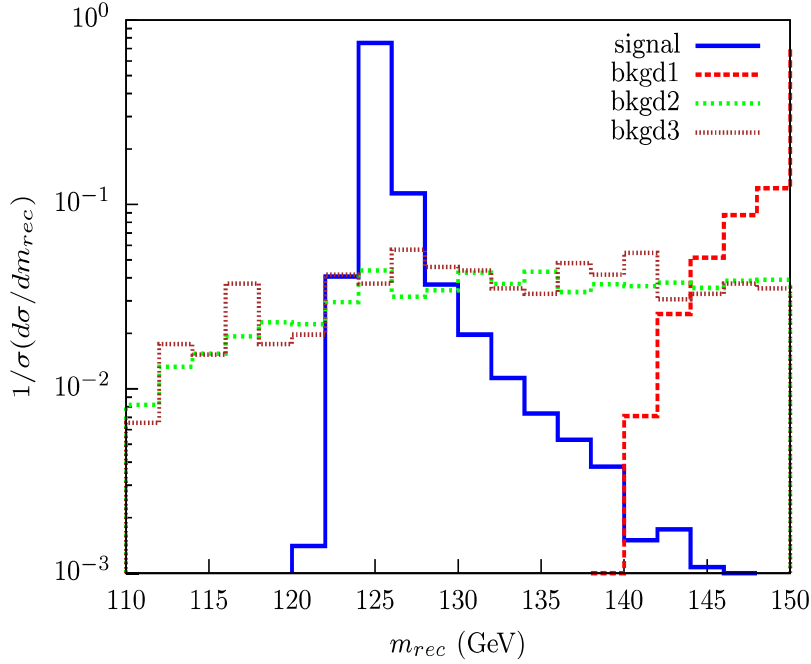


Figure 5.6: Normalized distribution for m_{rec} for the signal process ($d_1 = 5.0$, $d_2 = 5.0$) and the backgrounds at $\sqrt{s} = 250$ GeV. “bkgd1” refers to $e^+e^- \rightarrow Zh\gamma, Z \rightarrow \ell^+\ell^-, h \rightarrow b\bar{b}$, “bkgd2” to $e^+e^- \rightarrow \ell^+\ell^-b\bar{b}\gamma$ and “bkgd3” to $e^+e^- \rightarrow \ell^+\ell^-jj\gamma$ respectively.

Although the $\ell^+\ell^-b\bar{b}\gamma$ final state is capable of probing the d_1 , d_2 couplings at a reasonable luminosity, it is at the same time interesting to explore the invisible decay of the Z , which has a three times larger branching ratio than that of $Z \rightarrow \ell^+\ell^-$. In addition, the $\nu\bar{\nu}b\bar{b}\gamma$ final state can get contribution from the W -fusion process as mentioned earlier. This additional contribution becomes dominant at higher center-of-mass energies ($\sqrt{s} \gtrsim 500$ GeV) and hence for this analysis, we present our results for $\sqrt{s} = 250$ GeV and 500 GeV. The major SM backgrounds to this final state are as follows:

1. $e^+e^- \rightarrow \nu\bar{\nu}h\gamma, h \rightarrow b\bar{b}$
2. $e^+e^- \rightarrow \nu\bar{\nu}b\bar{b}\gamma$
3. $e^+e^- \rightarrow \nu\bar{\nu}jj\gamma$. with one j faking a b -jet.
4. $e^+e^- \rightarrow t\bar{t}, t \rightarrow bW^-, W^- \rightarrow \ell^-\nu$

We use the following criteria **(I0)** to pre-select our signal events:

- We impose veto on any charged lepton with energy greater than 20 GeV.

Process	$\sqrt{s} = 250 \text{ GeV}$
	$\sigma \text{ (pb)}$
$e^+e^- \rightarrow Zh, Z \rightarrow \ell^+\ell^-, h \rightarrow b\bar{b}\gamma$	2.79×10^{-4}

Table 5.4: Cross-section for the signal process ($d_1 = 5.0, d_2 = 5.0$) presented at $\sqrt{s} = 250$ GeV, before applying the cuts **C0**, **D1** and **D2**.

Process	$\sqrt{s} = 250 \text{ GeV}$			
	$\sigma \text{ (fb)}$	NEV ($\mathcal{L} = 250 \text{ fb}^{-1}$)		
		C0	D1	D2
$e^+e^- \rightarrow Zh$ $Z \rightarrow \ell^+\ell^-, h \rightarrow b\bar{b}\gamma$	0.279	13	11	11
$e^+e^- \rightarrow Zh\gamma$ $Z \rightarrow \ell^+\ell^-, h \rightarrow b\bar{b}$	0.079	1	-	-
$e^+e^- \rightarrow \ell^+\ell^-b\bar{b}\gamma$	0.990	19	3	1
$e^+e^- \rightarrow \ell^+\ell^-jj\gamma$	3.059	8	1	1

Table 5.5: Cross-section and expected number of events at 250 fb^{-1} luminosity for the signal and various processes contributing to background at $\sqrt{s} = 250$ GeV. We have used $d_1 = d_2 = 5.0$, with $\Lambda = 1$ TeV.

- Since we are working in a leptonic environment, the presence of ISR jets is unlikely. Hence we restrict the number of jets in the final state, demanding $N_j = 2$.
- Taking into account the b -jet tagging efficiency, as before, we demand $1 \leq N_b \leq 2$.
- We restrict number of hard photons in the final state: $N_\gamma = 1$.

Further, the following kinematic selections are made to reduce the SM background contributions:

- **I1:** Given the fact that the signal has direct source of missing energy (\cancel{E}), and that one can measure the net amount of \cancel{E} at an e^+e^- collider, we demand $\cancel{E} > 110$ GeV for $\sqrt{s} = 250$ GeV and $\cancel{E} > 280$ GeV for $\sqrt{s} = 500$ GeV. For illustration, in Fig. 5.7 we

have shown the \cancel{E} distribution for both the signal and background events at $\sqrt{s} = 500$ GeV.

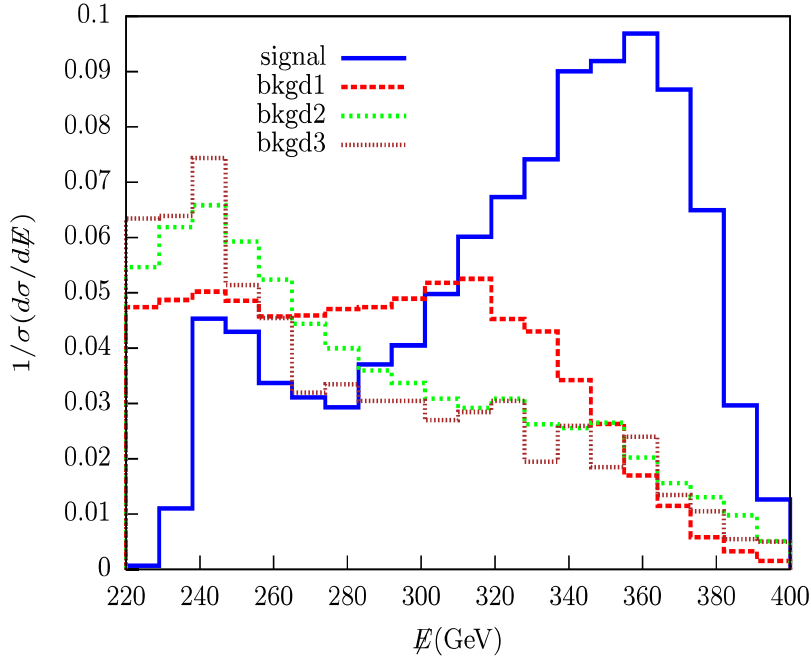


Figure 5.7: Normalized distribution for \cancel{E} for the signal process and the backgrounds at $\sqrt{s} = 500$ GeV. “bkgd1” refers to $e^+e^- \rightarrow \nu\bar{\nu}h\gamma, h \rightarrow b\bar{b}$, “bkgd2” to $e^+e^- \rightarrow \nu\bar{\nu}b\bar{b}\gamma$ and “bkgd3” to $e^+e^- \rightarrow \nu\bar{\nu}jj\gamma$ respectively.

- **I2:** Invariant mass reconstructed with the two hardest jets after ensuring that at least one of them is a b -jet, and the sole photon in the event should lie within the window (see Fig. 5.8): $90 \text{ GeV} \leq M_{b\bar{b}(j)\gamma} \leq 126 \text{ GeV}$.
- **I3:** Moreover, the invariant mass of the jet pair with $1 \leq N_b \leq 2$ should lie within the window (see Fig. 5.9): $20 \text{ GeV} \leq M_{b\bar{b}(j)} \leq 70 \text{ GeV}$.

Note that the charged lepton veto as well as the restriction on the number of jets together with the demand of a photon in the final state suppress the $t\bar{t}$ background. In addition **I1**, **I2** and **I3** turn out to be quite effective in killing the background. Once more the inclusion of **I2** plays an effective role in reducing the contribution from showering photons.

We summarise the results of our analysis in Tables 5.6 and 5.7. Table 5.6 shows the individual contributions of the Z -associated and W -fusion Higgs production channels to the total cross-section of $e^+e^- \rightarrow \nu\bar{\nu}b\bar{b}\gamma$ for $\sqrt{s} = 250$ and $\sqrt{s} = 500$ GeV.

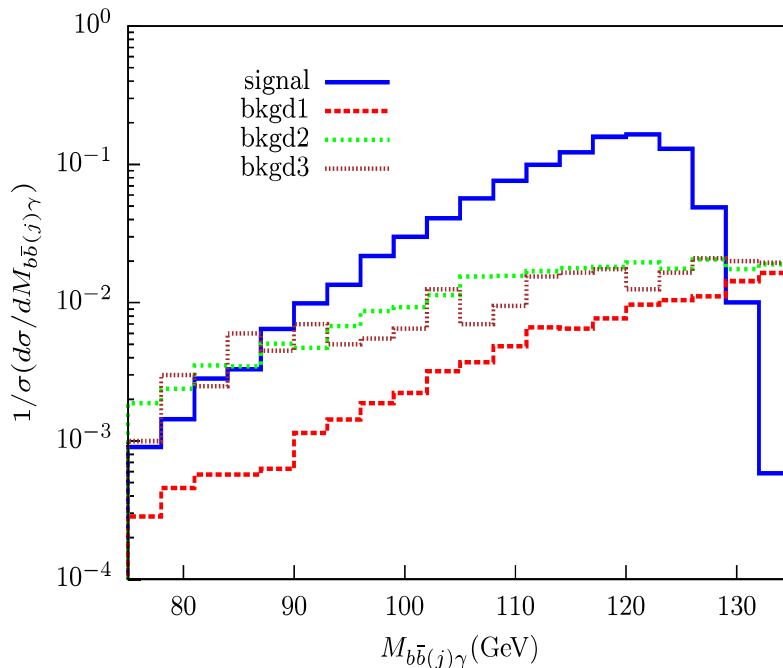


Figure 5.8: Normalized distribution for $M_{b\bar{b}(j)\gamma}$ for the signal process and the backgrounds at $\sqrt{s} = 500$ GeV.

In Table 5.7 we present the numerical results for $\sqrt{s} = 250$ GeV and $\sqrt{s} = 500$ GeV for $e^+e^- \rightarrow \nu\bar{\nu}h, h \rightarrow b\bar{b}\gamma$ and the corresponding SM backgrounds subjected to the cuts **(I0 - I3)**. It is evident from the cut-flow table that the cuts on the missing energy **(I1)** and the invariant mass of the $b\bar{b}\gamma$ system **(I2)** are highly effective in killing the SM background, so that a 3σ significance can be achieved with an integrated luminosity of $\sim 12 \text{ fb}^{-1}$ and $\sim 7 \text{ fb}^{-1}$ for $\sqrt{s} = 250$ GeV and $\sqrt{s} = 500$ GeV respectively. Thus the $\nu\bar{\nu}b\bar{b}\gamma$ final state is way more prospective compared to $\ell\bar{\ell}b\bar{b}\gamma$ final state and can be probed at a much lower luminosity at an e^+e^- collider.

Let us also comment on the CP-violating nature of the couplings $\{d_1, d_2\}$ and any such observable effect it might have on the kinematic distributions. Let us, for example, consider looking for some CP-violating asymmetry in the process $e^+e^- \rightarrow Zh \rightarrow \ell^+\ell^-b\bar{b}\gamma$. New physics only appears at the Higgs decay vertex and since the Higgs is produced on-shell, the decay part of the amplitude can be factored out from the production process. Evidently, CP-violating nature of any observable can arise out of interference terms linear in d_2 in the squared matrix element resulting from the interference of the CP-violating term in the Lagrangian with the CP-even terms (coming from the SM or the new physics vertex). However, for our case, all terms linear in d_2 vanish, either because of the masslessness of the on-shell

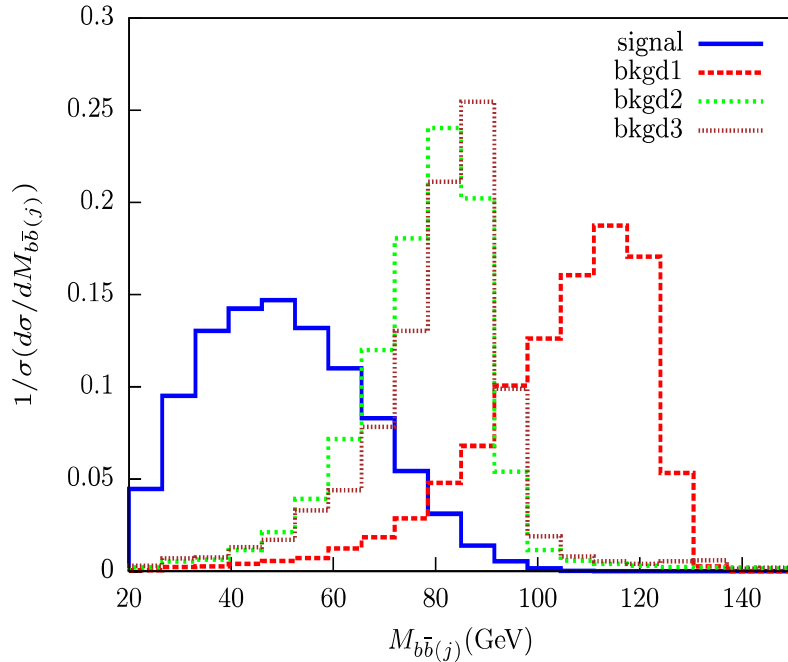


Figure 5.9: Normalized distribution for $M_{b\bar{b}(j)}$ for the signal process and the backgrounds at $\sqrt{s} = 500$ GeV.

photon or due to lack of more than three independent momenta in the Higgs decay. Although the terms proportional to $|d_2|^2$ are non-zero, they do not lead to CP-asymmetry. At the same time photon-mediated contributions to $e^+e^- \rightarrow b\bar{b}h$, too, fail to elicit any signature of CP-violation. This is again because the terms linear in d_2 in the squared matrix element multiplies the trace of four γ -matrices times γ_5 , which vanishes due to the absence of four independent four-momenta in the final state.

5.3.2 Effective $hb\bar{b}$ scenario

As mentioned earlier, the final state discussed so far may also arise for the h - b - \bar{b} effective vertex scenario where the γ is radiated from one of the b -jets. For this analysis, we choose values of c_1 and c_2 from their allowed ranges as indicated in section 5.2.2 to obtain the maximum possible signal cross-section, the choices of the parameters being $c_1 = -2.0$ and $c_2 = 0.5$, which corresponds to $\text{BR}(h \rightarrow b\bar{b}\gamma) \approx 10^{-4}$. The generation level cuts on the partonic events remain same as mentioned in the beginning of section 5.3.

As discussed earlier, the existing constraints on the $hb\bar{b}$ anomalous coupling values do not allow $\text{BR}(h \rightarrow b\bar{b}\gamma)$ to be significant. In practice it turns out to be smaller than what we

Process	$\sqrt{s} = 250 \text{ GeV}$	$\sqrt{s} = 500 \text{ GeV}$
	$\sigma \text{ (fb)}$	$\sigma \text{ (fb)}$
$e^+e^- \rightarrow Zh, Z \rightarrow \nu\bar{\nu}, h \rightarrow b\bar{b}\gamma$	0.997	0.261
$W\text{-fusion: } e^+e^- \rightarrow \nu\bar{\nu}h, h \rightarrow b\bar{b}\gamma$	0.169	1.618

Table 5.6: Individual cross-sections of the contributing production channels for the signal process $e^+e^- \rightarrow \nu\bar{\nu}h, h \rightarrow b\bar{b}\gamma$ presented at $\sqrt{s} = 250$ and $\sqrt{s} = 500$ GeV, before applying the cuts **I0 - I3**. We have used $d_1 = d_2 = 5.0$, with $\Lambda = 1$ TeV.

allowed in $hb\bar{b}\gamma$ anomalous coupling scenario by about two orders of magnitude. Hence the signal event rates expected at the LHC will be negligibly small even at very high luminosities. We therefore discuss the possibility of exploring such a scenario in the context of e^+e^- colliders.

Search at e^+e^- colliders

Similar to the analysis with d_1 and d_2 , the choices for the final state are $\ell^+\ell^-b\bar{b}\gamma$ and $b\bar{b}\gamma + \cancel{E}$. However, here we consider only the latter channel, since the former suffers from the branching suppression of the leptonic Z -decays in addition to the small value of $\text{BR}(h \rightarrow b\bar{b}\gamma)$, thus being visible at very high luminosities only.

In this case, since the new physics effect shows up in the $b\bar{b}h$ vertex, the radiatively obtained final state involving the Higgs passes off as signal. Therefore, in addition to the process in Eq. 5.3.3, the following processes also contribute to the signal now:

$$(a) e^+e^- \rightarrow \nu\bar{\nu}h\gamma, h \rightarrow b\bar{b} \quad (b) e^+e^- \rightarrow \nu\bar{\nu}h, h \rightarrow b\bar{b} \quad (5.3.5)$$

where the photon is produced in the hard scattering in (a), while in (b), it may arise from initial-state or final-state radiation⁴. Other SM processes not involving the Higgs giving rise to the same final state including a photon generated either via hard scattering or through showering will contribute to the background. The SM background contributions that we have considered here are:

1. (a) $e^+e^- \rightarrow \nu\bar{\nu}b\bar{b}\gamma$ (b) $e^+e^- \rightarrow \nu\bar{\nu}b\bar{b}$
2. (a) $e^+e^- \rightarrow \nu\bar{\nu}jj\gamma$ (b) $e^+e^- \rightarrow \nu\bar{\nu}jj$

⁴Note that, these two processes were contributing to the background in the $hb\bar{b}\gamma$ effective vertex scenario.

Process	$\sqrt{s} = 250 \text{ GeV}$					$\sqrt{s} = 500 \text{ GeV}$				
	$\sigma \text{ (fb)}$	NEV ($\mathcal{L} = 100 \text{ fb}^{-1}$)				$\sigma \text{ (fb)}$	NEV ($\mathcal{L} = 100 \text{ fb}^{-1}$)			
		I0	I1	I2	I3		I0	I1	I2	I3
$e^+e^- \rightarrow \nu\bar{\nu}h$ $h \rightarrow b\bar{b}\gamma$	1.17	41	37	36	31	1.86	70	57	53	46
$e^+e^- \rightarrow \nu\bar{\nu}h\gamma$ $h \rightarrow b\bar{b}$	0.36	4	2	1	-	1.76	62	25	3	1
$e^+e^- \rightarrow \nu\bar{\nu}b\bar{b}\gamma$	1.22	24	19	14	5	2.16	76	24	9	4
$e^+e^- \rightarrow \nu\bar{\nu}jj\gamma$	4.87	10	7	5	1	8.40	34	10	3	1
$e^+e^- \rightarrow t\bar{t}$	-	-	-	-	-	548.4	40	11	2	-

Table 5.7: Cross-section and expected number of events at 100 fb^{-1} luminosity for the signal and various processes contributing to background at $\sqrt{s} = 250$ and $\sqrt{s} = 500 \text{ GeV}$. We have used $d_1 = d_2 = 5.0$, with $\Lambda = 1 \text{ TeV}$.

Here also the background events are categorised in (a) and (b) depending on whether the photon is produced via hard scattering process or generated via showering. Here because of the choice of new physics vertex (unlike in $hb\bar{b}\gamma$ case), the showered photons may have a small contribution to the total background. The analysis has been done for two different center-of-mass energies, $\sqrt{s} = 500 \text{ GeV}$ and 1 TeV ⁵.

One needs to avoid double-counting of the signal and background events by separating the ‘hard’ photons from those produced in showers. Thus, for events with photons produced in the hard scattering process (including three body Higgs decay) we demand $p_T^\gamma > 20 \text{ GeV}$. On the other hand, photons that arise as a result of showering are taken to contribute to final states with $p_T^\gamma < 20 \text{ GeV}$.

We use the same event selection (**I0**) cuts as the previous e^+e^- analysis. We use the same \cancel{E} cut (**I1**) of 280 GeV and 750 GeV for $\sqrt{s} = 500 \text{ GeV}$ and 1 TeV respectively. We have used the same invariant mass ($M_{b\bar{b}(j)\gamma}$) cut (**I2**) for the $b\bar{b}(j)\gamma$ system. Here j is the hardest jet in those cases where only one b is tagged. However, the cut (**I3**) on the invariant mass of

⁵Our analysis with $\sqrt{s} = 250 \text{ GeV}$ reveals that, in order to probe such a scenario at an e^+e^- collider one needs a luminosity beyond 1000 fb^{-1} . Such a high luminosity is improbable for the 250 GeV run and hence those results are not discussed here.

$b\bar{b}(j)$ system has to be different in this scenario. One of the reasons for this is the fact that the radiative decay is enhanced for $p_b \approx m_b$, the emitted photon being thus often on the softer side. This can be understood in terms of the enhancement of the cross section under low momentum transfer, owing to the presence of a b -quark propagator in the radiative Higgs decay diagram. In Fig. 5.10 we have shown the two $M_{b\bar{b}(j)}$ distributions corresponding to the two scenarios considered here for the signal process $e^+e^- \rightarrow \nu\bar{\nu}h, h \rightarrow b\bar{b}\gamma$. The distribution corresponding to the $hb\bar{b}\gamma$ anomalous coupling peaks at a lower invariant mass value as compared to the $hb\bar{b}$ vertex, signaling that the photon is relatively harder in that case, as compared to that for the $hb\bar{b}$ anomalous vertex where it is produced in a radiative decay, hence is relatively softer. Accordingly, we modify **I3** to demand $50 \text{ GeV} \leq M_{b\bar{b}(j)} \leq 110 \text{ GeV}$.

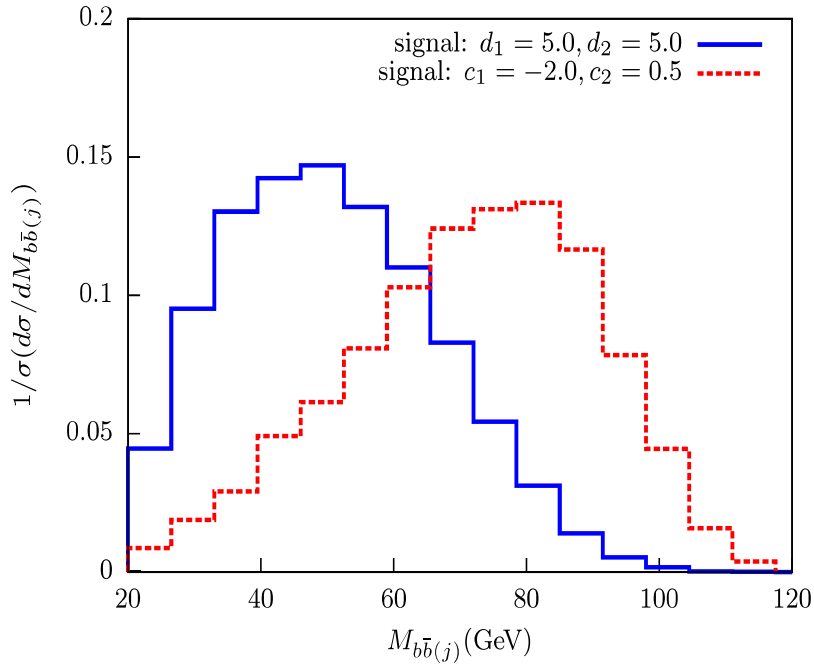


Figure 5.10: Normalized distribution for $M_{b\bar{b}(j)}$ for the signal process $e^+e^- \rightarrow \nu\bar{\nu}h, h \rightarrow b\bar{b}\gamma$ corresponding to the $hb\bar{b}\gamma$ and $hb\bar{b}$ effective vertex scenarios at $\sqrt{s} = 500 \text{ GeV}$.

In Tables 5.8 and 5.9, we present our results corresponding to the signal and background processes analysed at $\sqrt{s} = 500 \text{ GeV}$ and 1 TeV. The production cross-sections listed in Table 5.8 indicate that the rate for $e^+e^- \rightarrow \nu\bar{\nu}h, h \rightarrow b\bar{b}\gamma$ is small due to the suppression of $\text{BR}(h \rightarrow b\bar{b}\gamma)$. However, this scenario can still mimic the signal obtained in the $hb\bar{b}\gamma$ effective vertex scenario due to the large contributions to the signal process arising from the other two channels⁶.

⁶Note that an anomalous $hb\bar{b}$ vertex can be probed more effectively by studying the $h \rightarrow b\bar{b}$ decay solely.

Process	$\sqrt{s} = 500 \text{ GeV}$	$\sqrt{s} = 1 \text{ TeV}$
	$\sigma \text{ (pb)}$	$\sigma \text{ (pb)}$
$e^+e^- \rightarrow \nu\bar{\nu}h, h \rightarrow b\bar{b}\gamma$	9.98×10^{-5}	0.00023
$e^+e^- \rightarrow \nu\bar{\nu}h\gamma, h \rightarrow b\bar{b}$	0.0017	0.00523
$e^+e^- \rightarrow \nu\bar{\nu}h, h \rightarrow b\bar{b}$	0.058	0.14042

Table 5.8: cross sections for various processes contributing to signal at $\sqrt{s} = 500 \text{ GeV}$ and 1 TeV. Here $c_1 = -2.0$ and $c_2 = 0.5$.

As indicated in Table 5.9, these *other* signal contributions are significantly reduced due to our event selection and kinematic cuts which have been devised in a way such that the three-body decay of the h is revealed in the signal events more prominently. Table 5.9 shows the number of signal background events surviving after each cuts at $\mathcal{L} = 500 \text{ fb}^{-1}$. As before, in this case also the most dominant contributions to the SM background arise from $e^+e^- \rightarrow \nu\bar{\nu}b\bar{b}\gamma$ and $e^+e^- \rightarrow \nu\bar{\nu}jj\gamma$ production channels. The cuts on \mathcal{E} and $M_{b\bar{b}(j)\gamma}$ particularly help to reduce the background events. The Higgs-driven events in Table 5.9 come overwhelmingly (96-97%) from SM contributions, thus demonstrating that the $\{c_1, c_2\}$ couplings are unlikely to make a serious difference.

Since there are multiple channels contributing to signal process, it would be nice if one could differentiate among the various contributions by means of some kinematic variables or distributions. For this purpose we propose an observable $\Delta\phi(\gamma, \vec{\mathcal{E}})$ which can be distinctly different for the process where the γ is generated from h decay or produced otherwise. We show the distribution of $\Delta\phi(\gamma, \vec{\mathcal{E}})$ for the two most dominant production channels for comparison in Fig. 5.11.

The figure clearly shows the difference in the kinematic distribution between the two most dominant signal processes. For the process $e^+e^- \rightarrow \nu\bar{\nu}h, h \rightarrow b\bar{b}\gamma$, there is a sharp peak at larger $\Delta\phi$ as expected since the γ is always generated from the h decay. This feature can be used further in order to distinguish between the events arising from a two-body or a three-body decay of the Higgs.

Thus our study indicates that only the $hb\bar{b}\gamma$ coupling can be probed at a relatively smaller integrated luminosity at an e^+e^- collider. So far, in this section, we have discussed

Such analyses have already been performed in the context of e^+e^- collider [234]. Here we only study the production channels listed in Table 5.8 as complementary signal to our $hb\bar{b}\gamma$ effective vertex scenario.

Process	$\sqrt{s} = 500 \text{ GeV}$					$\sqrt{s} = 1 \text{ TeV}$				
	σ (pb)	NEV ($\mathcal{L} = 500 \text{ fb}^{-1}$)				σ (pb)	NEV ($\mathcal{L} = 500 \text{ fb}^{-1}$)			
		I0	I1	I2	I3		I0	I1	I2	I3
$e^+e^- \rightarrow \nu\bar{\nu}h$ $h \rightarrow b\bar{b}\gamma$	9.98×10^{-5}	9	8	7	6	0.00023	21	16	14	12
$e^+e^- \rightarrow \nu\bar{\nu}h\gamma$ $h \rightarrow b\bar{b}$	0.0017	297	120	17	16	0.00523	1003	362	40	37
$e^+e^- \rightarrow \nu\bar{\nu}h$ $h \rightarrow b\bar{b}$	0.058	8	7	6	5	0.14042	20	17	15	14
$e^+e^- \rightarrow \nu\bar{\nu}b\bar{b}\gamma$	0.00216	381	122	47	44	0.00494	983	329	95	91
$e^+e^- \rightarrow \nu\bar{\nu}b\bar{b}$	0.058	4	3	-	-	0.10880	7	6	1	1
$e^+e^- \rightarrow \nu\bar{\nu}jj\gamma$	0.0084	169	48	15	14	0.01851	398	124	34	32
$e^+e^- \rightarrow \nu\bar{\nu}jj$	0.21376	7	4	-	-	0.39883	11	8	2	2

Table 5.9: Cross-section and expected number of events at 500 fb^{-1} luminosity for the signal and various processes contributing to background at $\sqrt{s} = 500 \text{ GeV}$ and 1 TeV . The Higgs-driven events include both the SM contributions and those due to non-vanishing $\{c_1, c_2\}$.

the discovery potential of such a scenario for $d_1 = d_2 = 5.0$ in two possible final states, $\ell\bar{\ell}b\bar{b}\gamma$ and $b\bar{b}\gamma + \cancel{E}$ corresponding to two different centre-of-mass energies, $\sqrt{s} = 250 \text{ GeV}$ and 500 GeV . Out of these, the latter final state at $\sqrt{s} = 500 \text{ GeV}$ turns out to be most advantageous. Table 5.10, lists the required integrated luminosities in order to attain 3σ statistical significance for different values of d_1 and d_2 for the $b\bar{b}\gamma + \cancel{E}$ final state at $\sqrt{s} = 500 \text{ GeV}$.

5.4 Summary

We have studied the collider aspects of possible anomalous couplings of the 125 GeV Higgs with a $b\bar{b}$ pair and a photon. Such couplings have been obtained from gauge-invariant effective interaction terms of dimension-six. The new effective coupling parameters have been constrained from the existing Higgs measurement data at the LHC. In order to study

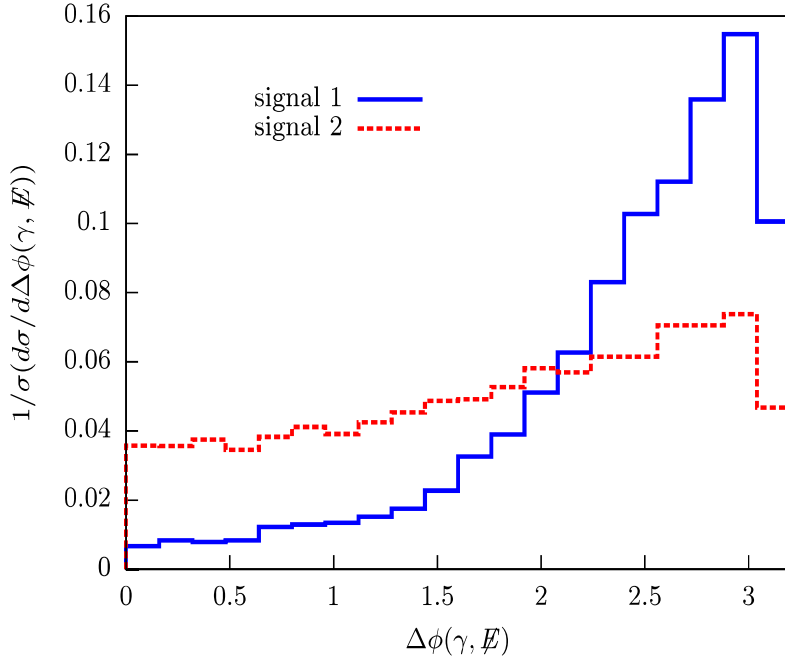


Figure 5.11: Normalized distribution for $\Delta\phi(\gamma, \vec{E})$ for the signal processes ($c_1 = -2.0$, $c_2 = 0.5$). “signal1” and “signal2” correspond to $e^+e^- \rightarrow \nu\bar{\nu}h, h \rightarrow b\bar{b}\gamma$ and $e^+e^- \rightarrow \nu\bar{\nu}h\gamma, h \rightarrow b\bar{b}$ respectively. The plot has been done with events generated at $\sqrt{s} = 500$ GeV.

the collider aspects of these new couplings we have concentrated on the three-body decay of the Higgs boson, $h \rightarrow b\bar{b}\gamma$. We have carried our analyses for the two different cases in the context of both LHC and a future e^+e^- collider.

The $hb\bar{b}\gamma$ effective coupling can be probed at the LHC with an integrated luminosity of the order of 2000 fb^{-1} with $\sqrt{s} = 14$ TeV. At an e^+e^- collider, on the other hand, such couplings can be probed at a low luminosity at $\sqrt{s} = 500$ GeV. Both results, as presented here, have been derived assuming $BR(h \rightarrow b\bar{b}\gamma) = 5\%$ for $d_1 = d_2 = 5.0$, which is allowed from the existing constraints on such non-standard couplings. With anomalous $hb\bar{b}\gamma$ interaction strengths consistent with the present constraints, integrated luminosities of the order of 7 fb^{-1} are sufficient to attain 3σ statistical significance. On the other hand, even smaller values of d_1 and d_2 can be probed at an e^+e^- collider. However, with the same centre-of-mass energy, in order to probe d_1, d_2 with values below 1, one has to go beyond 1000 fb^{-1} of integrated luminosity. In contrast, $hb\bar{b}$ anomalous couplings are much more constrained from the Higgs measurement data and thus events driven by them give rise to smaller signal excess.

The radiative decay $h \rightarrow b\bar{b}\gamma$ with potential contributions from anomalous $hb\bar{b}$ interac-

Process	Required Luminosity (fb⁻¹) at $\sqrt{s} = 500$ GeV (Final State: $b\bar{b}\gamma + \cancel{E}$)
$d_1 = d_2 = 5.0$	6.79
$d_1 = d_2 = 1.5$	337.5
$d_1 = d_2 = 1.0$	1572.6

Table 5.10: Required integrated luminosities to attain 3σ statistical significance corresponding to the final state $b\bar{b}\gamma + \cancel{E}$ at the centre-of-mass energy, $\sqrt{s} = 500$ GeV for different values of $hb\bar{b}\gamma$ anomalous couplings, $\{d_1, d_2\}$.

tions also contributes to similar final states and hence has been studied separately. Our analysis reveals that the expected event rates from three-body Higgs decay driven by $hb\bar{b}$ anomalous couplings, are unlikely to be statistically significant. It was found that the possible enhancement in the signal rates over the SM predictions because of the presence of the non-standard couplings $\{c_1, c_2\}$, consistent with their existing constraints, can be at most by a factor of 1.12. In such cases the final state arising from the three-body decay of the Higgs boson can also be mimicked by its two-body decay if a photon generated via hard scattering (contributed by processes involving t -channel W exchange, and not photon from Higgs decay) is tagged after the cuts. Hence we have proposed a kinematic variable $(\Delta\phi(\gamma, \vec{\cancel{E}}))$ (Fig. 5.11) that can be used to differentiate between these final state events.

Chapter 6

Two-Higgs doublet models

In the quest for new physics at colliders, especially in the electroweak symmetry breaking sector, we have adopted a model-independent approach in Chapters 3-5, using effective operators. The power of this approach lies in the fact that one can be unbiased about UV completion, and build from low-energy features manifest through effective operators and the corresponding Wilson coefficients. However, it is often instructive to simultaneously focus on specific renormalizable scenarios, with specific issues in view, and see which features of these models address some particular questions. Such a model-dependent study will be discussed in this and the next chapter. We concentrate in particular on one of the simplest possible extensions of the SM Lagrangian, where we extend the scalar sector of the SM by adding another scalar doublet. Such an extension, as we will argue in what follows, has wide-ranging phenomenological implications, out of which we shall discuss a chosen few.

6.1 Two-Higgs doublet models (2HDM) : Motivation

The extension of the scalar sector of the SM to incorporate two Higgs doublets can be motivated in various ways. One of the reasons stems from the fact that some popular theories like supersymmetry (SUSY) require at least two Higgs doublets.

Furthermore, though not in SUSY, a 2HDM can be make the scalar sector the source of extra CP violating phase(s), thus raising hopes for an explanation of baryon asymmetry [249–255]. People have also been interested to make the scalar sector a repository of dark matter particles, for example, through the formulation of ‘inert doublet’ models [256–266]. It has also been shown recently that the addition of just one doublet may make the electroweal

vacuum stable all the way to the Planck scale [267, 268]

2HDMs with a richer scalar sector offer new collider signatures, like decays of charged Higgs bosons, that can be verified at the LHC or future e^+e^- colliders. Such signatures offer a window to the elementary particle spectrum around the TeV scale.

In any extension of the electroweak symmetry-breaking sector, one has to ensure that the experimentally measured value of the ρ -parameter [24] defined as

$$\rho = \frac{M_W^2}{M_Z^2 \cos^2 \theta_W} \quad (6.1.1)$$

is very close to 1. In a $SU(2) \times U(1)$ gauge theory with n scalar multiplets of weak isospin T_i and hypercharge Y_i and corresponding vacuum expectation value of the neutral component being v_i , the ρ parameter at tree level [269] is given by

$$\rho = \frac{\sum_{i=1}^n \left[T_i(T_i + 1) - \frac{1}{4} Y_i^2 \right] v_i}{\sum_{i=1}^n \frac{1}{2} Y_i^2 v_i} \quad (6.1.2)$$

The tree level constraint of $\rho = 1$ in an extended Higgs sector can be satisfied with having additional $SU(2)$ singlets with $Y = 0$ and also with $SU(2)$ doublets with $Y = \pm 1$. This is due to the fact that in both cases one has $T_i(T_i + 1) = \frac{3}{4} Y^2$. The loop contributions to ρ do not impose any appreciable restriction on the scalar sector. There are other scalar extensions which can in principle also lead to $\rho = 1$ but these are more contrived than a minimalistic 2HDM scenario. Overall, any 2HDM emerges unscathed by this crucial constraint.

Another constraint that restricts the allowed possibilities in the Higgs sector is provided by the severe limits on the flavor-changing neutral currents (FCNCs). Within SM, the FCNCs do not pose a problem because the process of diagonalizing the fermion mass matrix also results in diagonal Yukawa couplings. This is because there is only one Higgs doublet to which the fermions couple. However, within a 2HDM scenario the situation is different. Consider a general coupling of the down type quarks to the 2 scalar doublets Φ_1 and Φ_2 given by

$$\mathcal{L}_Y = y_{ij}^1 \bar{d}_L d_R \Phi_1 + y_{ij}^2 \bar{d}_L d_R \Phi_2 \quad (6.1.3)$$

The indices 1 and 2 on $y_{ij}^{1,2}$ index the corresponding doublet to which the quarks couple and i, j are the generation indices. The resulting mass matrix becomes

$$M_{ij} = y_{ij}^1 \frac{v_1}{\sqrt{2}} + y_{ij}^2 \frac{v_2}{\sqrt{2}} \quad (6.1.4)$$

In general, the Yukawa matrices will not be simultaneously diagonalizable and thus the Yukawa couplings will not be flavor diagonal. This could result in flavor off-diagonal interactions of the kind $\bar{d}s\phi$. The presence of such flavor changing interactions have phenomenological consequences. Such a term if present, can lead to $K - \bar{K}$ mixing at the tree level. If one assumes such a coupling to have strength of the order of b -quark Yukawa coupling in SM, then the mass of the scalar mediating the oscillation is pushed to scales greater than 10 TeV [270–272]. This is slightly an undesirable situation from a phenomenological point of view. Another way to avoid tree level FCNCs comes from what is known as the Paschos-Glashow-Weinberg theorem [273, 274]. This theorem tells that one can avoid tree level FCNCs if all fermions of a given electric charge couple to the same Higgs doublet. This constrains the possible ways of coupling the fermions to the two doublets where the FCNCs are avoided by imposing certain discrete symmetries. Thus we have the following four 2HDM models with natural flavor conservation:

- **Type I 2HDM** : All quarks and leptons couple to just one doublet (Φ_2).
- **Type II 2HDM** : Up-type quarks (u_R) couple to Φ_2 and down-type quarks and leptons couple to Φ_1 .
- **Lepton-specific (type X) 2HDM** : Quarks couple to Φ_2 and leptons to Φ_1 .
- **Flipped (type Y) 2HDM** : Up-type quarks couple to Φ_2 , down-type quarks to Φ_1 (like in type II case), and leptons couple to Φ_2 .

The discrete symmetry transformations that ensure flavor-diagonal currents in the above 2HDMs are different. For example, in type I 2HDM demanding the invariance of the Lagrangian under $\Phi_1 \rightarrow -\Phi_1$ does the trick. For type II 2HDM symmetry is demanded under $\Phi_1 \rightarrow -\Phi_1$ and $d_R^i \rightarrow -d_R^i$. Thus one can find a discrete \mathbb{Z}_2 symmetry which ensures natural flavor conservation in the above models. The four possibilities are tabulated in Table 6.1.

Having discussed the various possible 2HDM scenarios that respect tree level flavor conservation, we turn now to discuss the scalar sector of these models and the couplings of the scalar sector to gauge bosons and fermions.

Model	u_R^i	d_R^i	e_R^i
Type I	Φ_2	Φ_2	Φ_2
Type II	Φ_2	Φ_1	Φ_1
Type X	Φ_2	Φ_2	Φ_1
Type Y	Φ_2	Φ_1	Φ_2

Table 6.1: Models which lead to natural flavour conservation. The superscript i is a generation index.

6.2 The scalar potential in 2HDM models

The most general form of the 2HDM scalar potential comprising of doublets Φ_1 and Φ_2 is

$$\begin{aligned}
V_{\text{2HDM}} = & m_{11}^2 \Phi_1^\dagger \Phi_1 + m_{22}^2 \Phi_2^\dagger \Phi_2 - [m_{12}^2 \Phi_1^\dagger \Phi_2 + \text{h.c.}] + \frac{1}{2} \lambda_1 (\Phi_1^\dagger \Phi_1)^2 + \frac{1}{2} \lambda_2 (\Phi_2^\dagger \Phi_2)^2 \\
& + \lambda_3 (\Phi_1^\dagger \Phi_1) (\Phi_2^\dagger \Phi_2) + \lambda_4 (\Phi_1^\dagger \Phi_2) (\Phi_2^\dagger \Phi_1) + \left\{ \frac{1}{2} \lambda_5 (\Phi_1^\dagger \Phi_2)^2 + [\lambda_6 (\Phi_1^\dagger \Phi_1) \right. \\
& \left. + \lambda_7 (\Phi_2^\dagger \Phi_2)] (\Phi_1^\dagger \Phi_2) + \text{h.c.} \right\}, \tag{6.2.1}
\end{aligned}$$

In general, the coefficients m_{12}^2 , λ_5 , λ_6 and λ_7 can be complex. For models respecting tree level flavor conservation, $\lambda_6 = \lambda_7 = 0$ is ensured via enforcing the \mathbb{Z}_2 symmetry under $\Phi_1 \rightarrow -\Phi_1$. This would dictate m_{12}^2 also to vanish. But we allow a soft breaking of \mathbb{Z}_2 symmetry by this quadratic term. In the study to be presented next, we restrict ourselves for simplicity to a CP-conserving 2HDM scenario, implying that all the coefficients in Eq. 7.2.2 are real. Under spontaneous symmetry breaking the neutral components of the two doublets acquire vacuum expectation values

$$\langle \Phi_1 \rangle = \frac{1}{\sqrt{2}} \begin{pmatrix} 0 \\ v_1 \end{pmatrix}, \quad \langle \Phi_2 \rangle = \frac{1}{\sqrt{2}} \begin{pmatrix} 0 \\ v_2 \end{pmatrix} \tag{6.2.2}$$

With this vacuum structure, the two scalar doublets can be parameterized as

$$\Phi_i = \begin{pmatrix} H_i^+ \\ \frac{v_i + h_i + iA_i}{\sqrt{2}} \end{pmatrix}, \quad i = 1, 2 \tag{6.2.3}$$

The mass matrices for the various fields are diagonalized using

$$\begin{pmatrix} H \\ h \end{pmatrix} = \begin{pmatrix} c_\alpha & s_\alpha \\ -s_\alpha & c_\alpha \end{pmatrix} \begin{pmatrix} h_1 \\ h_2 \end{pmatrix} \quad (6.2.4)$$

where H and h are the neutral CP-even scalars and c_α , $s_\alpha = \cos \alpha$, $\sin \alpha$ where α is the diagonalizing angle.

Also we have

$$\begin{pmatrix} G^0 \\ A \end{pmatrix} = \begin{pmatrix} c_\beta & s_\beta \\ -s_\beta & c_\beta \end{pmatrix} \begin{pmatrix} A_1 \\ A_2 \end{pmatrix} \quad (6.2.5)$$

and

$$\begin{pmatrix} G^\pm \\ H^\pm \end{pmatrix} = \begin{pmatrix} c_\beta & s_\beta \\ -s_\beta & c_\beta \end{pmatrix} \begin{pmatrix} H_1^\pm \\ H_2^\pm \end{pmatrix} \quad (6.2.6)$$

where G^0 , G^\pm are the neutral and charged Goldstone bosons, A is the pseudoscalar and H^\pm are the charged scalars. The neutral and the charged Goldstone bosons are absorbed to give masses to Z and W^\pm . Thus we are left with five physical scalars h , H (CP-even), A (CP-odd) and H^\pm , the charged Higgs bosons. Conventionally we take $M_H > M_h$. The second diagonalizing angle β is related to the vacuum expectation values via

$$\tan \beta = \frac{v_1}{v_2} \quad (6.2.7)$$

The coupling constants of the scalar potential can be expressed in terms of the physical mass states via the relations

$$\begin{aligned} \lambda_1 &= \frac{M_H^2 c_\alpha^2 + M_h^2 s_\alpha^2 - m_{12}^2 \tan \beta}{v^2 c_\beta^2}, \\ \lambda_2 &= \frac{M_H^2 s_\alpha^2 + M_h^2 c_\alpha^2 - m_{12}^2 \cot \beta}{v^2 s_\beta^2}, \\ \lambda_3 &= \frac{(M_H^2 - m_h^2) c_\alpha s_\alpha + 2M_{H^\pm}^2 s_\beta c_\beta - m_{12}^2}{v^2 s_\beta c_\beta}, \\ \lambda_4 &= \frac{(M_A^2 - 2M_{H^\pm}^2) s_\beta c_\beta + m_{12}^2}{v^2 s_\beta c_\beta}, \\ \lambda_5 &= \frac{m_{12}^2 - M_A^2 s_\beta c_\beta}{v^2 s_\beta c_\beta}. \end{aligned} \quad (6.2.8)$$

where $v = \sqrt{v_1^2 + v_2^2} \simeq 246$ GeV.

6.3 Couplings to gauge bosons and fermions

The phenomenological consequences of 2HDM models are dictated by the couplings of the scalars to gauge bosons and fermions. The couplings of the Higgs bosons to gauge bosons are the same for the above listed 2HDM models. But owing to different \mathbb{Z}_2 symmetries, the Yukawa couplings are model specific.

Three point vertices involving the scalars and the gauge bosons are [275–277]

$$\begin{aligned} hZ_\mu Z_\nu &: 2i\frac{m_Z^2}{v}\sin(\beta-\alpha)g_{\mu\nu}, & HZ_\mu Z_\nu &: 2i\frac{m_Z^2}{v}\cos(\beta-\alpha)g_{\mu\nu}, \\ hW_\mu^+ W_\nu^- &: 2i\frac{m_W^2}{v}\sin(\beta-\alpha)g_{\mu\nu}, & HW_\mu^+ W_\nu^- &: 2i\frac{m_W^2}{v}\cos(\beta-\alpha)g_{\mu\nu} \end{aligned} \quad (6.3.1)$$

and

$$\begin{aligned} hAZ_\mu &: \frac{g_Z}{2}\cos(\beta-\alpha)(p+p')_\mu, & HAZ_\mu &: -\frac{g_Z}{2}\sin(\beta-\alpha)(p+p')_\mu, \\ H^+H^-Z_\mu &: -\frac{g_Z}{2}\cos 2\theta_W(p+p')_\mu, & H^+H^-\gamma_\mu &: -ie(p+p')_\mu, \\ H^\pm hW_\mu^\mp &: \mp i\frac{g_W}{2}\cos(\beta-\alpha)(p+p')_\mu, & H^\pm HW_\mu^\mp &: \pm i\frac{g_W}{2}\sin(\beta-\alpha)(p+p')_\mu, \\ H^\pm AW_\mu^\mp &: \frac{g_W}{2}(p+p')_\mu, \end{aligned} \quad (6.3.2)$$

where p_μ and p'_μ are outgoing four-momenta of the first and the second scalars, respectively, and $g_Z = g_W/\cos\theta_W$. For a more exhaustive list one can refer to [275].

Notice that the couplings of the pseudoscalar A to gauge boson pairs vanishes due to CP invariance *i.e.* $g_{AVV} = 0$. From the above list of gauge-Higgs couplings one can see that $g_{hVV} = \sin(\beta-\alpha)g_{hVV}^{\text{SM}}$ and $g_{HVV} = \cos(\beta-\alpha)g_{HVV}^{\text{SM}}$. In the limit when $\beta-\alpha \rightarrow \frac{\pi}{2}$ (alignment limit), the couplings of the lighter CP-even Higgs approach that of the SM Higgs while $g_{HVV} \rightarrow 0$. Also, if a vertex involves atleast one gauge boson and exactly one of the non-minimal Higgs (H , A , H^\pm), it is proportional to $\cos(\beta-\alpha)$ and thus the corresponding coupling vanishes in the alignment limit.

The general Lagrangian for the Yukawa sector of the 2HDMs can be written as

$$\mathcal{L}_{\text{Yukawa}}^{\text{2HDM}} = -\bar{Q}_L Y_u \tilde{\Phi}_u u_R - \bar{Q}_L Y_d \Phi_d d_R - \bar{L}_L Y_\ell \Phi_\ell \ell_R + \text{h.c.}, \quad (6.3.3)$$

where the suffixes R and L denote right- and left-handed fermions, respectively. Subscripts u , d , and l refer to the up-type quarks, down-type quarks, and charged leptons, respectively. The choice of $\Phi_{f=u,d,\ell}$ from Φ_1 or Φ_2 is done so as to keep the interaction terms \mathbb{Z}_2 invariant, according to the Table 6.1. The Lagrangian in 6.3.3 written in terms of physical Higgs states

becomes

$$\mathcal{L}_{\text{Yukawa}}^{\text{Physical}} = - \sum_{f=u,d,\ell} \frac{m_f}{v} \left(\xi_h^f \bar{f} h f + \xi_H^f \bar{f} H f - i \xi_A^f \bar{f} \gamma_5 A f \right) - \left\{ \frac{\sqrt{2} V_{ud}}{v} \bar{u} (m_u \xi_A^u P_L + m_d \xi_A^d P_R) H^+ d + \frac{\sqrt{2} m_l}{v} \xi_A^l \bar{\nu}_L H^+ l_R + \text{h.c.} \right\}, \quad (6.3.4)$$

The multiplicative factors of the Yukawa couplings, *i.e.* ξ_h^f , ξ_H^f and ξ_A^f for the different 2HDM models [272] are given in Table 6.2. For $\sin(\beta - \alpha) \approx 1$ the Yukawa coupling with the SM-like Higgs (h) are similar to that of the SM.

	ξ_h^u	ξ_h^d	ξ_h^ℓ	ξ_H^u	ξ_H^d	ξ_H^ℓ	ξ_A^u	ξ_A^d	ξ_A^ℓ
Type-I	c_α/s_β	c_α/s_β	c_α/s_β	s_α/s_β	s_α/s_β	s_α/s_β	$\cot \beta$	$-\cot \beta$	$-\cot \beta$
Type-II	c_α/s_β	$-s_\alpha/c_\beta$	$-s_\alpha/c_\beta$	s_α/s_β	c_α/c_β	c_α/c_β	$\cot \beta$	$\tan \beta$	$\tan \beta$
Type-X	c_α/s_β	c_α/s_β	$-s_\alpha/c_\beta$	s_α/s_β	s_α/s_β	c_α/c_β	$\cot \beta$	$-\cot \beta$	$\tan \beta$
Type-Y	c_α/s_β	$-s_\alpha/c_\beta$	c_α/s_β	s_α/s_β	c_α/c_β	s_α/s_β	$\cot \beta$	$\tan \beta$	$-\cot \beta$

Table 6.2: The multiplicative factors in each type of Yukawa interactions in Eq. (6.3.4)

Let us proceed next to discuss the constraints on various 2HDM parameter spaces.

6.4 Constraints on 2HDM parameters

The parameter space of any 2HDM gets constrained from theoretical considerations of perturbativity and vacuum stability. In addition, the observed discrepancy in the muon $g - 2$ limits the parameter space of type X and type II models due to their Yukawa structure. Since the scalar sector of these models can contribute towards the two-point functions of the gauge bosons, EWP data also provides correlations between the allowed masses of the heavy Higgs bosons and the pseudoscalar. There are model specific constraints from direct searches at colliders and B -physics observables for the neutral and charged Higgs bosons. In what follows, we shall review these constraints and try to correlate them with the coupling structures in different 2HDMs.

6.4.1 Constraints from perturbativity and vacuum stability

The various couplings in the quartic terms λ_i ($i = 1..5$) have an upper bound from the requirements of the theory to be perturbative in those couplings, i.e.

$$\lambda_i \leq 4\pi \quad (6.4.1)$$

The vacuum stability requires the scalar potential to be bounded from below. Thus there should be no directions in the field space of the two doublets where $V_{2\text{HDM}} \rightarrow -\infty$. To ensure this we need to consider the quartic terms in the potential as the field values become very large. Realising this condition for the following directions gives us three constraints [272]:

- The direction $|\Phi_1| \rightarrow \infty$ and $|\Phi_2| = 0$ implies

$$\lambda_1 > 0. \quad (6.4.2)$$

- $|\Phi_2| \rightarrow \infty$ and $|\Phi_1| = 0$ gives

$$\lambda_2 > 0. \quad (6.4.3)$$

- The direction with $|\Phi_1| \rightarrow \infty$ and $|\Phi_2| \rightarrow \infty$ but $\Phi_1^\dagger \Phi_2 = 0$ implies

$$\lambda_3 > -\sqrt{\lambda_1 \lambda_2}. \quad (6.4.4)$$

- Another constraint comes from the field direction for which $\sqrt{\lambda_1}|\Phi_1|^2 = \sqrt{\lambda_2}|\Phi_2|^2$ and $|\Phi_1|^2|\Phi_2|^2 = |\Phi_1^\dagger \Phi_2|^2$ which leads to

$$\lambda_3 + \lambda_4 - |\lambda_5| > -\sqrt{\lambda_1 \lambda_2}. \quad (6.4.5)$$

In [278, 279] it was argued that when one has $\lambda_6 = \lambda_7 = 0$, these are actually necessary and sufficient conditions to ensure the positivity of the quartic potential along all directions. In addition, the requirement of the existence of global minimum imposes the following constraint [280]:

$$m_{12}^2(m_{11}^2 - m_{22}^2\sqrt{\lambda_1/\lambda_2})(\tan \beta - (\lambda_1/\lambda_2)^{1/4}) > 0 \quad (6.4.6)$$

The constraints on the coefficients listed above correspond to the requirement of a stable vacuum rather than a metastable one. The evolution of these coefficients under the renormalization group flow however can lead to these parameters becoming non-perturbative or the vacuum stability criteria being violated beyond a certain cut-off scale. Requiring that

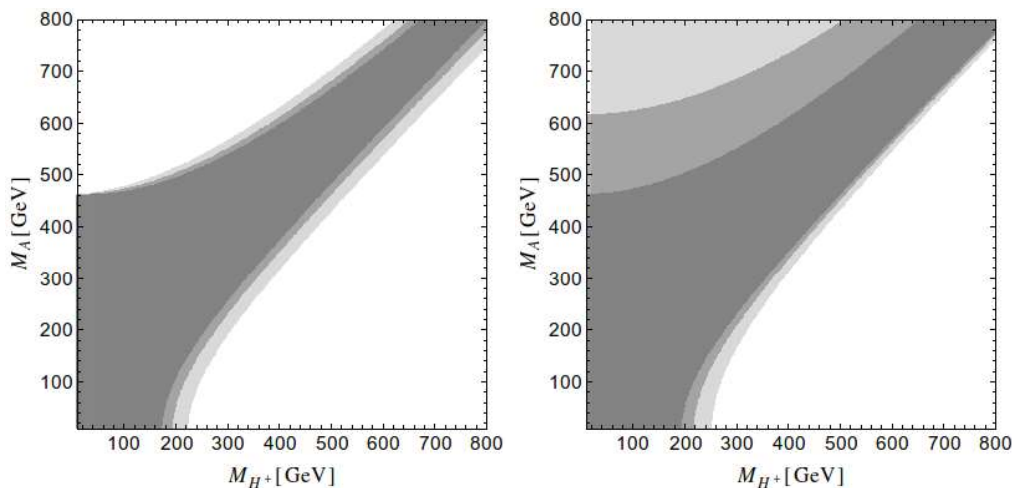


Figure 6.1: M_A - M_{H^\pm} plane in 2HDMs with $\beta - \alpha = \pi/2$ and $M_h = 126$ GeV. The darker to lighter gray regions in the left panel correspond to $\Delta M \equiv M_H - M_{H^\pm} = \{20, 0, -30\}$ GeV and $\lambda_1 = \sqrt{4\pi}$. The allowed regions in the right panel correspond to $\lambda_1 = \{\sqrt{4\pi}, 2\pi, 4\pi\}$ and vanishing ΔM . Both plots are obtained for $\tan \beta = 50$, but the change with respect to values of $\tan \beta \in [5, 100]$ is negligible. Figure taken from [16].

the couplings satisfy perturbativity and vacuum stability up to a given high scale (for example the GUT scale or the Planck scale) constrains the 2HDM parameter space. Studies exploring these issues have been taken up in [267, 268].

We can translate the above constraints into those on the scalar masses. The equations for λ_4 and λ_5 in Eq. 6.2.8 yield

$$M_{H^\pm}^2 = M_A^2 + \frac{1}{2}v^2(\lambda_5 - \lambda_4). \quad (6.4.7)$$

Notice that the difference $\lambda_5 - \lambda_4$ has to satisfy 6.4.5 from vacuum stability. If one assumes the alignment limit, then for $\tan \beta \gg 1$ the parameters λ_2 , λ_3 and m_{12}^2 can be expressed in terms of physical masses and λ_1 [16] through

$$\begin{aligned} \lambda_2 v^2 &\simeq M_h^2 + \lambda_1 v^2 / \tan^4 \beta, \\ \lambda_3 v^2 &\simeq 2M_{H^\pm}^2 - 2M_H^2 + M_h^2 + \lambda_1 v^2 / \tan^2 \beta, \\ m_{12}^2 &\simeq M_H^2 / \tan \beta + (M_h^2 - \lambda_1 v^2) / \tan^3 \beta \end{aligned} \quad (6.4.8)$$

Using the above relations coupled with the perturbativity bounds on λ_1 , the constraints on the mass plane $M_A - M_{H^\pm}$ have been derived in [16] and are shown in Figure 6.1.

One can observe that for a light pseudoscalar of $M_A < 100$ GeV, the charged Higgs mass

has an upper bound of $M_{H^\pm} \lesssim 200$ GeV. Also, for heavier charged Higgs boson, M_A is bounded from below.

6.4.2 EWP constraints

The contributions of the extended Higgs sector to the electroweak precision observables have been analyzed in [16, 281, 282]. The resulting constraints on the allowed mass splittings between the heavy Higgs bosons are shown in Figure 6.2. From Figure 6.2 it is clear that for degenerate masses of M_{H^\pm} and M_H , a wide range is allowed for M_A . But for a larger splitting of $M_H - M_{H^\pm}$, M_A is required to be almost degenerate with M_{H^\pm} .

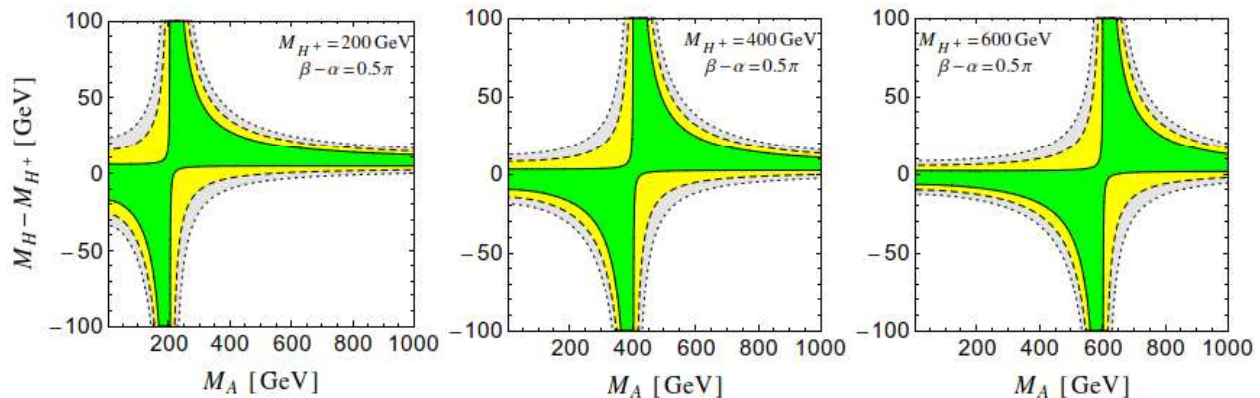


Figure 6.2: Allowed region in the M_A vs. $\Delta M_H = M_H - M_{H^\pm}$ plane from EWP constraints for different values of $M_{H^\pm} = 200, 400$ and 600 GeV. Plots are benchmarked for $\beta - \alpha = \pi/2$ and $M_h = 126$ GeV. The green, yellow, gray regions correspond to 68.3, 95.4, and 99.7% confidence intervals respectively, of a chi-square fit to the EWP data. Figure taken from [16].

6.4.3 Flavor constraints on M_{H^\pm} and $\tan \beta$

Experimental data on flavor observables provides constraints on the allowed values of M_{H^\pm} and $\tan \beta$. This is due to the contributions of the charged Higgs to the same at the tree or loop level [277]. Since these contributions are a function of the Yukawa structure, flavor physics constraints depend on the specific 2HDM scenario in context. Flavor constraints on couplings have been interpreted in terms of limits on M_{H^\pm} vs. $\tan \beta$ for the various 2HDM Yukawa couplings in [283–286]. The branching of $B \rightarrow X_s \gamma$ [287] provides a $\tan \beta$ independent lower bound of $M_{H^\pm} \gtrsim 380$ GeV [288, 289] for type II and type Y 2HDM models.

In a more recent analysis by BELLE collaboration the lower bound has been tightened to $M_{H^\pm} \gtrsim 580$ GeV [290]. For type I and type X 2HDMs $\tan \beta \lesssim 1$ is ruled out for $M_{H^\pm} \lesssim 800$ GeV, but there is no lower bound on M_{H^\pm} . This can be inferred from the fact that in type I and type X models the charged Higgs coupling to quarks is proportional to $\cot \beta$ whereas in type II and type Y 2HDMs a part of the vertex is proportional to $\tan \beta$ and the other to $\cot \beta$. From $B_d^0 - \bar{B}_d^0$ mixing, regions for which $\tan \beta \leq 1$ and $M_{H^\pm} \lesssim 500$ GeV are excluded [277, 287] for all the four 2HDM scenarios. Upper bounds on $\tan \beta$ from leptonic meson decays *i.e.* $B \rightarrow \tau \nu$ [291] and $D_s \rightarrow \tau \nu$ [292] exist for only type II 2HDM because here $\xi_A^d \xi_A^\ell = \tan^2 \beta$, whereas for type I, the product $\xi_A^d \xi_A^\ell = \cot^2 \beta$ and for type X and type Y it is equal to -1.

6.4.4 Collider constraints

Searches for the additional Higgs bosons in their leptonic or hadronic decay modes have been performed at LEP, Tevatron and LHC. These have led to constraints on the parameter spaces of the 2HDM models in terms of the allowed mass thresholds and $\tan \beta$ limits. The extent of the constraints is a reflection of the sensitivity of the probed channel to the 2HDM parameters. From neutral Higgs searches at LEP the value of $M_H + M_A < 185$ GeV has been excluded at 95% confidence level [293, 294]. Assuming that $BR(H^+ \rightarrow \tau^+ \nu) + BR(H^+ \rightarrow c\bar{s}) = 1$ combined searches for H^\pm give the mass bound of $M_{H^\pm} > 80$ GeV [295–297], which is independent of the branching ratios into individual fermionic modes. Searches at Tevatron by CDF and D0 collaborations in the channel $p\bar{p} \rightarrow b\bar{b}H/A$, $H/A \rightarrow b\bar{b}$ or $H/A \rightarrow \tau^+\tau^-$ have put limits on $\tan \beta$ vs. M_A in type II and type Y models [298–300]. The constraints arise owing to the sensitivity of the $\tau^+\tau^-$ ($b\bar{b}$) decay mode for type II (type II and type Y) models. For the $\tau^+\tau^-$ ($b\bar{b}$) mode, upper bounds of $\tan \beta$ have been obtained from around 25 – 80 (40 – 90) for M_A in the range 100 – 300 GeV, respectively.

Charged Higgs searches at Tevatron have been performed in the production channel involving decay of the top quark $t \rightarrow bH^\pm$ and subsequent decay modes of $H^\pm \rightarrow \tau \nu$ and $H^\pm \rightarrow cs$ [301–303]. Upper bounds on the branching ratio $BR(t \rightarrow bH^\pm)$ have been obtained, which can be translated into the bound on $\tan \beta$ in various scenarios. In the type I 2HDM, for $M_H^\pm > m_t$, upper bounds on $\tan \beta$ have been obtained in the range 20 – 70 for M_{H^\pm} from 180 – 190 GeV, respectively [301].

In Run I, CMS experiment has searched for H and A decaying to the $\tau^+\tau^-$ final state, and upper limits on $\tan \beta$ have been obtained for the MSSM scenario or the type II 2HDM from 3.8 to 52.7 for M_A from 140 GeV to 900 GeV, respectively [304]. Similar searches by

ATLAS collaboration [305] provide exclusion limits in the M_A vs. $\tan \beta$ plane within the context of MSSM. CMS search in the $pp \rightarrow b\bar{b}H/A, H/A \rightarrow b\bar{b}$ channel within type II and type Y 2HDMs, [306], provides exclusion limits on $\tan \beta$, *i.e.*, $\tan \beta \gtrsim 16$ (28) is excluded at $M_A = 100$ GeV (350 GeV).

In the charged Higgs searches, ATLAS has reported exclusion of an extended parameter region in the τ +jets final state [307,308] in the mass range $90 \text{ GeV} \lesssim M_{H^\pm} \lesssim 150 \text{ GeV}$ with $\tan \beta \gtrsim 1$. For $200 < M_{H^\pm} < 250 \text{ GeV}$, higher values of $\tan \beta > 50$ are excluded.

6.4.5 Constraints from muon $g-2$

An attempt to reconcile the observed $\sim 3\sigma$ discrepancy in the anomalous magnetic moment of the muon (a_μ) provides a compelling argument in favour of 2HDM models. As discussed in Chapter 2, the gap between the theoretical and experimental values *i.e.*

$$\Delta a_\mu \equiv a_\mu^{\text{EXP}} - a_\mu^{\text{SM}} = +262 (85) \times 10^{-11} \quad (6.4.9)$$

can be potentially reconciled via contributions from the extended Higgs sector [15,309–312]. It is obvious that a positive contribution from the new physics sector is desirable. At one-loop, the contributions from the neutral Higgs bosons h and H are positive and those from A and H^\pm are negative [313–315]. These scale as the fourth power of the muon mass [16]. Apart from these, there are two-loop contributions from the Barr-Zee diagrams [309,316] involving couplings of the neutral scalars to fermions that can give substantial positive contributions in certain regions of parameter space that can become larger than those at one loop (see Figure 6.3).

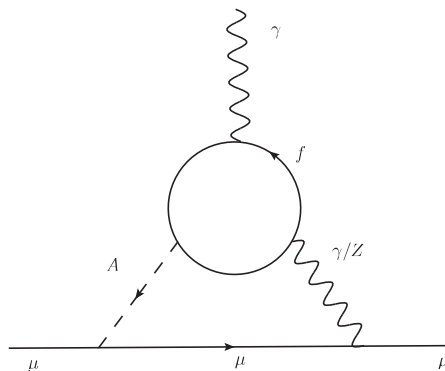


Figure 6.3: Two-loop contribution to muon $g - 2$ from a Barr-Zee diagram with a light A and a fermion loop.

This is aided by the fact that the two loop contribution scales as $\frac{m_f^2}{m_\mu^2}$ relative to that at one-loop. At two-loop the form factor corresponding to the CP-even scalars h and H has negative sign and that corresponding to A has positive sign, *i.e.* opposite to the one-loop behaviour. The negative sign of H contribution would make a heavier H a preferred choice to enhance Δa_μ . The above arguments are suggestive to the fact that a sufficiently light pseudoscalar in a two-loop diagram can generate a large positive correction to Δa_μ . One can see from Table 6.2 that Yukawa structures of type II and type X 2HDMs, both have a leptophilic A ($\xi_A^\ell = \tan \beta$). Thus one can expect an enhanced contribution to muon $g - 2$ from a τ loop, coupled with a light A , that is proportional to $\tan^2 \beta (m_\tau^2/m_\mu^2)$ in the large $\tan \beta$ limit. On the other hand for type I and type Y models since $\xi_A^\ell = -\cot \beta$, the two-loop contribution is proportional to $\cot^2 \beta$ and thus is weakened strongly at high $\tan \beta$. We have seen in section 6.4.1 (Figure 6.1) that for a light A of $M_A \lesssim 100$ GeV, M_{H^\pm} has an upper bound of ~ 200 GeV. But flavor constraints require M_{H^\pm} to be $\gtrsim 580$ GeV for type II and type Y models (see section 6.4.3). For type X models, there are no such strong bounds from flavor observables, and so they can accommodate a viable parameter space with a light A and high $\tan \beta$ to reconcile muon $g - 2$. Figure 6.4 shows the allowed region in M_A vs. $\tan \beta$ plane for $M_{h(H)} = 126, 200$ GeV. The constraints coming from the electron $g - 2$ (a_e) are also shown. The present gap between the experimental value and SM prediction for a_e stands at 1.3σ [16] where

$$\Delta a_e \equiv a_e^{\text{EXP}} - a_e^{\text{SM}} = -10.5(8.1) \times 10^{-13} \quad (6.4.10)$$

6.5 Summary

In this chapter we overviewed the four possible types of naturally flavor conserving 2HDM models and analyzed the couplings of the scalar sector to gauge bosons and fermions. It is seen that while these HDMs have a universal gauge-Higgs sector, the Yukawa couplings are dependent on the kind of \mathbb{Z}_2 symmetry imposed to avoid FCNCs at the tree level.

Constraints on these models from electroweak precision tests, vacuum stability and perturbativity, direct searches at colliders, muon and electron $g - 2$, and those from B -physics observables were interpreted in terms of allowed range of the masses of the additional Higgs bosons and $\tan \beta$. In these models, because of the universality of the gauge-Higgs couplings, the electroweak constraints (along with the perturbativity and vacuum stability ones) are

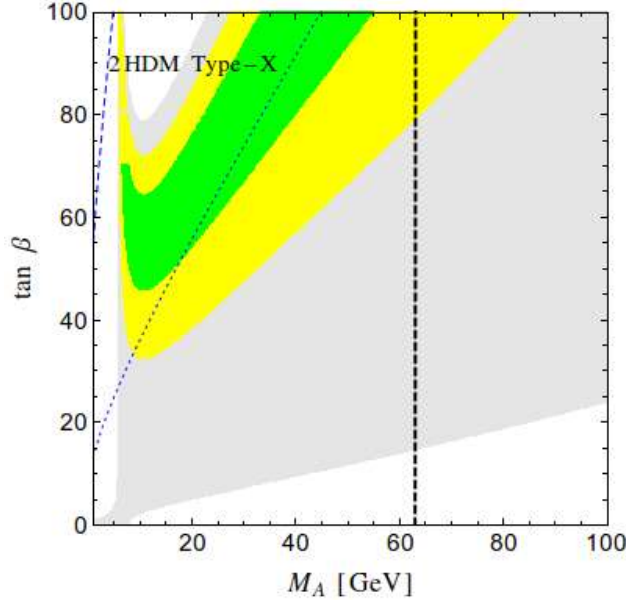


Figure 6.4: The 1σ , 2σ and 3σ regions allowed by Δa_μ in the M_A - $\tan\beta$ plane taking the limit of $\beta - \alpha = \pi/2$ and $M_{h(H)} = 126$ (200) GeV in type X 2HDM. The regions below the dashed (dotted) lines are allowed at 3σ (1.4σ) by Δa_e . The vertical dashed line corresponds to $M_A = M_h/2$. Figure taken from [16].

common to all of them, while the rest of the constraints, being dependent on the Yukawa structure, vary from model to model. Using a stringent set of precision electroweak measurements it is seen that, in the limit $(\beta - \alpha) \rightarrow \pi/2$ consistent with the LHC results on Higgs boson searches, all values of M_A are allowed when M_H and M_{H^\pm} are almost degenerate.

It was shown that a light pseudoscalar with Yukawa couplings proportional to $\tan\beta$ could be a possible solution to reconcile the muon $g - 2$ problem. This is only feasible in type II and type X models because of a leptophilic pseudoscalar. In contrast, type I and type Y models cannot accommodate Δa_μ because for them $\xi_A^\ell = -\cot\beta$. But a stringent lower bound on the mass of the charged scalar ($M_{H^\pm} \gtrsim 580$ GeV) in type II scenario coming from $B \rightarrow X_s \gamma$, coupled with the constraints from vacuum stability and perturbativity, leaves no room for a light pseudoscalar in type II model.

The above observations leave us with only type X as the favoured scenario to bridge the muon $g - 2$ discrepancy while at the same time satisfying all the other constraints. In the next chapter we shall explore the possibility of searching for these light pseudoscalars within the context of type X 2HDM at the 14 TeV run of the LHC and explore the discovery potential in the region of the parameter space for which $M_A \lesssim M_h/2$ and $\tan\beta \sim 50$.

Chapter 7

Reconstructing a light pseudoscalar in the type X Two-Higgs doublet model

7.1 Introduction

In Chapter 6 we have argued that extension of the electroweak symmetric sector of the standard model (SM) to two or more Higgs doublets is well-motivated. Out of these, the two-Higgs doublet models (2HDMs) occupy the centre stage. We have seen that such models in general suffer from the flavour changing neutral current (FCNC) problem. To avoid tree level FCNCs, a discrete symmetry (or something that effectively leads to it) is imposed, which restricts the Yukawa interactions of the two doublets. Based on the nature of such symmetry, four types of 2HDM were tabulated, namely, type I, type II, type X (or lepton specific) and type Y (or flipped) [272, 275, 276].

Of the four types of 2HDM models quoted above, only type X 2HDM emerges as a possible choice to reconcile the muon $g - 2$ discrepancy, while respecting the constraints from vacuum stability, EWP data, Flavor physics and collider data. It is seen to have an allowed region in its parameter space with a light pseudoscalar coupled with a high value of $\tan \beta$ that can give sufficiently high and positive contribution to Δa_μ [15, 312, 317–319] through the Barr-Zee two-loop diagram (see section 6.4.5).

As listed earlier, in this scenario, one scalar doublet in the flavour basis has Yukawa couplings with quarks only, while the other one couples to leptons alone. The physical states other than the SM-like 125-GeV scalar, obtained on diagonalizing the mass matrices, have very small coupling with quarks compared to those with leptons, once all constraints

including those from the Large Hadron Collider (LHC) are taken into account. This considerably relaxes the lower bounds on some of the physical masses. In particular, it has been found [16, 17, 320] that the neutral pseudoscalar A in type X 2HDM can be as light at 40-60 GeV or even lighter in certain regions in the parameter space, thanks to its generally low direct production rate at the LHC and other colliders that have run so far.¹ It is therefore important not only to look for LHC signals of this scenario [17], but also to *actually reconstruct the mass of the light A* . We suggest a method of doing precisely that.

The light pseudoscalar, for large $\tan\beta$, has a $\tau^+\tau^-$ branching ratio close to unity, and a $\mu^+\mu^-$ branching ratio on the order of 0.35%. Signals have been suggested in the multi-tau channels like $pp \rightarrow HA \rightarrow \tau^+\tau^- \tau^+\tau^-$ [17, 324–326]. However, the taus cannot be reconstructed in the collinear approximation [18] since there are four neutrinos in the final state. Besides, even if only one A decays into a τ -pair, the visible τ -decay product (like a τ -induced jet) cannot be treated in the collinear approximation at such low energies as that possessed by the τ produced from an A as light as 50 – 60 GeV. Therefore, we cannot reliably obtain M_A using the τ -pair(s). We find that the $\mu^+\mu^-$ pair can come to one’s rescue here. With $pp \rightarrow hX \rightarrow AA \rightarrow \tau^+\tau^- \mu^+\mu^-$, one may reconstruct M_A from the muon pair, in association with a pair of tau-jets. We show after a detailed simulation that such a strategy, combined with that for suppressing SM backgrounds, isolates the signal events carrying clear information on the pseudoscalar mass. It is thus possible to achieve discovery-level statistical significance with an integrated luminosity of about 100 fb^{-1} or less at 14 TeV.

In what follows, in section 7.2 we briefly review the generic features of the type X 2HDM with respect to the structure of the Yukawa and gauge couplings of the physical scalars and point out how the parameter space of the model gets constrained by the muon $g - 2$ and precision observables. Section 7.3 is devoted to the the LHC analysis of our signal that identifies the pseudoscalar resonance, detailing the event selection criteria that helps in suppressing the backgrounds. Section 7.4 includes a discussion of the results in the context of the efficacy of the analysis scheme used for our signal. We summarize and conclude in section 7.5.

¹Such light pseudoscalars may also occur in further extensions of the SM [321–323].

7.2 The type X 2HDM Model and Constraints

The type X 2HDM with $\Phi_{1,2}$ as the two doublets is characterised by the following Yukawa structure:

$$\mathcal{L}_Y = -Y_u \bar{Q}_L \tilde{\Phi}_2 u_R + Y_d \bar{Q}_L \Phi_2 d_R + Y_\ell \bar{L}_L \Phi_1 \ell_R + h.c., \quad (7.2.1)$$

where family indices are suppressed and $\tilde{\Phi}_2 = i\sigma_2 \Phi_2^*$. This Yukawa Lagrangian is the result of a \mathbb{Z}_2 symmetry [273] which prevents tree level flavor changing neutral current. Under \mathbb{Z}_2 , the fields transform as $\Phi_2 \rightarrow \Phi_2$ and $\Phi_1 \rightarrow -\Phi_1$ combined with $\ell_R \rightarrow -\ell_R$ while the other fermions are even under it. Thus Φ_2 couples only to the quarks whereas Φ_1 couples exclusively to the leptons. The most general form of the scalar potential is

$$\begin{aligned} V_{2\text{HDM}} = & m_{11}^2 \Phi_1^\dagger \Phi_1 + m_{22}^2 \Phi_2^\dagger \Phi_2 - [m_{12}^2 \Phi_1^\dagger \Phi_2 + h.c.] + \frac{1}{2} \lambda_1 (\Phi_1^\dagger \Phi_1)^2 + \frac{1}{2} \lambda_2 (\Phi_2^\dagger \Phi_2)^2 \\ & + \lambda_3 (\Phi_1^\dagger \Phi_1) (\Phi_2^\dagger \Phi_2) + \lambda_4 (\Phi_1^\dagger \Phi_2) (\Phi_2^\dagger \Phi_1) + \left\{ \frac{1}{2} \lambda_5 (\Phi_1^\dagger \Phi_2)^2 + [\lambda_6 (\Phi_1^\dagger \Phi_1) \right. \\ & \left. + \lambda_7 (\Phi_2^\dagger \Phi_2)] (\Phi_1^\dagger \Phi_2) + h.c. \right\}, \end{aligned} \quad (7.2.2)$$

where all the couplings are assumed to be real. The \mathbb{Z}_2 symmetry implies $\lambda_6 = \lambda_7 = 0$. However, the term proportional to m_{12}^2 , which softly breaks \mathbb{Z}_2 can be non zero to keep the quartic coupling λ_1 below perturbativity limit. This can be appreciated from the fact that for $m_{12}^2 = 0$, the expression for λ_1 in Eq. 6.2.8 reads

$$\lambda_1 = \frac{M_H^2 c_\alpha^2 + M_h^2 s_\alpha^2}{v^2 c_\beta^2}$$

which in the limit of $\tan \beta \gg 1$ and for $M_H \gg M_h$ becomes

$$\lambda_1 \simeq \frac{M_H^2}{v^2} \tan^2 \beta$$

which can threaten perturbativity of λ_1 in the limit of large $\tan \beta$ [17, 275, 327]. Parameter-

izing the doublets as $\Phi_i = \begin{pmatrix} H_i^+ \\ \frac{v_i + h_i + iA_i}{\sqrt{2}} \end{pmatrix}$, we obtain the five physical massive states A , h ,

H , H^\pm in terms of the two diagonalizing angles α and β :

$$\begin{aligned} A &= -s_\beta A_1 + c_\beta A_2, & H^+ &= -s_\beta H_1^+ + c_\beta H_2^+, \\ h &= -s_\alpha h_1 + c_\alpha h_2, & H &= c_\alpha h_1 + s_\alpha h_2, \end{aligned} \quad (7.2.3)$$

where s_α and c_β stand for $\sin \alpha$ and $\cos \beta$, etc. The CP-even state h corresponds to the SM-like Higgs with mass $M_h = 125$ GeV. Furthermore we look for the mass hierarchy $M_A <$

	ξ_h^u	ξ_h^d	ξ_h^ℓ	ξ_H^u	ξ_H^d	ξ_H^ℓ	ξ_A^u	ξ_A^d	ξ_A^ℓ
Type-X	c_α/s_β	c_α/s_β	$-s_\alpha/c_\beta$	s_α/s_β	s_α/s_β	c_α/c_β	$\cot \beta$	$-\cot \beta$	$\tan \beta$

Table 7.1: The multiplicative factors of Yukawa interactions in type X 2HDM

$M_h < M_H \simeq M_{H^\pm}$ which can be realised by setting $\lambda_4 + \lambda_5 \approx 0$. The SM-like Higgs couples to the pseudoscalar with strength $\lambda_{hAA} = -(\lambda_3 + \lambda_4 - \lambda_5)v$, where $v = \sqrt{v_1^2 + v_2^2} = 246$ GeV.

The Yukawa Lagrangian of Eq.(7.2.1) can be rewritten in terms of the physical Higgs bosons, h, H, A and H^\pm :

$$\begin{aligned} \mathcal{L}_{\text{Yukawa}}^{\text{Physical}} = & - \sum_{f=u,d,\ell} \frac{m_f}{v} \left(\xi_h^f \bar{f} h f + \xi_H^f \bar{f} H f - i \xi_A^f \bar{f} \gamma_5 A f \right) \\ & - \left\{ \frac{\sqrt{2} V_{ud}}{v} \bar{u} (m_u \xi_A^u P_L + m_d \xi_A^d P_R) H^+ d + \frac{\sqrt{2} m_l}{v} \xi_A^l \bar{\nu}_L H^+ l_R + \text{h.c.} \right\} \end{aligned} \quad (7.2.4)$$

where f runs over all of the quarks and charged leptons, and u, d , and l refer to the up-type quarks, down-type quarks, and charged leptons, respectively. The multiplicative factors of the Yukawa couplings, *i.e.* ξ_h^f, ξ_H^f and ξ_A^f are given in Table 7.1. For $\sin(\beta - \alpha) \approx 1$ the Yukawa coupling with the SM-like Higgs (h) are similar to that of the SM. In any type of the 2HDM, the couplings of scalars with a pair of gauge bosons are given by [275–277]:

$$g_{hVV} = \sin(\beta - \alpha) g_{hVV}^{\text{SM}}, \quad g_{HVV} = \cos(\beta - \alpha) g_{hVV}^{\text{SM}}, \quad g_{AVV} = 0, \quad (7.2.5)$$

where $V = Z, W^\pm$. The couplings of Z boson with the neutral scalars are,

$$hAZ_\mu : \frac{g_Z}{2} \cos(\beta - \alpha)(p + p')_\mu, \quad HAZ_\mu : -\frac{g_Z}{2} \sin(\beta - \alpha)(p + p')_\mu, \quad (7.2.6)$$

where p_μ and p'_μ are outgoing four-momenta of the first and the second scalars, respectively, and $g_Z = g_W / \cos \theta_W$.

For reasons already stated, we are concerned with the region corresponding to $\tan \beta \equiv v_2/v_1 \gg 1$. Constraints on 2HDM parameter space coming from $(g-2)_\mu$ have been analyzed in Refs. [15–17, 311, 312, 315, 328–333] and it was shown in the updated analysis [320] that light A in type X 2HDM can explain $(g-2)_\mu$ at 2σ while evading collider as well as precision data constraints. As stated previously in section 6.4.5, type II 2HDM also has a leptophilic pseudoscalar, but there the charged Higgs mass is bounded from below $M_{H^\pm} > 580$ GeV from the $B \rightarrow X_s \gamma$ measurement [290]. Such a heavy charged Higgs is not compatible with

the requirement of a light pseudoscalar [16] because of vacuum stability and perturbativity requirements. Also, in type I and type Y 2HDM, pseudoscalar is leptophobic ($\xi_A^\ell = -\cot \beta$) and its enhanced coupling with the muon and tau would also imply comparably strong coupling to at least one type of quarks (proportional to $\cot \beta$, see Table 6.2). This would lead to unacceptably large A production at hadron colliders. Besides, those models where the A couples to muon and tau proportionally to $\cot \beta$ cannot explain $(g-2)_\mu$, since $\tan \beta \leq 1$ is disfavoured by a number of considerations (see section 6.4.3). It is only in the type X that a light A can have enhanced coupling to the μ and the τ , concomitantly suppressed coupling to all quarks, and all phenomenological and other theoretical constraints (vacuum stability, perturbativity etc.) duly satisfied [334]. Keeping this in mind, we proceed to find a strategy for reconstructing M_A at the LHC.

7.3 Signal of a light A : An analysis for the LHC

The light pseudoscalar in type X 2HDM can be produced at the LHC via associated production along with the SM Higgs and also via the decay of the SM like Higgs. The associated production is proportional to $\cos^2(\beta - \alpha)$ and is suppressed for $(\beta - \alpha) \simeq \pi/2$, leaving $h \rightarrow AA$ as the dominant production mode for the pseudoscalar. The pseudoscalar is leptophilic and almost exclusively decays to τ lepton for large $\tan \beta$ with a very small branching ratio to di-muon ($BR(A \rightarrow \mu\mu) \simeq (m_\mu/m_\tau)^2 \simeq 0.35\%$). This will lead to copious production of four- τ events ($AA \rightarrow \tau^+\tau^-\tau^+\tau^-$), the characteristic Type-X signal which was analyzed in detail in Refs. [17, 324–326]. Since the decay of the τ involves neutrinos, full reconstruction of the four- τ system is not possible which rules out any possibility of identifying a resonance peak. On the other hand if we consider the decay $AA \rightarrow \mu^+\mu^-\tau^+\tau^-$ it is straightforward to identify the events owing to clean di-muon invariant mass ($M_{\mu\mu}$) peak at M_A which will be the ‘smoking gun’ signal for a light spin-0 resonance. We show later that, in spite of the limited branching ratio for $A \rightarrow \mu^+\mu^-$, the $2\mu 2\tau$ final state can identify the A peak well within the luminosity reach of the 14 TeV LHC.

The signal we are exploring contains a pair of oppositely charged muons with exactly two τ -tagged jets produced via :

$$p p \rightarrow h \rightarrow A A \rightarrow \mu^+\mu^-\tau^+\tau^- \rightarrow \mu^+\mu^- j_\tau j_\tau + \cancel{E}_T, \quad (7.3.1)$$

where j_τ is a τ -tagged jet as a result of hadronic τ -decay. The NNLO cross section for the Higgs production via gluon fusion at 14 TeV LHC is 50.35 pb [335].

Parameters	M_A (GeV)	$\tan \beta$	$\cos(\beta - \alpha)$	λ_{hAA}/v
BP1	50	60	0.03	0.02
BP2	60	60	0.03	0.03

Table 7.2: Benchmark points for studying the discovery prospects of light pseudoscalar in Type X 2HDM model at 14 TeV run of LHC. λ_{hAA} is in units of $v = 246$ GeV.

The Type-X 2HDM model have been encoded using `FeynRules` [153, 231] in order to generate the model files for implementation in `MadGraph5_aMC@NLO` [152, 241] which was used for computing the required cross-sections and generating events for collider analyses.

We have chosen the benchmark points (BP) given in Table 7.2 for our analysis. As we have explained in the previous section, we want a light pseudoscalar which can explain the muon $g - 2$ anomaly at 2σ . The benchmark points in the parameter space used here, corresponding to $M_A = 50, 60$ GeV, are consistent with all phenomenological constraints. They also satisfy theoretical constraints such as perturbativity and a stable electroweak vacuum [16]. The signal of a light A , which is our main focus here, does not depend on M_H or M_{H^\pm} . For both of our benchmark points, each of these masses is 200 GeV. For the chosen benchmark scenarios, the branching ratio of Higgs to AA is $BR(h \rightarrow AA) \simeq 15\%$ which is well below the upper limit of about 23% [14] on any non-standard decay branching ratio (BR) of the SM-like Higgs boson. The choice of $\tan \beta$ ensures that the lepton universality bounds originating from Z and τ decays are satisfied [320].

7.3.1 Backgrounds

The major backgrounds to our signal process : $\mu^+\mu^- j_\tau j_\tau$ come from the following channels (A) $pp \rightarrow \mu^+\mu^- + jets$, (B) $pp \rightarrow VV + jets(V = Z, W, \gamma^*)$ and (C) $pp \rightarrow t\bar{t} + jets$. All the background events are generated with two additional partons and the events are matched up to two jets using MLM matching scheme [336, 337] using the *shower- kT* algorithm with p_T ordered showers. We use NNLO production cross section for $\mu^\pm \mu^\mp j j$ [338] and ZZ [339], whereas $t\bar{t}$ production cross section is computed at N³LO [340].

Apart from these three backgrounds there exist other SM processes like VVV , $t\bar{t}V$ and $W^\pm Z$ which in principle could fake the proposed signal ($2\mu 2\tau$) [341]. However lower cross-section and the requirement of exactly two muons and two tau-tagged jets satisfying a tight

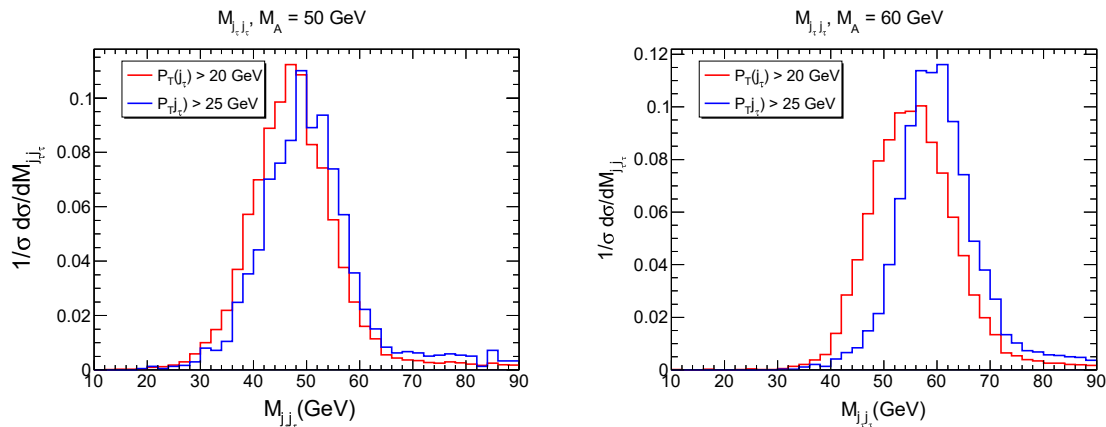


Figure 7.1: The invariant mass of the 2 tau-tagged jets for $M_A = 50$ and $M_A = 60$. The figures illustrate how the higher $p_T(j_\tau)$ threshold leads to more precise reconstruction of the peak at M_A .

invariant mass window around the pseudoscalar mass effectively eliminates the contribution from these additional channels.

7.3.2 Simulation and event selection

After generating both signal and background events with `MadGraph5_aMC@NLO`, we have used `PYTHIA6` [221] for the subsequent decay, showering and hadronization of the parton level events. Decay of τ leptons is incorporated using `TAUOLA` [342] integrated in `MadGraph5_aMC@NLO`. Both one- and three-prong τ decays have been included in our analysis. For event generation we have used the `NN23L01` [26] parton distribution function and the default dynamic renormalisation and factorisation scales [242] in `MadGraph5_aMC@NLO`. Finally, detector simulation was done using `Delphes3` [222]. Jets were reconstructed using the anti-kT algorithm [245] with $R = 0.4$. The τ -tagging efficiency and mistagging efficiencies of the light jets as τ -jets are incorporated in `Delphes3` as reported by the ATLAS collaboration [343]. We operate our simulation on the Medium tag point for which the tagging efficiency of 1-prong (3-prong) τ decay is 70% (60%) and the corresponding mistagging rate is 1% (2%).

The hadronic decays of the τ are associated with some missing transverse energy in the events. For the signal events the τ leptons originate from the decay of a light pseudoscalar (A) with mass 50 or 60 GeV. Hence, if the p_T of the τ -tagged jet has to be very close to $m_A/2$, the corresponding missing energy in the final state is suppressed. The invariant

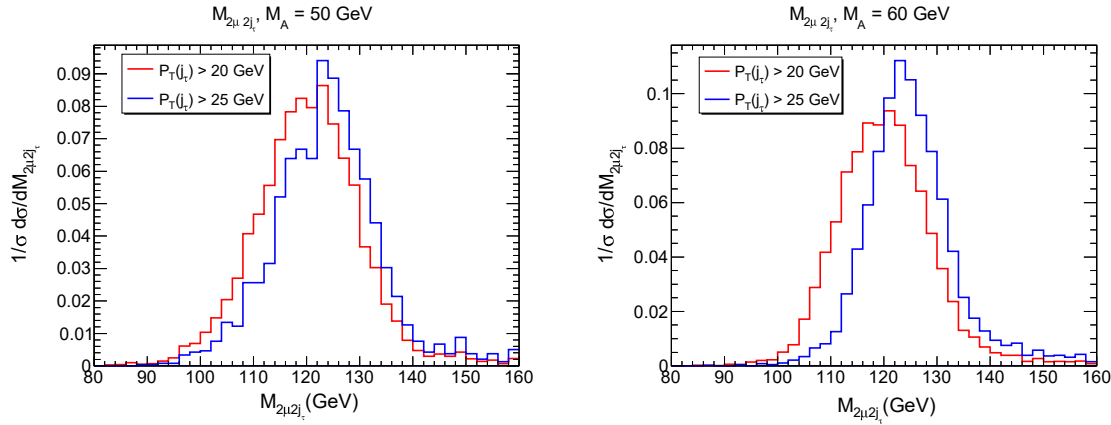


Figure 7.2: The invariant mass of the 2μ and 2 tau-tagged jets for $M_A = 50$ and $M_A = 60$. The figures illustrate how the higher $p_T(j_\tau)$ threshold leads to more precise reconstruction of the peak at $M_h = 125$ GeV.

mass of the τ -tagged jets will thus peak very close to the parent mass. In Figure 7.1 we substantiate this claim by plotting the invariant mass of the $j_\tau j_\tau$ system for two different jet p_T thresholds. One can clearly see that for $p_T(j_\tau) > 25$ GeV the invariant mass peaks at the parent pseudoscalar mass, whereas $M(j_\tau j_\tau)$ is peaking at a lower value than M_A for $p_T(j_\tau) > 20$ GeV. Also the invariant mass peak is sharper for the higher p_T threshold. The four-body invariant mass $M_{2\mu 2j_\tau}$ also shows the same features and peaks close to $M_h = 125$ GeV as depicted in Figure. 7.2. It is evident that these variables can be very efficient in minimizing the background events.

We use the following selection cuts to select our signal and reduce the accompanying backgrounds:

- **Preselection Cuts:** We require the final state to have two oppositely charged muons of minimum $p_T > 10$ GeV and $|\eta| < 2.5$. We also require two tau-tagged jets (j_τ) of minimum p_T , $p_T(j_\tau) > 20, 25$ GeV within $|\eta| < 2.5$.
- The invariant mass of the di-muon system ($M_{\mu\mu}$) satisfies the window,

$$|M_{\mu\mu} - M_A| < 7.5 \text{ GeV.}$$

- The invariant mass of the two tau-tagged jets ($M_{j_\tau j_\tau}$) satisfies:
 - for $p_T(j_\tau) > 20$ GeV : $(M_A - 20) < M_{j_\tau j_\tau} < (M_A + 10)$ GeV
 - for $p_T(j_\tau) > 25$ GeV : $|M_{j_\tau j_\tau} - M_A| < 15$ GeV.

- The invariant mass of two muons and two taujets ($M_{2\mu 2j_\tau}$) lies within the range :
 - for $p_T(j_\tau) > 20$ GeV : $(M_h - 20) < M_{2\mu 2j_\tau} < (M_h + 10)$ GeV.
 - for $p_T(j_\tau) > 20$ GeV : $|M_{2\mu 2j_\tau} - M_h| < 15$ GeV.

Notice that we have taken asymmetric cut-windows with respect to M_A for $M_{j_\tau j_\tau}$ and $M_{2\mu 2j_\tau}$ for $p_T(j_\tau) > 20$ GeV and symmetric ones for $p_T(j_\tau) > 25$ GeV. This has to do with the fact that for lower $p_T(j_\tau)$ cut, the invariant mass peaks at a lower value compared to the parent mass.

7.4 Results and Discussion

In Table 7.3, we present the cut flow for the signal and the various backgrounds for the benchmark points BP1 (BP2) where the number of events are calculated at the integrated luminosity of 3000 fb^{-1} . Note that some of the background events are estimated as upper bound (marked by an asterisk), as the number of simulated events passing the cuts drop down to very small values at some point in the cut flow table, even after simulating with 2×10^7 events for the background analysis. Since we adopt the Medium Tag point for tau-tagging, the mistagging rate for a pair of light jets is $\sim 10^{-4}$. This, along with a tight invariant mass window around M_A helps to get rid of a major fraction of the various background channels. Demanding that $|M_{\mu\mu} - M_A| < 7.5$ GeV should take care of the Z contribution in $pp \rightarrow \mu^+\mu^- + jets$ and $pp \rightarrow VV + jets$. After the cut on $M_{\mu\mu}$ only a feeble contribution from the photon (and partly off-shell Z) continuum can contribute in the $pp \rightarrow \mu^+\mu^- + jets$ channel.

We compute the statistical significance by using the formula

$$\mathcal{S} = \sqrt{2 \left[(S + B) \ln \left(1 + \frac{S}{B} \right) - S \right]} \quad (7.4.1)$$

where $S(B)$ are number of signal (background) events which survive the cuts. This is a more general formula to calculate the significance, which for $S \ll B$ reduces to $\mathcal{S} \sim S/\sqrt{B}$. In Figure 7.3 we have plotted the significance \mathcal{S} as a function of integrated luminosity for both the benchmark points where BP1(BP2) corresponds to $M_A = 50(60)$ GeV. For BP1 it is possible to reach 5σ sensitivity at integrated luminosity of $70(400) \text{ fb}^{-1}$ with $p_T(j_\tau) > 20(25)$ GeV. For BP2 the 5σ sensitivity is achievable at $40(125) \text{ fb}^{-1}$ integrated luminosity. Increasing the minimum $p_T(j_\tau)$ from 20 GeV to 25 GeV results in better invariant

Cuts	Signal	$pp \rightarrow \mu^+\mu^-$ +jets	$pp \rightarrow VV$ +jets	$pp \rightarrow t\bar{t}$ +jets
$p_T(j_\tau) > 20$ GeV				
Preselection	858 (1480)	41041 (41041)	107890 (107890)	14486 (14486)
$ M_{\mu\mu} - M_A < 7.5$ GeV	836 (1430)	909 (779)	1189 (1325)	1637 (1697)
$M_{j_\tau j_\tau} > M_A - 20$ & $M_{j_\tau j_\tau} < M_A + 10$ GeV	760 (1336)	130 (390)	307 (654)	330 (419)
$M_{2\mu 2j_\tau} > M_h - 20$ & $M_{2\mu 2j_\tau} < M_h + 10$ GeV	698 (1283)	< 130 (< 390)*	81 (109)	65 (51)
$p_T(j_\tau) > 25$ GeV				
Preselection	277 (493)	28833 (28833)	75209 (75209)	11629 (11629)
$ M_{\mu\mu} - M_A < 7.5$ GeV	269 (475)	649 (390)	794 (924)	1324 (1396)
$ M(j_\tau j_\tau) - M_A < 15$ GeV	228 (420)	< 649 (130)	112 (416)	182 (196)
$ M_{2\mu 2j_\tau} - M_h < 15$ GeV	211 (410)	< 649 (< 130)*	20 (15)	27 (27)

Table 7.3: Cut flow table for signal BP1(BP2) and different background processes with two different set of $p_T(j_\tau)$ cuts as described in Section 7.3.2. The number of events are computed with integrated luminosity of 3000 fb^{-1} . The number of background events also depends on benchmark points as M_A changes.

mass peaks but provides fewer number of events which decreases the discovery prospect of the model. However the luminosity requirement is well within the reach of high luminosity run at the LHC.

The benchmarks chosen in this work allowing for the $BR(h \rightarrow AA) \sim 15\%$ are close to the borderline of the exclusion limit on $\sigma(h) \times BR(h \rightarrow AA) \times BR(A \rightarrow \mu\mu)^2$ [344, 345], when this is translated for $A \rightarrow 2\mu 2\tau$. However, one can still allow for a lower branching ratio for $h \rightarrow AA$, for example, close to 10%, which keeps one well within the exclusion limit, satisfying all the other constraints. This would entail the required luminosity for a 5σ discovery to be nearly double the values quoted above.

If A were a scalar instead of a pseudoscalar, then it would also have decays into W^*W^*

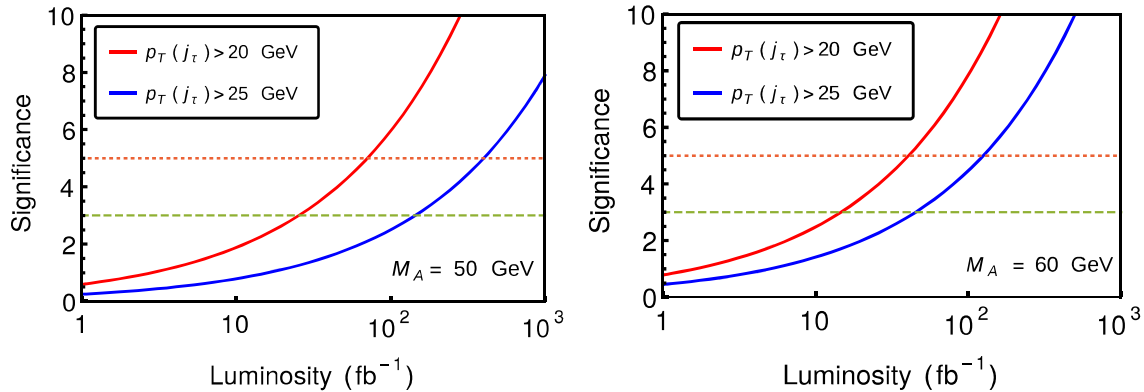


Figure 7.3: Discovery potential of the light pseudoscalar decaying to di-muon and di-tau channel using invariant mass variables for BP1(left panel) and BP2(right panel) at 14 TeV LHC.

and Z^*Z^* competing with the $\mu^+\mu^-$ mode. The non-observation of such final states, even with accumulating luminosity, should act as a pointer to the CP -odd nature of A . Secondly, the presence of such channels eats into the branching ratio of the A , and suppresses the $\mu^+\mu^-$ channel rate, reducing it below detectability. The fact that we can reconstruct the A via the $\mu\mu$ peak (which is the main point we make in this work) owes itself to the non-negligible branching ratio for this mode, which would not have been possible if it were a scalar instead of a pseudoscalar.

On the other hand, if A were a superposition of a scalar and a pseudoscalar field (i.e. if CP were violated), then the taus coming from the decay of the other A would consist of unequal admixtures of right- and left-polarised states (both for τ^- and τ^+). In principle, suitable triple products of vectors constructed out of the tau-decay products would have asymmetric distributions if CP -violation had taken place. However, the construction of such CP -asymmetric triple products would have required us to reconstruct the taus fully. This would warrant the so-called collinear approximation, where the τ , the decay product jet and a neutrino would all move along the same straight line. This approximation is valid if the tau has an energy of at least about 40 GeV. In our case, for a light (50 – 60 GeV) A this energy is not possessed by the taus, and thus their reconstruction is not reliable. Therefore, while one can distinguish a pure pseudoscalar from a pure scalar in this channel, identifying a CP -admixture is difficult.

It is possible to search for the heavy scalar H and the pseudoscalar using the $pp \rightarrow Z \rightarrow HA$ production channel. In principle, this enables one to reconstruct the H mass.

However, this associated production rate will be two orders of magnitude smaller than the rate for $pp \rightarrow h \rightarrow AA$, principally due to the large Higgs production rate from gluon fusion. Nevertheless, if one notices a low-mass $\mu^+\mu^-$ peak from A , one can look for a tau-pair peak simultaneously in such events. It is relatively easy to reconstruct tau-leptons from the tau-jets in such a case, since these taus are quite energetic and the collinear approximation [18] will work for them. Thus, in association with a light A constructed in the way suggested in our paper, a heavy H can also be looked for, albeit at higher luminosity.

In addition, a light A may of course be responsible for 4τ final states. Some channels leading to such a final state have been analyzed in [17, 325, 326]. We observe that the $\geq 3\tau$ final state fares better in terms of the statistical significance owing to the dominant branching ratio of $A \rightarrow \tau^+\tau^-$ as compared to the much smaller branching ratio of $A \rightarrow \mu^+\mu^-$. For instance, for a 5σ discovery of $M_A = 60$ GeV with $M_H = 200$ GeV, the required luminosity is approximately 70 fb^{-1} as against 218 fb^{-1} for the $2\mu 2\tau$ final state. However, the di-muon pair is a lot cleaner to reconstruct, and gives an accurate handle on the mass determination for the parent pseudoscalar. Thus the $2\mu 2\tau$ state is more informative when it comes to “identifying” the pseudoscalar.

7.5 Summary and Conclusion

While the type X 2HDM admits of a light pseudoscalar, the explicit reconstruction of its mass is a challenging task. We propose to meet this challenge by making use of the small but non-negligible branching ratio for $A \rightarrow \mu^+\mu^-$, especially in the region of the parameter space, which best explains the muon anomalous magnetic moment. We have studied the channel $pp \rightarrow h \rightarrow AA \rightarrow \mu^+\mu^- \tau^+\tau^-$, with the taus decaying into a jet each. The $\mu^+\mu^-$ pair shows a conspicuous invariant mass peak at M_A . Besides, an appropriate p_T cut on the tau-tagged jets also creates a $j_\tau j_\tau$ mass distribution that has a peak in the neighbourhood of M_A . A proper window demanded of the latter invariant mass helps the effective tagging and background reduction for the $\mu^+\mu^-$ peak. We find that, for M_A between 50 and 60 GeV, M_A can be reconstructed in this manner, with statistical significance of 4-5 σ well within the luminosity reach of the 14 TeV run.

Chapter 8

Summary and conclusions

The works included in this thesis incorporate both the model-independent and model-dependent approaches towards seeking new physics at colliders. While the two methods have a different formulation, the unifying feature that has been the emphasis of all the studies taken up here, is the role of kinematic observables in bringing out the signatures of new physics over and above the SM background. We summarise below the key points addressed in various chapters.

In Chapter 1, we surveyed the SM particle directory and reviewed the various couplings and interactions resulting from the gauge symmetry of the SM Lagrangian. We also reviewed the various experimental findings that established the SM as a well defined perturbative QFT.

This was followed up in Chapter 2 by arguing for why SM, despite its long standing successful experimental validation cannot be the full story. Several theoretical considerations and experimental inputs were summarized that strongly point towards the need for new physics beyond SM.

Chapter 3 addresses the issue of parameterizing new physics in the gauge-Higgs sector using effective field theory approach. The emphasis is on the CP-violating sector, motivated by the need to bring in extra CP violation needed to explain the baryon asymmetry in the universe. Here we considered a set of independent $SU(2) \times U(1)$ invariant CP-violating operators of dimension-six, which contribute to VVh interactions ($V = W, Z, \gamma$). Our aim is to constrain any CP-violating new physics above the electroweak scale via the effective couplings that arise when such physics is integrated out. For this purpose, we have used electroweak precision data, global fits of Higgs data at the Large Hadron Collider and the electric dipole moments of the neutron and the electron. Constraints were analyzed mainly on two-parameter and three-parameter spaces. We find that the constraints from the electroweak

precision data are the weakest. Among the existing Higgs search channels, considerable constraints come from the diphoton signal strength. We note that potential contribution to $h \rightarrow \gamma Z$ may in principle be a useful constraining factor, but it can be utilized only in the high energy run. The contributions to electric dipole moments mostly lead to the strongest constraints, though somewhat fine-tuned combinations of more than one parameter with large magnitudes are allowed. We also discussed constraints on gauge boson trilinear couplings which depend on the parameters of the CP-violating operators.

After constraining the parameter space of the CP-odd gauge-Higgs operators, in Chapter 4 we consider the observable effects of CP-violating anomalous ZZh interaction arising from gauge-invariant dimension-six operators at the Large Hadron Collider (LHC). The purpose is to distinguish them from not only the standard model effects but also those of CP-even anomalous interactions of similar nature. The postulation of a gauge-invariant origin makes various couplings of this kind interrelated. The role of CP-odd and naive Time reversal odd (\hat{T} -odd) observables in singling out the CP-odd effects was pointed out. We used the asymmetry parameter constructed out of such observables, since it has no contribution from standard or CP-even anomalous interactions. Parton showering and detector level simulation was included to make the analysis as realistic as possible. On the whole, we concluded that gauge invariant interaction of strength $\geq 40/\text{TeV}^2$ can be successfully isolated using integrated luminosities in the 1.5-3.0 ab^{-1} range.

Continuing within the ambit of EFT, Chapter 5 includes the study of the $h \rightarrow b\bar{b}\gamma$ decay via effective $hb\bar{b}\gamma$ interaction terms arising out of gauge-invariant dimension-six operators, as a potential source of new physics. Their role in some detectable final states have been compared with those coming from anomalous $hb\bar{b}$ interactions. We have considered the bounds coming from the existing collider and other low energy experimental data in order to derive constraints on the potential new physics couplings and predict possible collider signals for the two different new physics scenarios in the context of 14 TeV LHC and a future e^+e^- machine. We conclude that the anomalous $hb\bar{b}\gamma$ coupling can be probed at the 14 TeV LHC at 3σ level with an integrated luminosity of $\sim 2000 \text{ fb}^{-1}$, which an e^+e^- collider can probe at 3σ level with $\sim 12(7) \text{ fb}^{-1}$ at $\sqrt{s} = 250(500) \text{ GeV}$. It is also found that anomalous $hb\bar{b}$ interactions, subject to the existing LHC constraints, can not compete with the rates driven by $hb\bar{b}\gamma$ effective interactions.

In Chapter 6, we switch from model-independent to model-dependent approach. We discuss the construct of two-Higgs doublet models and list the constraints on their parameter space from theoretical requirements of vacuum stability and perturbativity and from

experimental inputs from electroweak precision data, Flavor physics and collider searches. It is seen that out of the four possible choices of 2HDMs (type I, II, X and Y), only type X (lepton-specific) 2HDM can accommodate the reconciliation of muon $g - 2$ discrepancy, satisfying all the above constraints.

Following this, in Chapter 7 we investigate the detectability as well as reconstructibility of a light pseudoscalar A of mass in the 50 – 60 GeV range, which is still allowed in a type X two-Higgs doublet scenario. Such a pseudoscalar can be pair-produced in the decay $h \rightarrow AA$ of the 125 GeV scalar h . The light pseudoscalar in the aforementioned range, helpful in explaining the muon anomalous magnetic moment, has not only substantial branching ratio in the $\tau^+\tau^-$ channel but also one of about 0.35% in the $\mu^+\mu^-$ final state. We show how to faithfully reconstruct the A mass using the $\mu^+\mu^-$ mode, and establish the existence of a pseudoscalar around 50 – 60 GeV, using the process $pp \rightarrow h \rightarrow AA \rightarrow \mu^+\mu^- \tau^+\tau^-$. This is found to be a reliable way of reconstructing the light A mass, with a statistical significance that amounts to discovery, with a few hundred fb^{-1} of integrated luminosity.

In conclusion, in the light of studies mentioned here and the wealth of data that is going to accumulate in the Run-II of the LHC, we can say that kinematic observables will play an ever-increasing role in collider searches. The need would be not just to compare a new physics signal against the SM background, but also to differentiate between two or more competing scenarios leading to the same final state. In this regard we might need to carefully analyze new corners of the phase space, which are yet unexplored.

Appendix A

Higher Dimensional Operators: The Gauge-Higgs Story

A.1 Gauge boson two-point functions in presence of CP-odd couplings

We define the two-point function for electroweak gauge bosons V_1 and V_2 as,

$$\Pi_{V_1 V_2}^{\mu\nu}(p^2) = g^{\mu\nu} \Pi_{V_1 V_2}(p^2) + p^\mu p^\nu \tilde{\Pi}_{V_1 V_2}(p^2). \quad (\text{A.1.1})$$

In electroweak precision observables only $\Pi_{V_1 V_2}(p^2)$ contribute. Below we give their expressions due to CP-odd couplings in terms of one-loop scalar functions A_0 and B_0 .

$$\begin{aligned} \Pi_{\gamma\gamma}(p^2) = & \frac{g^2 m_W^2}{18\Lambda^4} \left(3p^2 (C_{\gamma\gamma h}^2 (2m_h^2 - p^2) B_0(p^2, 0, m_h^2) - 2C_{WW\gamma}^2 (2m_W^2 + p^2) B_0(p^2, m_W^2, m_W^2)) \right. \\ & + C_{\gamma Zh}^2 A_0(m_Z^2) + 4C_{WW\gamma}^2 A_0(m_W^2) - 3C_{\gamma\gamma h}^2 m_h^4 B_0(p^2, 0, m_h^2) - 3C_{\gamma Zh}^2 (m_h^4 - 2m_h^2 (m_Z^2 + p^2) \\ & + (m_Z^2 - p^2)^2) B_0(p^2, m_Z^2, m_h^2) + 3A_0(m_h^2) (C_{\gamma\gamma h}^2 (m_h^2 + p^2) + C_{\gamma Zh}^2 (m_h^2 - m_Z^2 + p^2)) \\ & + 3C_{\gamma Zh}^2 A_0(m_Z^2) (m_Z^2 - m_h^2) + p^2 (7C_{\gamma\gamma h}^2 (p^2 - 3m_h^2) + 7C_{\gamma Zh}^2 (p^2 - 3(m_h^2 + m_Z^2))) \\ & \left. + 2C_{WW\gamma}^2 (12m_W^2 + 7p^2) \right), \quad (\text{A.1.2}) \end{aligned}$$

$$\Pi_{\gamma Z}(p^2) = \frac{g^2 m_W^2}{18\Lambda^4} \left(-3C_{\gamma\gamma h} C_{\gamma Zh} (m_h^2 - p^2)^2 B_0(p^2, 0, m_h^2) - 3C_{\gamma Zh} C_{ZZh} (m_h^4 - 2m_h^2 (m_Z^2 + p^2)) \right)$$

$$\begin{aligned}
& + (m_Z^2 - p^2)^2 B_0(p^2, m_Z^2, m_h^2) - 6C_{WW\gamma}C_{WWZ}p^2 (2m_W^2 + p^2) B_0(p^2, m_W^2, m_W^2) \\
& + 3C_{\gamma Zh}A_0(m_h^2) (C_{\gamma\gamma h} (m_h^2 + p^2) + C_{ZZh} (m_h^2 - m_Z^2 + p^2)) + 3C_{\gamma Zh}C_{ZZh}A_0(m_Z^2) \\
& (-m_h^2 + m_Z^2 + p^2) + 12C_{WW\gamma}C_{WWZ}p^2 A_0(m_W^2) + p^2 (7p^2(C_{\gamma Zh}(C_{\gamma\gamma h} + C_{ZZh}) \\
& + 2C_{WW\gamma}C_{WWZ}) - 21C_{\gamma Zh} (m_h^2(C_{\gamma\gamma h} + C_{ZZh}) + C_{ZZh}m_Z^2) + 24C_{WW\gamma}C_{WWZ}m_W^2)),
\end{aligned} \tag{A.1.3}$$

$$\begin{aligned}
\Pi_{ZZ}(p^2) &= \frac{g^2 m_W^2}{18\Lambda^4} (3p^2 (C_{\gamma Zh}^2 (2m_h^2 - p^2) B_0(p^2, 0, m_h^2) - 2C_{WWZ}^2 (2m_W^2 + p^2) B_0(p^2, m_W^2, m_W^2) \\
& + 4C_{WWZ}^2 A_0(m_W^2) + C_{ZZh}^2 A_0(m_Z^2)) - 3C_{\gamma Zh}^2 m_h^4 B_0(p^2, 0, m_h^2) - 3C_{ZZh}^2 (m_h^4 - 2m_h^2 (m_Z^2 + p^2) \\
& + (m_Z^2 - p^2)^2) B_0(p^2, m_Z^2, m_h^2) + 3A_0(m_h^2) (C_{\gamma Zh}^2 (m_h^2 + p^2) + C_{ZZh}^2 (m_h^2 - m_Z^2 + p^2)) \\
& + 3C_{ZZh}^2 A_0(m_Z^2) (m_Z^2 - m_h^2) + p^2 (7C_{\gamma Zh}^2 (p^2 - 3m_h^2) + 2C_{WWZ}^2 (12m_W^2 + 7p^2) \\
& + 7C_{ZZh}^2 (p^2 - 3(m_h^2 + m_Z^2))))),
\end{aligned} \tag{A.1.4}$$

$$\begin{aligned}
\Pi_{WW}(p^2) &= \frac{g^2 m_W^2}{18\Lambda^4 p^2} \left(3 \left(-C_{WW\gamma}^2 (m_W^2 - p^2)^2 (m_W^2 + p^2) B_0(p^2, m_W^2, 0) + C_{WW h}^2 (-p^2) (m_h^4 \right. \right. \\
& - 2m_h^2 (m_W^2 + p^2) + (m_W^2 - p^2)^2) B_0(p^2, m_W^2, m_h^2) - C_{WWZ}^2 (m_W^6 - m_W^4 (2m_Z^2 + p^2) \\
& + m_W^2 (m_Z^4 + 8m_Z^2 p^2 - (p^2)^2) + p^2 (m_Z^2 - p^2)^2) B_0(p^2, m_W^2, m_Z^2) - C_{WWZ}^2 A_0(m_Z^2) (m_W^2 + p^2) \\
& (m_W^2 - m_Z^2 - p^2)) + 3A_0(m_W^2) (C_{WW\gamma}^2 (m_W^4 - 10m_W^2 p^2 + (p^2)^2) + C_{WW h}^2 p^2 (-m_h^2 + m_W^2 + p^2) \\
& + C_{WWZ}^2 (m_W^4 - m_W^2 (m_Z^2 + 10p^2) + p^2 (p^2 - m_Z^2))) + 3C_{WW h}^2 p^2 A_0(m_h^2) (m_h^2 - m_W^2 + p^2) \\
& + p^2 (C_{WW\gamma}^2 (87m_W^4 - 14m_W^2 p^2 + 7(p^2)^2) + 7C_{WW h}^2 p^2 (p^2 - 3(m_h^2 + m_W^2)) + C_{WWZ}^2 \\
& (-7p^2 (2m_W^2 + 3m_Z^2) + 87m_W^2 (m_W^2 + m_Z^2) + 7(p^2)^2))).
\end{aligned} \tag{A.1.5}$$

Out of these, $\Pi_{\gamma\gamma}$, $\Pi_{\gamma Z}$ and Π_{ZZ} vanish at $p^2 = 0$. Note that in Π_{WW} there is an overall $1/p^2$ dependence. We would like to mention that both Π_{WW} and its derivative converge smoothly in $p^2 \rightarrow 0$ limit. The one-loop scalar functions in $n = 4 - 2\epsilon$ dimensions are given by,

$$\begin{aligned}
A_0(m_0^2) &= \int \frac{d^n l}{(2\pi)^n} \frac{1}{l^2 - m_0^2} \\
&\equiv \frac{1}{16\pi^2} m_0^2 \left[\frac{1}{\epsilon} + 1 - \ln(m_0^2) \right], \\
B_0(p^2, m_0^2, m_1^2) &= \int \frac{d^n l}{(2\pi)^n} \frac{1}{(l^2 - m_0^2) ((l+p)^2 - m_1^2)}
\end{aligned} \tag{A.1.6}$$

$$\equiv \frac{1}{16\pi^2} \left[\frac{1}{\epsilon} - \Delta(p^2, m_0^2, m_1^2) \right], \quad (\text{A.1.7})$$

where,

$$\Delta(p^2, m_0^2, m_1^2) = \int_0^1 dx \ln [-x(1-x)p^2 + x(m_1^2 - m_0^2) + m_0^2]. \quad (\text{A.1.8})$$

This form is suitable for computing B_0 and its derivative with respect to p^2 at $p^2 = 0$, which we require to calculate S, T and U parameters discussed in section 3.

Bibliography

- [1] ATLAS Collaboration, G. Aad et al., *Observation of a new particle in the search for the Standard Model Higgs boson with the ATLAS detector at the LHC*, *Phys. Lett.* **B716** (2012) 1–29, [[arXiv:1207.7214](#)].
- [2] CMS Collaboration, S. Chatrchyan et al., *Observation of a new boson at a mass of 125 GeV with the CMS experiment at the LHC*, *Phys. Lett.* **B716** (2012) 30–61, [[arXiv:1207.7235](#)].
- [3] W. Buchmüller and D. Wyler, *Effective lagrangian analysis of new interactions and flavour conservation*, *Nuclear Physics B* **268** (1986), no. 3 621 – 653.
- [4] M. C. Gonzalez-Garcia, *Anomalous Higgs couplings*, *Int. J. Mod. Phys.* **A14** (1999) 3121–3156, [[hep-ph/9902321](#)].
- [5] T. Han and J. Jiang, *CP violating $Z Z H$ coupling at e^+e^- linear colliders*, *Phys. Rev.* **D63** (2001) 096007, [[hep-ph/0011271](#)].
- [6] T. Plehn, D. L. Rainwater, and D. Zeppenfeld, *Determining the structure of Higgs couplings at the LHC*, *Phys. Rev. Lett.* **88** (2002) 051801, [[hep-ph/0105325](#)].
- [7] V. Barger, T. Han, P. Langacker, B. McElrath, and P. Zerwas, *Effects of genuine dimension-six Higgs operators*, *Phys. Rev.* **D67** (2003) 115001, [[hep-ph/0301097](#)].
- [8] S. S. Biswal, R. M. Godbole, R. K. Singh, and D. Choudhury, *Signatures of anomalous VVH interactions at a linear collider*, *Phys. Rev.* **D73** (2006) 035001, [[hep-ph/0509070](#)]. [Erratum: *Phys. Rev.* **D74**, 039904(2006)].
- [9] T. Han, Y.-P. Kuang, and B. Zhang, *Anomalous gauge couplings of the Higgs boson at high energy photon colliders*, *Phys. Rev.* **D73** (2006) 055010, [[hep-ph/0512193](#)].

- [10] R. M. Godbole, D. J. Miller, and M. M. Muhlleitner, *Aspects of CP violation in the H ZZ coupling at the LHC*, *JHEP* **12** (2007) 031, [[arXiv:0708.0458](#)].
- [11] N. D. Christensen, T. Han, and Y. Li, *Testing CP Violation in ZZH Interactions at the LHC*, *Phys. Lett.* **B693** (2010) 28–35, [[arXiv:1005.5393](#)].
- [12] B. Grzadkowski, M. Iskrzynski, M. Misiak, and J. Rosiek, *Dimension-Six Terms in the Standard Model Lagrangian*, *JHEP* **10** (2010) 085, [[arXiv:1008.4884](#)].
- [13] N. Desai, D. K. Ghosh, and B. Mukhopadhyaya, *CP-violating HWW couplings at the Large Hadron Collider*, *Phys. Rev.* **D83** (2011) 113004, [[arXiv:1104.3327](#)].
- [14] **ATLAS** Collaboration, G. Aad et al., *Constraints on new phenomena via Higgs boson couplings and invisible decays with the ATLAS detector*, *JHEP* **11** (2015) 206, [[arXiv:1509.0067](#)].
- [15] K.-m. Cheung, C.-H. Chou, and O. C. W. Kong, *Muon anomalous magnetic moment, two Higgs doublet model, and supersymmetry*, *Phys. Rev.* **D64** (2001) 111301, [[hep-ph/0103183](#)].
- [16] A. Broggio, E. J. Chun, M. Passera, K. M. Patel, and S. K. Vempati, *Limiting two-Higgs-doublet models*, *JHEP* **11** (2014) 058, [[arXiv:1409.3199](#)].
- [17] E. J. Chun, Z. Kang, M. Takeuchi, and Y.-L. S. Tsai, *LHC τ -rich tests of lepton-specific 2HDM for $(g - 2)_\mu$* , *JHEP* **11** (2015) 099, [[arXiv:1507.0806](#)].
- [18] D. L. Rainwater, D. Zeppenfeld, and K. Hagiwara, *Searching for $H \rightarrow \tau^+\tau^-$ in weak boson fusion at the CERN LHC*, *Phys. Rev.* **D59** (1998) 014037, [[hep-ph/9808468](#)].
- [19] **ZEUS, H1** Collaboration, H. Abramowicz et al., *Combination of measurements of inclusive deep inelastic $e^\pm p$ scattering cross sections and QCD analysis of HERA data*, *Eur. Phys. J.* **C75** (2015), no. 12 580, [[arXiv:1506.0604](#)].
- [20] **BCDMS** Collaboration, A. C. Benvenuti et al., *A High Statistics Measurement of the Proton Structure Functions $F(2)$ (x, Q^{*2}) and R from Deep Inelastic Muon Scattering at High Q^{*2}* , *Phys. Lett.* **B223** (1989) 485–489.
- [21] M. Arneodo, A. Arvidson, B. Badeek, M. Ballintijn, G. Baum, J. Beaufays, I. Bird, P. Bjrkholm, M. Botje, C. Brogini, W. Breckner, A. Brill, W. Burger, J. Ciborowski, R. van Dantzig, A. Dyring, H. Engelen, M. Ferrero, L. Fluri, U. Gaul, T. Granier,

- M. Grosse-Perdekamp, D. von Harrach, M. van der Heijden, C. Heusch, Q. Ingram, M. de Jong, E. Kabu, R. Kaiser, T. Ketel, F. Klein, S. Kullander, U. Landgraf, T. Lindqvist, G. Mallot, C. Mariotti, G. van Middelkoop, A. Milsztajn, Y. Mizuno, A. Most, A. Mcklich, J. Nassalski, D. Nowotny, J. Oberski, A. Pai, C. Peroni, B. Povh, K. Prytz, R. Rieger, K. Rith, K. Rhrich, E. Rondio, L. Ropelewski, A. Sandacz, D. Sanders, C. Scholz, R. Seitz, F. Sever, T.-A. Shibata, M. Siebler, A. Simon, A. Staiano, M. Szleper, W. Taczaa, Y. Tzamouranis, M. Virchaux, J. Vuilleumier, T. Walcher, R. Windmolders, A. Witzmann, K. Zaremba, and F. Zetsche, *Measurement of the proton and deuteron structure functions, f_2p and f_2d , and of the ratio lt* , *Nuclear Physics B* **483** (1997), no. 1 3 – 43.
- [22] M. R. Adams, S. Aïd, P. L. Anthony, D. A. Averill, M. D. Baker, B. R. Baller, A. Banerjee, A. A. Bhatti, U. Bratzler, H. M. Braun, T. J. Carroll, H. L. Clark, J. M. Conrad, R. Davisson, I. Derado, F. S. Dietrich, W. Dougherty, T. Dreyer, V. Eckardt, U. Ecker, M. Erdmann, G. Y. Fang, J. Figiel, R. W. Finlay, H. J. Gebauer, D. F. Geesaman, K. A. Griffioen, R. S. Guo, J. Haas, C. Halliwell, D. Hantke, K. H. Hicks, H. E. Jackson, D. E. Jaffe, G. Jancso, D. M. Jansen, Z. Jin, S. Kaufman, R. D. Kennedy, E. R. Kinney, H. G. E. Kobrak, A. V. Kotwal, S. Kunori, J. J. Lord, H. J. Lubatti, D. McLeod, P. Madden, S. Magill, A. Manz, H. Melanson, D. G. Michael, H. E. Montgomery, J. G. Morfin, R. B. Nickerson, J. Novak, S. O’Day, K. Olkiewicz, L. Osborne, R. Otten, V. Papavassiliou, B. Pawlik, F. M. Pipkin, D. H. Potterveld, E. J. Ramberg, A. Röser, J. J. Ryan, C. W. Salgado, A. Salvarani, H. Schellman, M. Schmitt, N. Schmitz, G. Siegert, A. Skuja, G. A. Snow, S. Söldner-Rembold, P. Spentzouris, H. E. Stier, P. Stopa, R. A. Swanson, H. Venkataramania, M. Wilhelm, R. Wilson, W. Wittek, S. A. Wolbers, A. Zghiche, and T. Zhao, *Proton and deuteron structure functions in muon scattering at 470 gev*, *Phys. Rev. D* **54** (Sep, 1996) 3006–3056.
- [23] L. W. Whitlow, E. M. Riordan, S. Dasu, S. Rock, and A. Bodek, *Precise measurements of the proton and deuteron structure functions from a global analysis of the SLAC deep inelastic electron scattering cross-sections*, *Phys. Lett.* **B282** (1992) 475–482.
- [24] **Particle Data Group** Collaboration, C. Patrignani et al., *Review of Particle Physics*, *Chin. Phys.* **C40** (2016), no. 10 100001.

- [25] S. Schael et al., *Precision electroweak measurements on the z resonance*, *Physics Reports* **427** (2006), no. 5 257 – 454.
- [26] **NNPDF** Collaboration, R. D. Ball et al., *Parton distributions for the LHC Run II*, *JHEP* **04** (2015) 040, [[arXiv:1410.8849](#)].
- [27] **NNPDF** Collaboration, E. R. Nocera, R. D. Ball, S. Forte, G. Ridolfi, and J. Rojo, *A first unbiased global determination of polarized PDFs and their uncertainties*, *Nucl. Phys.* **B887** (2014) 276–308, [[arXiv:1406.5539](#)].
- [28] **ATLAS, CMS** Collaboration, G. Aad et al., *Measurements of the Higgs boson production and decay rates and constraints on its couplings from a combined ATLAS and CMS analysis of the LHC pp collision data at $\sqrt{s} = 7$ and 8 TeV*, *JHEP* **08** (2016) 045, [[arXiv:1606.0226](#)].
- [29] <https://twiki.cern.ch/twiki/bin/view/LHCPhysics/CrossSections>.
- [30] **The ATLAS and CMS Collaborations** Collaboration, *ATLAS-CONF-2015-044*, tech. rep., 2015.
- [31] R. P. Feynman and M. Gell-Mann, *Theory of Fermi interaction*, *Phys. Rev.* **109** (1958) 193–198.
- [32] E. C. G. Sudarshan and R. e. Marshak, *Chirality invariance and the universal Fermi interaction*, *Phys. Rev.* **109** (1958) 1860–1860.
- [33] S. L. Glashow, *Partial Symmetries of Weak Interactions*, *Nucl. Phys.* **22** (1961) 579–588.
- [34] S. Weinberg, *A Model of Leptons*, *Phys. Rev. Lett.* **19** (1967) 1264–1266.
- [35] A. Salam, *Weak and Electromagnetic Interactions*, *Conf. Proc.* **C680519** (1968) 367–377.
- [36] **UA1** Collaboration, G. Arnison et al., *Experimental Observation of Isolated Large Transverse Energy Electrons with Associated Missing Energy at $\sqrt{s} = 540$ GeV*, *Phys. Lett.* **122B** (1983) 103–116. [,611(1983)].
- [37] G. Arnison et al., *Experimental observation of lepton pairs of invariant mass around 95 gev/c^2 at the CERN SPS collider*, *Physics Letters B* **126** (1983), no. 5 398 – 410.

- [38] **UA2** Collaboration, M. Banner et al., *Observation of Single Isolated Electrons of High Transverse Momentum in Events with Missing Transverse Energy at the CERN $\bar{p}p$ Collider*, *Phys. Lett.* **122B** (1983) 476–485.
- [39] **UA2** Collaboration, P. Bagnaia et al., *Evidence for $Z^0 \rightarrow e^+e^-$ at the CERN $\bar{p}p$ Collider*, *Phys. Lett.* **129B** (1983) 130–140.
- [40] **CDF Collaboration** Collaboration, F. Abe et al., *Observation of top quark production in $\bar{p}p$ collisions with the collider detector at Fermilab*, *Phys. Rev. Lett.* **74** (Apr, 1995) 2626–2631.
- [41] **D0** Collaboration, S. Abachi et al., *Observation of the top quark*, *Phys. Rev. Lett.* **74** (1995) 2632–2637, [[hep-ex/9503003](#)].
- [42] F. Englert and R. Brout, *Broken Symmetry and the Mass of Gauge Vector Mesons*, *Phys. Rev. Lett.* **13** (1964) 321–323.
- [43] P. W. Higgs, *Broken Symmetries and the Masses of Gauge Bosons*, *Phys. Rev. Lett.* **13** (1964) 508–509.
- [44] G. S. Guralnik, C. R. Hagen, and T. W. B. Kibble, *Global Conservation Laws and Massless Particles*, *Phys. Rev. Lett.* **13** (1964) 585–587.
- [45] M. Veltman, *Limit on mass differences in the weinberg model*, *Nuclear Physics B* **123** (1977), no. 1 89 – 99.
- [46] M. Chanowitz, M. Furman, and I. Hinchliffe, *Weak interactions of ultra heavy fermions*, *Physics Letters B* **78** (1978), no. 2 285 – 289.
- [47] P. Sikivie, L. Susskind, M. Voloshin, and V. Zakharov, *Isospin breaking in technicolor models*, *Nuclear Physics B* **173** (1980), no. 2 189 – 207.
- [48] R. A. Diaz and R. Martinez, *The Custodial symmetry*, *Rev. Mex. Fis.* **47** (2001) 489–492, [[hep-ph/0302058](#)].
- [49] N. Cabibbo, *Unitary symmetry and leptonic decays*, *Phys. Rev. Lett.* **10** (Jun, 1963) 531–533.
- [50] M. Kobayashi and T. Maskawa, *CP Violation in the Renormalizable Theory of Weak Interaction*, *Prog. Theor. Phys.* **49** (1973) 652–657.

- [51] E. D. Bloom, D. H. Coward, H. DeStaebler, J. Drees, G. Miller, L. W. Mo, R. E. Taylor, M. Breidenbach, J. I. Friedman, G. C. Hartmann, and H. W. Kendall, *High-energy inelastic $e - p$ scattering at 6° and 10°* , *Phys. Rev. Lett.* **23** (Oct, 1969) 930–934.
- [52] M. Breidenbach, J. I. Friedman, H. W. Kendall, E. D. Bloom, D. H. Coward, H. DeStaebler, J. Drees, L. W. Mo, and R. E. Taylor, *Observed behavior of highly inelastic electron-proton scattering*, *Phys. Rev. Lett.* **23** (Oct, 1969) 935–939.
- [53] J. D. Bjorken, *Asymptotic sum rules at infinite momentum*, *Phys. Rev.* **179** (Mar, 1969) 1547–1553.
- [54] R. P. Feynman, *Photon-hadron interactions*, .
- [55] J. D. Bjorken and E. A. Paschos, *Inelastic electron-proton and γ -proton scattering and the structure of the nucleon*, *Phys. Rev.* **185** (Sep, 1969) 1975–1982.
- [56] J. I. Friedman and H. W. Kendall, *Deep inelastic electron scattering*, *Annual Review of Nuclear Science* **22** (1972), no. 1 203–254,
[\[https://doi.org/10.1146/annurev.ns.22.120172.001223\]](https://doi.org/10.1146/annurev.ns.22.120172.001223).
- [57] H. W. Kendall, *Deep inelastic scattering: Experiments on the proton and the observation of scaling*, *Rev. Mod. Phys.* **63** (Jul, 1991) 597–614.
- [58] J. I. Friedman, *Deep inelastic scattering: Comparisons with the quark model*, *Rev. Mod. Phys.* **63** (Jul, 1991) 615–627.
- [59] **TASSO** Collaboration, R. Brandelik et al., *Evidence for Planar Events in e^+e^- Annihilation at High-Energies*, *Phys. Lett.* **86B** (1979) 243–249.
- [60] D. P. Barber et al., *Discovery of Three Jet Events and a Test of Quantum Chromodynamics at PETRA Energies*, *Phys. Rev. Lett.* **43** (1979) 830.
- [61] **PLUTO** Collaboration, C. Berger et al., *Evidence for Gluon Bremsstrahlung in e^+e^- Annihilations at High-Energies*, *Phys. Lett.* **86B** (1979) 418–425.
- [62] **JADE** Collaboration, W. Bartel et al., *Observation of Planar Three Jet Events in e^+e^- Annihilation and Evidence for Gluon Bremsstrahlung*, *Phys. Lett.* **91B** (1980) 142–147.

- [63] D. J. Gross and F. Wilczek, *Ultraviolet behavior of non-abelian gauge theories*, *Phys. Rev. Lett.* **30** (Jun, 1973) 1343–1346.
- [64] H. D. Politzer, *Reliable perturbative results for strong interactions?*, *Phys. Rev. Lett.* **30** (Jun, 1973) 1346–1349.
- [65] S. Bethke, *The 2009 world average of α_s* , *The European Physical Journal C* **64** (Dec, 2009) 689–703.
- [66] F. Hasert, H. Faissner, W. Krenz, J. V. Krogh, D. Lanske, J. Morfin, K. Schultze, H. Weerts, G. Bertrand-Coremans, J. Lemonne, J. Sacton, W. V. Doninck, P. Vilain, C. Baltay, D. Cundy, D. Haidt, M. Jaffre, P. Musset, A. Pullia, S. Natali, J. Pattison, D. Perkins, A. Rousset, W. Venus, H. Wachsmuth, V. Brisson, B. Degrange, M. Haguenaer, L. Kluberg, U. Nguyen-Khac, P. Petiau, E. Bellotti, S. Bonetti, D. Cavalli, C. Conta, E. Fiorini, M. Rollier, B. Aubert, L. Chounet, P. Heusse, A. Lagarrigue, A. Lutz, J. Vialle, F. Bullock, M. Esten, T. Jones, J. McKenzie, A. Michette, G. Myatt, J. Pinfold, and W. Scott, *Search for elastic muon-neutrino electron scattering*, *Physics Letters B* **46** (1973), no. 1 121 – 124.
- [67] F. Hasert, S. Kabe, W. Krenz, J. V. Krogh, D. Lanske, J. Morfin, K. Schultze, H. Weerts, G. Bertrand-Coremans, J. Sacton, W. V. Doninck, P. Vilain, U. Camerini, D. Cundy, R. Baldi, I. Danilchenko, W. Fry, D. Haidt, S. Natali, P. Musset, B. Osculati, R. Palmer, J. Pattison, D. Perkins, A. Pullia, A. Rousset, W. Venus, H. Wachsmuth, V. Brisson, B. Degrange, M. Haguenaer, L. Kluberg, U. Nguyen-Khac, P. Petiau, E. Belotti, S. Bonetti, D. Cavalli, C. Conta, E. Fiorini, M. Rollier, B. Aubert, D. Blum, L. Chounet, P. Heusse, A. Lagarrigue, A. Lutz, A. Orkin-Lecourtois, J. Vialle, F. Bullock, M. Esten, T. Jones, J. McKenzie, A. Michette, G. Myatt, and W. Scott, *Observation of neutrino-like interactions without muon or electron in the gargamelle neutrino experiment*, *Physics Letters B* **46** (1973), no. 1 138 – 140.
- [68] C. Prescott, W. Atwood, R. Cottrell, H. DeStaebler, E. L. Garwin, A. Gonidec, R. Miller, L. Rochester, T. Sato, D. Sherden, C. Sinclair, S. Stein, R. Taylor, J. Clendenin, V. Hughes, N. Sasao, K. Schler, M. Borghini, K. Lbelsmeyer, and W. Jentschke, *Parity non-conservation in inelastic electron scattering*, *Physics Letters B* **77** (1978), no. 3 347 – 352.

- [69] C. Prescott, W. Atwood, R. Cottrell, H. DeStaebler, E. L. Garwin, A. Gonidec, R. Miller, L. Rochester, T. Sato, D. Sherden, C. Sinclair, S. Stein, R. Taylor, C. Young, J. Clendenin, V. Hugnes, N. Sasao, K. Schler, M. Borghini, K. Lbelsmeyer, and W. Jentschke, *Further measurements of parity non-conservation in inelastic electron scattering*, *Physics Letters B* **84** (1979), no. 4 524 – 528.
- [70] D. P. Barber, U. Becker, G. D. Bei, G. Berghoff, A. Böhm, J. G. Branson, J. Bron, D. Buikman, J. D. Burger, M. Capell, C. C. Chang, G. F. Chen, H. S. Chen, M. Chen, C. P. Cheng, Y. S. Chu, R. Clare, P. Duinker, G. Y. Fang, Z. Y. Feng, H. S. Fesefeldt, D. Fong, M. Fukushima, J. C. Guo, A. Hariri, D. Harting, G. Hertel, M. C. Ho, T. T. Hsu, M. M. Ilyas, D. Z. Jiang, R. Kadel, W. Krenz, Q. Z. Li, D. Luckey, E. J. Luit, C. M. Ma, G. G. G. Massaro, T. Matsuda, H. Newman, M. Pohl, F. P. Poschmann, J. P. Revol, M. Rohde, H. Rykaczewski, I. Schulz, K. Sinram, M. Steuer, G. M. Swider, H. W. Tang, D. Teuchert, S. C. C. Ting, K. L. Tung, F. Vannucci, Y. X. Wang, J. Warnock, M. White, S. X. Wu, P. C. Yang, C. C. Yu, Y. Q. Zeng, N. L. Zhang, and R. Y. Zhu, *Experimental study of electroweak parameters at PETRA energies $12 \leq E_{c.m.} \leq 36.7$ GeV*, *Phys. Rev. Lett.* **46** (Jun, 1981) 1663–1667.
- [71] P. Duinker, *Review of e^+e^- physics at PETRA*, *Rev. Mod. Phys.* **54** (Apr, 1982) 325–387.
- [72] J. E. Kim, P. Langacker, M. Levine, and H. H. Williams, *A theoretical and experimental review of the weak neutral current: a determination of its structure and limits on deviations from the minimal $SU(2)_L \times U(1)$ electroweak theory*, *Rev. Mod. Phys.* **53** (Apr, 1981) 211–252.
- [73] G. Hooft, *Renormalizable lagrangians for massive Yang-Mills fields*, *Nuclear Physics B* **35** (1971), no. 1 167 – 188.
- [74] G. 't Hooft and M. Veltman, *Regularization and renormalization of gauge fields*, *Nuclear Physics B* **44** (1972), no. 1 189 – 213.
- [75] M. E. Peskin and T. Takeuchi, *Estimation of oblique electroweak corrections*, *Phys. Rev. D* **46** (Jul, 1992) 381–409.
- [76] M. D. Schwartz, *Quantum Field Theory and the Standard Model*. Cambridge University Press, 2014.

- [77] H. Georgi and S. L. Glashow, *Unity of all elementary-particle forces*, *Phys. Rev. Lett.* **32** (Feb, 1974) 438–441.
- [78] J. C. Pati and A. Salam, *Lepton number as the fourth "color"*, *Phys. Rev. D* **10** (Jul, 1974) 275–289.
- [79] P. Langacker, *Grand Unified Theories and Proton Decay*, *Phys. Rept.* **72** (1981) 185.
- [80] H. Georgi, H. R. Quinn, and S. Weinberg, *Hierarchy of interactions in unified gauge theories*, *Phys. Rev. Lett.* **33** (Aug, 1974) 451–454.
- [81] U. Amaldi, A. Böhm, L. S. Durkin, P. Langacker, A. K. Mann, W. J. Marciano, A. Sirlin, and H. H. Williams, *Comprehensive analysis of data pertaining to the weak neutral current and the intermediate-vector-boson masses*, *Phys. Rev. D* **36** (Sep, 1987) 1385–1407.
- [82] J. Ellis, S. Kelley, and D. Nanopoulos, *Probing the desert using gauge coupling unification*, *Physics Letters B* **260** (1991), no. 1 131 – 137.
- [83] U. Amaldi, W. de Boer, and H. Frstenau, *Comparison of grand unified theories with electroweak and strong coupling constants measured at lep*, *Physics Letters B* **260** (1991), no. 3 447 – 455.
- [84] P. Langacker and M. Luo, *Implications of precision electroweak experiments for m_t , ρ_0 , $\sin^2\theta_W$, and grand unification*, *Phys. Rev. D* **44** (Aug, 1991) 817–822.
- [85] C. GIUNTI, C. W. KIM, and U. W. LEE, *Running coupling constants and grand unification models*, *Modern Physics Letters A* **06** (1991), no. 19 1745–1755, [<http://www.worldscientific.com/doi/pdf/10.1142/S0217732391001883>].
- [86] M. J. G. Veltman, *Second Threshold in Weak Interactions*, *Acta Phys. Polon.* **B8** (1977) 475.
- [87] M. J. G. Veltman, *The Infrared - Ultraviolet Connection*, *Acta Phys. Polon.* **B12** (1981) 437.
- [88] S. P. Martin, *A Supersymmetry primer*, [hep-ph/9709356](http://arxiv.org/abs/hep-ph/9709356). [Adv. Ser. Direct. High Energy Phys.18,1(1998)].

- [89] C. A. Baker, D. D. Doyle, P. Geltenbort, K. Green, M. G. D. van der Grinten, P. G. Harris, P. Iaydjiev, S. N. Ivanov, D. J. R. May, J. M. Pendlebury, J. D. Richardson, D. Shiers, and K. F. Smith, *Improved experimental limit on the electric dipole moment of the neutron*, *Phys. Rev. Lett.* **97** (Sep, 2006) 131801.
- [90] R. Crewther, P. D. Vecchia, G. Veneziano, and E. Witten, *Chiral estimate of the electric dipole moment of the neutron in quantum chromodynamics*, *Physics Letters B* **88** (1979), no. 1 123 – 127.
- [91] R. D. Peccei, *The Strong CP problem and axions*, *Lect. Notes Phys.* **741** (2008) 3–17, [[hep-ph/0607268](#)]. [,3(2006)].
- [92] M. C. Gonzalez-Garcia and Y. Nir, *Neutrino masses and mixing: evidence and implications*, *Rev. Mod. Phys.* **75** (Mar, 2003) 345–402.
- [93] R. N. Mohapatra and A. Y. Smirnov, *Neutrino Mass and New Physics*, *Ann. Rev. Nucl. Part. Sci.* **56** (2006) 569–628, [[hep-ph/0603118](#)].
- [94] M. Gell-Mann, P. Ramond, and R. Slansky, *Complex Spinors and Unified Theories*, *Conf. Proc.* **C790927** (1979) 315–321, [[arXiv:1306.4669](#)].
- [95] P. Ramond, *The Family Group in Grand Unified Theories*, in *International Symposium on Fundamentals of Quantum Theory and Quantum Field Theory Palm Coast, Florida, February 25-March 2, 1979*, pp. 265–280, 1979. [hep-ph/9809459](#).
- [96] R. N. Mohapatra and G. Senjanović, *Neutrino mass and spontaneous parity nonconservation*, *Phys. Rev. Lett.* **44** (Apr, 1980) 912–915.
- [97] F. Zwicky, *Die Rotverschiebung von extragalaktischen Nebeln*, *Helv. Phys. Acta* **6** (1933) 110–127. [Gen. Rel. Grav.41,207(2009)].
- [98] F. Zwicky, *On the Masses of Nebulae and of Clusters of Nebulae*, *The Astrophysical Journal* **86** (Oct., 1937) 217.
- [99] V. C. Rubin, *Dark matter in spiral galaxies*, *Scientific American* **248** (June, 1983) 96–106.
- [100] **Planck** Collaboration, P. A. R. Ade et al., *Planck 2015 results. XIII. Cosmological parameters*, *Astron. Astrophys.* **594** (2016) A13, [[arXiv:1502.0158](#)].

- [101] G. Hinshaw, D. Larson, E. Komatsu, D. N. Spergel, C. L. Bennett, J. Dunkley, M. R. Nolta, M. Halpern, R. S. Hill, N. Odegard, L. Page, K. M. Smith, J. L. Weiland, B. Gold, N. Jarosik, A. Kogut, M. Limon, S. S. Meyer, G. S. Tucker, E. Wollack, and E. L. Wright, *Nine-year Wilkinson Microwave Anisotropy Probe (WMAP) Observations: Cosmological Parameter Results, The Astrophysical Journal Supplement Series* **208** (2013), no. 2 19.
- [102] A. D. Sakharov, *Violation of CP Invariance, c Asymmetry, and Baryon Asymmetry of the Universe, Pisma Zh. Eksp. Teor. Fiz.* **5** (1967) 32–35. [Usp. Fiz. Nauk161,61(1991)].
- [103] V. A. Kuzmin, V. A. Rubakov, and M. E. Shaposhnikov, *On anomalous electroweak baryon-number non-conservation in the early universe, Physics Letters B* **155** (May, 1985) 36–42.
- [104] V. A. Rubakov and M. E. Shaposhnikov, *Electroweak baryon number nonconservation in the early universe and in high-energy collisions, Usp. Fiz. Nauk* **166** (1996) 493–537, [[hep-ph/9603208](#)]. [Phys. Usp.39,461(1996)].
- [105] **Muon g-2** Collaboration, H. N. Brown et al., *Precise measurement of the positive muon anomalous magnetic moment, Phys. Rev. Lett.* **86** (2001) 2227–2231, [[hep-ex/0102017](#)].
- [106] **Muon g-2** Collaboration, G. W. Bennett et al., *Final Report of the Muon E821 Anomalous Magnetic Moment Measurement at BNL, Phys. Rev.* **D73** (2006) 072003, [[hep-ex/0602035](#)].
- [107] A. Czarnecki and W. J. Marciano, *The Muon anomalous magnetic moment: A Harbinger for 'new physics', Phys. Rev.* **D64** (2001) 013014, [[hep-ph/0102122](#)].
- [108] **LHC Higgs Cross Section Working Group** Collaboration, D. de Florian et al., *Handbook of LHC Higgs Cross Sections: 4. Deciphering the Nature of the Higgs Sector*, [arXiv:1610.0792](#).
- [109] **ATLAS** Collaboration, G. Aad et al., *Constraints on non-Standard Model Higgs boson interactions in an effective Lagrangian using differential cross sections measured in the $H \rightarrow \gamma\gamma$ decay channel at $\sqrt{s} = 8\text{TeV}$ with the ATLAS detector, Phys. Lett.* **B753** (2016) 69–85, [[arXiv:1508.0250](#)].

- [110] K. Hagiwara, R. Szalapski, and D. Zeppenfeld, *Anomalous Higgs boson production and decay*, *Phys. Lett.* **B318** (1993) 155–162, [[hep-ph/9308347](#)].
- [111] G. F. Giudice, C. Grojean, A. Pomarol, and R. Rattazzi, *The strongly-interacting light higgs*, *Journal of High Energy Physics* **2007** (2007), no. 06 045.
- [112] R. Contino, M. Ghezzi, C. Grojean, M. Muhlleitner, and M. Spira, *Effective Lagrangian for a light Higgs-like scalar*, *JHEP* **07** (2013) 035, [[arXiv:1303.3876](#)].
- [113] **CMS** Collaboration, V. Khachatryan et al., *Constraints on the spin-parity and anomalous HVV couplings of the Higgs boson in proton collisions at 7 and 8 TeV*, *Phys. Rev.* **D92** (2015), no. 1 012004, [[arXiv:1411.3441](#)].
- [114] P. P. Giardino, K. Kannike, M. Raidal, and A. Strumia, *Reconstructing Higgs boson properties from the LHC and Tevatron data*, *JHEP* **06** (2012) 117, [[arXiv:1203.4254](#)].
- [115] M. Klute, R. Lafaye, T. Plehn, M. Rauch, and D. Zerwas, *Measuring Higgs Couplings from LHC Data*, *Phys. Rev. Lett.* **109** (2012) 101801, [[arXiv:1205.2699](#)].
- [116] S. Banerjee, S. Mukhopadhyay, and B. Mukhopadhyaya, *New Higgs interactions and recent data from the LHC and the Tevatron*, *JHEP* **10** (2012) 062, [[arXiv:1207.3588](#)].
- [117] M. B. Einhorn and J. Wudka, *Higgs-Boson Couplings Beyond the Standard Model*, *Nucl. Phys.* **B877** (2013) 792–806, [[arXiv:1308.2255](#)].
- [118] **Gfitter Group** Collaboration, M. Baak, J. Cth, J. Haller, A. Hoecker, R. Kogler, K. Mnig, M. Schott, and J. Stelzer, *The global electroweak fit at NNLO and prospects for the LHC and ILC*, *Eur. Phys. J.* **C74** (2014) 3046, [[arXiv:1407.3792](#)].
- [119] J. R. Espinosa, C. Grojean, M. Muhlleitner, and M. Trott, *Fingerprinting Higgs Suspects at the LHC*, *JHEP* **05** (2012) 097, [[arXiv:1202.3697](#)].
- [120] A. Azatov, R. Contino, and J. Galloway, *Model-Independent Bounds on a Light Higgs*, *JHEP* **04** (2012) 127, [[arXiv:1202.3415](#)]. [Erratum: JHEP04,140(2013)].
- [121] E. Masso, *An Effective Guide to Beyond the Standard Model Physics*, *JHEP* **10** (2014) 128, [[arXiv:1406.6376](#)].

- [122] A. Falkowski, *Effective field theory approach to LHC Higgs data*, *Pramana* **87** (2016), no. 3 39, [[arXiv:1505.0004](#)].
- [123] A. V. Manohar and M. B. Wise, *Modifications to the properties of the Higgs boson*, *Phys. Lett.* **B636** (2006) 107–113, [[hep-ph/0601212](#)].
- [124] S. S. Biswal and R. M. Godbole, *Use of transverse beam polarization to probe anomalous VVH interactions at a Linear Collider*, *Phys. Lett.* **B680** (2009) 81–87, [[arXiv:0906.5471](#)].
- [125] S. S. Biswal, R. M. Godbole, B. Mellado, and S. Raychaudhuri, *Azimuthal Angle Probe of Anomalous HWW Couplings at a High Energy ep Collider*, *Phys. Rev. Lett.* **109** (2012) 261801, [[arXiv:1203.6285](#)].
- [126] T. Corbett, O. J. P. Eboli, J. Gonzalez-Fraile, and M. C. Gonzalez-Garcia, *Constraining anomalous Higgs interactions*, *Phys. Rev.* **D86** (2012) 075013, [[arXiv:1207.1344](#)].
- [127] I. Low, J. Lykken, and G. Shaughnessy, *Have We Observed the Higgs (Imposter)?*, *Phys. Rev.* **D86** (2012) 093012, [[arXiv:1207.1093](#)].
- [128] D. McKeen, M. Pospelov, and A. Ritz, *Modified Higgs branching ratios versus CP and lepton flavor violation*, *Phys. Rev.* **D86** (2012) 113004, [[arXiv:1208.4597](#)].
- [129] E. Mass and V. Sanz, *Limits on anomalous couplings of the Higgs boson to electroweak gauge bosons from LEP and the LHC*, *Phys. Rev.* **D87** (2013), no. 3 033001, [[arXiv:1211.1320](#)].
- [130] A. Freitas and P. Schwaller, *Higgs CP Properties From Early LHC Data*, *Phys. Rev.* **D87** (2013), no. 5 055014, [[arXiv:1211.1980](#)].
- [131] T. Corbett, O. J. P. Eboli, J. Gonzalez-Fraile, and M. C. Gonzalez-Garcia, *Robust Determination of the Higgs Couplings: Power to the Data*, *Phys. Rev.* **D87** (2013) 015022, [[arXiv:1211.4580](#)].
- [132] W. Dekens and J. de Vries, *Renormalization Group Running of Dimension-Six Sources of Parity and Time-Reversal Violation*, *JHEP* **05** (2013) 149, [[arXiv:1303.3156](#)].

- [133] A. Djouadi and G. Moreau, *The couplings of the Higgs boson and its CP properties from fits of the signal strengths and their ratios at the 7+8 TeV LHC*, *Eur. Phys. J.* **C73** (2013), no. 9 2512, [[arXiv:1303.6591](#)].
- [134] W.-F. Chang, W.-P. Pan, and F. Xu, *Effective gauge-Higgs operators analysis of new physics associated with the Higgs boson*, *Phys. Rev.* **D88** (2013), no. 3 033004, [[arXiv:1303.7035](#)].
- [135] R. Godbole, D. J. Miller, K. Mohan, and C. D. White, *Boosting Higgs CP properties via VH Production at the Large Hadron Collider*, *Phys. Lett.* **B730** (2014) 275–279, [[arXiv:1306.2573](#)].
- [136] S. Banerjee, S. Mukhopadhyay, and B. Mukhopadhyaya, *Higher dimensional operators and the LHC Higgs data: The role of modified kinematics*, *Phys. Rev.* **D89** (2014), no. 5 053010, [[arXiv:1308.4860](#)].
- [137] I. Anderson et al., *Constraining anomalous HVV interactions at proton and lepton colliders*, *Phys. Rev.* **D89** (2014), no. 3 035007, [[arXiv:1309.4819](#)].
- [138] C.-Y. Chen, S. Dawson, and C. Zhang, *Electroweak Effective Operators and Higgs Physics*, *Phys. Rev.* **D89** (2014), no. 1 015016, [[arXiv:1311.3107](#)].
- [139] J. Ellis, V. Sanz, and T. You, *Complete Higgs Sector Constraints on Dimension-6 Operators*, *JHEP* **07** (2014) 036, [[arXiv:1404.3667](#)].
- [140] H. Belusca-Maito, *Effective Higgs Lagrangian and Constraints on Higgs Couplings*, [[arXiv:1404.5343](#)].
- [141] Y. Chen, A. Falkowski, I. Low, and R. Vega-Morales, *New Observables for CP Violation in Higgs Decays*, *Phys. Rev.* **D90** (2014), no. 11 113006, [[arXiv:1405.6723](#)].
- [142] R. M. Godbole, D. J. Miller, K. A. Mohan, and C. D. White, *Jet substructure and probes of CP violation in Vh production*, *JHEP* **04** (2015) 103, [[arXiv:1409.5449](#)].
- [143] A. Falkowski and F. Riva, *Model-independent precision constraints on dimension-6 operators*, *JHEP* **02** (2015) 039, [[arXiv:1411.0669](#)].
- [144] A. Riotto, *Theories of baryogenesis*, in *Proceedings, Summer School in High-energy physics and cosmology: Trieste, Italy, June 29-July 17, 1998*, pp. 326–436, 1998. [[hep-ph/9807454](#)].

- [145] M. B. Voloshin, *CP Violation in Higgs Diphoton Decay in Models with Vectorlike Heavy Fermions*, *Phys. Rev.* **D86** (2012) 093016, [[arXiv:1208.4303](#)].
- [146] M. B. Gavela, J. Gonzalez-Fraile, M. C. Gonzalez-Garcia, L. Merlo, S. Rigolin, and J. Yepes, *CP violation with a dynamical Higgs*, *JHEP* **10** (2014) 044, [[arXiv:1406.6367](#)].
- [147] K.-M. Ruan, J. Shu, and J. Yepes, *CP violation from spin-1 resonances in a left-right dynamical Higgs context*, *Commun. Theor. Phys.* **66** (2016), no. 1 93–103, [[arXiv:1507.0474](#)].
- [148] C. Lim, *Cp violation in higher dimensional theories*, *Physics Letters B* **256** (1991), no. 2 233 – 238.
- [149] C. S. Lim, N. Maru, and K. Nishiwaki, *CP Violation due to Compactification*, *Phys. Rev.* **D81** (2010) 076006, [[arXiv:0910.2314](#)].
- [150] R. D. Peccei and H. R. Quinn, *CP conservation in the presence of pseudoparticles*, *Phys. Rev. Lett.* **38** (Jun, 1977) 1440–1443.
- [151] R. D. Peccei and H. R. Quinn, *Constraints imposed by CP conservation in the presence of pseudoparticles*, *Phys. Rev. D* **16** (Sep, 1977) 1791–1797.
- [152] J. Alwall, R. Frederix, S. Frixione, V. Hirschi, F. Maltoni, O. Mattelaer, H. S. Shao, T. Stelzer, P. Torrielli, and M. Zaro, *The automated computation of tree-level and next-to-leading order differential cross sections, and their matching to parton shower simulations*, *JHEP* **07** (2014) 079, [[arXiv:1405.0301](#)].
- [153] N. D. Christensen and C. Duhr, *FeynRules - Feynman rules made easy*, *Comput. Phys. Commun.* **180** (2009) 1614–1641, [[arXiv:0806.4194](#)].
- [154] J. Pumplin, D. R. Stump, J. Huston, H. L. Lai, P. M. Nadolsky, and W. K. Tung, *New generation of parton distributions with uncertainties from global QCD analysis*, *JHEP* **07** (2002) 012, [[hep-ph/0201195](#)].
- [155] **ATLAS** Collaboration, G. Aad et al., *Measurement of Higgs boson production in the diphoton decay channel in pp collisions at center-of-mass energies of 7 and 8 TeV with the ATLAS detector*, *Phys. Rev.* **D90** (2014), no. 11 112015, [[arXiv:1408.7084](#)].

- [156] CMS Collaboration, V. Khachatryan et al., *Observation of the diphoton decay of the Higgs boson and measurement of its properties*, *Eur. Phys. J.* **C74** (2014), no. 10 3076, [[arXiv:1407.0558](#)].
- [157] ATLAS Collaboration, G. Aad et al., *Measurements of Higgs boson production and couplings in the four-lepton channel in pp collisions at center-of-mass energies of 7 and 8 TeV with the ATLAS detector*, *Phys. Rev.* **D91** (2015), no. 1 012006, [[arXiv:1408.5191](#)].
- [158] CMS Collaboration, S. Chatrchyan et al., *Measurement of the properties of a Higgs boson in the four-lepton final state*, *Phys. Rev.* **D89** (2014), no. 9 092007, [[arXiv:1312.5353](#)].
- [159] *Observation and measurement of Higgs boson decays to WW* with ATLAS at the LHC*, Tech. Rep. ATLAS-CONF-2014-060, CERN, Geneva, Oct, 2014.
- [160] CMS Collaboration, S. Chatrchyan et al., *Measurement of Higgs boson production and properties in the WW decay channel with leptonic final states*, *JHEP* **01** (2014) 096, [[arXiv:1312.1129](#)].
- [161] CMS Collaboration, S. Chatrchyan et al., *Search for a Higgs boson decaying into a Z and a photon in pp collisions at $\sqrt{s} = 7$ and 8 TeV*, *Phys. Lett.* **B726** (2013) 587–609, [[arXiv:1307.5515](#)].
- [162] ATLAS Collaboration, G. Aad et al., *Search for Higgs boson decays to a photon and a Z boson in pp collisions at $\sqrt{s} = 7$ and 8 TeV with the ATLAS detector*, *Phys. Lett.* **B732** (2014) 8–27, [[arXiv:1402.3051](#)].
- [163] CMS Collaboration, V. Khachatryan et al., *Constraints on the Higgs boson width from off-shell production and decay to Z-boson pairs*, *Phys. Lett.* **B736** (2014) 64–85, [[arXiv:1405.3455](#)].
- [164] C. Englert, A. Freitas, M. M. Hlleitner, T. Plehn, M. Rauch, M. Spira, and K. Walz, *Precision Measurements of Higgs Couplings: Implications for New Physics Scales*, *J. Phys.* **G41** (2014) 113001, [[arXiv:1403.7191](#)].
- [165] M. Pospelov and A. Ritz, *Electric dipole moments as probes of new physics*, *Annals Phys.* **318** (2005) 119–169, [[hep-ph/0504231](#)].

- [166] J. Engel, M. J. Ramsey-Musolf, and U. van Kolck, *Electric Dipole Moments of Nucleons, Nuclei, and Atoms: The Standard Model and Beyond*, *Prog. Part. Nucl. Phys.* **71** (2013) 21–74, [[arXiv:1303.2371](#)].
- [167] A. Czarnecki and B. Krause, *Neutron electric dipole moment in the standard model: Valence quark contributions*, *Phys. Rev. Lett.* **78** (1997) 4339–4342, [[hep-ph/9704355](#)].
- [168] C. A. Baker et al., *An Improved experimental limit on the electric dipole moment of the neutron*, *Phys. Rev. Lett.* **97** (2006) 131801, [[hep-ex/0602020](#)].
- [169] **ACME** Collaboration, J. Baron et al., *Order of Magnitude Smaller Limit on the Electric Dipole Moment of the Electron*, *Science* **343** (2014) 269–272, [[arXiv:1310.7534](#)].
- [170] C. Dib, A. Faessler, T. Gutsche, S. Kovalenko, J. Kuckei, V. E. Lyubovitskij, and K. Pumsa-ard, *The Neutron electric dipole form-factor in the perturbative chiral quark model*, *J. Phys.* **G32** (2006) 547–564, [[hep-ph/0601144](#)].
- [171] T. M. Ito, *Plans for a Neutron EDM Experiment at SNS*, *J. Phys. Conf. Ser.* **69** (2007) 012037, [[nucl-ex/0702024](#)].
- [172] M. Raidal et al., *Flavour physics of leptons and dipole moments*, *Eur. Phys. J.* **C57** (2008) 13–182, [[arXiv:0801.1826](#)].
- [173] J.-C. Peng, *Neutron Electric Dipole Moment Experiments*, *Mod. Phys. Lett.* **A23** (2008) 1397–1408, [[arXiv:0804.4254](#)].
- [174] **CDF**, **D0** Collaboration, H. T. Diehl, *Vector Boson Pair Production and Trilinear Gauge Boson Couplings: Results from the Tevatron*, in *High-energy physics. Proceedings, 29th International Conference, ICHEP’98, Vancouver, Canada, July 23-29, 1998. Vol. 1, 2*, pp. 520–524, 1998. [hep-ex/9810006](#).
- [175] **D0** Collaboration, V. M. Abazov et al., *$W\gamma$ production and limits on anomalous $WW\gamma$ couplings in $p\bar{p}$ collisions*, *Phys. Rev. Lett.* **107** (2011) 241803, [[arXiv:1109.4432](#)].
- [176] **ATLAS** Collaboration, G. Aad et al., *Measurement of WZ production in proton-proton collisions at $\sqrt{s} = 7$ TeV with the ATLAS detector*, *Eur. Phys. J.* **C72** (2012) 2173, [[arXiv:1208.1390](#)].

- [177] **ATLAS** Collaboration, G. Aad et al., *Measurement of W^+W^- production in pp collisions at $\sqrt{s} = 7\text{TeV}$ with the ATLAS detector and limits on anomalous WWZ and $WW\gamma$ couplings*, *Phys. Rev.* **D87** (2013), no. 11 112001, [[arXiv:1210.2979](#)].
[Erratum: *Phys. Rev.D* 88, no.7, 079906(2013)].
- [178] **CMS** Collaboration, S. Chatrchyan et al., *Measurement of the W^+W^- Cross section in pp Collisions at $\sqrt{s} = 7\text{TeV}$ and Limits on Anomalous $WW\gamma$ and WWZ couplings*, *Eur. Phys. J.* **C73** (2013), no. 10 2610, [[arXiv:1306.1126](#)].
- [179] **CMS** Collaboration, S. Chatrchyan et al., *Measurement of the $W\gamma$ and $Z\gamma$ inclusive cross sections in pp collisions at $\sqrt{s} = 7\text{TeV}$ and limits on anomalous triple gauge boson couplings*, *Phys. Rev.* **D89** (2014), no. 9 092005, [[arXiv:1308.6832](#)].
- [180] K. Hagiwara, R. D. Peccei, D. Zeppenfeld, and K. Hikasa, *Probing the Weak Boson Sector in $e^+e^- \rightarrow W^+W^-$* , *Nucl. Phys.* **B282** (1987) 253–307.
- [181] S. Dawson, S. K. Gupta, and G. Valencia, *CP violating anomalous couplings in $W\gamma$ and $Z\gamma$ production at the LHC*, *Phys. Rev.* **D88** (2013), no. 3 035008, [[arXiv:1304.3514](#)].
- [182] J. Beringer et al., *Review of particle physics*, *Phys. Rev. D* **86** (Jul, 2012) 010001.
- [183] D. E. Morrissey and M. J. Ramsey-Musolf, *Electroweak baryogenesis*, *New J. Phys.* **14** (2012) 125003, [[arXiv:1206.2942](#)].
- [184] C. N. Leung, S. T. Love, and S. Rao, *Low-energy manifestations of a new interactions scale: Operator analysis*, *Zeitschrift für Physik C Particles and Fields* **31** (Sep, 1986) 433–437.
- [185] R. Rattazzi, *Anomalous interactions at the Z^0 -pole*, *Zeitschrift für Physik C Particles and Fields* **40** (Dec, 1988) 605–611.
- [186] K. Hagiwara and M. L. Stong, *Probing the scalar sector in $e^+e^- \rightarrow f\bar{f}H$* , *Z. Phys.* **C62** (1994) 99–108, [[hep-ph/9309248](#)].
- [187] D. Chang, W.-Y. Keung, and I. Phillips, *CP odd correlation in the decay of neutral Higgs boson into ZZ , W^+W^- , or $t\bar{t}$* , *Phys. Rev.* **D48** (1993) 3225–3234, [[hep-ph/9303226](#)].

- [188] A. Skjold and P. Osland, *Signals of CP violation in Higgs decay*, *Phys. Lett.* **B329** (1994) 305–311, [[hep-ph/9402358](#)].
- [189] G. J. Gounaris, F. M. Renard, and N. D. Vlachos, *Tests of anomalous Higgs boson couplings through $e^-e^+ \rightarrow HZ$ and $H\gamma$* , *Nucl. Phys.* **B459** (1996) 51–74, [[hep-ph/9509316](#)].
- [190] B. Grzadkowski and J. F. Gunion, *Using decay angle correlations to detect CP violation in the neutral Higgs sector*, *Phys. Lett.* **B350** (1995) 218–224, [[hep-ph/9501339](#)].
- [191] K. Hagiwara, S. Ishihara, J. Kamoshita, and B. A. Kniehl, *Prospects of measuring general Higgs couplings at e^+e^- linear colliders*, *Eur. Phys. J.* **C14** (2000) 457–468, [[hep-ph/0002043](#)].
- [192] D. J. Miller, S. Y. Choi, B. Eberle, M. M. Muhlleitner, and P. M. Zerwas, *Measuring the spin of the Higgs boson*, *Phys. Lett.* **B505** (2001) 149–154, [[hep-ph/0102023](#)]. [1825(2001)].
- [193] S. Y. Choi, D. J. Miller, M. M. Muhlleitner, and P. M. Zerwas, *Identifying the Higgs spin and parity in decays to Z pairs*, *Phys. Lett.* **B553** (2003) 61–71, [[hep-ph/0210077](#)].
- [194] B. Zhang, Y.-P. Kuang, H.-J. He, and C. P. Yuan, *Testing anomalous gauge couplings of the Higgs boson via weak boson scatterings at the CERN LHC*, *Phys. Rev.* **D67** (2003) 114024, [[hep-ph/0303048](#)].
- [195] V. Hankele, G. Klamke, D. Zeppenfeld, and T. Figy, *Anomalous Higgs boson couplings in vector boson fusion at the CERN LHC*, *Phys. Rev.* **D74** (2006) 095001, [[hep-ph/0609075](#)].
- [196] V. Hankele, G. Klamke, and D. Zeppenfeld, *Higgs + 2 jets as a probe for CP properties*, in *Meeting on CP Violation and Non-standard Higgs Physics Geneva, Switzerland, December 2-3, 2004*, pp. 58–62, 2006. [[hep-ph/0605117](#)].
- [197] S. S. Biswal, D. Choudhury, R. M. Godbole, and Mamta, *Role of polarization in probing anomalous gauge interactions of the Higgs boson*, *Phys. Rev.* **D79** (2009) 035012, [[arXiv:0809.0202](#)].

- [198] S. Dutta, K. Hagiwara, and Y. Matsumoto, *Measuring the Higgs-Vector boson Couplings at Linear e^+e^- Collider*, *Phys. Rev.* **D78** (2008) 115016, [[arXiv:0808.0477](#)].
- [199] T. Han and Y. Li, *Genuine CP-odd Observables at the LHC*, *Phys. Lett.* **B683** (2010) 278–281, [[arXiv:0911.2933](#)].
- [200] Y. Gao, A. V. Gritsan, Z. Guo, K. Melnikov, M. Schulze, and N. V. Tran, *Spin determination of single-produced resonances at hadron colliders*, *Phys. Rev.* **D81** (2010) 075022, [[arXiv:1001.3396](#)].
- [201] A. De Rujula, J. Lykken, M. Pierini, C. Rogan, and M. Spiropulu, *Higgs look-alikes at the LHC*, *Phys. Rev.* **D82** (2010) 013003, [[arXiv:1001.5300](#)].
- [202] R. Boughezal, T. J. LeCompte, and F. Petriello, *Single-variable asymmetries for measuring the ‘Higgs’ boson spin and CP properties*, [arXiv:1208.4311](#).
- [203] D. Stolarski and R. Vega-Morales, *Directly Measuring the Tensor Structure of the Scalar Coupling to Gauge Bosons*, *Phys. Rev.* **D86** (2012) 117504, [[arXiv:1208.4840](#)].
- [204] S. Bolognesi, Y. Gao, A. V. Gritsan, K. Melnikov, M. Schulze, N. V. Tran, and A. Whitbeck, *On the spin and parity of a single-produced resonance at the LHC*, *Phys. Rev.* **D86** (2012) 095031, [[arXiv:1208.4018](#)].
- [205] C. Englert, D. Goncalves-Netto, K. Mawatari, and T. Plehn, *Higgs Quantum Numbers in Weak Boson Fusion*, *JHEP* **01** (2013) 148, [[arXiv:1212.0843](#)].
- [206] A. Djouadi, R. M. Godbole, B. Mellado, and K. Mohan, *Probing the spin-parity of the Higgs boson via jet kinematics in vector boson fusion*, *Phys. Lett.* **B723** (2013) 307–313, [[arXiv:1301.4965](#)].
- [207] J. Ellis, V. Sanz, and T. You, *Associated Production Evidence against Higgs Impostors and Anomalous Couplings*, *Eur. Phys. J.* **C73** (2013) 2507, [[arXiv:1303.0208](#)].
- [208] C. Delaunay, G. Perez, H. de Sandes, and W. Skiba, *Higgs Up-Down CP Asymmetry at the LHC*, *Phys. Rev.* **D89** (2014), no. 3 035004, [[arXiv:1308.4930](#)].

- [209] Y. Sun, X.-F. Wang, and D.-N. Gao, *CP mixed property of the Higgs-like particle in the decay channel $h \rightarrow ZZ^* \rightarrow 4l$* , *Int. J. Mod. Phys. A* **29** (2014) 1450086, [[arXiv:1309.4171](#)].
- [210] F. Maltoni, K. Mawatari, and M. Zaro, *Higgs characterisation via vector-boson fusion and associated production: NLO and parton-shower effects*, *Eur. Phys. J.* **C74** (2014), no. 1 2710, [[arXiv:1311.1829](#)].
- [211] G. Amar, S. Banerjee, S. von Buddenbrock, A. S. Cornell, T. Mandal, B. Mellado, and B. Mukhopadhyaya, *Exploration of the tensor structure of the Higgs boson coupling to weak bosons in $e^+ e^-$ collisions*, *JHEP* **02** (2015) 128, [[arXiv:1405.3957](#)].
- [212] M. Beneke, D. Boito, and Y.-M. Wang, *Anomalous Higgs couplings in angular asymmetries of $H \rightarrow Z\ell^+\ell^-$ and $e^+ e^- \rightarrow HZ$* , *JHEP* **11** (2014) 028, [[arXiv:1406.1361](#)].
- [213] **CMS Collaboration** Collaboration, *Constraints on anomalous HVV interactions using H to $4l$ decays*, Tech. Rep. CMS-PAS-HIG-14-014, CERN, Geneva, 2014.
- [214] **CMS Collaboration** Collaboration, *Constraints on Anomalous HWW Interactions using Higgs boson decays to W^+W^- in the fully leptonic final state*, Tech. Rep. CMS-PAS-HIG-14-012, CERN, Geneva, 2014.
- [215] B. Bhattacharjee, T. Modak, S. K. Patra, and R. Sinha, *Probing Higgs couplings at LHC and beyond*, [arXiv:1503.0892](#).
- [216] S. Dwivedi, D. K. Ghosh, B. Mukhopadhyaya, and A. Shivaji, *Constraints on CP-violating gauge-Higgs operators*, *Phys. Rev.* **D92** (2015), no. 9 095015, [[arXiv:1505.0584](#)].
- [217] D. Choudhury, R. Islam, and A. Kundu, *Anomalous Higgs Couplings as a Window to New Physics*, *Phys. Rev.* **D88** (2013), no. 1 013014, [[arXiv:1212.4652](#)].
- [218] M. Dahiya, S. Dutta, and R. Islam, *Investigating perturbative unitarity in the presence of anomalous couplings*, *Phys. Rev.* **D93** (2016), no. 5 055013, [[arXiv:1311.4523](#)].
- [219] G. Valencia, *Constructing CP odd observables*, in *Theoretical Advanced Study Institute in Elementary Particle Physics (TASI 94): CP Violation and the limits of*

- the Standard Model Boulder, Colorado, May 29-June 24, 1994*, pp. 0235–270, 1994.
[hep-ph/9411441](#).
- [220] R. D. Ball et al., *Parton distributions with LHC data*, *Nucl. Phys.* **B867** (2013) 244–289, [[arXiv:1207.1303](#)].
- [221] T. Sjostrand, S. Mrenna, and P. Z. Skands, *PYTHIA 6.4 Physics and Manual*, *JHEP* **05** (2006) 026, [[hep-ph/0603175](#)].
- [222] **DELPHES 3** Collaboration, J. de Favereau, C. Delaere, P. Demin, A. Giammanco, V. Lematre, A. Mertens, and M. Selvaggi, *DELPHES 3, A modular framework for fast simulation of a generic collider experiment*, *JHEP* **02** (2014) 057, [[arXiv:1307.6346](#)].
- [223] R. Brun and F. Rademakers, *ROOT: An object oriented data analysis framework*, *Nucl. Instrum. Meth.* **A389** (1997) 81–86.
- [224] S. Banerjee, T. Mandal, B. Mellado, and B. Mukhopadhyaya, *Cornering dimension-6 HVV interactions at high luminosity LHC: the role of event ratios*, *JHEP* **09** (2015) 057, [[arXiv:1505.0022](#)].
- [225] **CMS** Collaboration, S. Chatrchyan et al., *Search for the standard model Higgs boson produced in association with a W or a Z boson and decaying to bottom quarks*, *Phys. Rev.* **D89** (2014), no. 1 012003, [[arXiv:1310.3687](#)].
- [226] **ATLAS** Collaboration, G. Aad et al., *Observation and measurement of Higgs boson decays to WW^* with the ATLAS detector*, *Phys. Rev.* **D92** (2015), no. 1 012006, [[arXiv:1412.2641](#)].
- [227] **ATLAS** Collaboration, G. Aad et al., *Search for the $b\bar{b}$ decay of the Standard Model Higgs boson in associated $(W/Z)H$ production with the ATLAS detector*, *JHEP* **01** (2015) 069, [[arXiv:1409.6212](#)].
- [228] **CMS** Collaboration, S. Chatrchyan et al., *Evidence for the 125 GeV Higgs boson decaying to a pair of τ leptons*, *JHEP* **05** (2014) 104, [[arXiv:1401.5041](#)].
- [229] **ATLAS** Collaboration, G. Aad et al., *Study of $(W/Z)H$ production and Higgs boson couplings using $H \rightarrow WW^*$ decays with the ATLAS detector*, *JHEP* **08** (2015) 137, [[arXiv:1506.0664](#)].

- [230] **ATLAS** Collaboration, G. Aad et al., *Evidence for the Higgs-boson Yukawa coupling to tau leptons with the ATLAS detector*, *JHEP* **04** (2015) 117, [[arXiv:1501.0494](#)].
- [231] A. Alloul, N. D. Christensen, C. Degrande, C. Duhr, and B. Fuks, *FeynRules 2.0 - A complete toolbox for tree-level phenomenology*, *Comput. Phys. Commun.* **185** (2014) 2250–2300, [[arXiv:1310.1921](#)].
- [232] J. Brod, U. Haisch, and J. Zupan, *Constraints on CP-violating Higgs couplings to the third generation*, *JHEP* **11** (2013) 180, [[arXiv:1310.1385](#)].
- [233] J. F. Gunion and X.-G. He, *Determining the CP Nature of a Neutral Higgs Boson at the CERN Large Hadron Collider*, *Phys. Rev. Lett.* **76** (Jun, 1996) 4468–4471.
- [234] V. Braguta, A. Chalov, A. Likhoded, and R. Rosenfeld, *Future e^+e^- colliders' sensitivity to $h\bar{b}b$ coupling and cp violation*, *Phys. Rev. Lett.* **90** (Jun, 2003) 241801.
- [235] T. Han and B. Mellado, *Higgs Boson Searches and the $H b$ anti- b Coupling at the LHeC*, *Phys. Rev.* **D82** (2010) 016009, [[arXiv:0909.2460](#)].
- [236] T. Han, Z. Liu, Z. Qian, and J. Sayre, *Improving Higgs coupling measurements through ZZ Fusion at the ILC*, *Phys. Rev.* **D91** (2015) 113007, [[arXiv:1504.0139](#)].
- [237] F. Boudjema, R. M. Godbole, D. Guadagnoli, and K. A. Mohan, *Lab-frame observables for probing the top-Higgs interaction*, *Phys. Rev.* **D92** (2015), no. 1 015019, [[arXiv:1501.0315](#)].
- [238] K. Hagiwara, K. Ma, and H. Yokoya, *Probing CP violation in e^+e^- production of the Higgs boson and toponia*, *JHEP* **06** (2016) 048, [[arXiv:1602.0068](#)].
- [239] S. Dwivedi, D. K. Ghosh, B. Mukhopadhyaya, and A. Shivaji, *Distinguishing CP-odd couplings of the Higgs boson to weak boson pairs*, *Phys. Rev.* **D93** (2016) 115039, [[arXiv:1603.0619](#)].
- [240] **CMS** Collaboration, V. Khachatryan et al., *Combined search for anomalous pseudoscalar HVV couplings in $VH(H \rightarrow b\bar{b})$ production and $H \rightarrow VV$ decay*, *Phys. Lett.* **B759** (2016) 672–696, [[arXiv:1602.0430](#)].
- [241] J. Alwall, M. Herquet, F. Maltoni, O. Mattelaer, and T. Stelzer, *MadGraph 5 : Going Beyond*, *JHEP* **06** (2011) 128, [[arXiv:1106.0522](#)].

- [242] <http://cp3.irmp.ucl.ac.be/projects/madgraph/wiki/FAQ> General-13.
- [243] **The ATLAS Collaborations** Collaboration, *ATL-PHYS-PUB-2015-022*, tech. rep., 2015.
- [244] **CMS** Collaboration, S. Chatrchyan et al., *Identification of b -quark jets with the CMS experiment*, *JINST* **8** (2013) P04013, [[arXiv:1211.4462](#)].
- [245] M. Cacciari, G. P. Salam, and G. Soyez, *The Anti- $k(t)$ jet clustering algorithm*, *JHEP* **04** (2008) 063, [[arXiv:0802.1189](#)].
- [246] H. Abramowicz et al., *The International Linear Collider Technical Design Report - Volume 4: Detectors*, [arXiv:1306.6329](#).
- [247] <https://twiki.cern.ch/twiki/bin/view/LHCPhysics/LHCHXSWG>.
- [248] A. Arbey et al., *Physics at the e^+e^- Linear Collider*, *Eur. Phys. J.* **C75** (2015), no. 8 371, [[arXiv:1504.0172](#)].
- [249] M. Trodden, *Electroweak baryogenesis: A Brief review*, in *Proceedings, 33rd Rencontres de Moriond 98 electroweak interactions and unified theories: Les Arcs, France, Mar 14-21, 1998*, pp. 471–480, 1998. [hep-ph/9805252](#).
- [250] N. Turok and J. Zadrozny, *Electroweak baryogenesis in the two doublet model*, *Nucl. Phys.* **B358** (1991) 471–493.
- [251] K. Funakubo, A. Kakuto, and K. Takenaga, *The Effective potential of electroweak theory with two massless Higgs doublets at finite temperature*, *Prog. Theor. Phys.* **91** (1994) 341–352, [[hep-ph/9310267](#)].
- [252] A. T. Davies, C. D. Froggatt, G. Jenkins, and R. G. Moorhouse, *Baryogenesis constraints on two Higgs doublet models*, *Phys. Lett.* **B336** (1994) 464–470.
- [253] J. M. Cline, K. Kainulainen, and A. P. Vischer, *Dynamics of two Higgs doublet CP violation and baryogenesis at the electroweak phase transition*, *Phys. Rev.* **D54** (1996) 2451–2472, [[hep-ph/9506284](#)].
- [254] M. Laine and K. Rummukainen, *Two Higgs doublet dynamics at the electroweak phase transition: A Nonperturbative study*, *Nucl. Phys.* **B597** (2001) 23–69, [[hep-lat/0009025](#)].

- [255] L. Fromme, S. J. Huber, and M. Seniuch, *Baryogenesis in the two-Higgs doublet model*, *JHEP* **11** (2006) 038, [[hep-ph/0605242](#)].
- [256] N. G. Deshpande and E. Ma, *Pattern of Symmetry Breaking with Two Higgs Doublets*, *Phys. Rev.* **D18** (1978) 2574.
- [257] E. Ma, *Verifiable radiative seesaw mechanism of neutrino mass and dark matter*, *Phys. Rev.* **D73** (2006) 077301, [[hep-ph/0601225](#)].
- [258] R. Barbieri, L. J. Hall, and V. S. Rychkov, *Improved naturalness with a heavy Higgs: An Alternative road to LHC physics*, *Phys. Rev.* **D74** (2006) 015007, [[hep-ph/0603188](#)].
- [259] D. Majumdar and A. Ghosal, *Dark Matter candidate in a Heavy Higgs Model - Direct Detection Rates*, *Mod. Phys. Lett.* **A23** (2008) 2011–2022, [[hep-ph/0607067](#)].
- [260] T. Hambye and M. H. G. Tytgat, *Electroweak symmetry breaking induced by dark matter*, *Phys. Lett.* **B659** (2008) 651–655, [[arXiv:0707.0633](#)].
- [261] L. Lopez Honorez, E. Nezri, J. F. Oliver, and M. H. G. Tytgat, *The Inert Doublet Model: An Archetype for Dark Matter*, *JCAP* **0702** (2007) 028, [[hep-ph/0612275](#)].
- [262] M. Gustafsson, E. Lundstrom, L. Bergstrom, and J. Edsjo, *Significant Gamma Lines from Inert Higgs Dark Matter*, *Phys. Rev. Lett.* **99** (2007) 041301, [[astro-ph/0703512](#)].
- [263] Q.-H. Cao, E. Ma, and G. Rajasekaran, *Observing the Dark Scalar Doublet and its Impact on the Standard-Model Higgs Boson at Colliders*, *Phys. Rev.* **D76** (2007) 095011, [[arXiv:0708.2939](#)].
- [264] P. Agrawal, E. M. Dolle, and C. A. Krenke, *Signals of Inert Doublet Dark Matter in Neutrino Telescopes*, *Phys. Rev.* **D79** (2009) 015015, [[arXiv:0811.1798](#)].
- [265] L. Lopez Honorez and C. E. Yaguna, *The inert doublet model of dark matter revisited*, *JHEP* **09** (2010) 046, [[arXiv:1003.3125](#)].
- [266] N. Chakrabarty, D. K. Ghosh, B. Mukhopadhyaya, and I. Saha, *Dark matter, neutrino masses and high scale validity of an inert Higgs doublet model*, *Phys. Rev.* **D92** (2015), no. 1 015002, [[arXiv:1501.0370](#)].

- [267] N. Chakrabarty and B. Mukhopadhyaya, *High-scale validity of a two Higgs doublet scenario: predicting collider signals*, *Phys. Rev.* **D96** (2017), no. 3 035028, [[arXiv:1702.0826](#)].
- [268] N. Chakrabarty and B. Mukhopadhyaya, *High-scale validity of a two Higgs doublet scenario: metastability included*, *Eur. Phys. J.* **C77** (2017), no. 3 153, [[arXiv:1603.0588](#)].
- [269] P. Langacker, *Grand unified theories and proton decay*, *Physics Reports* **72** (1981), no. 4 185 – 385.
- [270] B. McWilliams and L.-F. Li, *Virtual Effects of Higgs Particles*, *Nucl. Phys.* **B179** (1981) 62–84.
- [271] O. U. Shanker, *Flavor Violation, Scalar Particles and Leptoquarks*, *Nucl. Phys.* **B206** (1982) 253–272.
- [272] G. C. Branco, P. M. Ferreira, L. Lavoura, M. N. Rebelo, M. Sher, and J. P. Silva, *Theory and phenomenology of two-Higgs-doublet models*, *Phys. Rept.* **516** (2012) 1–102, [[arXiv:1106.0034](#)].
- [273] S. L. Glashow and S. Weinberg, *Natural conservation laws for neutral currents*, *Phys. Rev. D* **15** (Apr, 1977) 1958–1965.
- [274] E. A. Paschos, *Diagonal neutral currents*, *Phys. Rev. D* **15** (Apr, 1977) 1966–1972.
- [275] J. F. Gunion, H. E. Haber, G. L. Kane, and S. Dawson, *The Higgs Hunter’s Guide*, *Front. Phys.* **80** (2000) 1–404.
- [276] A. Djouadi, *The Anatomy of electro-weak symmetry breaking. II. The Higgs bosons in the minimal supersymmetric model*, *Phys. Rept.* **459** (2008) 1–241, [[hep-ph/0503173](#)].
- [277] S. Kanemura, H. Yokoya, and Y.-J. Zheng, *Complementarity in direct searches for additional Higgs bosons at the LHC and the International Linear Collider*, *Nucl. Phys.* **B886** (2014) 524–553, [[arXiv:1404.5835](#)].
- [278] K. G. Klimenko, *On Necessary and Sufficient Conditions for Some Higgs Potentials to Be Bounded From Below*, *Theor. Math. Phys.* **62** (1985) 58–65. [*Teor. Mat. Fiz.*62,87(1985)].

- [279] M. Maniatis, A. von Manteuffel, O. Nachtmann, and F. Nagel, *Stability and symmetry breaking in the general two-Higgs-doublet model*, *Eur. Phys. J.* **C48** (2006) 805–823, [[hep-ph/0605184](#)].
- [280] A. Barroso, P. M. Ferreira, I. P. Ivanov, and R. Santos, *Metastability bounds on the two Higgs doublet model*, *JHEP* **06** (2013) 045, [[arXiv:1303.5098](#)].
- [281] S. Bertolini, *Quantum Effects in a Two Higgs Doublet Model of the Electroweak Interactions*, *Nucl. Phys.* **B272** (1986) 77–98.
- [282] S. Kanemura, Y. Okada, H. Taniguchi, and K. Tsumura, *Indirect bounds on heavy scalar masses of the two-Higgs-doublet model in light of recent Higgs boson searches*, *Phys. Lett.* **B704** (2011) 303–307, [[arXiv:1108.3297](#)].
- [283] F. Mahmoudi and O. Stal, *Flavor constraints on the two-Higgs-doublet model with general Yukawa couplings*, *Phys. Rev.* **D81** (2010) 035016, [[arXiv:0907.1791](#)].
- [284] F. J. Botella, G. C. Branco, A. Carmona, M. Nebot, L. Pedro, and M. N. Rebelo, *Physical Constraints on a Class of Two-Higgs Doublet Models with FCNC at tree level*, *JHEP* **07** (2014) 078, [[arXiv:1401.6147](#)].
- [285] X.-D. Cheng, Y.-D. Yang, and X.-B. Yuan, *Phenomenological discriminations of the Yukawa interactions in two-Higgs doublet models with Z_2 symmetry*, *Eur. Phys. J.* **C74** (2014), no. 10 3081, [[arXiv:1401.6657](#)].
- [286] G. Bhattacharyya, D. Das, and A. Kundu, *Feasibility of light scalars in a class of two-Higgs-doublet models and their decay signatures*, *Phys. Rev.* **D89** (2014) 095029, [[arXiv:1402.0364](#)].
- [287] **Heavy Flavor Averaging Group** Collaboration, Y. Amhis et al., *Averages of B -Hadron, C -Hadron, and tau-lepton properties as of early 2012*, [arXiv:1207.1158](#).
- [288] T. Hermann, M. Misiak, and M. Steinhauser, *$\bar{B} \rightarrow X_s \gamma$ in the Two Higgs Doublet Model up to Next-to-Next-to-Leading Order in QCD*, *JHEP* **11** (2012) 036, [[arXiv:1208.2788](#)].
- [289] M. Misiak and M. Steinhauser, *NNLO QCD corrections to the $\bar{B} \rightarrow X_s \gamma$ matrix elements using interpolation in m_c* , *Nucl. Phys.* **B764** (2007) 62–82, [[hep-ph/0609241](#)].

- [290] **Belle** Collaboration, A. Abdesselam et al., *Measurement of the inclusive $B \rightarrow X_{s+d}\gamma$ branching fraction, photon energy spectrum and HQE parameters*, in *Proceedings, 38th International Conference on High Energy Physics (ICHEP 2016): Chicago, IL, USA, August 3-10, 2016*, 2016. [arXiv:1608.0234](#).
- [291] W.-S. Hou, *Enhanced charged Higgs boson effects in $B^- \rightarrow \tau\bar{\nu}$, $\mu\bar{\nu}$ and $b \rightarrow \tau\bar{\nu} + X$* , *Phys. Rev.* **D48** (1993) 2342–2344.
- [292] A. G. Akeroyd and F. Mahmoudi, *Constraints on charged Higgs bosons from $D(s)\pm \rightarrow \mu^\pm\nu$ and $D(s)^\pm \rightarrow \tau^\pm\nu$* , *JHEP* **04** (2009) 121, [[arXiv:0902.2393](#)].
- [293] **DELPHI** Collaboration, J. Abdallah et al., *Searches for neutral higgs bosons in extended models*, *Eur. Phys. J.* **C38** (2004) 1–28, [[hep-ex/0410017](#)].
- [294] **DELPHI, OPAL, ALEPH, LEP Working Group for Higgs Boson Searches, L3** Collaboration, S. Schael et al., *Search for neutral MSSM Higgs bosons at LEP*, *Eur. Phys. J.* **C47** (2006) 547–587, [[hep-ex/0602042](#)].
- [295] **L3** Collaboration, P. Achard et al., *Search for charged Higgs bosons at LEP*, *Phys. Lett.* **B575** (2003) 208–220, [[hep-ex/0309056](#)].
- [296] **DELPHI** Collaboration, J. Abdallah et al., *Search for charged Higgs bosons at LEP in general two Higgs doublet models*, *Eur. Phys. J.* **C34** (2004) 399–418, [[hep-ex/0404012](#)].
- [297] **LEP, DELPHI, OPAL, ALEPH, L3** Collaboration, G. Abbiendi et al., *Search for Charged Higgs bosons: Combined Results Using LEP Data*, *Eur. Phys. J.* **C73** (2013) 2463, [[arXiv:1301.6065](#)].
- [298] **CDF** Collaboration, T. Aaltonen et al., *Search for Higgs Bosons Produced in Association with b -quarks*, *Phys. Rev.* **D85** (2012) 032005, [[arXiv:1106.4782](#)].
- [299] **D0** Collaboration, V. M. Abazov et al., *Search for Higgs bosons of the minimal supersymmetric standard model in $p\bar{p}$ collisions at $\sqrt{s} = 1.96$ TeV*, *Phys. Lett.* **B710** (2012) 569–577, [[arXiv:1112.5431](#)].
- [300] **CDF, D0** Collaboration, T. Aaltonen et al., *Search for Neutral Higgs Bosons in Events with Multiple Bottom Quarks at the Tevatron*, *Phys. Rev.* **D86** (2012) 091101, [[arXiv:1207.2757](#)].

- [301] **D0** Collaboration, V. M. Abazov et al., *Search for charged Higgs bosons decaying to top and bottom quarks in $p\bar{p}$ collisions*, *Phys. Rev. Lett.* **102** (2009) 191802, [[arXiv:0807.0859](#)].
- [302] **D0** Collaboration, V. M. Abazov et al., *Search for Charged Higgs Bosons in Top Quark Decays*, *Phys. Lett.* **B682** (2009) 278–286, [[arXiv:0908.1811](#)].
- [303] **CDF** Collaboration, T. Aaltonen et al., *Search for charged Higgs bosons in decays of top quarks in p anti- p collisions at $s^{*(1/2)} = 1.96$ TeV*, *Phys. Rev. Lett.* **103** (2009) 101803, [[arXiv:0907.1269](#)].
- [304] **CMS** Collaboration, V. Khachatryan et al., *Search for neutral MSSM Higgs bosons decaying to a pair of tau leptons in pp collisions*, *JHEP* **10** (2014) 160, [[arXiv:1408.3316](#)].
- [305] **ATLAS** Collaboration, G. Aad et al., *Search for the neutral Higgs bosons of the Minimal Supersymmetric Standard Model in pp collisions at $\sqrt{s} = 7$ TeV with the ATLAS detector*, *JHEP* **02** (2013) 095, [[arXiv:1211.6956](#)].
- [306] **CMS** Collaboration, S. Chatrchyan et al., *Search for a Higgs boson decaying into a b -quark pair and produced in association with b quarks in proton-proton collisions at 7 TeV*, *Phys. Lett.* **B722** (2013) 207–232, [[arXiv:1302.2892](#)].
- [307] **ATLAS** Collaboration, G. Aad et al., *Search for charged Higgs bosons decaying via $H^+ \rightarrow \tau\nu$ in top quark pair events using pp collision data at $\sqrt{s} = 7$ TeV with the ATLAS detector*, *JHEP* **06** (2012) 039, [[arXiv:1204.2760](#)].
- [308] **ATLAS** Collaboration, G. Aad et al., *Search for charged Higgs bosons decaying via $H^\pm \rightarrow \tau^\pm\nu$ in fully hadronic final states using pp collision data at $\sqrt{s} = 8$ TeV with the ATLAS detector*, *JHEP* **03** (2015) 088, [[arXiv:1412.6663](#)].
- [309] D. Chang, W.-F. Chang, C.-H. Chou, and W.-Y. Keung, *Large two loop contributions to $g-2$ from a generic pseudoscalar boson*, *Phys. Rev.* **D63** (2001) 091301, [[hep-ph/0009292](#)].
- [310] F. Larios, G. Tavares-Velasco, and C. P. Yuan, *A Very light CP odd scalar in the two Higgs doublet model*, *Phys. Rev.* **D64** (2001) 055004, [[hep-ph/0103292](#)].
- [311] M. Krawczyk, *Precision muon $g-2$ results and light Higgs bosons in the 2HDM(II)*, *Acta Phys. Polon.* **B33** (2002) 2621–2634, [[hep-ph/0208076](#)].

- [312] K. Cheung and O. C. W. Kong, *Can the two Higgs doublet model survive the constraint from the muon anomalous magnetic moment as suggested?*, *Phys. Rev. D* **68** (2003) 053003, [[hep-ph/0302111](#)].
- [313] B. e. Lautrup, A. Peterman, and E. de Rafael, *Recent developments in the comparison between theory and experiments in quantum electrodynamics*, *Phys. Rept.* **3** (1972) 193–260.
- [314] J. P. Leveille, *The Second Order Weak Correction to $(G-2)$ of the Muon in Arbitrary Gauge Models*, *Nucl. Phys.* **B137** (1978) 63–76.
- [315] A. Dedes and H. E. Haber, *Can the Higgs sector contribute significantly to the muon anomalous magnetic moment?*, *JHEP* **05** (2001) 006, [[hep-ph/0102297](#)].
- [316] S. M. Barr, E. M. Freire, and A. Zee, *Mechanism for large neutrino magnetic moments*, *Phys. Rev. Lett.* **65** (Nov, 1990) 2626–2629.
- [317] F. Jegerlehner and A. Nyffeler, *The Muon $g-2$* , *Phys. Rept.* **477** (2009) 1–110, [[arXiv:0902.3360](#)].
- [318] M. Lisanti and J. G. Wacker, *Discovering the Higgs with Low Mass Muon Pairs*, *Phys. Rev. D* **79** (2009) 115006, [[arXiv:0903.1377](#)].
- [319] J. Cao, P. Wan, L. Wu, and J. M. Yang, *Lepton-Specific Two-Higgs Doublet Model: Experimental Constraints and Implication on Higgs Phenomenology*, *Phys. Rev. D* **80** (2009) 071701, [[arXiv:0909.5148](#)].
- [320] E. J. Chun and J. Kim, *Leptonic Precision Test of Leptophilic Two-Higgs-Doublet Model*, *JHEP* **07** (2016) 110, [[arXiv:1605.0629](#)].
- [321] P. Bandyopadhyay, C. Coriano, and A. Costantini, *Perspectives on a supersymmetric extension of the standard model with a $Y = 0$ Higgs triplet and a singlet at the LHC*, *JHEP* **09** (2015) 045, [[arXiv:1506.0363](#)].
- [322] P. Bandyopadhyay, C. Coriano, and A. Costantini, *Probing the hidden Higgs bosons of the $Y = 0$ triplet- and singlet-extended Supersymmetric Standard Model at the LHC*, *JHEP* **12** (2015) 127, [[arXiv:1510.0630](#)].
- [323] D. Goncalves and D. Lopez-Val, *Pseudoscalar searches with dileptonic tops and jet substructure*, *Phys. Rev. D* **94** (2016), no. 9 095005, [[arXiv:1607.0861](#)].

- [324] S. Su and B. Thomas, *The LHC Discovery Potential of a Leptophilic Higgs*, *Phys. Rev.* **D79** (2009) 095014, [[arXiv:0903.0667](#)].
- [325] S. Kanemura, K. Tsumura, and H. Yokoya, *Multi-tau-lepton signatures at the LHC in the two Higgs doublet model*, *Phys. Rev.* **D85** (2012) 095001, [[arXiv:1111.6089](#)].
- [326] S. Kanemura, K. Tsumura, K. Yagyu, and H. Yokoya, *Fingerprinting nonminimal Higgs sectors*, *Phys. Rev.* **D90** (2014) 075001, [[arXiv:1406.3294](#)].
- [327] J. F. Gunion and H. E. Haber, *The CP conserving two Higgs doublet model: The Approach to the decoupling limit*, *Phys. Rev.* **D67** (2003) 075019, [[hep-ph/0207010](#)].
- [328] M. Krawczyk, *The New $(g-2)$ for muon measurement and limits on the light Higgs bosons in 2HDM (II)*, [hep-ph/0103223](#).
- [329] L. Wang and X.-F. Han, *A light pseudoscalar of 2HDM confronted with muon $g-2$ and experimental constraints*, *JHEP* **05** (2015) 039, [[arXiv:1412.4874](#)].
- [330] V. Ilisie, *New Barr-Zee contributions to $(g - 2)_\mu$ in two-Higgs-doublet models*, *JHEP* **04** (2015) 077, [[arXiv:1502.0419](#)].
- [331] T. Abe, R. Sato, and K. Yagyu, *Lepton-specific two Higgs doublet model as a solution of muon $g - 2$ anomaly*, *JHEP* **07** (2015) 064, [[arXiv:1504.0705](#)].
- [332] T. Han, S. K. Kang, and J. Sayre, *Muon $g - 2$ in the aligned two Higgs doublet model*, *JHEP* **02** (2016) 097, [[arXiv:1511.0516](#)].
- [333] A. Cherchiglia, P. Kneschke, D. Stckinger, and H. Stckinger-Kim, *The muon magnetic moment in the 2HDM: complete two-loop result*, *JHEP* **01** (2017) 007, [[arXiv:1607.0629](#)].
- [334] F. Staub, *Reopen parameter regions in Two-Higgs Doublet Models*, [arXiv:1705.0367](#).
- [335] <https://twiki.cern.ch/twiki/bin/view/LHCPhysics/HiggsEuropeanStrategy>.
- [336] M. L. Mangano, M. Moretti, F. Piccinini, and M. Treccani, *Matching matrix elements and shower evolution for top-quark production in hadronic collisions*, *JHEP* **01** (2007) 013, [[hep-ph/0611129](#)].

- [337] S. Hoeche, F. Krauss, N. Lavesson, L. Lonnblad, M. Mangano, A. Schaliche, and S. Schumann, *Matching parton showers and matrix elements*, in *HERA and the LHC: A Workshop on the implications of HERA for LHC physics: Proceedings Part A*, pp. 288–289, 2005. [hep-ph/0602031](#).
- [338] S. Catani, L. Cieri, G. Ferrera, D. de Florian, and M. Grazzini, *Vector boson production at hadron colliders: a fully exclusive QCD calculation at NNLO*, *Phys. Rev. Lett.* **103** (2009) 082001, [[arXiv:0903.2120](#)].
- [339] F. Cascioli, T. Gehrmann, M. Grazzini, S. Kallweit, P. Maierhofer, A. von Manteuffel, S. Pozzorini, D. Rathlev, L. Tancredi, and E. Weihs, *ZZ production at hadron colliders in NNLO QCD*, *Phys. Lett.* **B735** (2014) 311–313, [[arXiv:1405.2219](#)].
- [340] C. Muselli, M. Bonvini, S. Forte, S. Marzani, and G. Ridolfi, *Top Quark Pair Production beyond NNLO*, *JHEP* **08** (2015) 076, [[arXiv:1505.0200](#)].
- [341] **CMS Collaboration** Collaboration, *A search for doubly-charged Higgs boson production in three and four lepton final states at $\sqrt{s} = 13$ TeV*, Tech. Rep. CMS-PAS-HIG-16-036, CERN, Geneva, 2017.
- [342] S. Jadach, Z. Was, R. Decker, and J. H. Kuhn, *The tau decay library TAUOLA: Version 2.4*, *Comput. Phys. Commun.* **76** (1993) 361–380.
- [343] *Reconstruction, Energy Calibration, and Identification of Hadronically Decaying Tau Leptons in the ATLAS Experiment for Run-2 of the LHC*, Tech. Rep. ATL-PHYS-PUB-2015-045, CERN, Geneva, Nov, 2015.
- [344] **CMS Collaboration** Collaboration, *Search for the exotic decay of the Higgs boson to two light pseudoscalar bosons with two taus and two muons in the final state at $\sqrt{s} = 8$ TeV*, Tech. Rep. CMS-PAS-HIG-15-011, CERN, Geneva, 2016.
- [345] R. Aggleton, D. Barducci, N.-E. Bomark, S. Moretti, and C. Shepherd-Themistocleous, *Review of LHC experimental results on low mass bosons in multi Higgs models*, *JHEP* **02** (2017) 035, [[arXiv:1609.0608](#)].